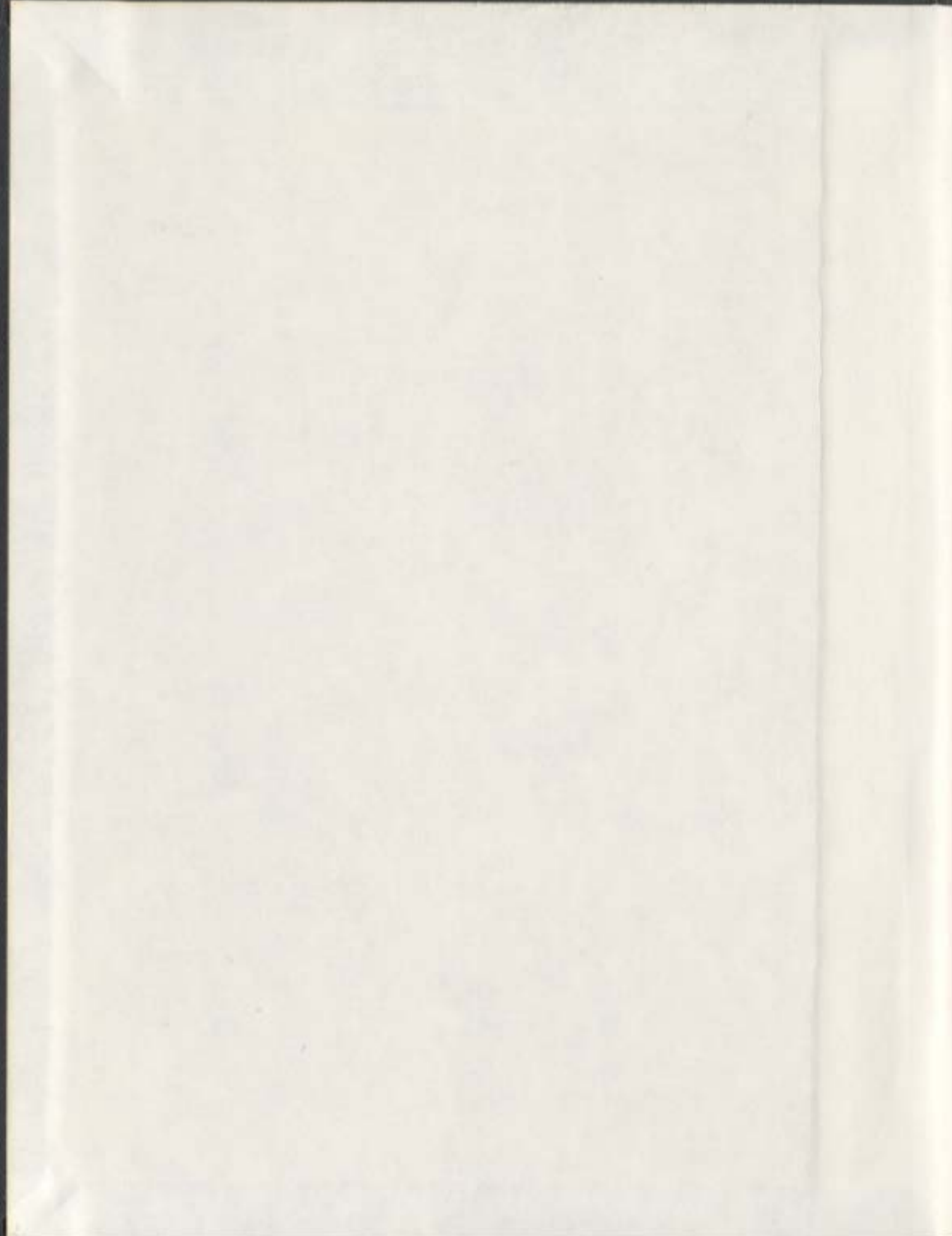


MASS SPECTROMETRIC ANALYSIS AND FINGERPRINT
IDENTIFICATION OF NATURAL LIPOPOLYSACCHARIDE
VACCINE CANDIDATES AND SYNTHETIC LIPOSOMAL
CHOLESTERYL NEOGLYCOLIPIDS

ANAS EL-ANEED



**Mass Spectrometric Analysis and Fingerprint Identification of Natural
Lipopolysaccharide Vaccine Candidates and Synthetic Liposomal Cholesteryl
Neoglycolipids**

by

Anas El-Aneed[©]

A thesis submitted to the School of Graduate Studies in partial fulfillment
of the requirements for the degree of
Doctor of Philosophy

Biochemistry Department
Memorial University of Newfoundland
September 2006

St. John's

Newfoundland and Labrador



Library and
Archives Canada

Bibliothèque et
Archives Canada

Published Heritage
Branch

Direction du
Patrimoine de l'édition

395 Wellington Street
Ottawa ON K1A 0N4
Canada

395, rue Wellington
Ottawa ON K1A 0N4
Canada

Your file *Votre référence*
ISBN: 978-0-494-31314-5
Our file *Notre référence*
ISBN: 978-0-494-31314-5

NOTICE:

The author has granted a non-exclusive license allowing Library and Archives Canada to reproduce, publish, archive, preserve, conserve, communicate to the public by telecommunication or on the Internet, loan, distribute and sell theses worldwide, for commercial or non-commercial purposes, in microform, paper, electronic and/or any other formats.

The author retains copyright ownership and moral rights in this thesis. Neither the thesis nor substantial extracts from it may be printed or otherwise reproduced without the author's permission.

AVIS:

L'auteur a accordé une licence non exclusive permettant à la Bibliothèque et Archives Canada de reproduire, publier, archiver, sauvegarder, conserver, transmettre au public par télécommunication ou par l'Internet, prêter, distribuer et vendre des thèses partout dans le monde, à des fins commerciales ou autres, sur support microforme, papier, électronique et/ou autres formats.

L'auteur conserve la propriété du droit d'auteur et des droits moraux qui protègent cette thèse. Ni la thèse ni des extraits substantiels de celle-ci ne doivent être imprimés ou autrement reproduits sans son autorisation.

In compliance with the Canadian Privacy Act some supporting forms may have been removed from this thesis.

Conformément à la loi canadienne sur la protection de la vie privée, quelques formulaires secondaires ont été enlevés de cette thèse.

While these forms may be included in the document page count, their removal does not represent any loss of content from the thesis.

Bien que ces formulaires aient inclus dans la pagination, il n'y aura aucun contenu manquant.


Canada

Abstract

Mass spectrometric fingerprint identification and structural elucidation of natural and synthetic compounds can be accomplished via the use of mass spectrometry techniques namely, electrospray ionization tandem mass spectrometry (ESI-MS/MS) and matrix assisted laser desorption ionization tandem mass spectrometry (MALDI-MS/MS). In this work, it was opted to use ESI-MS and MALDI-MS, since these are the softest ionization methods which do not require excessive manipulation of the analytes. The identification of MS fingerprints can be effectively used for any quantitative or qualitative studies.

Lipopolysaccharides (LPS) are poly-sugars enriched on the outer membrane of all gram-negative bacteria, most of which are pathogenic. These sugar complexes are potential candidates with relevance to bacterial vaccine developments. This study established the fragmentation pattern of native LPS extracts isolated from *Aeromonas salmonicida*, which infects various fish species. The exact molecular structure of lipid A portion and the core region of this bacterium have been precisely established providing evidence for the unreported presence of the reactive phosphate group at the reducing end of the core oligosaccharide.

LPS moieties (vaccines) have limited antigenic properties when injected alone due to their small size. Therefore a synthetic conjugate of LPS with a protein carrier or the encapsulation of LPS within liposomal carrier will result in the desired antigenic activity. One major limitation for the usage of liposomes is their tendency to aggregate as well as rapid clearance in the circulation system. Synthetic neoglycolipids have been successfully incorporated into liposomal formulations to prolong their half lives as alternative to pegylated liposomes (PEG-liposomes).

The fragmentation routes of a series of synthetic amphiphilic cholesteryl polyethoxy neoglycolipids were established with the aid of electrospray ionization mass spectrometry with a QqTOF-MS hybrid instrument. The results have shown the unique presence of specific common fingerprints such as [Cholestene]⁺, [(Sugar-spacer-OH)+H]⁺, [oxonium]⁺, [oxonium-H₂O]⁺ and, in some cases, [(Cholesterol-spacer-OH)+H]⁺. In addition, the “*in situ*” formation of an unexpected and unique [C-glycoside]⁺ product ion, resulting from an ion-molecule reaction, was observed. This reaction occurs in the collision cell and the ESI interface of the tandem mass spectrometer. Interestingly, this product ion was absent in the case of *O*-acetylated sugar species.

Acknowledgments

I would like to express my deep thanks and appreciation to my supervisor Dr. Joseph Banoub who provided me with guidance and valuable directions during my degree program; I value him as a mentor and a friend.

I would like to acknowledge the resources provided by Fisheries and Oceans (DFO), St. John's where I conducted my research. Special thanks to the technical staff in DFO; Mr. George Sheppard who assisted me in many of the mass spectrometric experiments. I have enjoyed his company and it was a pleasure to share the office space with him. Mr. Howard Hooder who generously corrected my thesis and all other publications, extracted from this work. Other DFO staff and students, namely Manjusri Wijekoon, Nadine Templeman, Jeanne Hart, Janice Lannon, Dr. Andry Ratsimandresy, and William (Bill) Hickey for their friendship and pleasant personalities. This list is by no means a complete list of the fantastic people I met in DFO.

It would have been very difficult to complete the work associated with this document without the numerous discussions with my colleague Dr. Alejandro Cohen. I value his friendship and the time spent working together on many projects/publications.

I thank Dr. Paul Boullanger, from Université Claude Bernard Lyon 1, France, for the chemical synthesis of the neoglycolipids tested in this thesis and Dr. Mariano Koen-Alonso, from DFO, for his assistance in the statistical analysis.

All colleagues in the Biochemistry department and the very active, friendly and helpful technical and secretary staff, namely Ms. Anne Sinnott, Ms. Betty Ann Lewis, Ms. Christine Squire, Mr. Barry Walters, and Ms. Donna Hunt. I appreciate their support and assistance.

Special thanks to Dr. Chet Jablonski, the Dean of the School of Graduate Studies, for his leadership and priceless advice during my academic studies at Memorial University.

I would also like to thank Dr. P. Davis and Dr. K. Nag for serving on my supervisory committee.

Thanks to the school of graduate studies and NSERC for the financial support during my degree programme.

The work accomplished in this thesis would have never been as pleasant without the support and the love of all friends I met in St. John's. I would like especially to thank my best friends Bisan Hazem and Charlene Kenny. Charlene was always there for me when needed and have given me affection, great company and many memorable moments.

Finally, I would like to express my love to my parents and two brothers. Their moral support will never be forgotten.

Table of contents:

Abstract.....	ii
Acknowledgements.....	iii
List of tables.....	ix
List of figures.....	x
List of abbreviations.....	xv
List of Appendices.....	xviii
CHAPTER 1: Introduction.....	1
1.1. Mass Spectrometry.....	1
1.1.1. Mass spectrometry; a historic perspective.....	1
1.1.2. Soft ionization techniques.....	3
1.1.2.1. Electrospray ionization-Mass spectrometry.....	5
1.1.2.2 Matrix assisted laser desorption ionization.....	9
1.1.2.3. Comparison between MALDI and ESI.....	13
1.1.3. Mass analyzers.....	15
1.1.3.1. Quadrupole analyzer.....	15
1.1.3.2. Time of flight (ToF) analyzer.....	17
1.1.3.3. Tandem mass spectrometry (MS/MS).....	20
1.1.3.4. Hybrid quadrupole orthogonal time-of-flight mass spectrometry (Q-ToF).....	23
1.2. Bacterial membranes and lipopolysaccharides.....	26
1.2.1. Background.....	26
1.2.2. Gram positive bacteria.....	26
1.2.3. Gram negative bacteria.....	26

1.2.4. Lipopolysaccharide (LPS).....	28
1.2.4.1. Lipid A.....	29
1.2.4.2. The core region.....	33
1.2.4.3. The O-antigen (the O-chain).....	35
1.2.5. LPS-derived vaccines.....	35
1.2.5.1. LPS-protein conjugates.....	35
1.2.5.2. Liposome-derived vaccines.....	37
1.2.5.3. Neoglycolipids-stabilized liposomes.....	39
1.3. Mass spectrometric analysis of carbohydrates.....	40
1.4. Research objectives.....	42
1.4.1. Natural lipopolysaccharide.....	42
1.4.2. Novel synthetic cholesteryl neoglycolipids.....	43
CHAPTER 2: Materials and Methods.....	45
2.1. Lipopolysaccharides.....	45
2.1.1. Bacterial culture.....	45
2.1.2. Purification of the lipopolysaccharides.....	45
2.1.3. Hydrolysis of the lipopolysaccharides.....	46
2.1.4. Methylation of the core oligosaccharide.....	47
2.1.5. Electrospray Quadrupole Orthogonal Time-of-Flight Mass Spectrometry.....	47
2.1.6. Electrospray Quadrupole-Hexapole-Quadrupole Mass Spectrometry.....	48
2.1.7. Matrix assisted laser/desorption ionization (MALDI)	

mass spectrometry.....	49
2.1.8. Gas chromatography-electron impact- mass spectrometry (GC-EI-MS).....	49
2.2. Synthetic cholesteryl neoglycolipids.....	50
2.2.1. The synthesis of the neoglycolipid derivatives.....	50
2.2.2. Electrospray Quadrupole Orthogonal Time-of-Flight Mass Spectrometry.....	52
2.2.3. The influence of Declustering Potential (DP) and Focusing Potential (FP) on ion formation.....	52
 CHAPTER 3: Mass Spectrometric Analysis of <i>A. salmonicida</i> Lipid A.....	54
3.1. Background.....	54
3.2. ESI- QqToF analysis.....	57
3.3. MS/MS analysis of the biphosphorylated and monophosphorylated lipid A.....	65
3.4. MS/MS analysis of the [C - H] ⁻ and [Y - H] ⁻ ions.....	73
3.5. Summary.....	84
 CHAPTER 4: Mass Spectrometric Analysis of the Core Oligosaccharide of Wild-Type <i>Aeromonas salmonicida</i>	85
4.1. Background.....	85
4.2. MS analysis of the homogenous mixture of the core oligosaccharide.....	91
4.2.1. Negative-ion mode QqToF-MS analysis.....	91
4.2.2. Negative-ion mode MS-MS analysis.....	94
4.2.3. MS/MS evidence for the presence of phosphorylated Kdo unit within the core oligosaccharide.....	101
4.2.4. Positive-ion mode MS and MS/MS analysis.....	103
4.3. MS analysis of the permethylated core oligosaccharide.....	108
4.3.1. QqToF-MS.....	108

4.3.2. MS/MS analysis of the permethylated core oligosaccharide.....	112
4.4. Summary.....	119
CHAPTER 5: Mass Spectrometric Analysis of the Core Oligosaccharide of Mutant <i>Areomonas salmonicida</i>	121
5.1. Background.....	121
5.2. MS analysis of the homogenous mixture of the inner-core oligosaccharide.....	123
5.2.1. Negative-ion mode MS analysis.....	123
5.2.2. Negative-ion mode ESI-QqToF-MS/MS analysis.....	123
5.3. MS analysis of the permethylated core oligosaccharide.....	130
5.3.1. ESI-QqToF-MS.....	130
5.3.2. Positive-ion mode MS/MS analysis.....	135
5.4. Summary.....	144
CHAPTER 6: Mass Spectrometric Fingerprints of Synthetic Cholesteryl Neoglycolipids: The Presence of a Unique C-Glycoside.....	146
5.1. Background.....	146
6.2. QqToF-MS Analysis.....	148
6.3. CID-MS/MS analysis.....	156
6.3.1. CID-MS/MS analysis of the precursor protonated molecules of the non-protected neoglycolipids.....	156
6.3.1.1. The formation of [C-Glycoside] ⁺	162
6.3.1.2. The influence of Declustering Potential (DP) and Focusing potential (FP) on the formation of C-Glycoside.	171
6.3.2. CID-MS/MS analysis of the precursor protonated molecules of the protected neoglycolipids.....	174
6.4. Summary.....	182

CHAPTER 7: Conclusions and Summary.....	184
7.1. Mass spectrometric analysis of LPS oligosaccharide.....	185
7.1.1. Lipid A.....	185
7.1.2. The core oligosaccharide.....	187
7.2. Synthetic neoglycolipids.....	189
7.2.1. Mass spectrometric fingerprints.....	189
7.2.2. C-glycosidation reaction.....	190
7.3. Future directions.....	193
7.4. Closing remarks.....	194
References.....	196
Appendix I.....	218
Appendix II.....	220
Appendix III.....	224
Appendix IV.....	231
Appendix V.....	233
Appendix VI.....	244
Appendix VI.....	247

List of Tables

Table 1-1: Summary of the various features of current ionization methods used in mass spectrometry.....	6
Table 3-1: Assignments of the diagnostic ions observed in QqToF mass spectrum of native lipid A extract acquired at DP= -60.....	59
Table 3-2: Assignments of the diagnostic product ions in CID- MS/MS analysis of the singly charged monophosphorylated Lipid A ion $[M_M - 2H]^-$ at m/z 1688.27.....	68
Table 3-3: Assignments of the diagnostic product ions in CID- MS/MS analysis of the doubly charged biphosphorylated Lipid A ion $[M_B - 2H]^{2-}$ at m/z 883.56.....	72
Table 4-2: Diagnostic product ions of the $[Y]^+$ series resulting from incremental addition of 14 Da, indicating the multiple methylated species of the 4,7-anhydro- α -keto acid derivatives 4A and 4A'.....	117
Table 6-1: list of characteristic ions observed within MS/MS analysis of 9 protonated molecules $[M+H]^+$ of the neoglycolipids bearing non-protected sugar species. Each neoglycolipid was designated based on the sugar portion (Figure 2-1) and the nature of the spacer.....	157
Table 6-2: Tabulated CID-MS/MS results of the $[C\text{-Glycoside}]^+$ ions.....	164
Table 6-3: list of characteristic ions observed within MS/MS analysis protonated molecules of the neoglycolipids bearing protected sugar species. Each neoglycolipid was designated based on the sugar portion (Scheme 1) and the nature of the spacer.....	175
Table 6-4: Tabulated CID-MS/MS results that established Figure 6-12.....	181

List of Figures

Figure 1-1: Conventional electron impact (EI) ionization process. (A) Formation of positively charged ions. (B) Formation of negatively charged ions.....	4
Figure 1-2: The formation of ions during electrospray ionization.....	8
Figure 1-3: MALDI ionization Process.....	11
Figure 1-4: the chemical structure of three commonly used matrices in MALDI-MS analysis.....	12
Figure 1-5: Representation of a quadrupole mass analyzer.....	16
Figure 1-6: Schematic representation of a conventional ToF (time of flight) analyzer (A) and a reflectron-type ToF (B).....	19
Figure 1-7: Comparison of one-stage mass spectrometry (top) and tandem mass spectrometry (bottom).....	21
Figure 1-8: Schematic representation of Applied Biosystems Q-ToF instrument (QSTAR hybrid QqToF).....	25
Figure 1-9: Simplified schematic representation of gram positive and gram negative bacterial membranes.....	30
Figure 1-10: Representation of LPS general structure with three distinctive components: the lipid A, the core oligosaccharide, and the O-specific antigen.....	31
Figure 1-11: Theoretical possible fragmentation of a lactose sugar.....	41
Figure 2-1: the molecular structure of cholysterly neoglycolipids evaluated in this study.....	51
Figure 3-1: Lipid A basic structure.....	55
Figure 3-2: Negative QqToF MS scan of the native lipid A extract from <i>A. salmonicida</i> acquired at DP = - 60.....	58
Figure 3-3: Schematic representation of the fully substituted biphosphorylated lipid A and the diagnostic ions [C - H] ⁻ and [Y - H] ⁻ observed in the QqToF MS scan.....	60

Figure 3-4: The presence of 7 Dalton signals lower and higher of the Biphosphorylated Lipid A $[M_B - 2H]^{2-}$ observed at m/z 883.5826 (A) and 14 Daltons of the Monophosphorylated Lipid A $[M_M - H]^-$ observed at m/z 1688.2144 (B).	62
Scheme 3-5: Four theoretical structures of the lipid A that can be proposed instead of the one illustrated in Figure 3-3.....	64
Figure 3-6: Negative ion CID-MS/MS of the singly charged Monophosphorylated Lipid A $[M_M - H]^-$ at m/z 1688.2 (A) and of the doubly charged Biphosphorylated Lipid A $[M_B - 2H]^{2-}$ at m/z 883.5 (B).....	66
Figure 3-7: Proposed fragmentation pathways of the product ion scan of the selected precursor Monophosphorylated Lipid A $[M_M - H]^-$ ion at m/z 1688.2.....	67
Figure 3-8: Schematic representation of the charge driven (a) and charge remote (b) processes.....	70
Figure 3-9: Negative ion CID-MS/MS of the diagnostic ions: $[C - H]^-$ at m/z 1074.7 (A), $[Y - H]^-$ at m/z 710.4 (B), and $[C - (C12:0(3-O(14:0)))ketene - H]^-$ at m/z 666.3 (C).....	74
Figure 3-10: Proposed fragmentation pathways of the product ion scan of the diagnostic ion $[C - (C12:0(3-O(14:0)))ketene - H]^-$ observed at m/z 666.3.....	76
Figure 3-11: Negative ion CID-MS/MS of the ions: $[M_M - (C12:0)ketene - H]^-$ at m/z 1768.18 (A); $[M_B - (C12:0)ketene - 2H]^{2-}$ at m/z 792.50 (B); $[M_M - (C12:0)ketene - H]^-$ at m/z 1506.04 (C); $[M_M - (C14:0(3-OH))Ketene - H]^-$ at m/z 1462.05 (D).....	79
Figure 3-12: Schematic representation of the rationalized fragmentation routes of the $[M_B - H]^-$ ion observed at m/z 1768.18.....	80
Figure 3-13: Fragmentation pattern of the doubly charged precursor ion $[M_B - (C12:0) Ketene - 2H]^{2-}$ observed at m/z 792.50.....	80
Figure 3-14: Fragmentation routes of the precursor ion $[M_M - (C12:0)Ketene - H]^-$ at m/z 1506.05.....	81
Figure 3-15: Fragmentation pattern of the precursor ion $[M_M - C14:0(3-OH)ketene - H]^-$ at m/z 1462.05.....	83
Figure 4-1: Facile elimination of <i>O</i> -4 phosphorylated Kdo to produce a furoic acid derivative by ring closure involving (C-2)-(O-5)-(C-5).....	87
Figure 4-2: Products formed after treatment of the LPS of <i>A. salmonicida</i>	

(Structure <u>1A</u>) with 1% acetic acid at 100°C for 90 minutes.....	89
Figure 4-3: Formation of the dephosphorylated core oligosaccharide containing the diastomeric mixture of the 5- <i>O</i> -glycosylated 4,8-anhydro- and 4,7-anhydro derivatives of the enolizable α -keto-acid.....	90
Figure 4.4: Negative ion mode ESI-MS spectrum of the homogeneous core oligosaccharide mixture using a declustering potential (DP) of -100V.....	93
Figure 4-5: (A) ESI-MS/MS spectrum of the precursor ion $[M-2H]^{2-}$ at m/z 933.30. (B) The proposed fragmentation routes and the product ions of $[M-2H]^{2-}$	96
Figure 4-6: Schematic representation of the fragmentation pattern of the core oligosaccharide of <i>A. salmonicida</i> recorded in the negative ion mode.....	97
Figure 4-7: (A) ESI-MS/MS spectrum of the precursor ion $[M-2H]^-$ at m/z 1867.84. (B) The proposed fragmentation routes and the product ions of $[M-2H]^-$	99
Figure 4-8: Diagnostic Z-type product ions resulting from the low energy CID-MS/MS of both the $[M-2H]^{2-}$ and $[M-H]^-$ precursor ions are illustrated.....	100
Figure 4-9: ESI-MS/MS spectrum and the proposed product ions of the precursor ion $[M_{PO_4}-2H]^{2-}$ at m/z 982.29.....	102
Figure 4-10: Positive ion mode ESI-MS spectra of the homogeneous core oligosaccharide mixture using a declustering potential (DP) of 80V.....	104
Figure 4-11: Positive ion mode ESI-MS spectra of the homogeneous core oligosaccharide mixture using a declustering potential (DP) of 80V. The proposed fragmentation routes and product ions are also shown.....	105
Figure 4-12: Fragmentation pattern of the core oligosaccharide of the wild-type <i>A. salmonicida</i> recorded in the positive ion mode.....	106
Figure 4-13: ESI-MS/MS spectrum of the precursor $[M+H]^+$ at m/z 1869.62 and the proposed fragmentation routes of the product ions.....	107
Figure 4-14: Positive ion mode ESI-MS (A) and MALDI-MS (B) spectra of the permethylated homogeneous core oligosaccharide mixture dissolved in methanol with the addition of trace amounts of formic acid.....	110
Figure 4-15: Schematic representation of the fragmentation patterns of the permethylated homogeneous mixture of core oligosaccharides recorded in the	

positive ion mode.....	113
Figure 4-16: ESI-MS/MS spectra of the permethylated precursor ions $[M+2H]^{2+}$ at m/z 1194.61 and the proposed fragmentation routes and product ions of this precursor.....	114
Figure 4-17: ESI-MS/MS spectra of the permethylated precursor ions $[M_5+2H]^+$ at m/z 1247.63 and the proposed fragmentation routes and product ions of this precursor.....	118
Figure 5-1: The molecular structure of the core oligosaccharide of the mutant form <i>A. salmonicida</i> lipopolysaccharide, containing an <i>O</i> -4 phosphorylated Kdo residue.....	122
Figure 5-2: Negative ion mode, full scan, ESI-QqTOF-MS of core oligosaccharide of mutant <i>A. salmonicida</i> at DP=15.....	124
Figure 5-3: Product ion scan of m/z 794.88. Peaks are labelled according to the proposed fragmentation routes.....	125
Figure 5-4: (A) Proposed major fragmentation patterns of the deprotonated molecule $[M-H]^-$ at m/z 794.88 (A). Types of product ions observed in this CID-MS/MS analysis (B).....	127
Figure 5-5: (A) Positive ion mode full scan MS of permethylated core oligosaccharide of mutant <i>A. salmonicida</i> by ESI-QhQ MS.....	132
(B) Positive ion mode full scan MS of permethylated core oligosaccharide of mutant <i>A. salmonicida</i> treated with traces of formic acid by ESI-QhQ MS.....	132
(C) Positive ion mode full scan MS of permethylated core oligosaccharide of mutant <i>A. salmonicida</i> by ESI-QqTOF MS.....	133
Figure 5-6: Product ion scan of m/z 1021.52 by ESI-QqTOF MS/MS using low energy CID at two different collision energies (A: 10eV and B: 15eV).....	136
Figure 5-7: Proposed major fragmentation patterns of the permethylated protonated molecules $[M+H]^+$ at m/z 1021.52, $[M_1+H]^+$ at m/z 1035.5134 and $[M_2+H]^+$ at m/z 1049.5251.....	137
Figure 5-8: Types of product ions observed in the CID-MS/MS analysis of the permethylated protonated molecule $[M+H]^+$ at m/z 1021.52.	138
Figure 5-9: Product ion scan of m/z 1113.15 by ESI-QqTOF MS/MS using low energy CID.....	141
Figure 5-10: Proposed major fragmentation patterns of the permethylated protonated molecule $[M_3+H]^+$ at m/z 1113.1562.....	142

Figure 5-11: Types of product ions observed in the CID-MS/MS analysis of the permethylated protonated molecule $[M_3+H]^+$ at m/z 1113.1562.....	143
Figure 6-1: Four examples of positive QqToF-MS scans of different amphiphilic neoglycolipids (structure shown within the figure).....	150
Figure 6-2: General schematic representation of the proposed fragmentation pattern of the cholesteryl neoglycolipids observed in ToF-MS analysis.....	152
Figure 6-3: Confirmation of the genesis of the ions designated as $[(\text{Sugar-spacer-OH})+H]^+$ using deuterated neoglycolipid species.....	155
Figure 6-4: MS/ MS experiments of neoglycolipids bearing (A) GlcNAc linked to the cholesterol portion via <i>O</i> -Glycoside; (B) GlcNAc linked to the cholesterol portion via $(\text{CH}_2\text{CH}_2\text{O})_3$ spacer; and (C) LacNAc linked to the cholesterol portion via $(\text{CH}_2\text{CH}_2\text{O})_3$ spacer.....	160
Figure 6-5: (A) MS/MS scan of neoglycolipid bearing GlcNAloc linked to the cholesterol portion via $(\text{CH}_2\text{CH}_2\text{O})_4$ spacer. (B) MS/MS of the fragment ion designated as $[(\text{Cholesterol-spacer-OH})+H]^+$. (C) MS/MS of the fragment ion designated as $[(\text{OH-Spacer-OH}) +H]^+$	163
Figure 6-6: MS/MS of the ion identified as $[C\text{-Glycoside}]^+$, extracted from the neoglycolipids bearing (A) GlcNAc and linked to the cholesterol through <i>O</i> -glycoside linkage and (B) the LacNAc and linked the cholesterol through $(\text{CH}_2\text{CH}_2)_3$ spacer.....	166
Figure 6-7: Schematic representation of the mechanistic process that leads to the formation of the $[C\text{-Glycoside}]^+$ ion within the ESI interface and during CID-MS/MS analysis.....	168
Figure 6-8: The proposed fragmentation pattern of the $[M+Na]^+$ of the neoglycolipid bearing GlcNAc with a $(\text{CH}_2\text{CH}_2\text{O})_3$ spacer.....	170
Figure 6-9: The relationship between $[C\text{-glycoside}]^+$ ion count and (A) DP values; (B) FP values.....	172
Figure 6-10: The influence of DP on the formation of $[C\text{-glycoside}]^+$, $[\text{Oxonium}]^+$, $[M+H]^+$, and $[(\text{Sugar-spacer})+H]^+$ ions within the ESI interface of the Q-Star Machine.....	173
Figure 6-11: CID-MS/MS of the $[\text{Oxonium}]^+$ ions extracted from neoglycolipid that bear GlcNAloc sugar species (A) and the per- <i>O</i> -acetylated GlcNAloc (B)...	177
Figure 6-12: The fragmentation pattern of the protected $[\text{GlcNAloc}]^+$	180

List of Abbreviations

Capillary electrophoresis-mass spectrometry	CE-MS
Chemical ionization	CI
Collision Induced Dissociation	CID
Declustering Potential	DP
Desorption electrospray ionization	DESI
D-glucosamine	GlcNH ₂
Direct current	DC
Electron impact	EI
Electrospray ionization	ESI
Fast atom bombardment	FAB
Focusing Potential	FP
Fourier transform ion cyclotron resonance	FT-ICR
Fourier transform-mass spectrometry	FT-MS
Full width at half maximum	FWHM
Galactose	Gal
Gas chromatography-Mass spectrometry	GC-MS
Glucose	Glc
<i>L-glycero-D-manno</i> -heptose	Hep
High pressure liquid chromatography	HPLC
L-fucose	Fuc
Linear acceleration pulsar high-pressure	LINAC

Lipooligosaccharides	LOS
Lipopolysaccharide	LPS
Liquid chromatography-mass spectrometry	LCMS
Liquid secondary ion mass spectrometry	LSIMS
Mass Spectrometry	MS
mass-to-charge ratio	<i>m/z</i>
Matrix assisted laser desorption ionization	MALDI
<i>N</i> -acetyl-glucosamine	GlcNAc
<i>N</i> -acetyllactosamine	LacNAc
<i>N</i> -allyloxycarbonyl-D-glucosamine	GlcNAloc
<i>N</i> -trideuterioacetyl-D-glucosamine	GlcNHCOCD ₃
Plasma desorption	PD
Poly Ethylene Glycol	PEG
Quadrupole	Q
Quadrupole ion trap	QIT
Quadrupole orthogonal time-of-flight	QqTOF
Quadrupole-Hexapole-Quadrupole	QhQ
Radio-frequency	rf
Surface enhanced laser desorption ionization	SELDI
Tandem mass spectrometry	MS/MS
Time of flight	ToF
Triple quadrupole	QqQ

α -3-deoxy-D-manno-oct-2-ulosonic acid

Kdo

List of Appendices

Appendix I: Lipid A.....	218
Appendix II: The CID-MS/MS spectra and the fragmentation patterns of the doubly charged series ions presented in Table 4-1.....	220
Appendix III: ESI-MS/MS and MALDI-MS/MS spectra of the mono-charged series of the protonated molecules shown in Table 4-1.....	224
Appendix IV: Additional positive ESI-MS/MS spectra that established the fragmentation pattern shown in Figure 5-7.....	231
Appendix V: Positive QqToF-MS spectra of all tested neoglycolipids (except for the ones presented in Figure 6-1).....	233
Appendix VI: Positive ESI-QqToF-MS spectra of the protected neoglycolipids.....	244
Appendix VII: ESI-QqToF-MS/MS spectra of the protonated molecules of the neoglycolipids, except for the ones presented within Chapter 7.....	247

CHAPTER 1: Introduction

1.1. Mass Spectrometry

1.1.1. Mass spectrometry; a historic perspective:

Mass spectrometry (MS) has rapidly evolved during the past 20 years with its various applications invading every discipline within the life and health sciences (Banoub *et al.*, 2005b; Henderson & McIndoe, 2005; Korfmacher, 2005). Mass spectrometry relies on the formation of gas phase ions (positively or negatively charged) that can be isolated electrically (or magnetically) based on their mass-to-charge ratio (m/z). In a MS spectrum, the x-coordinate represents m/z values while the y-axis indicates the relative abundances “quantity”. Mass spectrometric analysis can provide important information about the analytes including their structure, purity and composition.

Mass spectrometry was first described by physicists in the late 1880s. Wilhelm Wien, for example, was the first to demonstrate in 1898 that superimposed electric and magnetic fields can deflect positive ions and his work was preceded by the work of physicist, Eugen Goldstein who in 1886 discovered a new kind of radiation, “*Kanalstrahlen*”, and reached the conclusion that these “new” rays were merely positively charged particles (Grayson, 2002). Inspired by these findings, Sir Joseph John Thomson, a professor of experimental physics at Cambridge University, invented the first mass spectrometry instrumentation and in 1913 illustrated the value of his novel discovery within the field of analytical chemistry (Thomson, 1913). Mass spectrometry was critical for stable isotope/radionucleotide studies (Aston, 1942) and, eventually, commercial mass spectrometric instrumentation, that can diagnostically detect organic

substances, appeared on the market in the 1940s, as a response to the demands from the oil industry (Grayson, 2002).

The “marriage” between gas chromatography and mass spectrometry expanded the interest in this powerful technique to include biochemistry. Gas chromatography is capable of separating thermally stable biological compounds, such as fatty acids, steroids, and carbohydrates. This analytical tool was invented in 1952 (James & Martin, 1952) and coupling it to a mass spectrometer (i.e. GC-MS) was pioneered by Holmes and Morrell in 1957 (Holmes & Morrell, 1957). Early mass spectrometric instrumentation was limited to volatile compounds with a low molecule weight range (>1000 Da). This was due to the fact that the conventional ionization technique, namely electron impact (EI), is harsh and will result in the destruction of complex biomolecules (e.g. proteins, nucleotides, complex carbohydrates). In addition, the usage of mass spectrometry within biochemistry labs was limited to GC-MS instrumentation that separates volatile mixtures. Under such conditions, complex biological substances cannot be transmitted to the gas phase without significant destruction and degradation. It was only after the introduction of soft ionization techniques that mass spectrometry was used for structural biology. Mass spectrometry can now be interfaced with other separation techniques, such as high pressure liquid chromatography (HPLC-MS) and capillary electrophoresis (CE-MS). However, it is common to perform MS analysis for purified materials or synthetic conjugates, without the use of a separation procedure.

1.1.2. Soft ionization techniques:

Regardless of the method by which a sample is introduced into a mass spectrometer (i.e. GC, HPLC, direct injection), the ion source is the compartment where charged species are produced and is the “gate” to other sections of the instrument, namely the analyzer and the detector. Many ionization techniques are currently used with mass spectrometric instrumentations. The traditional ionization method, namely EI, utilizes energetic electron beams during the ionization process and operates only under vacuum while the analytes are already in the gas phase. A beam of electrons (negative charges) are formed from a heated metallic filament (e.g. tungsten) and these electrons are electrically accelerated and directed to collide with a vaporized sample, causing electron expulsion from the analytes and subsequent formation of positively charged radical-cations. These conditions are not suitable for large molecules or many biological materials. EI along with chemical ionization (introduced below) are, however, still the methods of choice for GC-MS equipment (Kitson *et al.*, 1996). Figure 1-1 illustrates the process by which ions are formed during EI ionization and it should be noted that with specific compounds, negatively charged species can be observed (Herbert & Johnstone, 2003) (Figure 1-1B).

Due to the limitations associated with EI ionization, chemical ionization (CI) and plasma desorption (PD) methods were introduced in 1966 (Munson & Field, 1966) and 1974 (Torgerson *et al.*, 1974), respectively. Both techniques will result predominantly in the formation of protonated (or deprotonated) ions which are more stable than the radical ions formed during EI-MS analysis. CI depends on the interaction between energetic electrons and neutral molecules, such as methane, resulting in the formation of charged

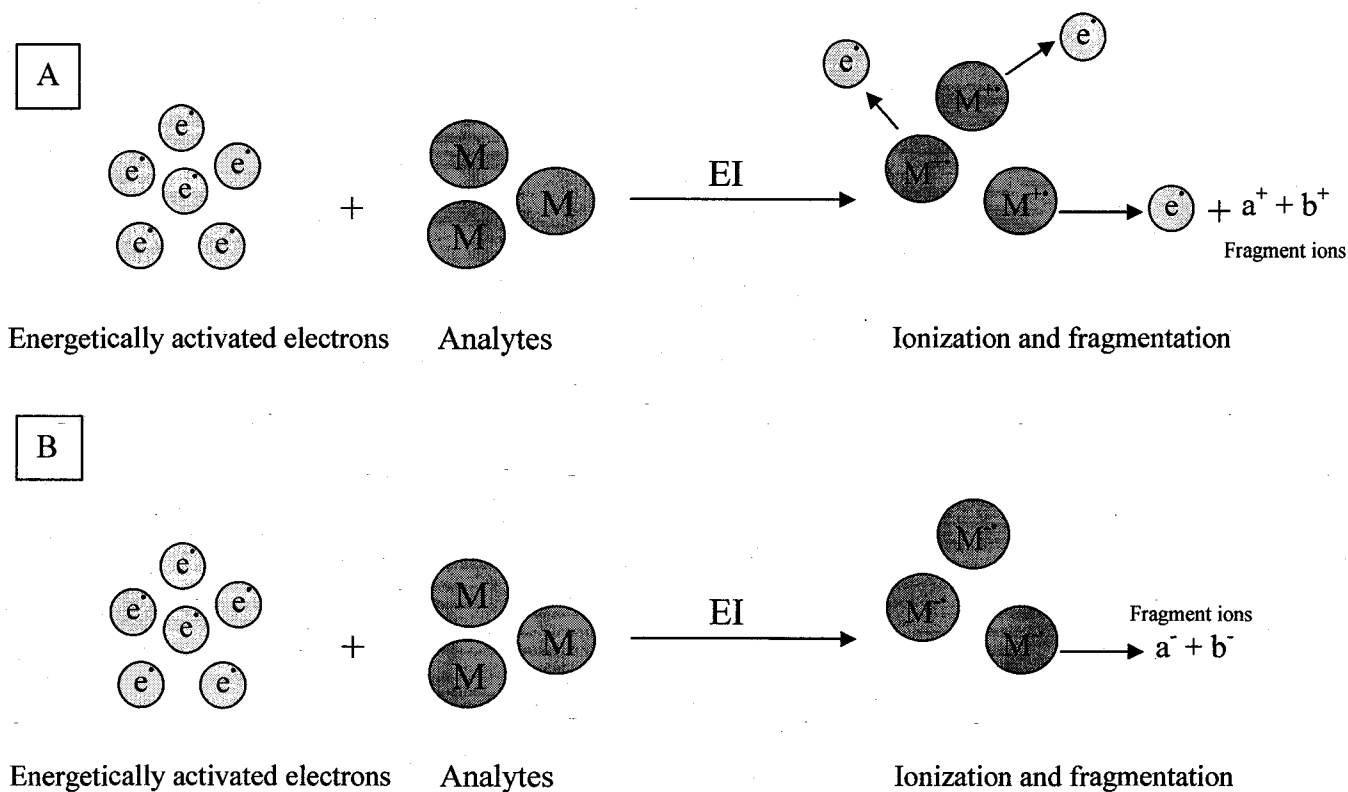


Figure 1-1: Conventional electron impact (EI) ionization process. (A) Formation of positively charged ions. (B) Formation of negatively charged ions.

ions that will interact with the analytes producing protonated species. Similar to EI ionization, this method poses some limitations in terms of mass range (<1000) and requires specific sample characteristics with regard to thermal stability and volatility. CI is, however, better than EI with respect to the production of the molecular ion. Nevertheless, both EI and CI were not capable of analyzing the most valuable, thermally instable, polar biological compounds.

PD ionization, on the other hand, is one of the early “soft” ionization techniques which were capable of analyzing biomolecules, up to a molecular weight (MW) of 100,000 Daltons (Da). The term “soft” indicates that minimum internal energy is

transmitted to the analytes during the ionization process. PD ionization was introduced after the design of field ionization and field desorption methods (Beckey, 1969; Inghram & Gomer, 1954). Subsequently, additional soft ionization methods were developed and replaced older techniques. These include fast atom bombardment (FAB) (Barber *et al.*, 1981; Morris *et al.*, 1981), liquid secondary ion mass spectrometry (LSIMS) (Shackleton & Straub, 1982), matrix assisted laser desorption ionization (MALDI) (Tanaka *et al.*, 1988) and electrospray ionization (ESI) (Yamashita & Fenn, 1984a; Yamashita & Fenn, 1984b). The last two ionization techniques, in particular, have revolutionized the usage of mass spectrometers and enabled researchers to easily study biological substances, such as glycoconjugates, proteins and DNA. The significance of the development of MALDI and ESI was globally recognized when the “inventors”, Koichi Tanaka of the Shimadzu Corp in Kyoto, Japan and John Fenn of the Virginia Commonwealth University, Richmond, USA shared the 2002 Nobel Prize in chemistry. Table 1-1 compares different commonly used ionization methods, summarizing their various characteristics; information in Table 1-1 is extracted from Herbert & Johnstone, (2003) and Henderson & McIndoe, (2005).

1.1.2.1. Electrospray ionization-Mass spectrometry (ESI-MS):

Development of electrospray ionization started in the late 1960s with the work of Dole and co-workers who successfully introduced a polystyrene polymer (average MW=51,000 Da) into the gas-phase as a charged species (Dole *et al.*, 1968). This technique was then linked to a quadrupole mass analyzer and was significantly optimized in the early 1980s (Yamashita & Fenn, 1984a; Yamashita & Fenn, 1984b). ESI-MS is

Ionization technique	Nature of analytes	Sample introduction	Mass Range	Brief description
Electron Impact EI	Volatile Thermally stable	Gas chromatography solid or liquid probe	<1000 Da	Hard method Mainly fragment ions
Chemical Ionization CI	Volatile Thermally stable	Gas chromatography solid or liquid probe	<1000 Da	Soft method Molecular ion
Fast atom bombardment FAB	Organometallic compounds	Liquid chromatography, direct injection	<5000 Da optimal range 200-2000	Soft method Require matrix
Matrix assisted laser desorption ionization (MALDI)	Biomolecules (Proteins, DNA, glycoconjugates)	Sample is co- crystallized with a matrix	Can go beyond 500,000 Da	Very soft method Singly charged ions
Electrospray ionization (ESI)	Organic & inorganic compounds	Sample in solution	From very low masses to extraordinarily high	Very soft method Multiply charged ions

Table 1-1: Summary of the various features of current ionization methods used in mass spectrometry.

currently used for qualitative and quantitative studies of a wide variety of nonvolatile and thermally labile simple inorganic chemicals as well as complex biological structures (Pramanik *et al.*, 2002).

In ESI-MS, the sample should be soluble in a preferably polar solvent which can be infused, under atmospheric pressure, into the ionization source via a thin needle. As the sample is being constantly sprayed, a high electrical potential is applied at the needle (3-4 Kv) resulting in the formation of highly charged droplets (i.e. nebulisation). These droplets are then driven electrically and are vaporized with the aid of a warm neutral gas (usually nitrogen). Under these conditions, the droplets break down and, while shifting inside the source, their size is continuously being reduced. Eventually, the repulsive forces, also termed the coulombic forces, among the ions on the surface of the shrinking droplets become very high. These forces will ultimately exceed the surface tension of the solvent, resulting in ions which desorb into the gas-phase. This theory of ESI ion formation is termed the ion evaporation method (Iribarne & Thomson, 1976; Kebarle, 2000) and is believed to favor ions with relatively low m/z values (Baldwin, 2005). An alternative theory, which is supposed to be dominant in the case of ions with very high m/z (Baldwin, 2005), is the charge residue model, which involves continuous evaporation of the solvent accompanied by droplet fragmentation so that a single ion (probably multiply charged) is formed at the end of this process (i.e. solvent is completely evaporated) (Dole *et al.*, 1968; Griffiths *et al.*, 2001; Kebarle, 2000). Figure 1-2 illustrates the different proposed mechanisms of ion formation during the ESI process.

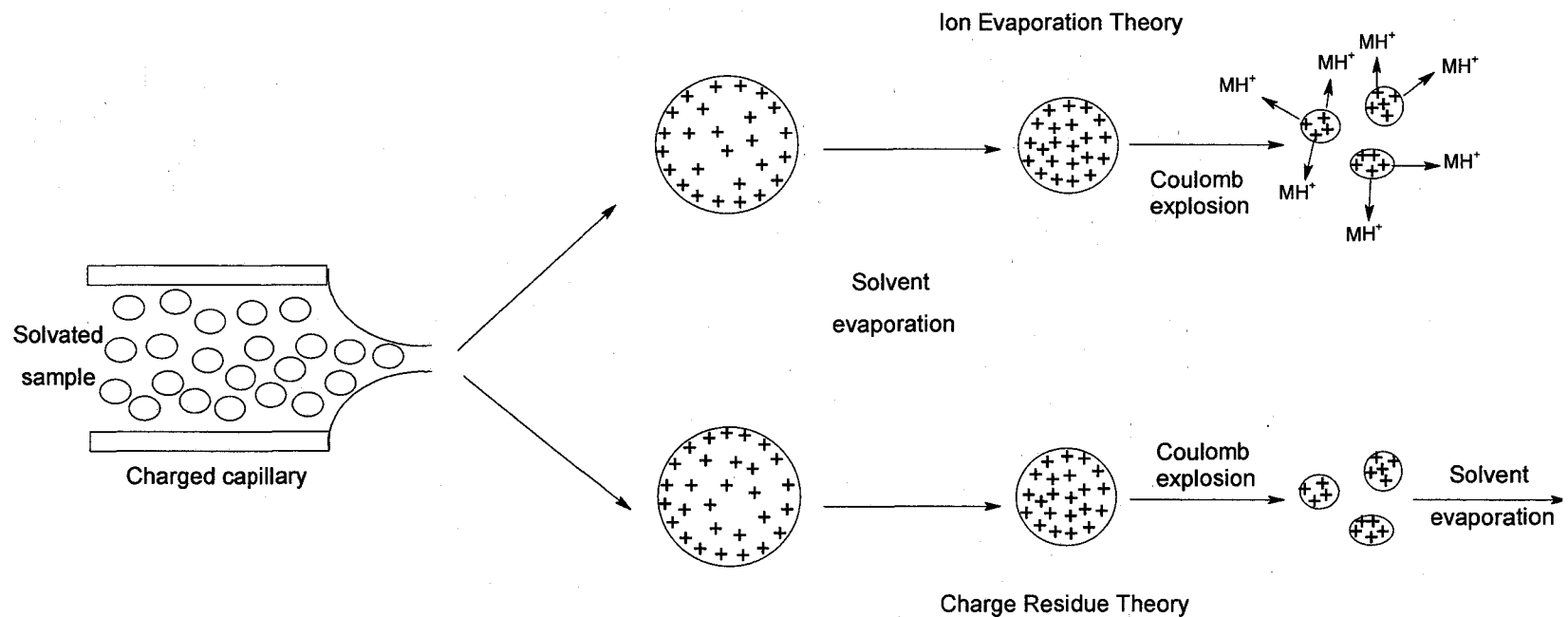


Figure 1-2: The formation of ions during electrospray ionization. The sample solution is passed through a charged capillary, resulting in the creation of charged droplets that evaporate with the aid of a stream of nitrogen. Coulomb explosion will break the highly charged droplets into smaller ones and eventually ions are desorbed from the surface according to the ion evaporation theory or solvent is completely evaporated as speculated based on the charge residue theory. This scheme represents ions as positively charged; the same mechanism applies in the case of negative ion mode.

ESI has obviously resolved the problems inherited in studying large biomaterials using traditional mass spectrometry and its performance can be further enhanced by linking it to liquid chromatography (a powerful analytical technique) in a process known as LCMS. In conventional ES pioneered by Fenn's group, samples were injected at a flow rate of 2-20 $\mu\text{l}/\text{min}$ (Whitehouse *et al.*, 1985) which posed some problems when dealing with limited biological samples. Therefore, additional research efforts (Emmett & Caprioli, 1994; Gale & Smith, 1993) resulted in the development of nanospray technology which operates at a very low flow rate in the order of nanoliters per minute (nl/min). The advantage of nanospray technology is not limited to minimized flow rates, but also to the mechanism of ion formation, improving, for example, glycoconjugate analysis (Karas *et al.*, 2000a). ESI continues to attract researchers from various disciplines who investigate both new applications as well as possible new improvements at the technical level.

1.1.2.2 Matrix assisted laser desorption ionization (MALDI):

MALDI is by far the leading mass spectrometric methodology currently being used for protein sequencing and proteomic research and is commonly utilized in tandem with ESI technology. Banoub's group, for example, have successfully characterized vitellogenin protein, a fish biomarker, by both ESI and MALDI (Banoub *et al.*, 2004a; Banoub *et al.*, 2003). Similar to ESI, however, MALDI is also powerful for studying DNA (Gut, 2004), lipids (Balazy, 2004) and glycoconjugates (Harvey, 2003).

In MALDI, ions are desorbed from the solid phase. A sample is first dissolved in a suitable solvent and mixed with an excessive amount of an appropriate matrix.

Subsequently, it is spotted on a MALDI plate and air-dried (or under a stream of nitrogen gas). Under these circumstances, the sample is co-crystallized with the matrix. The components in the mixture are brought into the gas-phase via a laser beam (usually a nitrogen laser at a wavelength of 337 nm) that hits the sample-matrix crystal, leading to absorption of the laser energy by the matrix and subsequent desorption and ionization of the analytes in the sample. Figure 1-3 represents the process by which ions are formed during MALDI-MS.

MALDI was initially operated under vacuum; however, atmospheric pressure (AP) MALDI was developed in 2000 (Laiko *et al.*, 2000). This development has reduced cost, enhanced ease of operation and improved the commercial production of mass spectrometers with interchangeable MALDI and ESI sources. The mechanisms by which ions are formed in MADLI are still not fully understood and the choice of a specific matrix is mainly experimental. Figure 1-4 shows the chemical structure of three of the most widely used MALDI matrices. In addition to its dependency on the nature of the analytes, the choice of the matrix can also be influenced by the ionization mode, whether positive or negative. Basic matrices are favored in the case of the latter, while acidic ones are more efficient in the case of the former (i.e. proton donor) (Baldwin, 2005; Henderson & McIndoe, 2005).

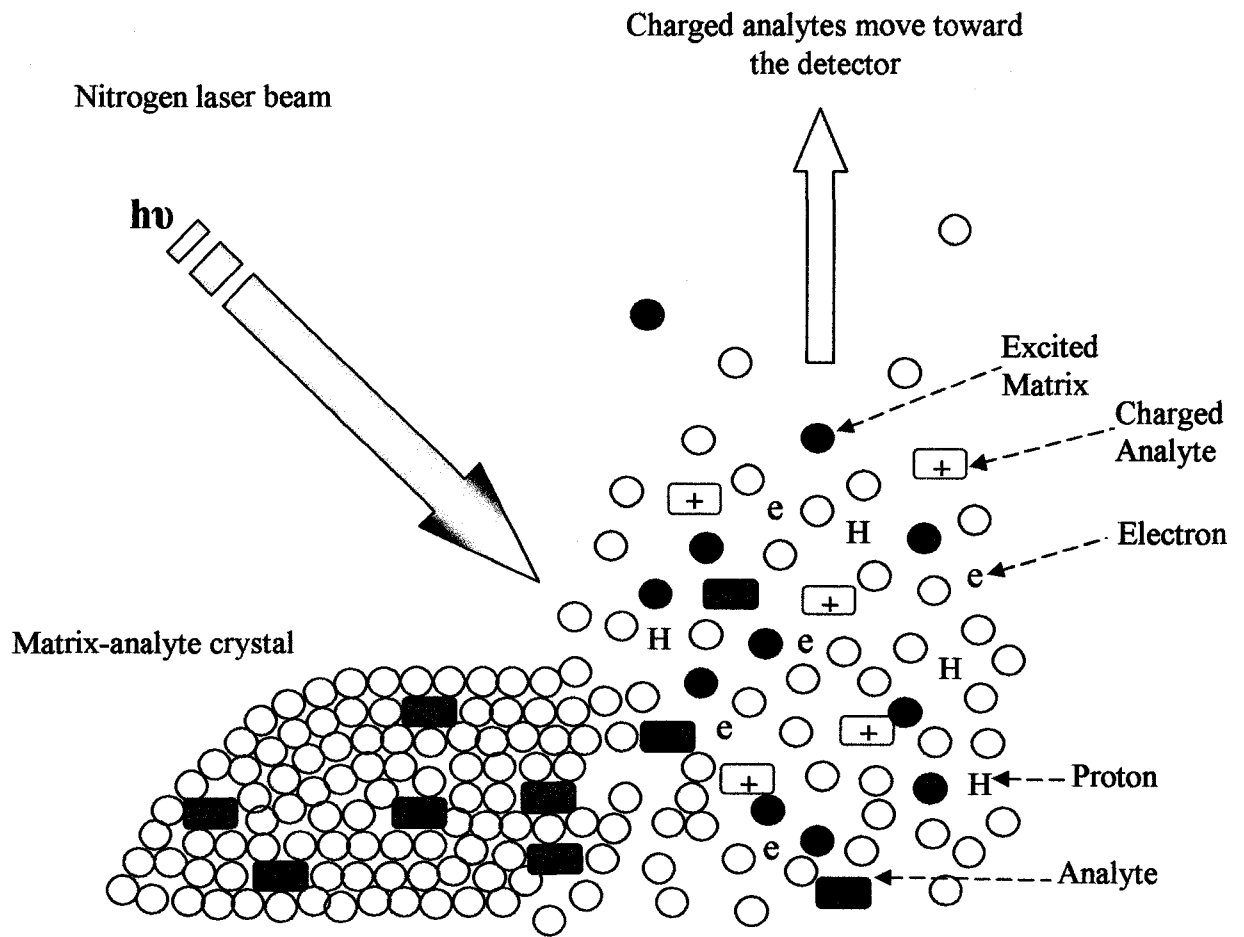
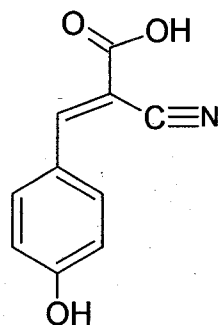
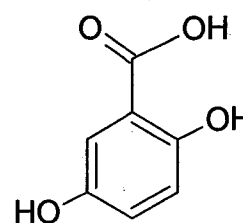


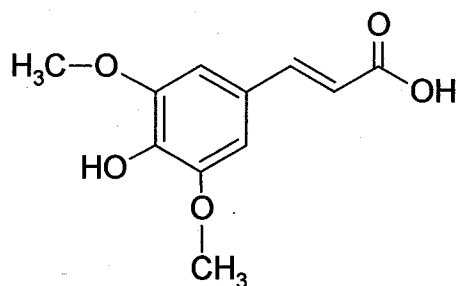
Figure 1-3: MALDI ionization Process. The matrix-analyte crystal is bombarded with a UV laser beam that excites the matrix which, in turn, transfers the energy to the analytes. This results in the ionization and desorption of the analytes, mainly as singly charged species.



α -cyano-4-hydroxycinnamic acid
CHCA



2,5-dihydroxybenzoic acid
DHB



Sinapinic acid
SA

Figure 1-4: The chemical structures of three commonly used matrices in MALDI-MS analysis.

1.1.2.3. Comparison between MALDI and ESI:

Both ESI and MALDI are very sensitive analytical techniques utilizing analyte concentrations which are as low as picomolar. One of the main differences, however, between MALDI and ESI is the state in which the sample is introduced to the ion source. ESI uses solvated sample which is infused into the instrument, while MALDI uses the solid state. Therefore, when interfaced with LC, it is possible to efficiently utilize ESI for quantitative measurements (Cohen *et al.*, 2006). Despite the fact that ESI is capable of reproducing data better than MALDI, it should be noted that relative abundance of various ions in an ESI spectrum is not a real representation of the sample concentration. Hence, a standard solution (when the objective is quantification) should be prepared with suitable calibration, preferably with the use of an isotopic analogue of the analyte (Cohen *et al.*, 2006). There were some attempts to expand the usage of MALDI from merely qualitative towards quantitative measurements (Biroccio *et al.*, 2005; Grant *et al.*, 2003) and it has been recently interfaced with LC (Fung *et al.*, 2004). However, the heterogeneity of a MALDI crystal sample poses a major difficulty for such an application. In fact, the quality of MALDI spectra can be significantly influenced by the position of the laser beam and the operator should identify a "sweet spot" within the sample crystal that can produce the most informative spectrum.

Attempts to interface MALDI to LC are, to some degree, related to the robustness of MALDI to the modest presence of salts and/or detergents (Breux *et al.*, 2000; Kallweit *et al.*, 1996). In contrast, when using ESI, contaminants adsorbed to the tubes through which a sample is infused into the ESI needle can compete with the analytes and may influence the results. Such a problem is not encountered in MALDI as analytes can

escape impurities during ionization in the same fashion they escape the bulk of the matrix. Finally, ESI tends to produce multiply charged species for biomolecules that are over 1000 Da. This is the reason why ESI can, theoretically, have unlimited mass range, as very large biomaterials can appear at lower m/z values. MALDI, however, tends to produce singly charged species and this phenomenon is of great importance for identifying the molecular ion of proteins, carbohydrates and lipids. Karas and co-workers hypothesized that in MALDI-MS, neutralization of multiple charged species occurs due to the production of neutralizing electrons during the photoionization process and hence, singly charged ions are “the lucky survivors” (Karas *et al.*, 2000b).

MALDI and ESI applications continue to grow within the scientific community and are the basis for newer ionization sources that can be used for specific purposes. Surface enhanced laser desorption ionization (SELDI), for example, was a development of MALDI (Hutchens & Yip, 1993) and it combines the power of MALDI with the selectivity of a protein chip technique. It is currently being optimized for cancer diagnosis (Semmes *et al.*, 2005) and biomarker discovery (El Aneed & Banoub, 2006). SELDI applications are not limited to human health; a recent investigation showed the usefulness of SELDI-MS profiling as a diagnostic tool in Atlantic salmon (Provan *et al.*, 2006). More recently, a desorption electrospray ionization (DESI) source was developed and mass spectra can now be recorded on a sample in its native environment (Cooks *et al.*, 2006; Takats *et al.*, 2004).

1.1.3. Mass analyzers:

A mass analyzer is the part of the instrument in which ions, before reaching the detector, are separated based on their m/z values. In a mass spectrometer, the isolation of ions is usually electrically-driven, although traditional analyzers, namely magnetic sectors, employ a magnetic field that influences ion separation. Similar to the ionization process in terms of the available methodologies, there are numerous systems that can isolate ions based on their m/z values. Currently, four main analyzers are widely used by mass spectroscopists, namely quadrupole (Q), quadrupole ion trap (QIT), time of flight (ToF) and Fourier transform ion cyclotrone resonance (FT-ICR). These analyzers vary in terms of size, price, resolution, mass range, and the ability to perform tandem mass spectrometry experiments (MS/MS). While QIT is capable of multiple mass spectrometric experiments (MS^n), FT-ICR is by far, the most powerful in terms of accurate mass measurements (Pasa-Tolic *et al.*, 2004). Both are, however, limited with regards to mass range.

The following sections will focus on quadrupole and time of flight analyzers and illustrate the development of hybrid instruments that link a quadrupole to a ToF analyzer with MS/MS capability (i.e. Q-ToF instrument).

1.1.3.1. Quadrupole analyzer:

The principle of a quadrupole mass analyzer was first described in the 1950s by Nobel Prize winning, physicist Paul Wolfgang and this ion filter was well-suited for GC-MS instrumentation (Grayson, 2002). This analyzer is composed of four parallel electrical rods (with a circular cross section), as shown in Figure 1-5. A direct current

(DC) potential (U) is applied to two of these rods, while the other two are linked to an alternating radio-frequency (rf) potential (the potential is termed V , while the frequency is termed ω). Ions, formed in the ionization chamber, are pulsed towards a quadrupole by an electrical field in the range of 5Kv. A positively charged ion, for example, will move in the direction of the negatively charged rod. However, once the polarity is changed, the ion will switch its movement path before striking the rod. In such a situation, ions will undergo complex oscillation (trajectory) and with the appropriate values of V , U and ω , only ions within a narrow range of m/z will survive the path towards the detector. The remaining ions will possess the “wrong” trajectory and will eventually collide with one of the rods. The ramping of V , U and ω values can result in the transmission of various ions (with different m/z) toward the detector (Downard, 2004; Henderson & McIndoe, 2005). This simplified illustration of a quadrupole is based on a complicated second-order differential equation, known as the Mathieu equation (March & Hughes, 1989).

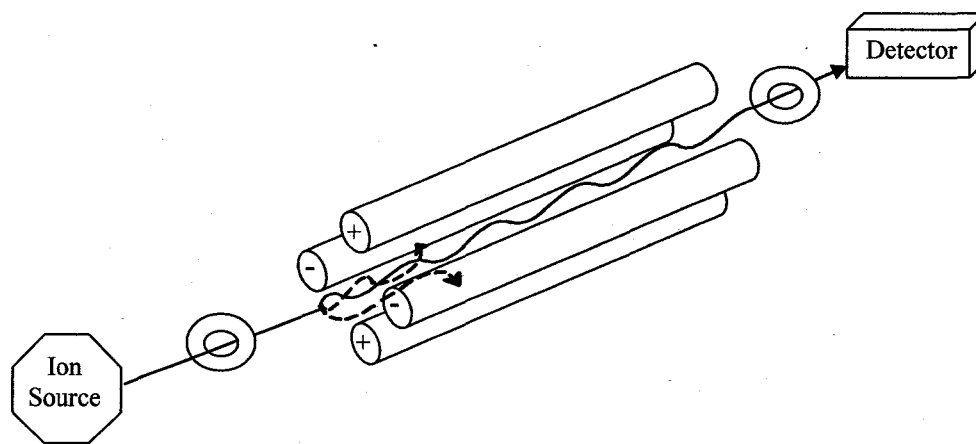


Figure 1-5: Representation of a quadrupole mass analyzer. Four parallel electrical rods with varying direct current and alternating radio-frequency potentials. Only one m/z value will possess the “right” trajectory and survive the path to reach the detector (solid line). The rest will collide with rods and will be ejected (dotted line).

The major advantages of quadrupole analyzers are the low cost, relatively small size, robustness and ease of maintenance. A quadrupole possesses, however, limited capability in terms of mass range (usually < 4000 Da), resolving power, and the ability to perform MS/MS analysis. The final disadvantage can be overcome by attaching a quadrupole to other analyzers such as additional quadrupoles (triple quadrupole instrument) or a quadrupole linked to a ToF (QqToF). An rf-only quadrupole (especially in a hybrid mass spectrometer) will function as an ion focusing device that guides ions to other components of the apparatus. Such functionality can be significantly improved with hexapoles and octapoles which cannot, however, perform as ion filters.

1.1.3.2. Time of flight (ToF) analyzer:

This ion separation methodology is one of the simplest and although it was first described in the middle of the 20th century (Stephens, 1946), it was not until the 1990s (Brown & Lennon, 1995), when it was rediscovered. Unlike other mass filters, this analyzer does not apply electrical or magnetic fields. ToF simply relies on the free flight of the ionized molecules in a tube of 1-2 m in length, before reaching the detector. As seen in Figure 1-6, if two ions (A_1 , and A_2) are formed at the same time with the same charge but the mass of $A_1 < A_2$, A_1 will reach the detector before A_2 . The main advantage of a ToF analyzer is that all formed ions will eventually reach the detector (unlike quadrupole or sector instruments). The equation that correlates m/z with total time of flight (t_f) is expressed in the following formula (Merchant & Weinberger, 2000):

$$m/z = t_f^2 \cdot 2 E s / (2s+x)$$

Where E is the voltage applied, s is the length of the ion acceleration region and x is the length of the free flight region. Theoretically E, s, And x are fixed, therefore, the above equation can be reduced to

$$m/z = K t_f^2$$

Where, K is the calibrating factor. This equation illustrates the direct relationship between the m/z value and the time of flight.

While ToF has the advantage of being able to detect a very high mass range, the tube linearity of a conventional ToF analyzer (Figure 1-6 A) can influence its resolving power, as ions entering the ToF carry different kinetic energies (KE) and this subsequently will affect resolution and molecular ion measurements. This drawback was overcome by the development of the reflectron (electrostatic ion mirror) (Mamyrin & Shmikk, 1979) which is an ion optic device that changes the path of the ions within the ToF, as shown in Figure 1-6B. Ions with higher KE will penetrate deeper into the ion mirror and hence ions will be gradually repelled, improving the resolution of the ToF spectrum. Another factor is the flight time; since ions (in reflectron-ToF) are traveling a longer path, better resolution as well as accurate mass measurements can be obtained due to the increase in the flight time (Clauser *et al.*, 1999). Most ToF analyzers currently have a resolution value $> 10,000$ (Edmondson & Russell, 1996), however, a resolution of 20,000 has been reported with commercial instruments having a second mirror (Ens & Standing, 2005). Resolution is defined based on the full width at half maximum (FWHM), or Δm , and can be obtained by dividing mass (m) / Δm .

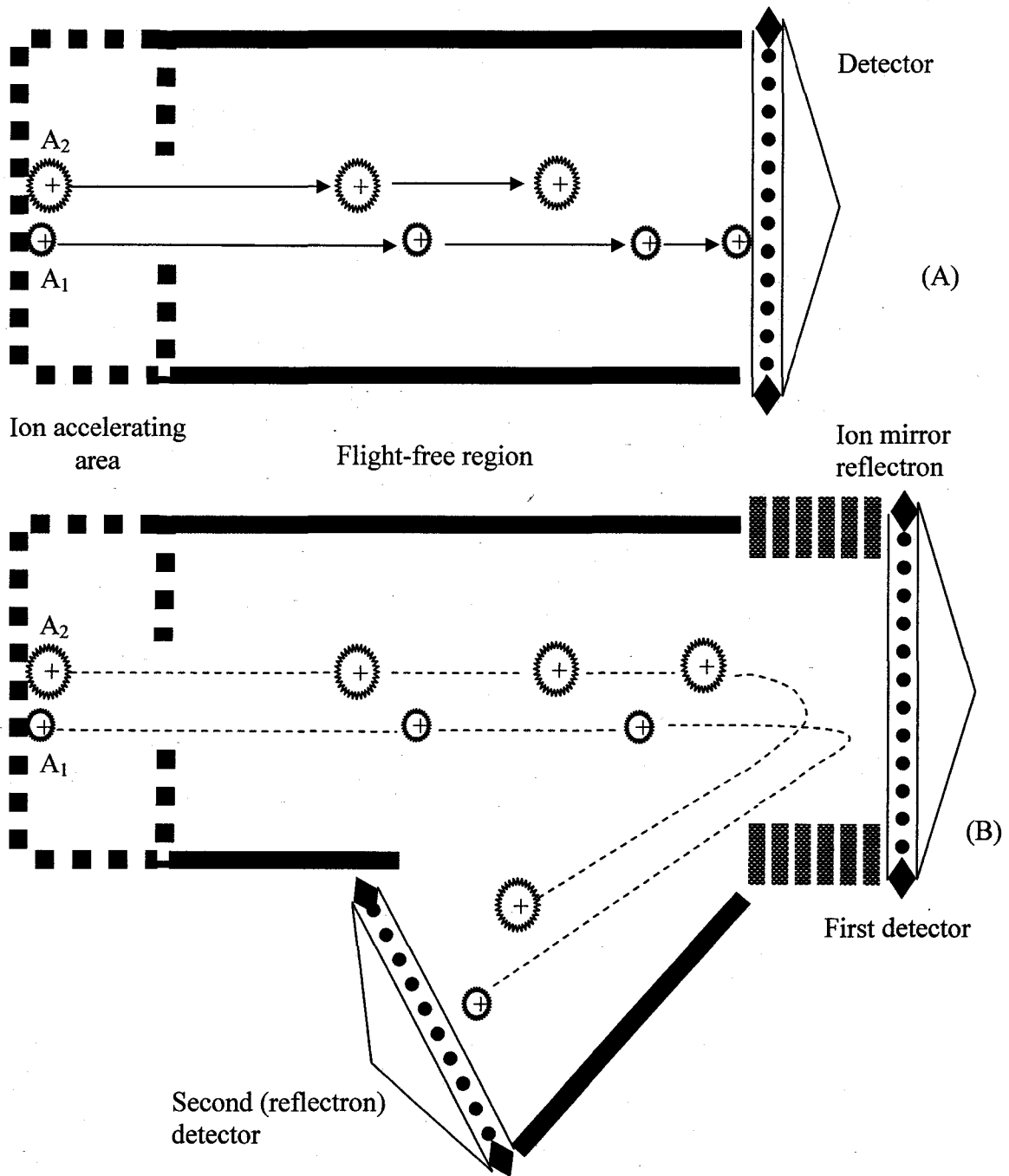


Figure 1-6: Schematic representation of a conventional ToF (time-of-flight) analyzer (A) and a reflectron-type ToF (B).

Most reflectron-type mass analyzers have two detectors: the first is beyond the ion mirror, and the second is at the end of the ion path. Due to the fact that a reflectron can result in ion loss, the operator can decide whether to compromise resolution, or sensitivity. Due to the nature of ToF, it is widely linked to the MALDI ion source (i.e. MALDI-ToF). Nevertheless, ToF can also be efficiently attached to an ESI source in hybrid instruments or orthogonal ToF, capable of performing tandem mass spectrometric experiments.

1.1.3.3. Tandem mass spectrometry (MS/MS):

Both single-stage ESI-MS and MALDI-MS are very valuable for molecular ion determination and can provide, under certain circumstances, useful structural information. These “circumstances” refer to the induction of fragmentation within the source, such as “post source decay” (Purcell & Gorman, 2001) and “in source fragmentation” (Joly *et al.*, 2005) in the case of MALDI and ESI, respectively. Tandem mass spectrometry relies on the isolation of a specific m/z (i.e. precursor ion) that can be then subjected to dissociation and subsequent production of fragment or product ions (previously known as daughter ions). The users’ task is to solve the “puzzle” created with an MS/MS spectrum, revealing valuable information with respect to the molecular structure of the analyte.

To achieve this goal, multiple mass analyzers can be connected in a series, so that ion isolation is performed by the first analyzer followed by ion fragmentation in the collision cell, while the final analyzer separates fragment ions based on their m/z values. Figure 1-7 illustrates the differences between one-stage mass spectrometry and MS/MS instrumentation. In fact, various combinations of mass analyzers can be assembled

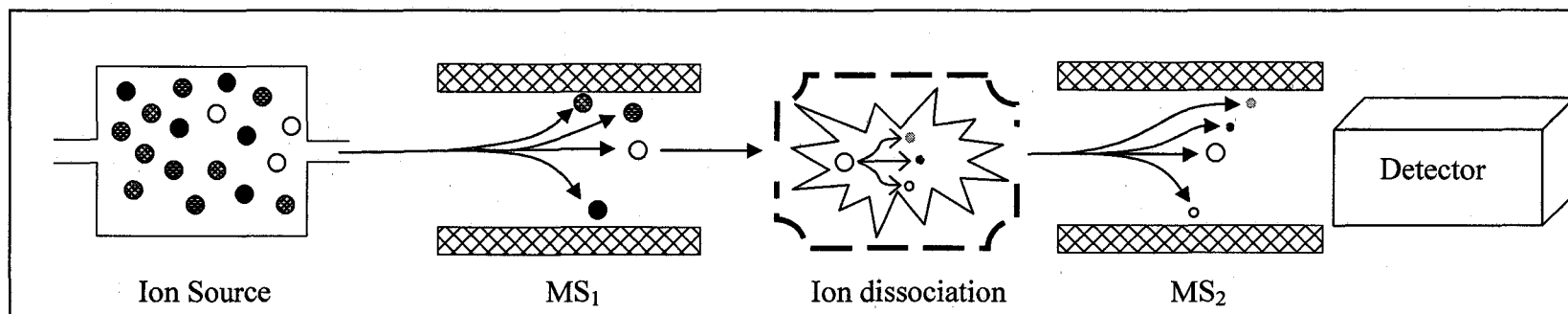
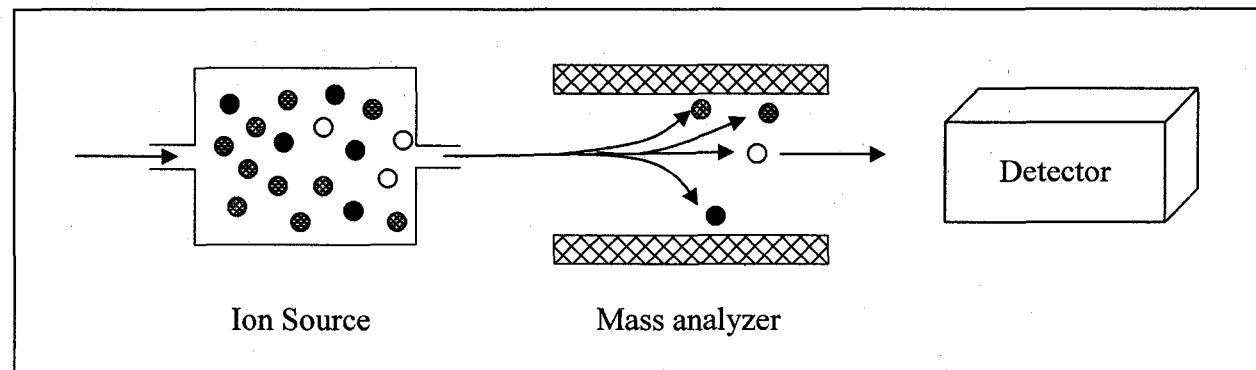


Figure 1-7: Comparison of one-stage mass spectrometry (top) and tandem mass spectrometry (bottom). In one-stage mass spectrometry, ions formed in the ion source are separated in the mass analyzer before reaching the detector. In tandem mass spectrometry, a specific ion is selected in the first mass analyzer (MS_1) and then subjected to collision in the collision cell, while the second analyzer (MS_2) separates the product ions before they reach the detector.

including sectors, quadrupoles, and ToF (Chernushevich *et al.*, 2001; Shukla & Futrell, 2000; Vestal & Campbell, 2005). Such MS/MS instruments are considered tandem-in-space since the analysis is performed by different mass analyzers “in different spaces”. Tandem-in-time, however, refers to trapping instruments where all ions are ejected except for one m/z that will be subsequently fragmented “in the same space”. These instruments include ITQ and FT-MS; both of which have one analyzer and can perform multiple MS experiments (MS^n), which are powerful tools for structural studies. It was shown, for example, that ion intensity is the only limitation to the extent of an MS^n analysis in an ITQ mass spectrometer (Louris *et al.*, 1990).

One of the commonly used tandem-in-space mass spectrometers is the triple quadrupole instrument, introduced in late 1970s (Yost & Enke, 1978). This instrumentation is currently abbreviated QqQ, where the lower q refers to the collision cell (an rf-only quadrupole). The selected ion for MS/MS analysis is filtered by the first quadrupole and undergoes collision with a stream of inert gas (e.g. helium, nitrogen, argon, xenon) within the collision cell. Such a collision will result in the transfer of some kinetic energy to internal one, causing ions to fragment. This process is referred to as *collisionally-activated dissociation* (CAD) or *collision-induced dissociation* (CID) (Jennings, 1968; McLafferty *et al.*, 1973). CID can in turn be divided into high and low-energy; the latter is associated with QqQ and Q-ToF (introduced below). High CID is observed with sector instruments that operate at high accelerating potential (in the order of Kilo electrvolts-keV) and it has been reported that charge driven fragmentation is dominant in case of high-energy CID (Gross, 1992). The accelerating potential is, however, less than 100 eV in the case of low-energy CID and it was shown that neutral

losses are the main mechanism by which fatty acids, for example, are fragmented (Kerwin *et al.*, 1996). CID is not the only process for precursor ion fragmentation, as alternative methods were developed including, for example, surface induced dissociation (Dongre *et al.*, 1996) and electron-capture-induced dissociation (Kelleher *et al.*, 1999).

In a QqQ mass spectrometer, three quadrupoles are connected; however, an MS/MS which carries different analyzers is termed a hybrid mass spectrometer. One of the most widely used ones, capable of low-energy CID analysis, is Q-ToF mass spectrometer.

1.1.3.4. Hybrid quadrupole orthogonal time-of-flight mass spectrometry (Q-ToF):

The Q-ToF instrument was first described in 1996 (Morris *et al.*, 1996) as a means of combining the scanning capabilities of a quadrupole and the resolving power of a ToF analyzer. It can provide high-quality, informative, simple, one-stage MS and tandem MS/MS spectra.

A diagrammatic representation of the Q-Star instrument, manufactured by *Applied Biosystems*, is shown in Figure 1-8. As seen in this figure, this mass spectrometer is composed of three quadrupoles linked to a ToF analyzer which is geometrically aligned in the orthogonal configuration with respect to the quadrupoles; and, hence, the name Q-ToF orthogonal mass spectrometry. The first and the third quadrupoles always operate in the rf-only mode. The first is utilized as an ion focusing device and to provide collisional cooling of the ions so that the quality of the ion beam is improved (Krutchinsky *et al.*, 1998). This quadrupole is usually referred to as q_0 , while the third quadrupole is the collision cell where low-energy CID fragmentation occurs. The second

quadrupole is the ion filter portion of the instrument, used during MS/MS analysis. It should be noted that all quadrupoles operate in the rf-only mode during simple single-stage MS analysis. The utilization of the second quadrupole as the analyzer, instead of the ToF, is only used for tuning the instrument since the ToF is more efficient for this purpose. Due to the crucial role of both the second and third quadrupoles during MS/MS analysis, these instruments are usually referred to as QqToF mass spectrometers, where the first Q refers to the mass-resolving quadrupole and the second q indicates the collision cell (rf-only quadrupole or hexapole).

One of the major advantages of QqToF instrumentation is its ability to be interfaced with either ESI or MALDI with little manipulation of the configuration. The association with MALDI is of great importance as conventional MALDI-ToF cannot perform MS/MS experiments. Due to the inherent limitation of a quadrupole in terms of mass range, there are, however, difficulties in orthogonal injection of large singly charged ions to the ToF.

Other advantages of QqToF instruments include ease of operation, high resolution, high mass accuracy and up to 100-fold increase in sensitivity when compared to triple quadrupole (Ens & Standing, 2005). Nevertheless, QqQ instruments are still favored for quantitative studies as well as for precursor ion scans in which the “parent” ion of a specific fragment can be identified. In such an analysis (with QqQ), the final quadrupole is fixed while the first one is scanning. Such functionality can not be as efficiently obtained with QqToF instruments as with QqQ mass spectrometers.

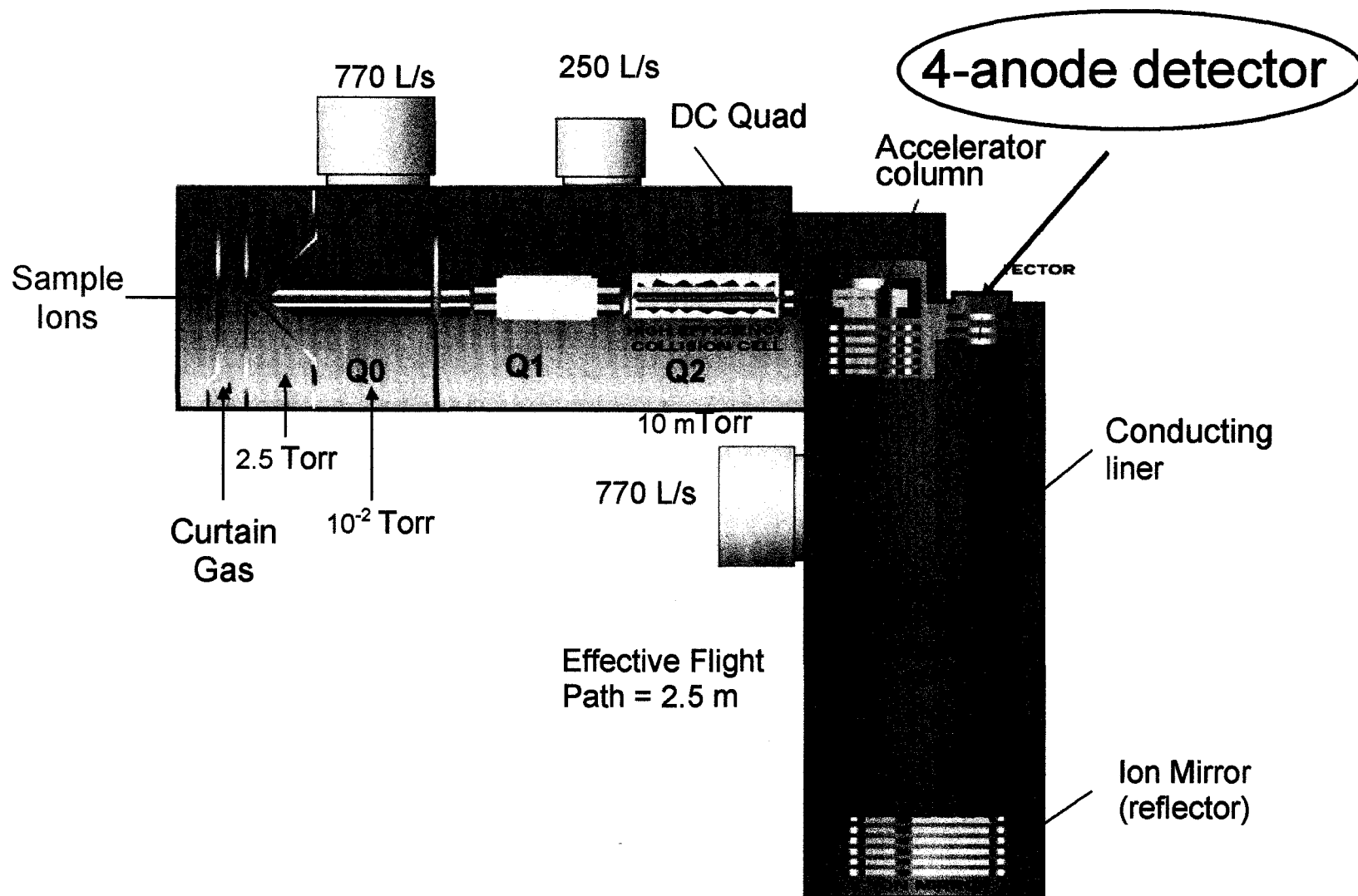


Figure 1-8: Schematic representation of Applied Biosystems Q-ToF instrument (QSTAR hybrid QqToF). This Scheme was generously provided by Applied Biosystems.

1.2. Bacterial membranes and lipopolysaccharides

1.2.1. Background:

In 1884, Hans C. J. Gram, a Danish bacteriologist, developed a simple staining methodology that was capable of distinguishing bacterial microorganisms into two major groups (Gram, 1884). This method was named after its inventor so that bacteria are either gram-positive (violet color) or gram-negative (red color). This discrepancy in the staining properties among various bacteria is directly associated with the structure and the composition of the surface membrane. The bacterial cell wall protects the interior from the outside environment and provides safe means for transporting substances from the inner part to the outside surroundings and vice versa.

1.2.2. Gram positive bacteria:

The cell wall of gram positive bacteria is mainly composed of the inner phospholipid bilayer, peptidoglycans, polysaccharides and proteins (Seltmann & Holst, 2002). The reason that these bacteria are colored violet (or dark blue) after gram staining is associated with the multilayered peptidoglycan ability to retain the crystal violet stain following decolourization with the solvent; this layer is significantly thicker within these bacteria than in gram negative ones (Dijkstra & Keck, 1996). Peptidoglycan, also known as murein, is a natural polymer that is composed of sugars and amino acids. It is a crucial part of the bacterial envelope and plays important role in the mechanical integrity of the membrane (Dijkstra & Keck, 1996). The interference in its formation by the

antimicrobial agent, penicillin, for example, can inhibit cell growth (Tipper & Strominger, 1965; Wise & Park, 1965).

Another component of the bacterial membrane are polysaccharides which can either be linked to peptidoglycans or be present within the membrane as separate entities. Those associated with peptidoglycans can be differentiated into two main groups, namely teichuronic acids (Ward, 1981) and teichoic acids (Archibald *et al.*, 1968). Other polysaccharides include lipoteichoic acids (Wicken & Knox, 1975) and lipoglycans (Seltmann & Holst, 2002). There is structural diversity among those carbohydrates which have multiple functions such as binding to proteins, attaching to metals, and providing phosphate moieties (Schaffer & Messner, 2005).

Mass spectrometry has been successfully employed for quantitative and qualitative research related to these biological glycoconjugates. ESI-MS/MS, for example, was coupled to high-performance anion-exchange liquid chromatography to study neutral and acidic sugars isolated from various bacteria (including bacilli), grown in phosphate-restricted environments (Wunschel *et al.*, 1997). The investigators successfully utilized this system for both structural confirmation and for selective quantification of these carbohydrates. Similarly, MALDI-ToF was recently used, in a study which evaluated the influence of acyl chains on lipoteichoic acid function, to confirm the deacylation process of pneumococcal lipoteichoic acid (Kim *et al.*, 2005). Despite its successful usage for studying polysugars isolated from gram positive bacteria, mass spectrometry has been much more appreciated, as shown below, for studying the molecular structure of lipopolysaccharides associated with gram negative bacterial membranes.

1.2.3. Gram negative bacteria:

The major structural differences between gram negative and gram positive bacterial membranes is the presence of inner and outer portions in the former as well as a coat of lipopolysaccharides (the outermost part of gram negative bacterial membrane). Both inner and outer membranes are composed of phospholipids (mainly glycerol-phospholipids) and proteins. The peptidoglycan layer is located within the gelatinous material, called periplasm, which separates the two layers. This peptidoglycan layer cannot retain gram staining; in fact, the gram procedure will dissolve the outer membrane and partially destroy the peptidoglycans (Beveridge & Davies, 1983) so that it cannot keep the original dye color. The outer leaflet of the outer membrane is mainly composed of the amphiphilic LPS moieties that contain a lipid portion (lipid A) embedded into the membrane environment. Figure 1-9 represents the configuration of gram positive and negative envelope structures.

1.2.4. Lipopolysaccharide (LPS):

LPS, also known as endotoxin, is a major component of gram negative bacterial membranes. Endotoxin as a concept was first described at the end of the 1800s by the German investigator, Richard Pfeiffer, “the father of endotoxin” (Rietschel & Cavaillon, 2003). LPS moieties can be isolated from the bacterial cell wall by the aqueous phenol method (Westphal *et al.*, 1952) and these isolates can then be subjected to biological and structural studies. Various portions of LPS have been used, in small amounts, for therapeutic purposes, such as, vaccines (Pupo *et al.*, 1999) and anticancer medications (Reisser *et al.*, 2002). LPS can be divided into three main parts: the lipid A, the core

region and the hydrophilic *O*-antigen. The general backbone of an LPS moiety is presented in Figure 1-10.

1.2. 4. 1. Lipid A:

Lipid A is the portion of the molecule by which LPS is anchored to the cell membrane. It is the most toxic part of LPS whose biological activity is strongly associated with this lipid. It gives the amphiphilic LPS moiety its hydrophobic characteristics and it is the least heterogeneous part of the LPS molecule. Lipid A is basically composed of a bi-phosphorylated β -(1 \rightarrow 6)-linked glucosamine backbone. Fatty acids are attached to this backbone at positions C-2, C-3, C-2', and C-3' via both ester and amide linkages. These fatty acids are commonly present in the hydroxylated form (usually at position C-3 or C-2 of the fatty acids) and hence the hydroxyl group can be esterified with additional fatty acid residues.

The number and the length of lipid A's fatty acids vary among different species. While ESI-MS-MS analysis of *Enterobacter agglomerans* lipid A, for example, revealed the presence of 6 fatty acids including three C₁₄ (3-OH), one C₁₄, one C₁₆, and two C₁₂ (Chan & Reinhold, 1994). The lipid A isolated from *Burkholderia cepacia*, a plant pathogen, bears 5 fatty acids, two C₁₆ (3-OH), two C₁₄ (3-OH) and one C₁₄ (Silipo *et al.*, 2005). MALDI-MS analysis has, however, shown that the latter extract was a mixture of penta- and tetra-acylated lipid As; the tetra-acylated one lacks the C₁₄ fatty acid residue (Silipo *et al.*, 2005). Despite the fact that lipid A fatty acids usually contain 10-16 carbon atoms, it has been shown that other unusual chains such as C₁₈ and C₂₀ exist within some isolates; for example, they are associated with the lipid A isolated from *Chlamydia*

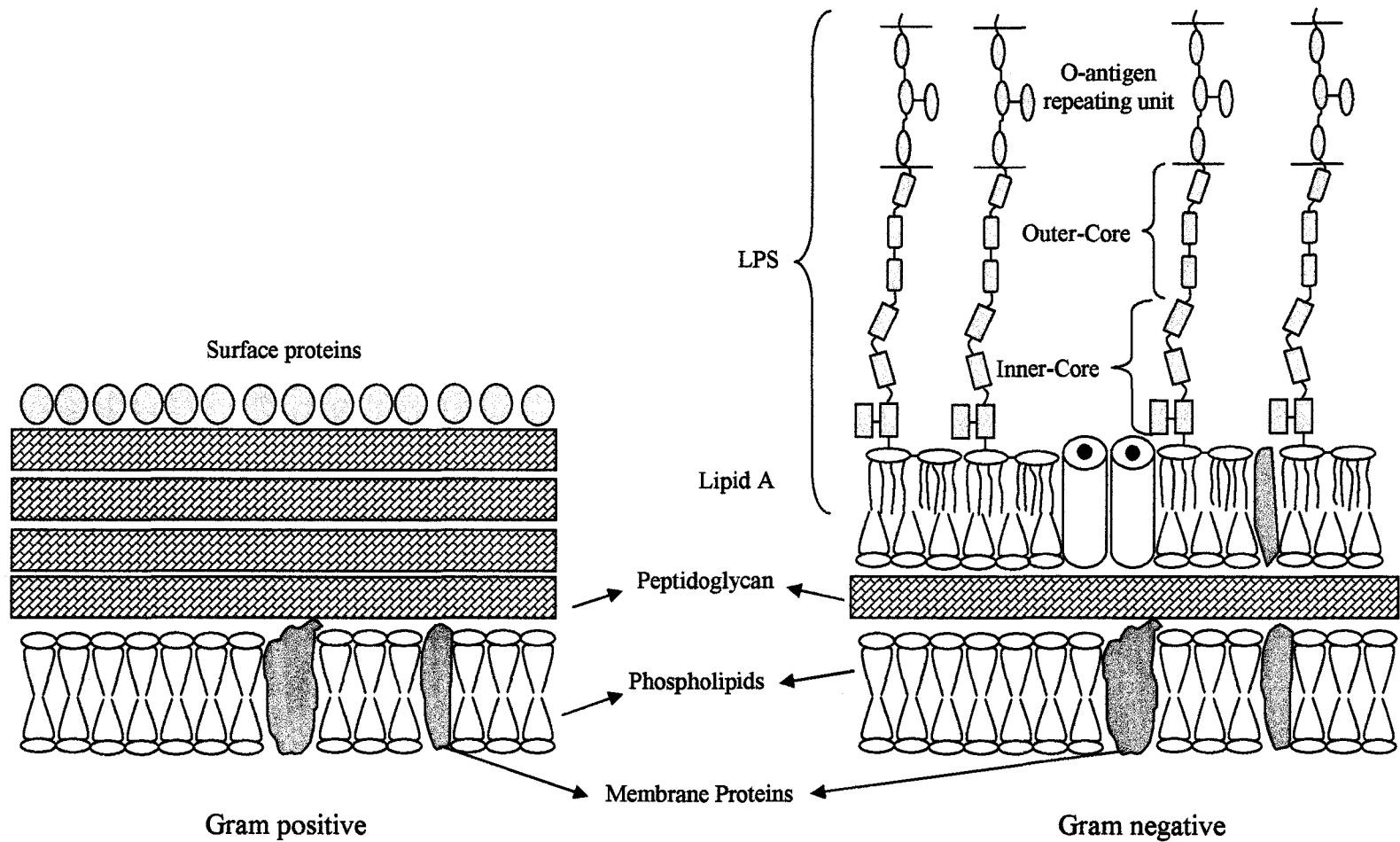


Figure 1-9: Simplified schematic representation of gram positive and gram negative bacterial membranes. The scheme presents the major differences between the two groups. LPS only exists on the gram negative bacteria which also contain inner and outer membranes. The peptidoglycan layer is significantly thicker in gram positive bacteria so that it can retain the initial gram dye.

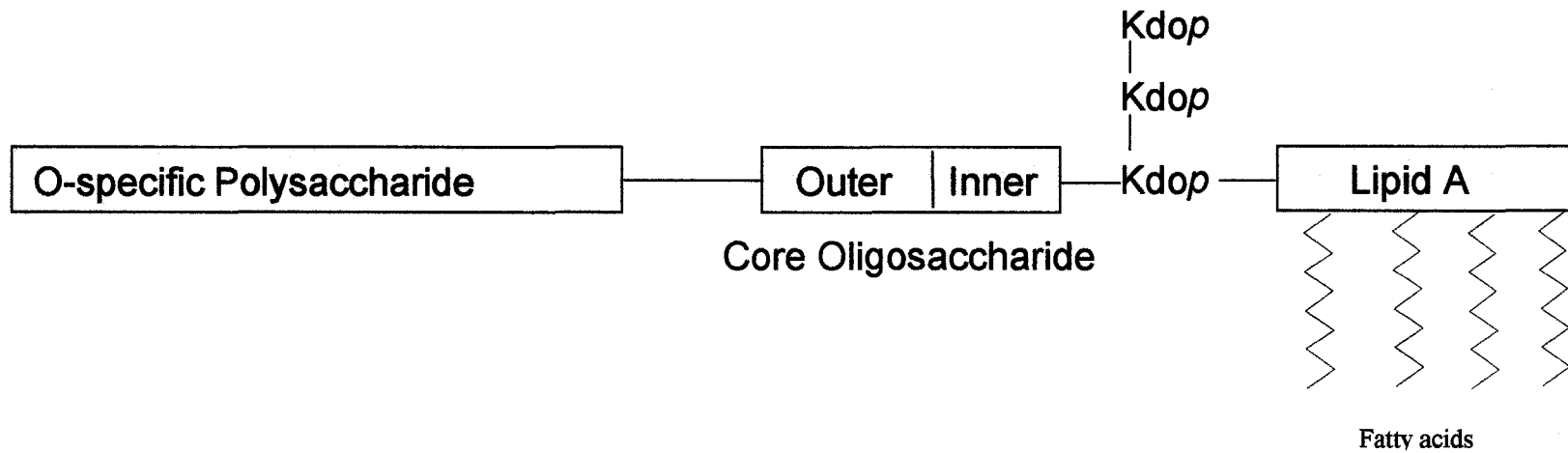


Figure 1-10: Representation of LPS general structure with three distinctive components: the lipid A, the core oligosaccharide, and the *O*-specific antigen.

trachomatis, a common infectious agent (Heine *et al.*, 2003). The length of these fatty acids has a major influence on the toxicity of lipid A, with the most toxic ones, bearing C₁₂, C₁₂(OH), C₁₄, and C₁₄(OH) (Caroff & Karibian, 2003). Unsaturated fatty acids are rarely observed and, if present, they usually exist as a mixture with the saturated counterparts (Schwudke *et al.*, 2003; Zdrovenko *et al.*, 2001). LPS natural extracts, including lipid A, are complex mixtures of structurally-related glycoforms. This is mainly due to the presence of various biosynthetic pathways and degradation during the isolation process. Mass spectrometry is capable of analyzing these mixtures, illustrating the exact molecular structure of each constituent (Mikhail *et al.*, 2005) which can vary depending on growth conditions such as the temperature (Corsaro *et al.*, 2004a). In addition, these complex biological glyco-mixtures are excellent candidates for qualitative and quantitative analysis by capillary electrophoresis interfaced with mass spectrometry (CE-MS) (Li *et al.*, 2005).

In addition to the substitution with fatty acids, phosphate, and sometimes pyrophosphate groups, usually exist at positions C-1 of the reducing glucosamine residue and C-4' of the non-reducing end (Rund *et al.*, 2000; Ummarino *et al.*, 2003). These phosphate groups can be in turn substituted with phosphoryl-ethanolamine (Kelly *et al.*, 1996), ethanolamine, or occasionally neutralized with other substituent, such as arabinosamine (Silipo *et al.*, 2005). Structural studies of lipid A, in which mass spectrometry is an instrumental tool, are highly important with respect to its biological activity. For example, lipid A is generally considered a pro-inflammatory agent; some synthetic analogues have, however, been evaluated successfully as antagonistic factors against *Escherichia Coli* lipid A (Demchenko *et al.*, 2003; Peri *et al.*, 2006). This

discrepancy in the effects among such related structures is related to the exact structure of these active biological substances.

1. 2. 4. 2. The core region:

The second portion of LPS, namely the core region, is less conserved among species in comparison to lipid A. This part can be further divided into two subdivisions, the inner and outer cores (see Figure 1-10). The use of mutant bacterial strains bearing only the inner core can efficiently facilitate mass spectrometric analysis and structural determination (Olsthoorn *et al.*, 1999; Radziejewska-Lebrecht *et al.*, 1994). These mutant bacteria are usually referred to as “rough mutant” because of the glossy colony morphology in comparison to the wild-type that are, in turn, termed “smooth” due to their unwrinkled visible colony texture. Notably, these rough-type bacteria can only grow *in vitro* and are more sensitive to antibiotics (Vaara, 1993).

The inner-core region is usually composed of 8-12 branched sugars including a unique 8-carbon residue at the reducing end of the chain, namely α -3-deoxy-D-manno-oct-2-ulosonic acid (“Kdo”), which has proven to be critical for the LPS biological activity (Haeffner-Cavaillon *et al.*, 1989). Kdo is the “linkage” between lipid A (usually through position C-6 of the non-reducing end) and the poly-sugar and this linkage is susceptible to mild-acid hydrolysis. Kdo can be substituted with additional one or two Kdo moieties. All of the sugar units within the inner core of *Chlamydophila psittaci*, which can infect both humans and animals, contained only Kdo units (Rund *et al.*, 2000). This inner core was composed of either three Kdo’s (α -Kdo-(2→8)- α -Kdo-(2→4)- α -Kdo-(2→6)-Lipid A) or four Kdo’s with a branched moiety (α -Kdo-(2→4)-[α -Kdo-(2→8)]- α -

Kdo-(2→4)- α -Kdo-(2→6)-Lipid A) (Rund *et al.*, 2000). Traditionally, the presence of Kdo moieties was determined by the thiobarbiturate-based colorimetric assay, used as a characteristic test for taxonomic classification (Jann *et al.*, 1973). This test, however, fails to detect LPS with a single Kdo as in the *Vibrio* family (Caroff *et al.*, 1987). Mass spectrometric analysis, however, has overcome this deficiency, illustrating its presence within many species which were previously believed to lack Kdo (Banoub *et al.*, 1983; Brade, 1985). While Kdo can be considered a characteristic sugar in LPS, a few bacterial species (e.g. *Yersinia pestis*) contain Kdo analogues, such as D-glycero-D-talo-oct-2-ulosonic acid (“KO”) (Vinogradov *et al.*, 2002). Similar to other sugars within LPS moiety, Kdo can be substituted with reactive groups such as phosphate or phosphoethanolamine (Li *et al.*, 2004). Another unique sugar within the LPS inner core region is L-glycero-D-manno-heptose (Hep) which is a 7-carbon sugar; some bacteria, however, lack Hep residues (Moll *et al.*, 1997).

The outer core varies greatly and consists of hexoses, primarily glucose (Glc), galactose (Gal), N-acetyl-galactosamine and N-acetyl-glucosamine (GlcNAc). All of the core sugars are in the pyranose form and, in general, have the α -anomeric configuration. It should be noted that heptoses can also be present in the outer core and hexoses were identified in the inner core region, as in the case of *Yersinia enterocolitica*, in which is composed of a heptasaccharide, including 2 units of D-Glc (Radziejewska-Lebrecht *et al.*, 1994). In all of the above investigations, mass spectrometry was an essential tool for studying the structure of these complex biological mixtures. Moreover, MS-MS has proven to be capable of evaluating these glycoconjugates without the need for tedious, time-consuming, separating techniques (Kondakova *et al.*, 2005).

1. 2. 4. 3. The O-antigen (the O-chain):

Despite its heterogeneity in comparison to lipid A, the core is in turn less heterogeneous than the O-antigen portion. The O-chain is composed of repeating oligosaccharide units of varying six-carbon sugars and its composition is different among various genera and bacterial serotypes. This variation can be related to the composition of the sugar units within the building block, the position of the *O*-glycosidic linkages, and the nature of the non-carbohydrate constituents. This O-chain is exposed directly to the host during infection and it has a protective role from the surrounding environment. It has been demonstrated, for example, that wild-type bacteria can resist antibiotics, however, their rough mutant counterparts (lacking the O-chain poly-sugar) are sensitive to antibiotic effects (Banemann *et al.*, 1998). O-antigen is also responsible for adhesion to the tissues during infection (Paradis *et al.*, 1994). This O-chain can be branched, substituted with non-carbohydrate substituents such as phosphate and amino acids (Caroff & Karibian, 2003). In some pathogens, the O-antigen is absent; however, the inner core is well-recognized and mono and oligosaccharide branches are extended from the core; such glyco-chains of the bacterial membrane are referred to as lipooligosaccharides (LOS) rather than lipopolysaccharides (LPS) (Raetz & Whitfield, 2002).

1.2.5. LPS-derived vaccines:

1.2.5.1. LPS-protein conjugates:

LPS derivatives have been mostly appreciated for their potential use as vaccine candidates. Bacterial LPS is the major contributor to the host immune reaction and hence, it has been successfully utilized for vaccination. The significance of LPS can be

illustrated with the use of LPS antibodies which can protect against infection (Bowden *et al.*, 1995; Fulop *et al.*, 2001). LPS when injected alone is not immunogenic as it can escape recognition by the immune system due to its relatively small size. LPS conjugated to a protein carrier, however, can provoke the desired immunological reaction and can induce prolonged immunity. The first attempts to test protein conjugates as immunogens dates back to the late 1920s by Landsteiner's group (Ada & Isaacs, 2003). Shortly after, Avery and Goebel illustrated that bacterial carbohydrate-protein conjugates can induce strong antibody response (Avery & Goebel, 1929). The sugar portion of a carbohydrate-protein conjugate is usually referred to as a hapten which originates from the Greek verb "haptein", meaning to fasten (Soanes & Stevenson, 2005).

The linkage between the LPS backbone and the protein carrier can be either a direct linkage or with the aid of a suitable spacer. Many protein carriers have been evaluated for the production of LPS-derived vaccines such as bacterial toxoids [e.g. tetanus toxoid (Gu *et al.*, 2003)], outer bacterial membrane proteins (Wu *et al.*, 2005) and bovine serum albumen (BSA) (Chernyak *et al.*, 2002). Regardless of the nature of the protein carrier, it should be stable, safe and capable of enhancing LPS immunogenicity. The first commercially available glycoconjugate vaccine was licensed in the late 1980s against *Haemophilus influenzae* type b (Hib) and this work was originally pioneered by Schneerson and co-workers (Schneerson *et al.*, 1980). The infection has been virtually eliminated in countries where widespread vaccination among the general public has been executed (Robbins *et al.*, 1996).

While many studies have focused on using natural LPS for the development of LPS vaccine conjugates, synthetic carbohydrate chains that mimic LPS epitopes (the part

of an antigen recognized by the immune system) seems to be evolving as a promising approach for the production of LPS-protein conjugates. Pavol Kováč's group, for example, has been spearheading the production of BSA-hapten conjugates that bear synthetic mono-, tetra- and hexa-sugars which mimic the terminal part of the O-specific polysaccharide of the *Vibrio cholerae*, serotype Ogawa (Ma *et al.*, 2003; Zhang *et al.*, 1998). Their novel conjugate (bearing the hexa-sugar) has shown protective immunity within mice (Chernyak *et al.*, 2002). BSA-LPS derived from the *Vibrio cholerae*, serotype Inaba (despite structural similarities to Ogawa) failed, however, to achieve this protective immunity (Meeks *et al.*, 2004). This has been attributed to the possibility that either the terminal sugars of Inaba are not protective epitopes or the delivery system was not optimized. The only difference between those two species lies within the terminal sugar which is characterized by a hydroxyl group at the 2 position in Inaba but a 2-*O*-methyl group in Ogawa. The investigators have successfully utilized SELDI-MS to evaluate the degree of BSA-sugar conjugation and have presented very promising results with respect to controlling the reaction and the degree of substitution (Ma *et al.*, 2003; Saksena *et al.*, 2003). These results, based on MS analysis, can have significant industrial impact during commercial production as it relates to quality control and quality assurance.

1.2.5. 2. Liposome-derived vaccines:

In addition to LPS-protein conjugates, liposomes have been used to present LPS as antigens within living organisms. Liposomes were first introduced in 1965 (Bangham *et al.*, 1965a; Bangham *et al.*, 1965b) as artificial cell membranes and were in 1974

evaluated as potential drug carriers (Gregoriadis *et al.*, 1974). Liposomes are self-assembled in an aqueous medium that contains a suitable lipid mixture. They are currently one of the most widely used drug delivery systems capable of encapsulating the newest biologically-derived drugs, namely proteins, DNA and carbohydrates.

Since liposomes have both hydrophobic and hydrophilic compartments, they can efficiently encapsulate amphiphilic LPS derivatives. Natural or modified lipid A-liposome complexes are well-established as potent non-toxic adjuvants (Alving *et al.*, 1992). Monophosphoryl lipid A, for example, has been used successfully for immunotherapy in a clinical setting as a vaccine adjuvant to treat colorectal cancer patients (Neidhart *et al.*, 2004). Similarly, a cocktail of complete-core LPSs of four gram negative bacteria were encapsulated within multilamellar liposomes, producing an immunogenic and nontoxic formulation (Bennett-Guerrero *et al.*, 2000; Erridge *et al.*, 2002). It should be mentioned that different LPS portions can have different effects in terms of toxicity and immunogenicity. LPS mutant-liposome complexes of *Neisseria meningitidis* were, for example, more potent and less toxic vaccines than the wild-type LPS or lipid A liposomal formulations (Arigita *et al.*, 2005).

Regardless of the composition of a liposomal drug delivery system, these lipid spheres have an inherent deficiency in terms of stability and short half life within the circulation. These drawbacks have been the target for considerable research activity. Testing various lipid mixtures, reducing the size, and manipulating the zeta potential value are few examples of variables which have been evaluated to encounter the stability/short-half life problem (Wu & Zern, 1996). The usage of pegylated liposomes (i.e. liposomes bearing polyethylene glycol (PEG)) have been very useful in increasing

stability and to enhance liposomal efficiency as drug carriers (Simoes *et al.*, 2004). In addition, these PEG chains can serve as arms to attach ligands for specific organ targeting (El Aneed, 2003). PEG influences liposomal formulation mainly through steric hindrance (sterically-stabilized liposomes). PEG-liposomes have been tested for different purposes including the encapsulation of LPS derived carbohydrate moieties, such as lipid A (Park & Huang, 1993).

1.2.5.3. Neoglycolipids-stabilized liposomes:

Synthetic carbohydrate residues linked to a lipid component via a suitable spacer can readily be incorporated into the surface bilayer of liposomal formulations. Such structures are termed neoglycolipids and have proven to efficiently enhance liposomal stability and to increase their circulatory half-life. In addition, the sugar portion of these novel glycoconjugates can effectively target liposomes to specific cells or organs (Duffels *et al.*, 2000). It is believed that the glycosylated species will create a repulsive steric barrier that prevents molecular aggregation and adhesion. It has shown for example that the addition of 5 % oligomaltose distearoylphatidylethanolamine conjugate to a liposomal formulation can eliminate lipid aggregation in comparison to conventional liposomes (Xu *et al.*, 2002). Over a 10-h period, the turbidity was increased eightfold in conventional liposomes in contrast to the merely 5 % in the neoglycolipid-stabilized liposomes. It was also shown that liposomal efficiency as drug carriers was significantly enhanced with the use of neoglycolipid-coated liposomes (Perouzel *et al.*, 2003).

These novel liposomal structures can encapsulate various compounds including antigens. Neoglycolipid-stabilized liposomes were loaded, for example, with HIV

glycoprotein antigen enhancing the targeting ability of these formulas towards antigen producing cells (Fukasawa *et al.*, 1998). To validate the molecular structure of these synthetic compounds, mass spectrometry has been efficiently used (Pohlentz & Drees, 2000; Pohlentz *et al.*, 1994).

1.3. Mass spectrometric analysis of carbohydrates

Carbohydrate chains are polymers of sugar units that are linked by glycoside bonds which resemble, in principle, peptide bonds in proteins. Mass spectrometry of proteins and peptides is a well-established science where significant information with regard to the sequence, structure and post-translational modifications are routinely obtained. During MS and MS/MS analysis, breakages at the peptide bonds are the most informative ones. Similarly, breakage at the glycoside bonds can be very useful in terms of structural determination of carbohydrates. Inner-sugar fragments can also serve as diagnostic fragment ions used to precisely illustrate the structure of the studied carbohydrate chains. Figure 1-11 is a theoretical representation of possible fragmentations of a simple di-sugar, namely lactose (β -D-Galp-(1 \rightarrow 4)-D-Glcp) where the reducing end is Glc (glucose) and the non-reducing unit is Gal (galactose). In this figure and in the following chapters, the systematic nomenclature for carbohydrate fragmentation by FAB MS/MS proposed by Domon and Costello (Domon & Costello, 1988a; Domon & Costello, 1988b) is used. As can be seen from Figure 1-11, fragments that result from the elimination of the reducing end and the formation of ions containing the non-reducing end are referred to as A, B, and C with A being related to inner sugar

fragments. The fragment ions, however, that bear the reducing end are termed Z, Y and X with the latter being associated with inner-sugar fragments. Due to the many possible inner sugar breakages, specific numbers that represent the bond being broken are used to distinguish a specific fragment (see Figure 1-11 for details). In addition, this letter-coded representation is also numbered based on the sugar where fragmentation occurs, with the non-reducing end being 1 in case of A, B, and C ions, while the reducing end is numbered 1 in the case of Z, Y. The X-type ions are numbered 0 if occurred within the reducing end group. Note that in a simple di-sugar B, C, Z, and Y fragments will not be assigned any number due to the absence of additional sugars (i.e. all can be numbered 1). However, both A and X ions are coded in this figure is based on the position of the breakage as well as on the sugar unit being fragmented.

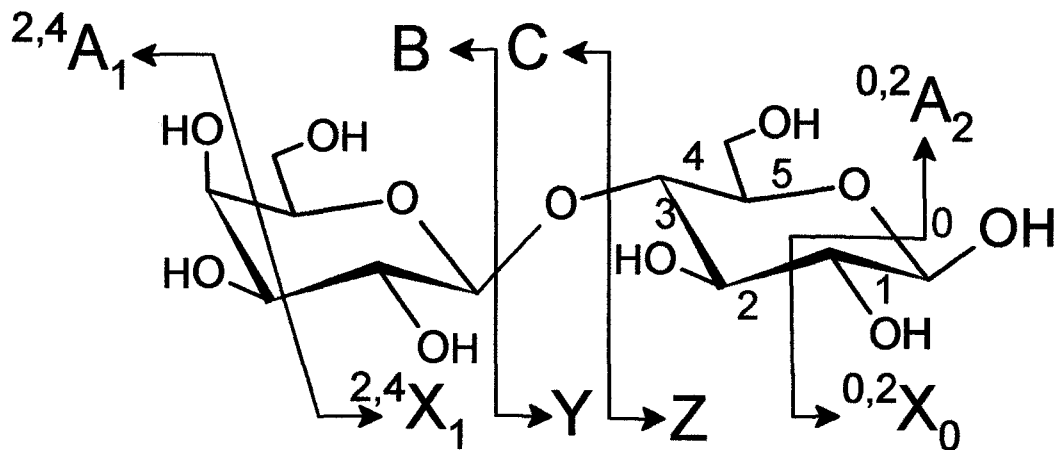


Figure 1-11: Theoretical possible fragmentation of a lactose sugar. Breakages at the glycoside linkage are termed B and C when retaining the non-reducing end sugar, while Z and Y refer to fragments that contain the reducing end. Inner sugar fragments are termed X and A ions, where the A ion retains the non-reducing end and X contains the reducing end. These inner sugar fragments are labelled based on the broken bond (numbered 0-5, as shown on the reducing end).

1.4. Research objective

The objective of this work is to generate mass spectrometric fingerprints and establish fragmentation patterns of natural and synthetic glycoconjugates. These fingerprints can be used to evaluate and predict the mass spectrometric patterns of similar structures and can be efficiently used for quantitative purposes. The state-of-the-art ESI-MS, MALDI-MS and MS/MS are used to achieve this goal and to elucidate the molecular structures of these compounds.

1.4.1. Natural lipopolysaccharide:

This study will evaluate the mass spectrometric fingerprints of both known and unknown structures of rough and smooth LPS isolated from the fish pathogen *Aeromonas salmonicida*. This gram negative bacterium is the etiological agent of a fatal disease, termed furunculosis, in salmonid fish which can result in significant loss in fish stocks. It is one of the oldest described fish pathogens and was first reported in 1894 (Austin & Austin, 1999). There are three main subspecies of *A. salmonicida* (Belland & Trust, 1988) and the one investigated in this document is *A. salmonicida* subspecies *salmonicida*. Similar to any LPS, *A. salmonicida* LPS can serve as a potential vaccine that can have a positive impact on aquaculture. An additional benefit of the use of LPS vaccines in farmed fish is related to the possible reduction in the use of antibiotics in a food product; furthermore, bacteria can develop resistance to these antibiotics over time, reducing their therapeutic efficiency. Over a 10-year time period in Norway, for example, the use of fish vaccines was increased almost 10 times while the use of

antibiotics was reduced from 48,500 Kg to merely 1,010 Kg (Hastein *et al.*, 2005). Both LPS-BSA conjugates and LPS-liposome complexes of *A. salmonicida* were successfully formulated (Banoub *et al.*, 1989; Nakhla, 1995).

The core and the lipid A antigens from *A. salmonicida* are both investigated in this work. While the exact molecular structure of lipid A is established for the first time, the structure of the core region was recognized over 20 years ago by Banoub and co-workers (Banoub *et al.*, 1983; Shaw *et al.*, 1992). However, there is no information with respect to the ESI-MS-MS and MALDI-MS-MS fragmentation pattern of this core. MS analysis in this study established for the first time the mass spectrometric fingerprints of these biological extracts and suggested the molecular structure of the lipid A. The proposed structure of the LPS core region was also confirmed by ToF-MS and MS-MS experiments. In addition, the analysis revealed the presence of a phosphate group at the reducing end (i.e. the Kdo residue) which had not previously been recognized.

1.4.2. Novel synthetic cholesteryl neoglycolipids:

Boullanger's research group at the Université Claude Bernard, France, has been pioneering the chemical synthesis of novel liposomal cholesteryl neoglycolipids that link sugar residues to a cholesterol moiety via a poly-ethoxy variable spacer (Boullanger *et al.*, 1995b; Kemoun *et al.*, 1999; Lafont *et al.*, 1996; Laurent *et al.*, 2006). These glycojugates can be arranged on the liposomal surfaces increasing stability and enhancing their targeting capabilities (Faivre *et al.*, 2003; Gelhausen *et al.*, 1998).

This investigation authenticated the proposed structure of a series of novel cholesteryl neoglycolipids by mass spectrometry and established the ESI-MS-MS

fingerprints. The most striking finding was, however, the presence of a unique ion-molecule reaction that yields the production of an unexpected C-glycoside species. This novel mass spectrometric phenomenon along with the establishment of a universal fragmentation pattern was evaluated in 18 new compounds that bear various sugars and spacers linked to the lipophilic cholesterol portion.

CHAPTER 2: Materials and Methods

2.1. Lipopolysaccharides:

2.1.1. Bacterial culture:

Both the rough mutant and the smooth wild-type strains of *A. salmonicida* ssp *salmonicida* were obtained from Dr. T.P.T. Evelyn (Department of Fisheries and Oceans, Nanaimo, British Columbia, Canada). It was isolated originally from Sockeye salmon and is numbered as Strain SJ-15, wild type, and SJ-83, rough mutant, of the collection of the Northwest Atlantic Fisheries Centre, St. John's, NL. The cultures were grown to medium-to-late stationary phase in Trypticase Soy Broth without added glucose (Baltimore Biological Laboratories Inc.) for almost 20 h at 25°C and aeration at 20-1/min in a New Brunswick MF-128S fermentor. They were then killed by the addition of 0.3 % formalin with continuous agitation for 16 hrs at room temperature. Cells were subsequently collected by centrifugation at 20,000 rpm in a Sorvall SS-34 rotor (48,200 × g), washed with NaCl (0.15 M) and finally lyophilized and stored at -50° C until required.

2.1.2. Purification of the lipopolysaccharides:

LPS was extracted by the hot-phenol method (Westphal *et al.*, 1952) and freeze-dried. Basically, stored cells (10 g) were suspended in deionized water (175 ml) and heated to 70° C. An equal volume of heated phenol (90 %) was added and the mixture was stirred for 20 min at 70° C. The mixture was then cooled on ice and centrifuged using Sorvall SS-34 rotor (3500 rpm, 1475 × g). The aqueous layer was isolated by

aspiration and the procedure was repeated twice. The aqueous layers were combined and dialysed against water to remove any traces of phenol. Furthermore, the volume of the combined water mixture was reduced by evaporation (under vacuum) and finally centrifuged at 39,000 rpm ($105,000 \times g$) for 3 hours. The LPS pellet was resuspended in water and centrifugation was repeated twice; LPS was finally lyophilized.

LPS isolates were further purified using polymyxin-coated Affi-prep beads (Bio-Rad Laboratories, Richmond, CA, USA). Fifteen milligrams of LPS was suspended in 15 ml of phosphate-buffered saline (PBS, PH=7.4). LPS solution was then mixed with washed polymyxin beads (the beads were originally washed first with 0.1 M NaOH and then distilled H₂O). The mixture was incubated overnight with agitation using an orbital shaker (1500 rpm). The mixture was then centrifuged ($2500 \times g$) for 10 min and the supernatant was collected. The beads were then washed twice with 15 ml and 5 ml 0.1 M NaOH. The supernatants were combined and LPS was dialysed against water and finally lyophilized.

2.1.3. Hydrolysis of the lipopolysaccharides:

LPS (100 mg) was hydrolyzed with 1% acetic acid for 90 min at 100°C. Centrifugation at $3000 \times g$ for 30 min resulted in the precipitation of lipid A, while the polysaccharide was present in aqueous media. Lipid A was removed and washed with water, and the core oligosaccharide was recovered from the supernatant by chromatography on Sephadex G-50 (Pharmacia Ltd.). Fractions were visualized using a differential refractive index monitor (Waters Associates).

2.1.4. Methylation of the core oligosaccharide:

Methylation was performed on the core region and was carried out according to the method of Hakomori (Hakomori, 1964). Briefly, 1-2 mg of the sample was dissolved in Dimethyl sulfoxide (DMSO) with the aid of stirring at room temperature (ultrasonicate if necessary). An aliquot of 0.4 ml of methylsulfinyl carbanion was added (methylsulfinyl carbanion was prepared by mixing NaH/oil (50 mg) with 1 ml DMSO with stirring and subsequent flushing with N₂ for 20 seconds. Subsequent agitation at 50-60° C for one hour; H₂ was allowed to escape the reaction vessel). The reaction mixture was stirred for 1 hr at room temperature. One ml of CH₃I is added to the mixture and agitate for 4 hrs. The methylated core oligosaccharide was purified on columns of Sephadex LH-20, eluted with chloroform, evaporated, weighed and dissolved in methanol for MALDI-MS, ESI-MS and CID-MS/MS analyses.

Please note that all the pre-mass spectrometric analysis work, namely isolation, purification and methylation of LPS, was performed by the technical staff in Fisheries and Oceans Canada (DFO), St. John's, NL, Canada.

2.1.5. Electrospray Quadrupole Orthogonal Time-of-Flight Mass Spectrometry:

Mass spectrometry was performed using an Applied Biosystems API QSTAR XL MS/MS quadrupole orthogonal time-of-flight (QqTOF)-MS/MS hybrid instrument capable of analyzing a mass range of m/z 5-40,000 with a resolution of 10,000 in both the positive and the negative ion modes. ESI was performed with a Turbo Ionspray source operated at 5.5 kV at a temperature of 80°C. Traces of lipid A were dissolved in dichloromethane/methanol (1:1) so that the final concentration was 0.5 mg/ml. The

solution was then electrosprayed underivatized in the negative ion mode. Aqueous 0.5% taurocholic acid solution (Applied Biosystems, Foster City, CA) was added to the sample for ToF calibration (exact mass $[M-H]^- = 514.2838$). Nitrogen was used as the collision gas for MS/MS analysis with collision energies (CE) varying between -35 to -100 eV.

In the cases of the core oligosaccharides, samples from the underivatized homogeneous mixture were dissolved in water for ESI in the negative ion mode while for the positive ion mode, the sample was dissolved in water/methanol/formic acid (90/9.9/0.1). Permethylated oligosaccharide mixtures were analyzed in the ESI-positive ion mode. Mixtures were prepared as 0.5 mg/ml solutions in methanol and aliquots (25 μ L) were infused into the mass spectrometer with an integrated Harvard syringe pump at a rate of 10 μ L/min using the Turbo Ionspray source, operated at 5.5 kV at a temperature of 80-100°C. For the positive ion mode, the ToF analyser was calibrated with renin (Applied Biosystems, Foster City, CA), exact mass $[M+H]^+ = 1758.9326$; $[M+2H]^{2+} = 879.9699$. For CID MS/MS, the CE was set so that the selected precursor ion remained abundant (10 to 100 eV), and CID gas pressure was varied between 4 and 12.

2.1.6. Electrospray Quadrupole-Hexapole-Quadrupole Mass Spectrometry:

The ESI mass spectra (negative and positive ion modes) were recorded with a Micromass Quattro quadrupole-hexapole-quadrupole mass spectrometer equipped with a megaflo ESI source capable of analyzing ions up to m/z 4000. A personal computer (Compaq PII 266 MHz processor running Windows NT 4, service pack 3) equipped with Micromass MASSLYNX 3.2.0 Mass Spectrometry Data System software was used for data acquisition and processing. The temperature of the ESI source was maintained at

75°C. The operating voltage of the ESI capillary was 3.00 kV and the high voltage lens was set to 0.40 throughout the whole operation. ESI-MS were recorded with a cone voltage of 25V. MS/MS experiments were conducted using the same instrument. Product ion scans of selected masses were induced by collision with argon in the (r.f. only) hexapole. The resulting product ions were analyzed by the second quadrupole. Collision energies varying from 20 to 35 eV and a collision gas pressure in the collision cell varying from 3.5×10^{-4} to 6.5×10^{-4} mbar (1 bar = 10^5 Pa) were used in all MS/MS experiments. The collision gas (nitrogen) pressure was increased to induce the dissociation of the sodium adduct ions. Precursor ion scans were performed when needed of mass-selected ions which were induced by collision with argon in the (r.f.-only).

2.1.7. Matrix assisted laser/desorption ionization (MALDI) mass spectrometry:

Samples for MALDI-MS analyses were prepared by mixing equal volumes of 2,5-dihydroxybenzoic acid (MALDI-QualityTM Matrix Solutions, Agilent Technologies) and a solution of 1 mg ml⁻¹ of the core oligosaccharide mixture. 0.5 µL of this solution was loaded onto the sample plate. Alternatively, matrix solution was first spotted on the MALDI plate followed by spotting the analyte. Mass spectra from MS and MS/MS experiments were acquired on the same QSTAR XL instrument described previously, equipped with a N₂ laser oMALDI[®] source. The laser parameters were set to 25 Hz pulsed frequency at 25% power energy. For MS/MS experiments, collision energy was ramped from 40 to 100eV to optimize the fragmentation of each individual precursor ion. Argon was used instead of nitrogen as CID gas, to ensure better fragmentation in the collision cell.

2.1.8. Gas chromatography-electron impact- mass spectrometry (GC-EI-MS):

GC-EI-MS analysis was performed on a Varian Saturn 2000 GC MS/MS instrument equipped with Zebron capillary column (30m × 0.25 mm). Helium was used as the carrier gas. Lipid A was treated with 2 M HCl in methanol (methanolysis) for 3 hrs at 100° C. Methyl esters were extracted by hexane and analyzed on GC-EI-MS in comparison with standard methyl esters (Supelco, Bellefonte, PA, USA). GC analysis of methyl esters was performed with following temperature program: 100° C for 5 min, 100° → 280° C at 5° C/ min, 280° C for 5 min. The methyl ester fatty acid analysis showed the presence of two major components namely 3-hydroxymyristic acid (C14:0(3-OH)) and lauric acid (C12:0) in a molar ratio of 2:1 and minor traces of myristic acid (C14:0), 3-hydroxytridecanoic acid (C13:0(3-OH)), palmitoleic acid (C16:1), palmitic acid (C16:0), and 3-hydroxypentadecanoic acid (C15:0(3-OH)).

2.2. Synthetic cholesteryl neoglycolipids:

2.2.1. The synthesis of the neoglycolipid derivatives:

In these amphiphilic neoglycolipid cholesteryl derivatives, the cholesterol and the carbohydrate moieties were attached either by means of a polyethoxy variable spacer or with no spacer, as in the case of simple *O*-glycosides. The general molecular structure of these compounds is presented in Figure 1-2. The synthesis of neoglycolipids 1-3 (Boullanger *et al.*, 1995a; Lafont *et al.*, 1996), 4 (Lafont *et al.*, 1997), 6 (Boullanger *et al.*, 1995a; Lafont *et al.*, 1996), 2 (with deuteriated chains) and 5 (Bardonnet *et al.*, 2005; Laurent *et al.*, 2006) were performed as reported earlier. The chosen carbohydrate

portion was: D-glucosamine (GlcNH₂) (1), N-acetyl-D-glucosamine (GlcNAc) (2), N-trideuterioacetyl-D-glucosamine (GlcNHCOCD₃) (3), N-acetyllactosamine (LacNAc) (4), L-fucose (Fuc) (5), N-allyloxycarbonyl-D-glucosamine (GlcNAloc) (6), and the corresponding per-O-acetylated derivatives of GlcNAloc and LacNAc carbohydrate residues (protected sugar species). The total number of neoglycolipids investigated in this study was 18.

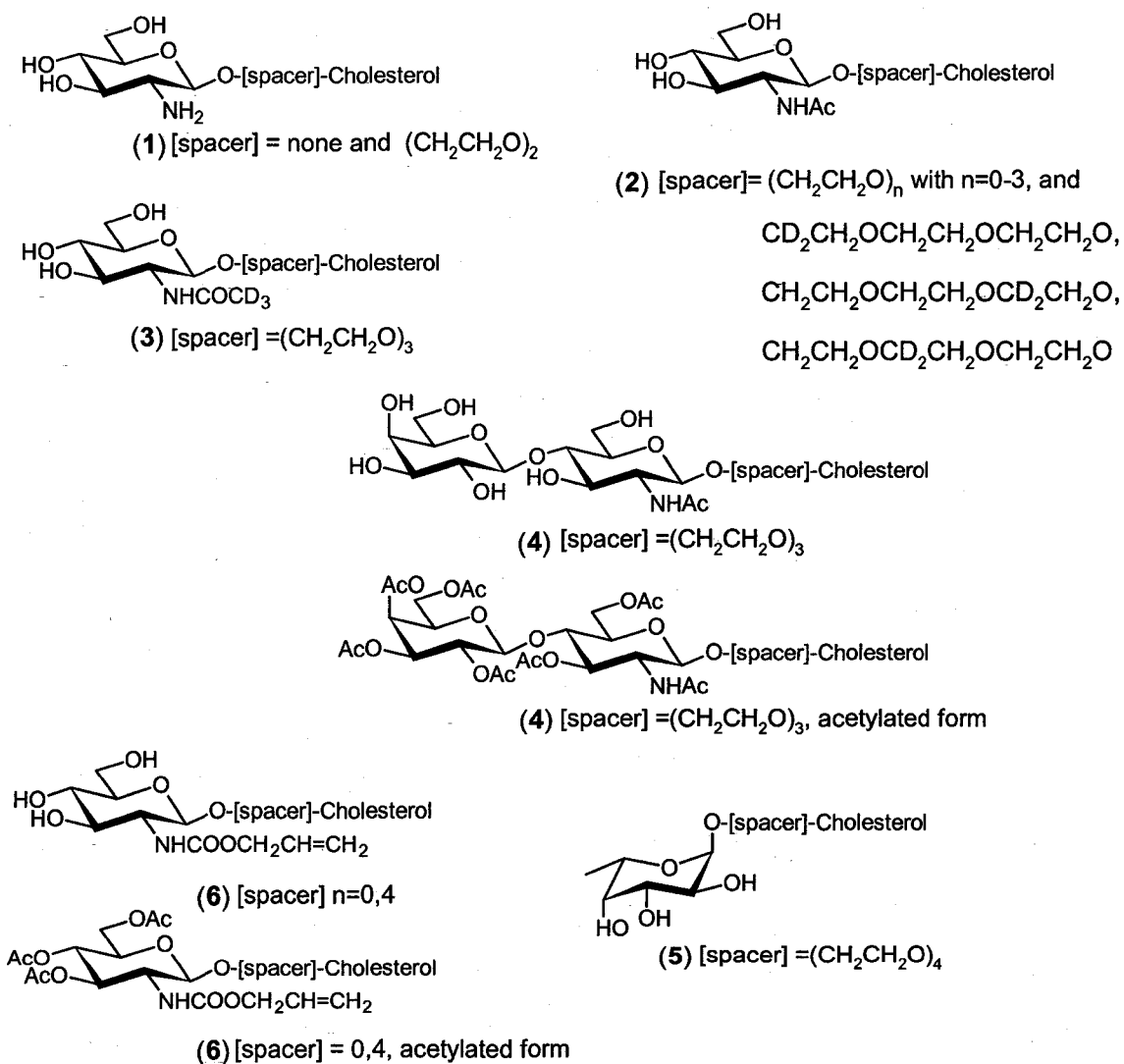


Figure 2-1: The molecular structures of cholysterly neoglycolipids evaluated in this study

2.2.2. Electrospray Quadrupole Orthogonal Time-of-Flight Mass Spectrometry:

Mass spectra of the neoglycolipid derivatives were acquired in the positive ion mode. All experiments were performed with an Applied Biosystems, API QSTAR XL MS/MS quadrupole orthogonal time-of-flight (QqToF-MS/MS) hybrid tandem mass spectrometer. Traces of the neoglycolipid derivatives were dissolved in methanol or methanol/dichloromethane (1:1). Sample solution was then infused into the mass spectrometer with an integrated Harvard syringe pump at a rate of 5 $\mu\text{L}/\text{min}$ using the Turbo IonSpray Source. Formic acid was added to increase the formation of the $[\text{M}+\text{H}]^+$ protonated molecules.

2.2.3. The influence of Declustering Potential (DP) and Focusing Potential (FP) on ion formation:

DP and FP are electrical voltages within the ESI ionization source that have the greatest effects on *in source* fragmentation. In order to study the influence of DP and FP on the ion count, the neoglycolipids were dissolved in methanol or methanol/dichloromethane (1:1) such that the final concentration was 100 nmol/ml. Randomly selected values of DP and FP were obtained using Microsoft Excel. Ion count of different ions was measured three times for each condition. All other instrument parameters were kept constant (Ion Source Gas 1= 25, Ion Source Gas 2= 0, Curtain Gas= 20, Temperature= 0, and DP2= 10).

DP and FP values were randomized within the instruments' allowed ranges (DP [-10,350] and FP [0,480]). The number of ion counts was performed for each combination of DP and FP values. Then, the correlation between ion counts and DP or FP values were

evaluated using the Spearman Rank Correlation coefficient ($r_{Spearman}$). (Conover, 1999)

After these initial tests (see Chapter 6), it was clear that only DP has influence on the ion count. Considering this result, the shape of the relationship between ion count and DP obtained from the formation of the C-Glycoside with the ones obtained from the formation of other ions, namely $[M+H]^+$ and $[(\text{Sugar-Spacer})+H]^+$ were compared. These pair-wise comparisons were made using the 2-samples Kolmogorov-Smirnov Test (Conover, 1999). Ion counts from each experimental run were normalized to its maximum to ensure comparability among experiments (i.e. comparing the shape of these distributions, not their absolute magnitudes).

CHAPTER 3: Mass Spectrometric Analysis of *A. salmonicida* Lipid A

3.1. Background:

Lipopolysaccharides (LPS) have been the center of considerable research activity. They have been recognized as the most significant biological components of the outer membranes of gram-negative bacterial cells and are the major contributor to the antigenic activity of these bacteria. It has been well established that LPS derivatives are potential candidates for bacterial vaccine development (Erridge *et al.*, 2002; Fattom *et al.*, 1999; Kawai *et al.*, 2002).

Lipid A, which is the most toxic part of the LPS, has been evaluated as a possible adjuvant in the therapy of immune diseases (Baldrige *et al.*, 2000; Persing *et al.*, 2002; Prince *et al.*, 2001), as well as a potential anticancer medication (Larmonier *et al.*, 2004; Reisser *et al.*, 2002; Won *et al.*, 2003). Therefore, the exact molecular structure of lipid A is required for the production of possible therapeutic formulations, for synthetic purposes and for the design of structure-activity relationships.

The basic general structure of lipid A is shown in Figure 3-1 and is universally composed of the biphosphorylated β -D-(1 \rightarrow 6) linked D-glucosamine (D-GlcN) disaccharide which is acylated at both the *N*- and *O*- positions. Various analytical techniques such as X-ray diffraction, Fourier transform infrared spectroscopy

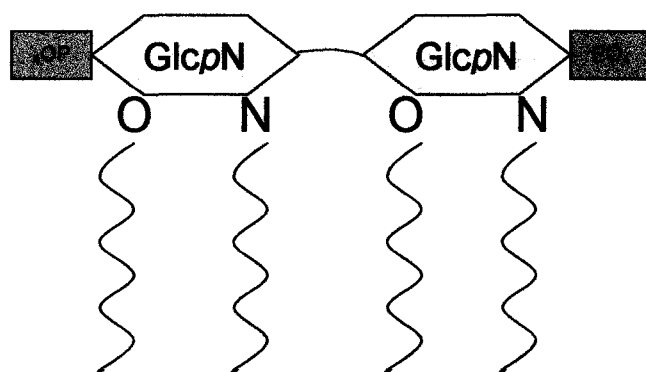


Figure 3-1: Lipid A basic structure; it is composed of the biphosphorylated β -D-(1 \rightarrow 6) linked D-glucosamine (D-GlcN) disaccharide which is acylated at both the *N*- and *O*-positions.

(Brandenburg *et al.*, 2002; Brandenburg *et al.*, 1998; Fukuoka *et al.*, 2001) and nuclear magnetic resonance (NMR) spectroscopy (Brecker, 2003; Hashimoto *et al.*, 2003) have been used to reveal the chemical structure of various lipid A moieties. Early MS methods such as laser desorption (LD) and fast atom bombardment (FAB), were used for the chemical identification of various lipid A extracts (Johnson *et al.*, 1990; Qureshi *et al.*, 1988; Seydel *et al.*, 1984). More recently, soft ionization methods, namely MALDI-MS and ESI-MS (as well as MS/MS) in both positive and negative ion modes were used to characterize lipid A (Boue & Cole, 2000; Chan & Reinhold, 1994; Corsaro *et al.*, 2002). MALDI-MS is usually associated with many adduct ions which can complicate the mass spectrum and it lacks the formation of multiply charged species. On the other hand, ESI tends to produce multiply charged ions allowing very high molecular weight compounds to appear at lower mass-to-charge (m/z) ratios with significant reduction of the interference associated with adduct ions. ESI-MS/MS has been successfully utilized to obtain the detailed chemical structure of lipid A derived from different bacterial species

such as *Enterobacter agglomerans* (Boue & Cole, 2000), *Pseudoalteromonas haloplanktis* (Corsaro et al., 2002) and *Shigella flexneri* (Chan & Reinhold, 1994). The negative ion mode has been shown to be of a particular advantage to lipid A analysis, since it requires no derivatization or manipulation of the molecule due to the natural existence of the easily ionized phosphate and hydroxyl groups.

In reality, lipid A extracts are usually formed as a microheterogeneous mixture composed of a major lipid A component, in addition to other minor products. This heterogeneity is most likely a result of complete and incomplete lipid A biosynthesis and differs mainly in the composition of fatty acid length and saturation and substitution of the phosphate by ethanolamine or various glycosyl groups (Chan & Reinhold, 1994; Krasikova et al., 2001; Zarrouk et al., 1997).

In the present study, ESI-QqToF tandem mass spectrometry is used to differentiate and elucidate the molecular structure of the main constituent of native Lipid As isolated from the bacterial species *A. salmonicida*. In addition, this analysis has illustrated the fragmentation pattern and the mass spectrometric fingerprints of this biological compound; these data can be used in the future to evaluate related lipid A's and to perform quantitative studies on its formulations.

The QqToF-MS/MS instrument equipped with LINAC (linear acceleration pulsar high-pressure) collision cell was used, since the collision induced dissociation (CID) tandem mass spectrometry analysis performed on a conventional quadrupole-hexapole-quadrupole tandem instrument, failed to fragment the selected precursor ions using different collision energies and gas pressure conditions in the collision cell (spectra shown in Appendix I).

3.2. ESI- QqToF analysis:

The negative ion QqToF-MS scan of the lipid A was acquired with a declustering potential (DP) value of -60 (Figure 3-2). The obtained mass spectrum indicated a major doubly charged ion and its corresponding singly charged minor species, which were observed at m/z 883.5826 and 1768.1972, respectively. These ions were assigned as the $[M_B - 2H]^{2-}$ and $[M_B - H]^-$, the biphosphorylated lipid A moiety bearing a phosphate group on each sugar. The monophosphorylated lipid A was also observed as a major ion at m/z 1688.2144, and was assigned as the $[M_M - H]^-$ ion. The loss of HPO_3 can occur either at the reducing or the non-reducing sugar group. Based on fatty acid analysis, the presence of two major components, namely myristic acid (C14:0(3-OH)) and lauric acid (C12:0) was observed. Therefore, it is feasible to propose that the major compound of this heterogeneous lipid A mixture, is the D-glucosamine-disaccharide in which the *O*- and *N*-“free positions” are substituted by myristyloxylauric (C14:0(3-*O*(12:0))) groups at the non-reducing end sugar, whereas the reducing sugar moiety “free positions” were substituted with a 3-OH myristic acid chain (C14:0(3-OH)).

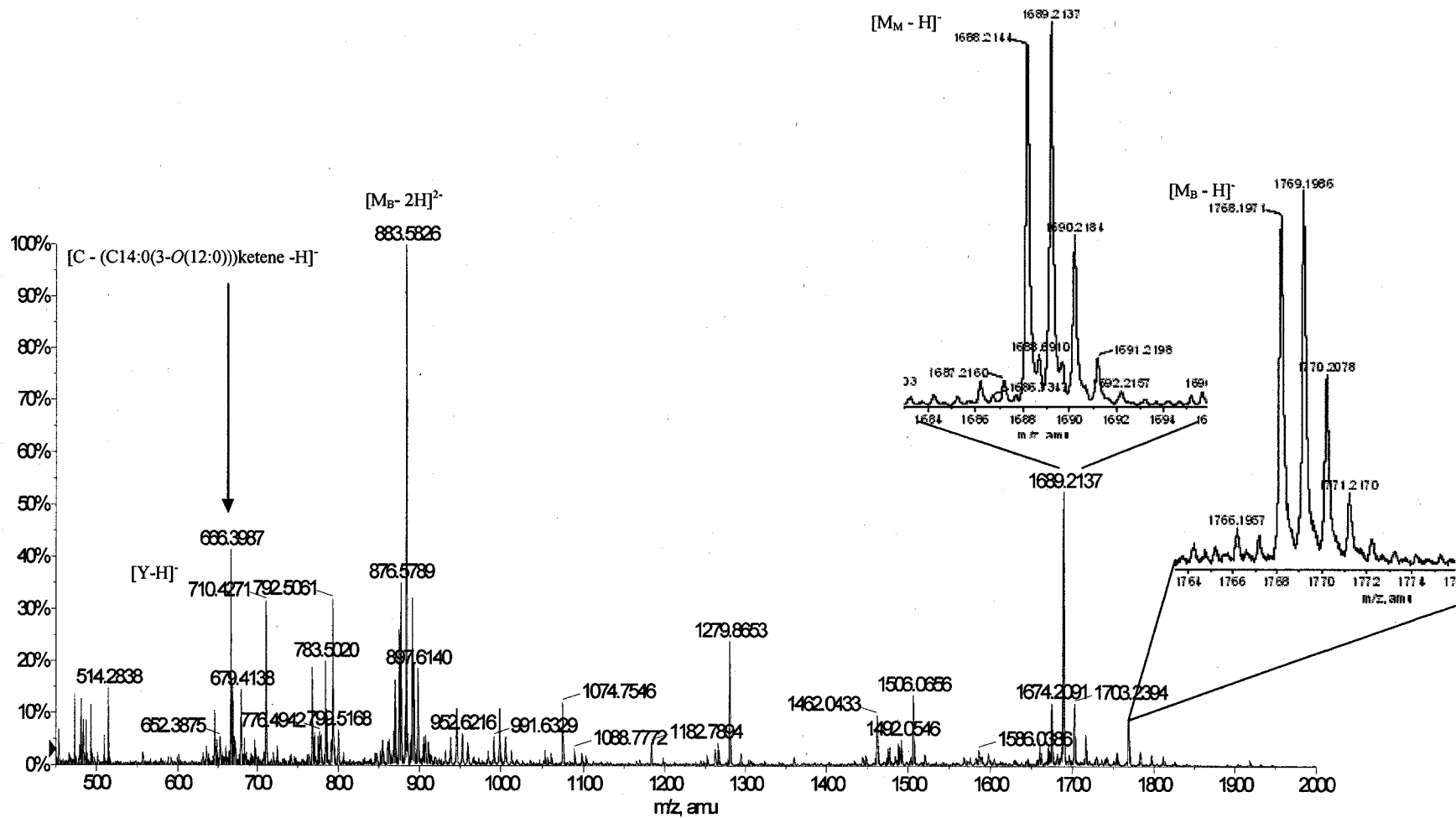
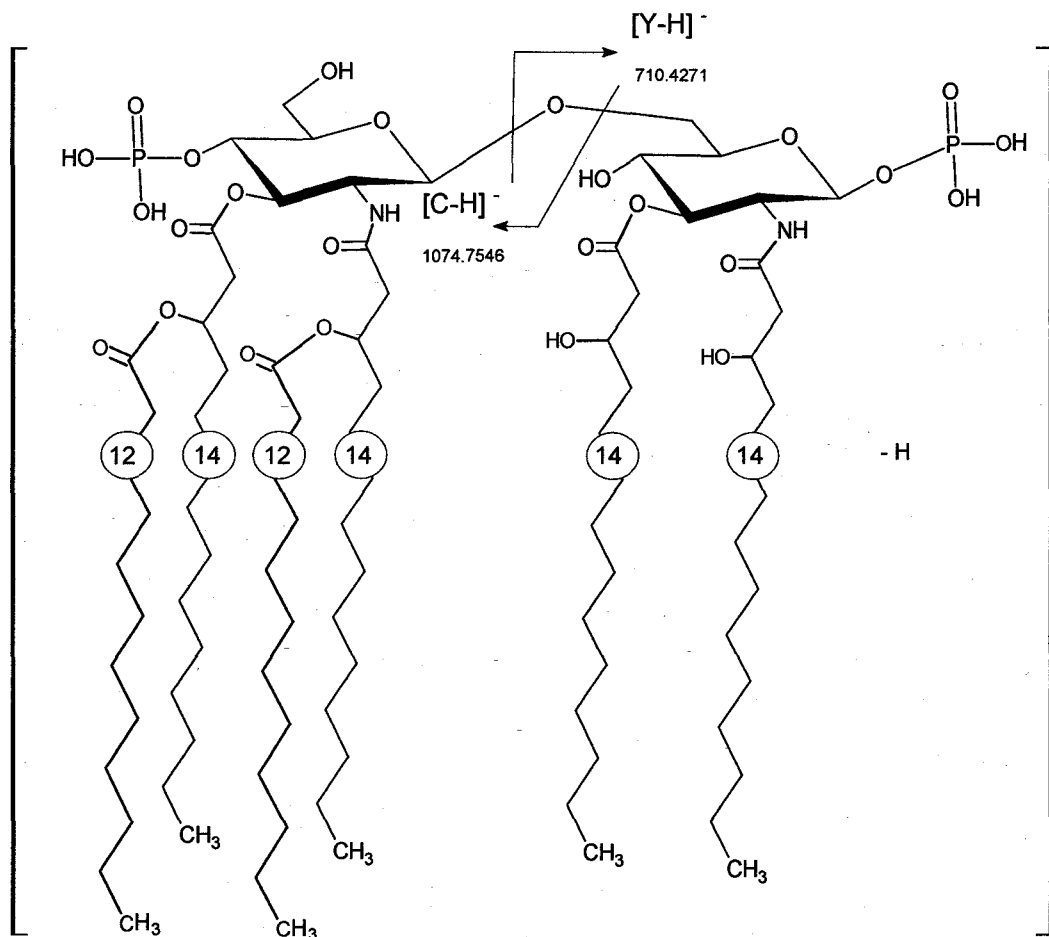


Figure 3-2: Negative QqToF MS scan of the native lipid A extract from *A. salmonicida* acquired at DP = - 60.

The proposed structure of the biphosphorylated lipid A and its distinctive ions observed in the QqToF-MS are illustrated in Table 3-1 and Figure 3-3. It should be noted, that at this stage of this study, the position of the esterified fatty acids was tentatively assigned and that there were many possible structures for the lipid A. The theoretical structure shown in Figure 3-3 corresponds to a biphosphorylated lipid A with a theoretical $[M_B - 2H]^{2-}$ and $[M_B - H]^-$ of m/z 883.5826 and 1768.1972, respectively. The structure shown in Figure 3-3 was, however, confirmed with a detailed analysis of the QqToF-MS and the MS/MS analysis of selected molecular anions, as described in the following sections.

Diagnostic Ion	Empirical Formula	m/z		Abundance - (%)
		Calculated	Observed	
$[M_B - H]^-$ *	$C_{92}H_{173}N_2O_{25}P_2$	1768.1802	1768.1972	9.18 %
$[M_B - 2H]^{2-}$	$C_{92}H_{172}N_2O_{25}P_2$	883.5862	883.5826	100 %
$[M_B - (C12:0)ketene - 2H]^{2-}$	$C_{80}H_{150}N_2O_{24}P_2$	792.5026	792.5061	31.92 %
$[M_B - (C12:0)ketene - H_2O - 2H]^{2-}$	$C_{80}H_{148}N_2O_{23}P_2$	783.4974	783.5020	20.00 %
$[M_M - H]^{*-}$	$C_{92}H_{172}N_2O_{22}P$	1688.2139	1688.2144	49.26 %
$[M_M - (C12:0)ketene - H]^-$	$C_{80}H_{150}N_2O_{21}P$	1506.0468	1506.0656	13.52 %
$[M_M - (C14:0(3-OH))ketene - H]^-$	$C_{78}H_{146}N_2O_{20}P$	1462.0206	1462.0433	9.73 %
$[M_M - (C12:0)ketene - (C14:0(3-OH))ketene - H]^-$	$C_{66}H_{124}N_2O_{19}P$	1279.8535	1279.8653	23.81 %
$[C - H]^-$	$C_{58}H_{109}NO_{14}P$	1074.7585	1074.7546	12.13 %
$[C - (C14:0(3-O(12:0)))ketene - H]^-$	$C_{32}H_{61}NO_{11}P$	666.3982	666.3987	41.42 %
$[Y - H]^-$	$C_{34}H_{63}NO_{12}P$	710.4244	710.4271	31.58 %

Table 3-1: Assignments of the diagnostic ions observed in QqToF mass spectrum of native lipid A extract acquired at DP= -60.



[Biphosphorylated Lipid A - H]⁻

[M_B - H]⁻

m/z 1768.1972

Figure 3-3: Schematic representation of the fully substituted biphosphorylated lipid A and the diagnostic ions [C - H]⁻ and [Y - H]⁻ observed in the QqToF MS scan.

Glycosidic cleavages induced by MS and MS/MS provide useful structural information and sugar sequencing of complex carbohydrates (Banoub *et al.*, 1990; Bateman *et al.*, 1996; Domon & Costello, 1988a; Domon & Costello, 1988b). In the conventional ESI-MS, two distinctive ions at m/z 1074.7546 and 710.4271 were observed and were assigned as the $[C - H]^-$ and $[Y - H]^-$ ions, respectively, and are shown in Figure 3-3. The ion observed at m/z 666.3987 was produced from the $[C - H]^-$ at m/z 1074.7546 and was assigned as the $[C - (C14:0(3-O(12:0))) \text{ ketene} - H]^-$.

In addition to the distinctive $[Y]^-$ and $[C]^-$ derived ions, four other structurally related ions were also observed. The first was a doubly-charged ion at m/z 792.5061, which was assigned as $[M_B - (C12:0)\text{ketene} - 2H]^{2-}$. It was deduced to stem from the characteristic ion $[M_B - 2H]^{2-}$ at m/z 883.5826 by the loss of one lauryl group (C12:0) as a neutral ketene ($R-CH=C=O$). Two others, however, originated from the monophosphorylated ion $[M_M - H]^-$ and were observed as singly-charged ion species at m/z 1506.0656 and 1279.8653. These ions were assigned as $[M_M - (C12:0)\text{ketene} - H]^-$ and $[M_M - (C12:0)\text{ketene} - (C14:0(3-OH))\text{ketene} - H]^-$, respectively. Similarly, monophosphorylated lipid A eliminated a molecule of (C14:0(3-OH))-ketene to afford the ion observed at m/z 1462.0433, assigned as $[M_M - (C14:0(3-OH))\text{ketene} - H]^-$.

Careful examination of the QqToF mass spectrum also revealed the presence of two higher and two lower signals with a difference of 14 Daltons for the major singly-charged ions and 7 Daltons for the major doubly-charged species. These ions were attributed to the microheterogenic nature of lipid A extract due to lipid A compounds being linked to various longer and/or shorter fatty acids. This assumption was in

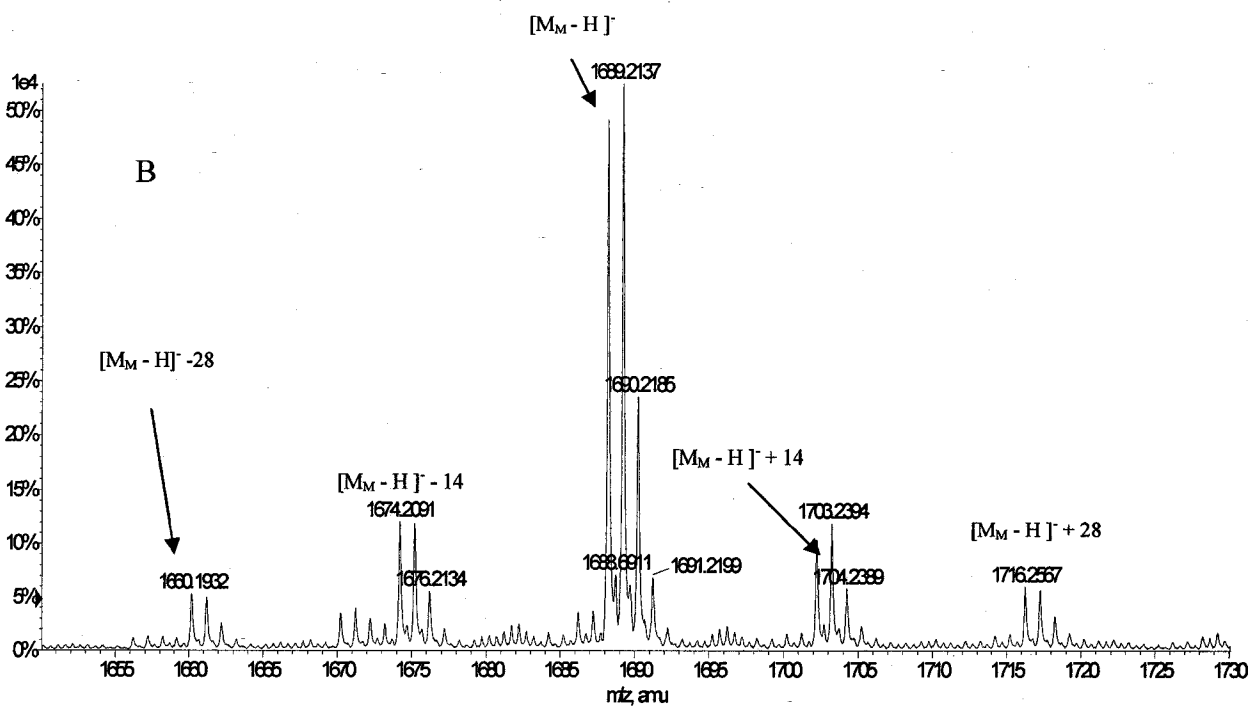
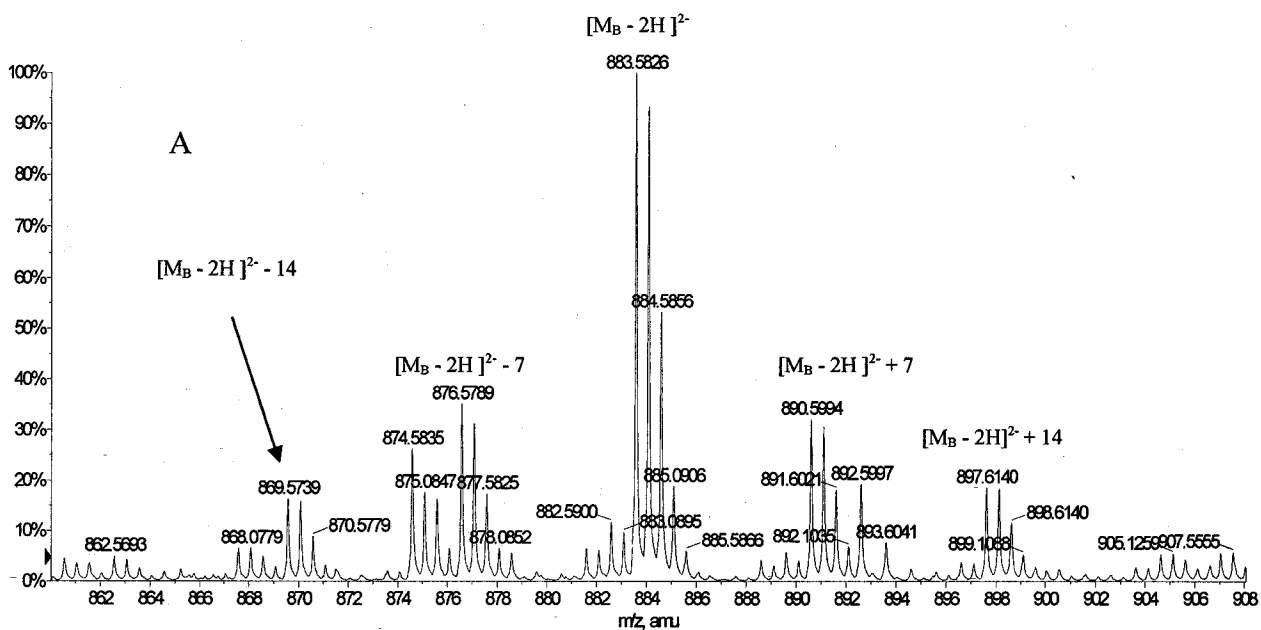
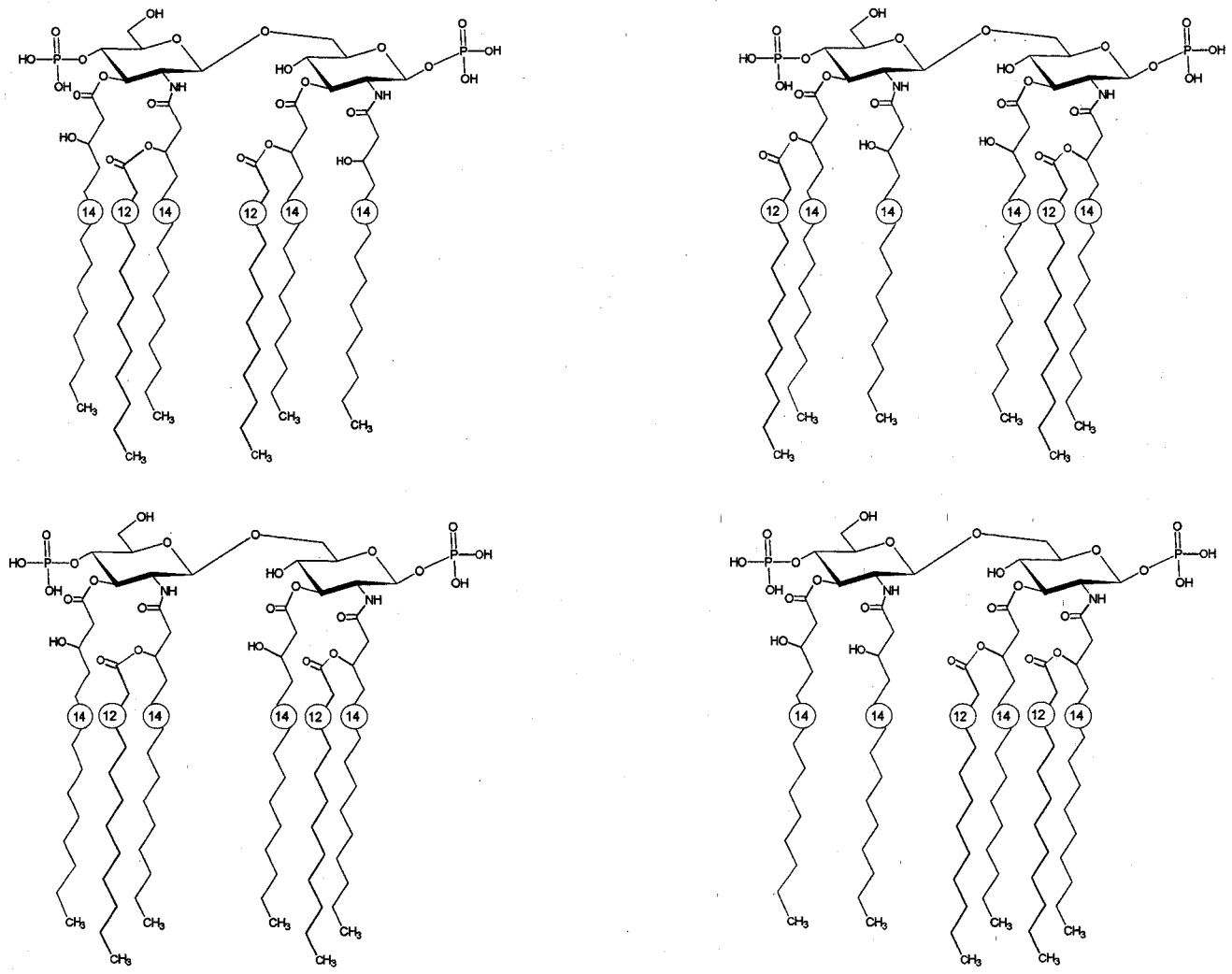


Figure 3-4: The presence of 7 Dalton signals lower and higher of the Biphosphorylated Lipid A $[M_B - 2H]^{2-}$ observed at m/z 883.5826 (A) and 14 Daltons of the Monophosphorylated Lipid A $[M_M - H]^-$ observed at m/z 1688.2144 (B).

agreement with the composition of methyl ester fatty acid data obtained by GC-EI-MS analysis, in which traces of myristic acid (C14:0), 3-OH tridecanoic acid (C13:0(3-OH)), palmitoleic acid (C16:1), palmitic acid (C16:0), and 3-OH pentadecanoic acid (C15:0(3-OH)) were also identified. Figure 3-4 shows these “satellite” signals for the $[M_B - 2H]^{2-}$ and $[M_M - H]^-$. Similarly, the ions lacking the fatty acid chains reported in Table 3-1 can, in reality, be either a by-product of the uncompleted biosynthesis process, a hydrolysis product or a fragment of the lipid A-fully substituted molecule. Lipid A extract was subjected to additional acid hydrolysis for 30 and 60 min and then evaluated with the mass spectrometer. This showed a substantial increase in the diagnostic ions resulting from the C and Y breakages, confirming the assumption that hydrolysis influences the spectrum outcome.

The assignment of the ions observed in the simple one-stage high resolution MS analysis is based on the exact molecular weight only, and additional evidence is usually required to validate these assignments. Therefore, without further confirmation, it would be possible to suggest various constitutional isomers structures of lipid A, as shown in Figure 3-5. For example, all the ions proposed in Table 3-1 and Figure 3-3 could also be correct, if the fatty acids were reversibly distributed between the two sugars. Tandem mass spectrometry, however, permitted the identification of the diagnostic product ions and to confirm the proposed molecular structure. It should be noted that both wild type and rough mutant lipid A extracts produced identical outcomes (see Appendix I).



Scheme 3-5: Four theoretical structures of the lipid A that can be proposed instead of the one illustrated in Figure 3-3. These structures share the same theoretical $[M_B - 2H]^{2-}$ and $[M_B - H]^-$ at m/z 883.5826 and 1768.1972, respectively.

3.3. MS/MS analysis of the biphosphorylated and monophosphorylated lipid A

The product ion scans of the selected precursor singly monophosphorylated $[M_M - H]^-$ and doubly charged biphosphorylated $[M_B - 2H]^{2-}$ ions at m/z 1688.2144 and 883.5826 were recorded with the QqToF-MS/MS instrument and are shown in Figure 3-6A and 3-6B, respectively. Collision energy (CE) and CID gas conditions were adjusted such that the precursor ion remained abundant. More energy and CID gas were required to break the singly charged monophosphorylated ion (CE= -75, CID= 8) in contrast to the doubly charged biphosphorylated ion (CE= -35, CID= 3).

The fragmentation pathway of the monophosphorylated lipid A at m/z 1688.28 was rationalized and is presented in Figure 3-7 and Table 3-2. The presence of a myristyloxylauric (C14:0(3-O(12:0))) group at position O-3' was evident from the consecutive losses of C12:0 acid followed by C14:1 either as neutral ketene or as a free fatty acid.

In the MS studies of lipid A, it is understood that the negative charge is localized on the highly ionized phosphate group. It has been established that the loss of fatty acid during collision induced dissociation (CID) of glycerolphospho-ethanolamine occurs either as a neutral free fatty acid retaining the charge on the phosphate group (charge remote process) or as a neutral ketene derivative relocalizing the charge on the oxygen (charge driven process) (Hsu & Turk, 2000). Similarly, the fatty acid at position O-3' of lipid A can also fragment via charge-remote or charge-driven mechanisms. These two competing processes are illustrated in Figure 3-8 for the ions $[M_M - (C12:0)acid - H]^-$, $[M_M - (C12:0)acid - (C14:1)acid - H]^-$, $[M_M - (C12:0)acid - (C14:1)ketene - H]^-$ observed at m/z 1488.09, 1261.87, and 1279.86, respectively. Similar losses can be rationalized for

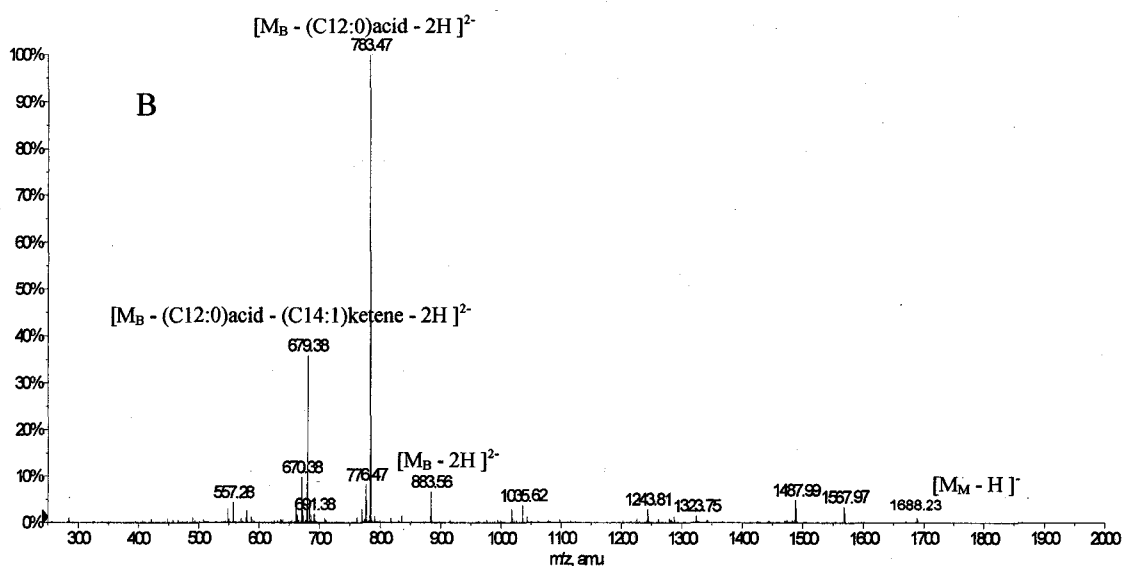
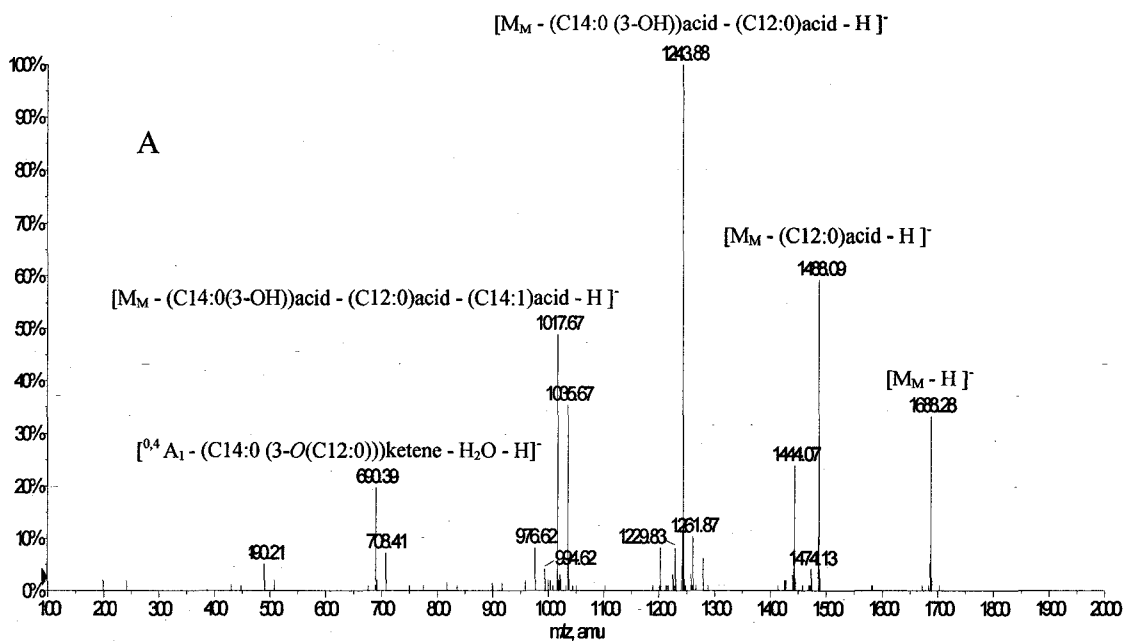


Figure 3-6: Negative ion CID-MS/MS of the singly-charged Monophosphorylated Lipid A $[M_M - H]^-$ at m/z 1688.2 (A) and of the doubly-charged Biphosphorylated Lipid A $[M_B - 2H]^{2-}$ at m/z 883.5 (B).

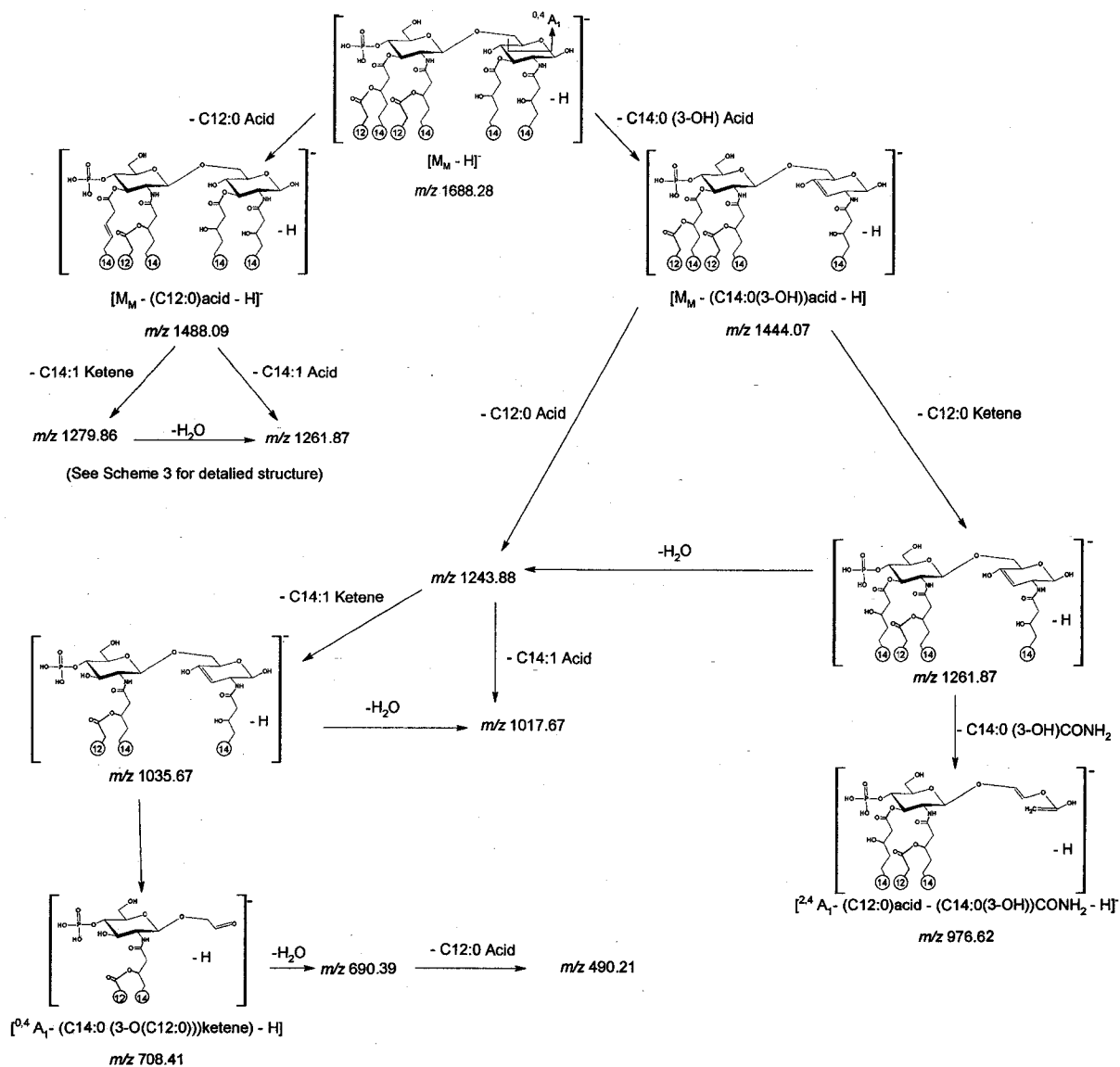


Figure 3-7: Proposed fragmentation pathways of the product ion scan of the selected precursor Monophosphorylated Lipid A $[M_M - H]^-$ ion at m/z 1688.2.

Table 3-2: Assignments of the diagnostic product ions in CID- MS/MS analysis of the singly charged monophosphorylated Lipid A ion $[M_M - 2H]^-$ at m/z 1688.27.

Diagnostic Ion	m/z		Abundance (%)
	Calculated	Observed	
$[M_M - H]^-$	1688.21	1688.28	33.65 %
$[M_M - (C14:0 (3-OH))acid - H]^-$	1444.01	1444.07	27.88 %
$[M_M - (C14:0 (3-OH))acid - (C12:0)ketene - H]^-$	1261.84	1261.87	12.50 %
$[M_M - (C12:0)acid - (C14:1)acid - H]^-$	1261.84	1261.87	12.50 %
$[M_M - (C14:0 (3-OH))acid - (C12:0)acid - H]^-$	1243.83	1243.88	100 %
$[M_M - (C14:0 (3-OH))acid - (C12:0)acid - (C14:1)ketene - H]^-$	1035.64	1035.67	38.46 %
$[M_M - (C14:0 (3-OH))acid - (C12:0)acid - (C14:1)acid - H]^-$	1017.63	1017.67	48.07 %
$[M_M - (C12:0)acid - H]^-$	1488.03	1488.09	68.26 %
$[M_M - (C12:0)acid - (C14:1)ketene - H]^-$	1279.85	1279.86	7.69 %
$[^{0,4}A_1 - (C14:0 (3-O(C12:0)))ketene - H]^-$	708.40	708.41	7.69 %
$[^{0,4}A_1 - (C14:0 (3-O(C12:0)))ketene - H_2O - (C12:0)acid - H]^-$	490.22	490.21	7.69 %
$[^{2,4}A_1 - (C12:0)ketene - (C14:0 (3-OH))CONH_2 - H]^-$	976.61	976.62	8.65 %

the major product ions assigned as $[M_M - (C14:0(3-OH))acid - (C12:0)acid - H]^-$, $[M_M - (C14:0(3-OH))acid - (C12:0)acid - (C14:1)ketene - H]^-$, and $[M_M - (C14:0(3-OH))acid - (C12:0)acid - (C14:1)acid - H]^-$ at m/z 1243.88, 1035.67 and 1017.67, respectively. In addition to these two aforementioned mechanisms, another fragmentation route cannot be excluded. This latter mechanism can occur simultaneously, allowing the product ion $[M_M - (C12:0)acid - (C14:1)ketene - H]^-$ at m/z 1279.86, for example, to lose a water molecule, and produce the ion $[M_M - (C12:0)acid - (C14:1)ketene - H_2O - H]^-$ at m/z 1261.85 instead of the one described earlier and designated as $[M_M - (C12:0)acid - (C14:1)acid - H]^-$ (see Figure 3-8). Similarly, it should also be noted that the ion at m/z 1261.87 can be obtained by two routes and support two different isomers structures which are illustrated in Figures 3-7 and 3-8.

The multiple origin of this series of isomer product ions is generated either by concerted or consecutive multiple neutral losses. The losses could be composed of either fatty acid and ketene molecules, or ketene and water molecules. In this context, note that “concerted” or “consecutive” losses of many such product ions in the MS/MS experiment simply means that they are both lost at the same time and within the same reaction region in the hybrid tandem mass spectrometer.

Furthermore, two diagnostic inner sugar fragment ions were distinguished at m/z 708.41, and 976.62. The first of these was assigned as the $[^{0,4}A_2 - (C14:0(3-O(C12:0)))ketene - H]^-$ ion and was a result of a cleavage of the product ion $[M_M - (C14:0(3-OH))acid - (C12:0)acid - (C14:1)ketene - H]^-$ at m/z 1035.67. The product ion observed at m/z 976.61, however, originated from the $[M_M - (C12:0)acid - (C14:1)acid - H]^-$

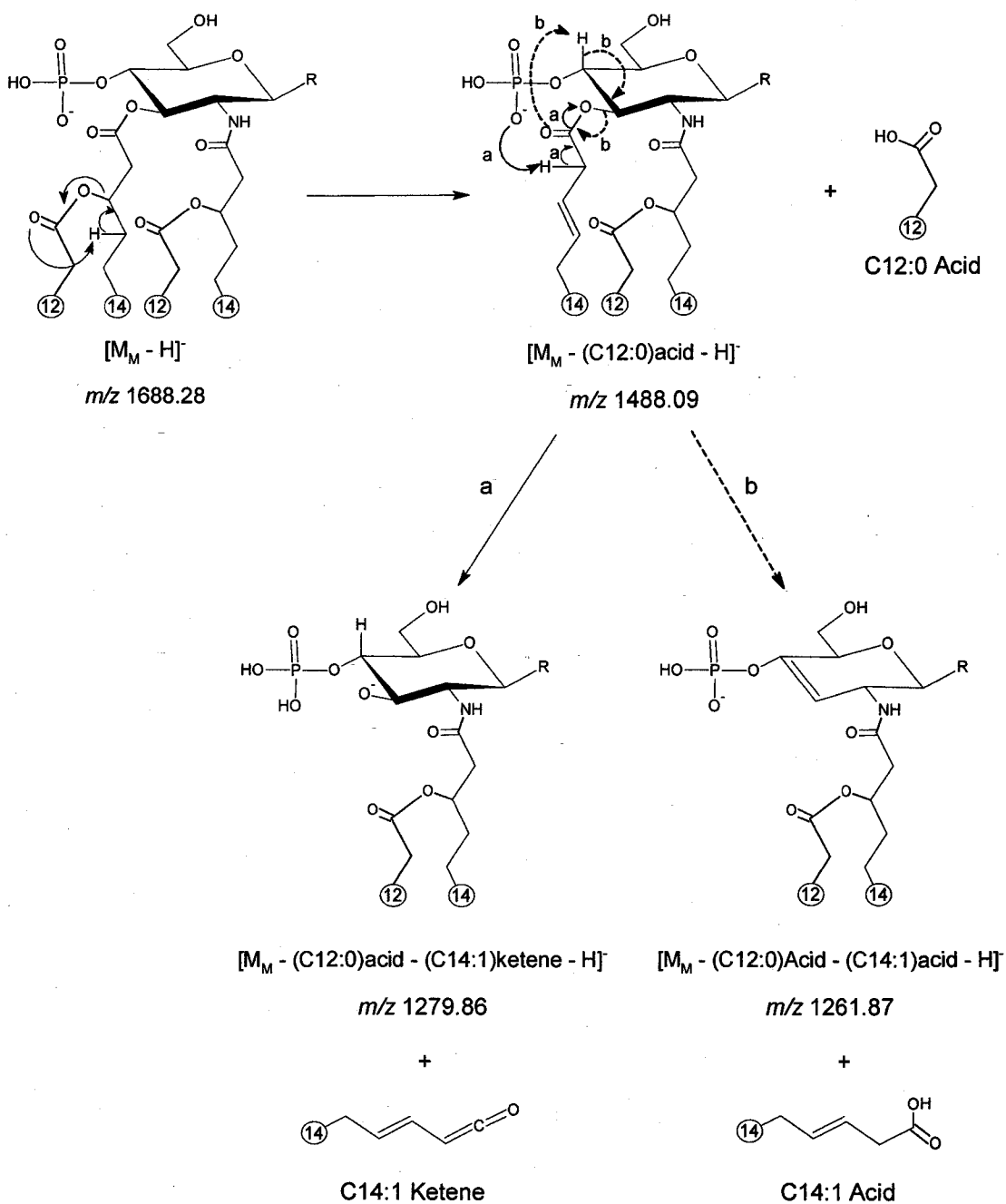


Figure 3-8: Schematic representation of the charge driven (a) and charge remote (b) processes illustrated on the product ions $[M_M - (C12:0)acid - H]^-$, $[M_M - (C12:0)acid - (C14:1)acid - H]^-$, $[M_M - (C12:0)acid - (C14:1)ketene - H]^-$ at *m/z* 1488.08, 1279.86, and 1261.87 respectively. R is the reducing end of the lipid A portion.

ion at m/z 1261.85 and was proposed as the $[\text{}^{2,4}\text{A}_2 - (\text{C12:0})\text{acid} - (\text{C14:0(3-OH)})\text{CONH}_2 - \text{H}]^-$ ion (structures shown in Figure 3-7). The presence of these fragment ions suggest that the phosphate group is retained at position 4', which is in agreement with the losses of ketene or free fatty acid at position O-3' through charge remote and charge driven processes. These two distinctive product ions predetermined the presence of C14:0 (3-OH) on the reducing end group of the D-GlcN disaccharide and authenticate the structure presented in Figure 3-3.

The MS/MS scan of the doubly-charged biphosphorylated lipid A $[\text{M}_B - 2\text{H}]^{2-}$ observed at m/z 883.80 (Figure 3-6B) did not provide evidence for the presence of any distinctive product ions which would indicate the locations of the fatty acids. However, the presence of C12:0, C14:0(3-O(12:0)) and C14:0 (3-OH) fatty acid groups were once again confirmed through the distinctive losses of these fatty acid chains. Table 3-3 summarizes the ions observed in this CID MS/MS.

Table 3-3: Assignments of the diagnostic product ions in CID- MS/MS analysis of the doubly-charged biphosphorylated lipid A ion $[M_B - 2H]^{2-}$ at m/z 883.56.

Diagnostic Ion	m/z		Abundance (%)
	Calculated	Observed	
$[M_B - 2H]^{2-}$	883.58	883.56	6.76 %
$[M_B - (C12:0)acid - 2H]^{2-}$	783.49	783.47	100 %
$[M_B - (C12:0)acid - CH_2 - 2H]^{2-}$	776.48	776.47	8.25 %
$[M_B - (C12:0)acid - (C14:1)ketene - 2H]^{2-}$	679.40	679.38	35.97 %
$[M_B - (C12:0)acid - (C14:1)acid - 2H]^{2-}$	670.40	670.38	9.90 %
$[M_B - (C12:0)acid - (C14:1)ketene - (C14:0 (3-OH))acid - H]^{2-}$	557.30	557.28	4.45 %
$[M_M - H]^-$	1688.21	1688.23	0.99 %
$[M_M - (C12:0)acid - H]^-$	1488.03	1487.99	4.95 %
$[M_M - (C12:0)acid - (C14:0)acid - H]^-$	1243.83	1243.81	2.97 %
$[M_B - (C12:0)acid - H]^-$	1568.00	1567.97	3.46 %
$[M_B - (C12:0)acid - (C14:0 (3-OH))acid - H]^-$	1323.79	1323.75	1.48 %

3.4. MS/MS analysis of the [C - H]⁻ and [Y - H]⁻ ions:

As mentioned earlier, three distinctive ions, namely [C - H]⁻, [Y - H]⁻ and [C - (C14:0(3-*O*(12:0)))ketene - H]⁻ associated with the glycosidic cleavages of the β-D-(1→6) of the D-GlcN disaccharide were observed in the QqToF MS at *m/z* 1074.7546, 710.4271 and 666.3987, respectively (see Figures 3-2 and 3-3). To confirm the proposed structure of these ions, MS/MS were acquired and are shown in Figures 3-9A, 3-9B, and 3-9C.

The product ion scan of the selected ion [C - H]⁻ at *m/z* 1074.74 (Figure 3-9A) showed the loss of a (C12:0) acid chain to yield the product ion assigned as [C - (C12:0)acid - H]⁻ observed at *m/z* 874.56 which can further fragment by losing a ((C14:1)ketene) molecule to afford the product ion observed at *m/z* 666.37. This latter loss probably takes place at the labile *O*- linked fatty acid rather than the more stable *N*-linked one. It is well-accepted that during MS/MS analysis of the lipid A moiety, the elimination of the fatty acid derivatives occurs mainly from the *O*- linked fatty acid esters (Boue & Cole, 2000; Chan & Reinhold, 1994). Therefore, it was projected that the major ion observed at *m/z* 648.37 would be associated with the loss of the ((C14:1)acid) at position *O*-3', rather than a loss of H₂O from the product ion observed at *m/z* 666.37, and it is very possible that these two processes occur simultaneously, as mentioned earlier. The latter product ion could further fragment by losing another C12:0 acid chain or H₃PO₄ to produce the distinctive product ions [C - (C12:0)acid - (C14:1)acid - (C12:0)acid - H]⁻ and [C - (C12:0)acid - (C14:1)acid - H₃PO₄ - H]⁻ appearing at *m/z* 448.19, and 550.40, respectively (see Figure 3-9A for proposed structures). These product ions confirmed the proposed structure of lipid A bearing two myristyloxylauric (C14:0(3-*O*(12:0))) and one phosphate group at its non-reducing end sugar.

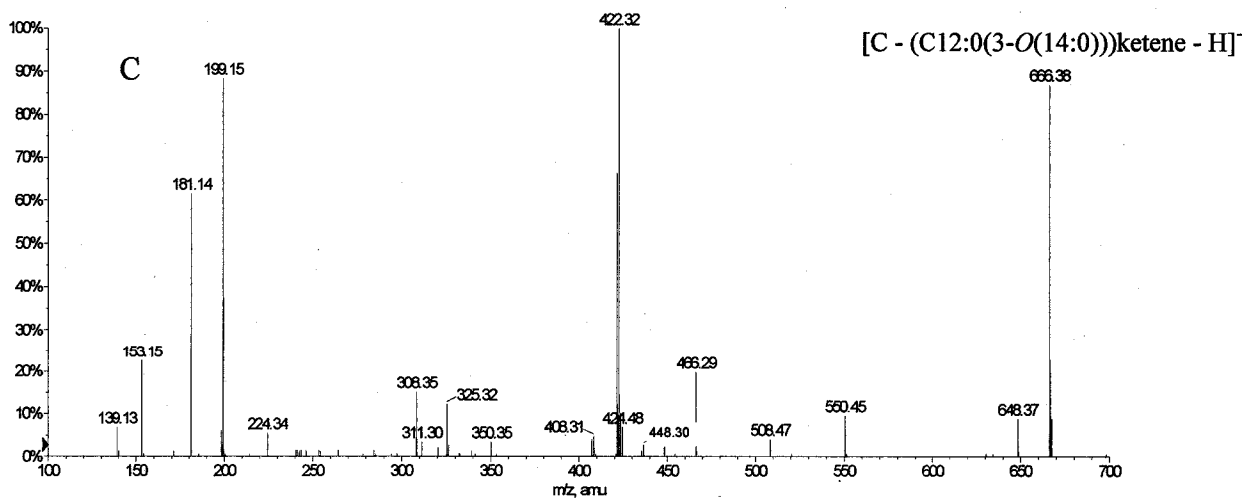
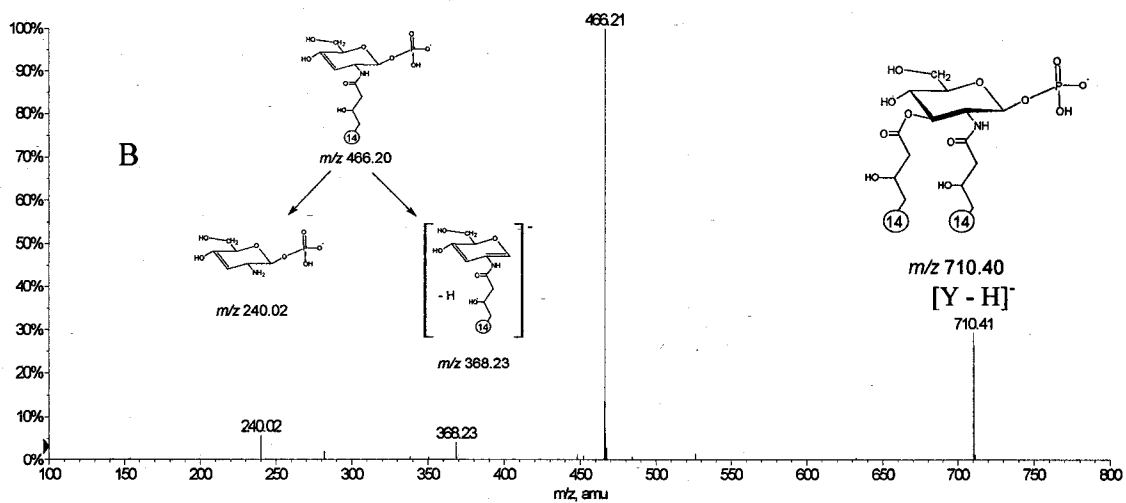
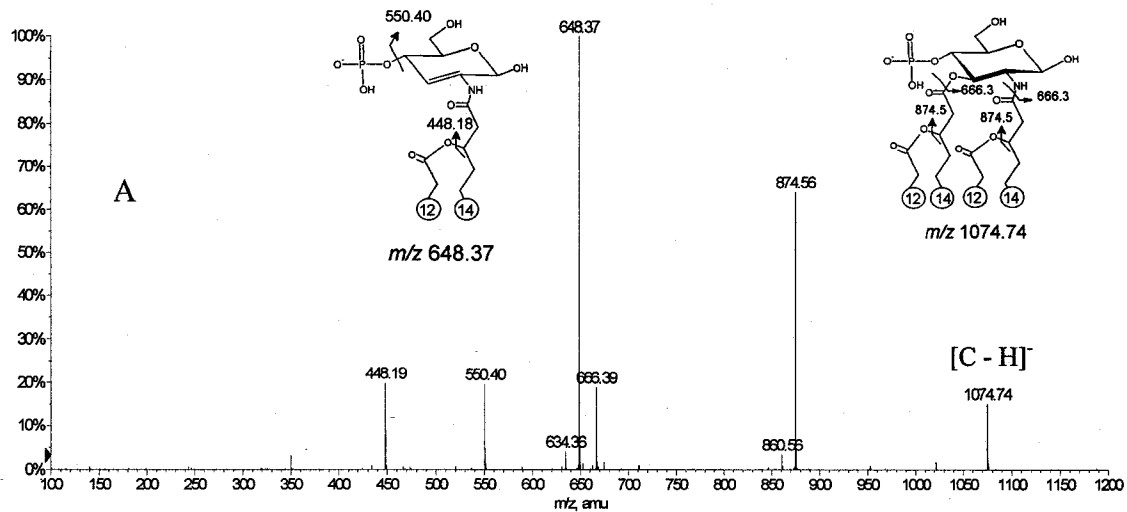


Figure 3-9: Negative ion CID-MS/MS of the diagnostic ions: $[C - H]^-$ at m/z 1074.7 (A), $[Y - H]^-$ at m/z 710.4 (B), and $[C - (C12:0(3-O(14:0)))ketene - H]^-$ at m/z 666.3 (C).

On the other hand, as shown in Fig 3-9B, MS/MS analysis of the [Y - H]⁻ ion at *m/z* 710.41 clearly illustrated, that the loss of the neutral acid C14:0(3-OH) at *m/z* 466.21 occurs initially, followed by C14:0(3-OH)ketene, to produce the distinctive ion observed at *m/z* 240.02, which was proposed to be 3-deoxy-1-phosphate glucosamine (structure shown in Fig 3-9B). Similar to the [C - H]⁻ fragmentation pathway, a distinctive loss of H₃PO₄ also occurs to produce the ion observed at *m/z* 368.23. This latter product ion spectrum supports the proposed original structure, which designated the presence of two C14:0 (3-OH) acid chains and one H₃PO₄ on the reducing end group of lipid A.

The fragmentation pathway of the [C- (C12:0(3-O(14:0)))ketene - H]⁻ ion at *m/z* 666.38 was also rationalized and is presented in the self-explanatory Figure 3-10. Despite the many possible fragmentation routes that can lead to the formation of the same ions observed in this spectrum, the fragmentation pattern presented in Figure 3-10 was confirmed by using precursor ion scan analysis. The precursor ion scan of the ion observed at *m/z* 193 is included in Figure 3-10, and it clearly illustrates that this ion was indeed produced from the ion observed at *m/z* 153 (losing CH₂) eliminating the theoretical possibility that this ion was obtained from the ion observed at 181 losing CH₂=C=O. The rationale presented in Figure 3-10 further confirms the proposed structure, and illustrates, once more, that this product ion retains the fatty acids at position O-2' due to the appearance of the diagnostic second generation product ions observed at *m/z* 224.33 and 325.31. These latter ions were identified as (myristene-3) acid amide ((C14:1)CONH₂) and a product of 2,4 inner-sugar elimination, respectively.

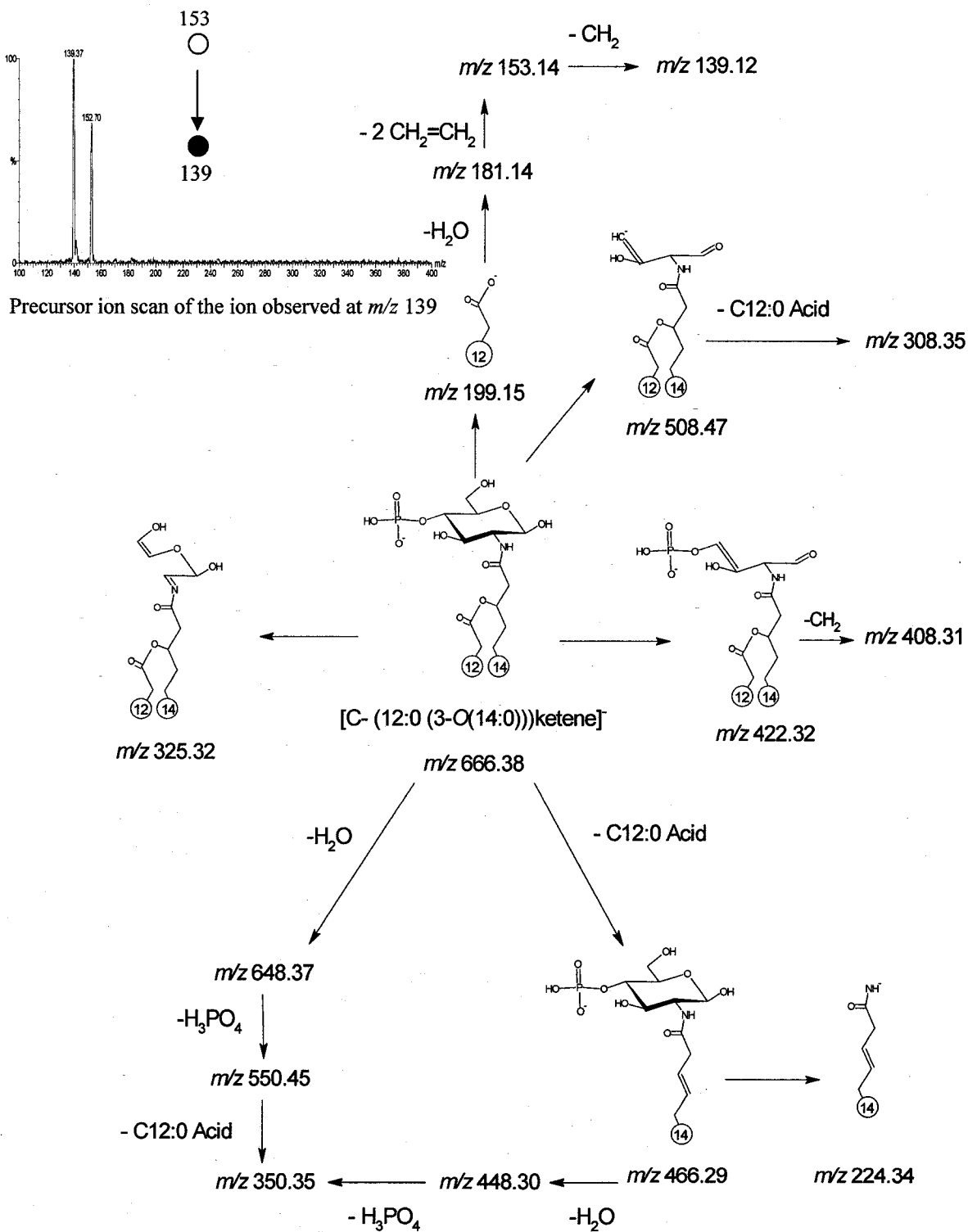
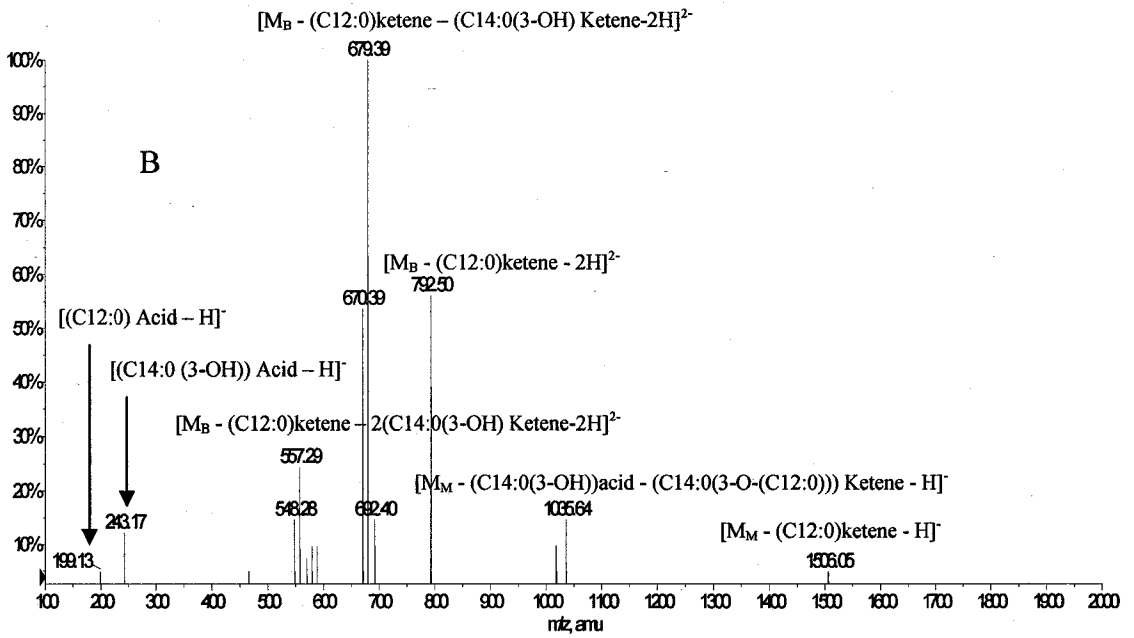
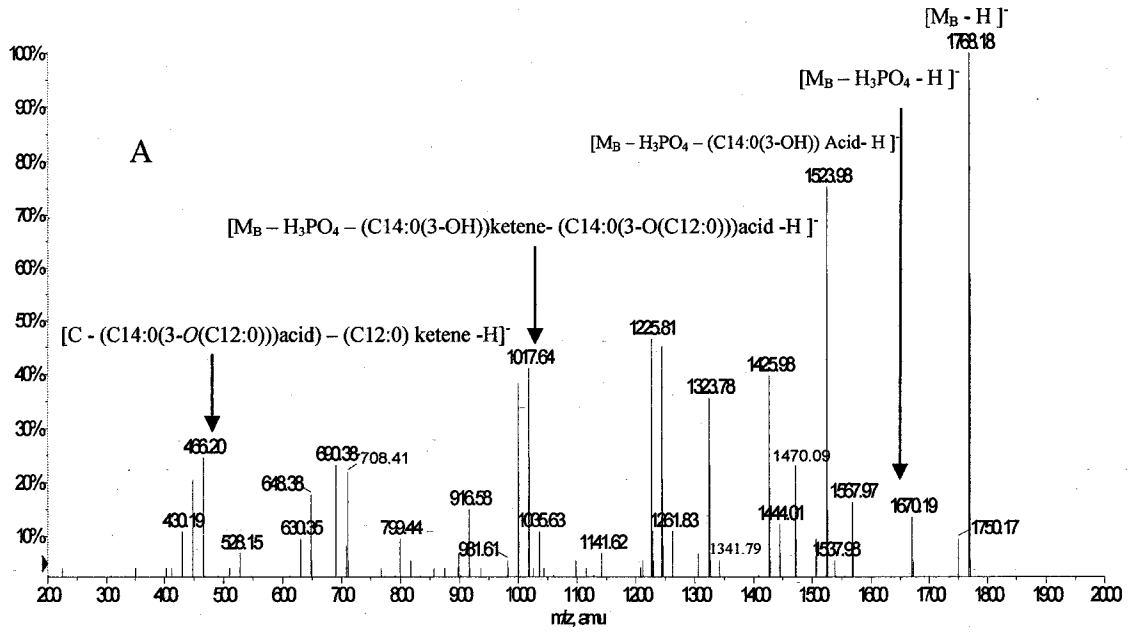


Figure 3-10: Proposed fragmentation pathways of the product ion scan of the diagnostic ion $[C - (C12:0(3-O(14:0)))ketene - H]^+$ observed at m/z 666.3.

The MS/MS of all the remaining ions observed in the conventional ESI-MS (Table 3-1) were also acquired and their fragmentation pathways were rationalized confirming the proposed structure of lipid A. Figure 3-11 shows the MS/MS of the precursor ions, $[M_B-H]^-$ m/z 1768.18, $[M_B - (C12:0)ketene - 2H]^{2-}$ at m/z 792.50, $[M_M - (C12:0)ketene - H]^-$ m/z 1506.04, and $[M_M - (C14:0(3-OH))Ketene - H]^-$ m/z 1462.05. The detailed fragmentation routes and the corresponding structures of the fragment ions are illustrated in figures 3-12, 3-13, 3-14 and 3-15, respectively. The elimination of fatty acids occurs either via charge-remote or charge-driven mechanisms, as discussed earlier. In addition, the presence of inner-sugar fragments can confirm the structure of the precursor ion as well as the proposed structure of other fragment ions. The loss of H_3PO_4 in Figure 3-12 was speculated, for example, to occur on the reducing-end. This assumption is based on the formation of the $^{0,4}A_2$ and the C fragment ions which confirm the presence of the phosphate group at position C-4' of the non-reducing end sugar. Similarly in Figures 3-13 and 3-14, the presence of diagnostic inner-sugar fragments confirmed the localization of the H_3PO_4 group at the non-reducing end. It should be noted that more than one possible fragmentation route can exist in some structures, especially in the case of fatty acid losses. The transition $[M_M-(C12:0)ketene-H]^-$ (m/z 1506.05) \rightarrow $[M_M-(C14:0(3-OH))acid-(C14:0(3-O(C12:0)))H]^-$ (m/z 1053.64) in Figure 3-13, for example, has been illustrated by a loss of (C14:0(3OH) ketene) at position C-3 of the reducing end while (C14:0(3OH) acid) was eliminated on position C-3' of the non-reducing end. The alternative assumption of (C14:0(3OH) ketene) elimination on position C-3' and (C14:0(3OH) acid) loss on position C-3 is also valid as no diagnostic ions were present to confirm either of these closely related structures.



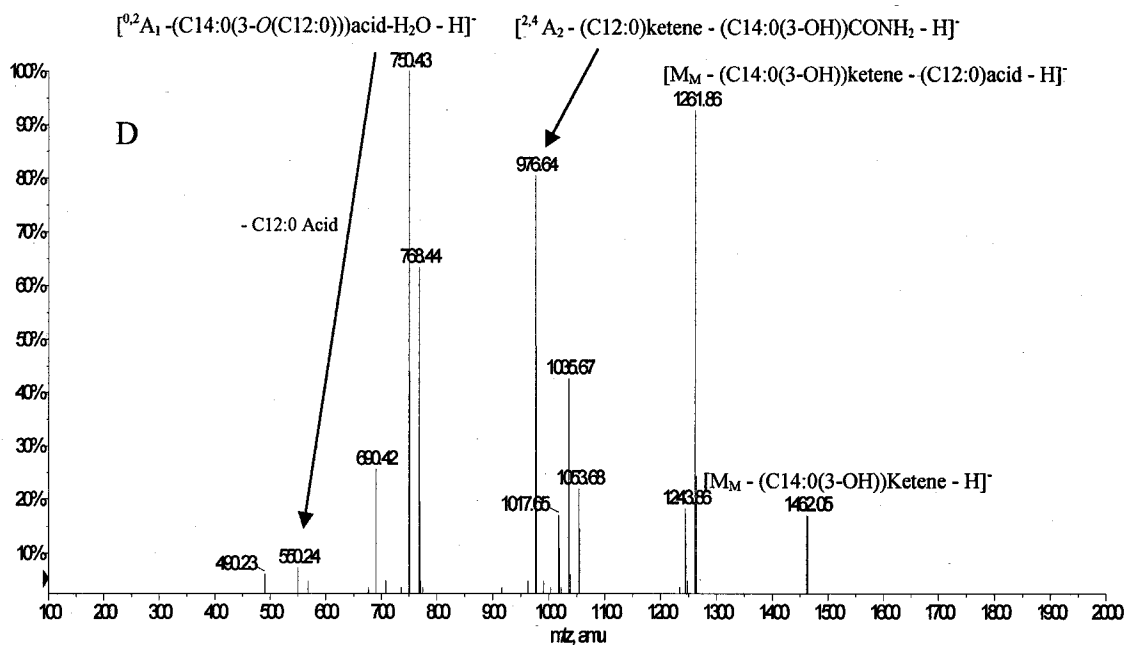
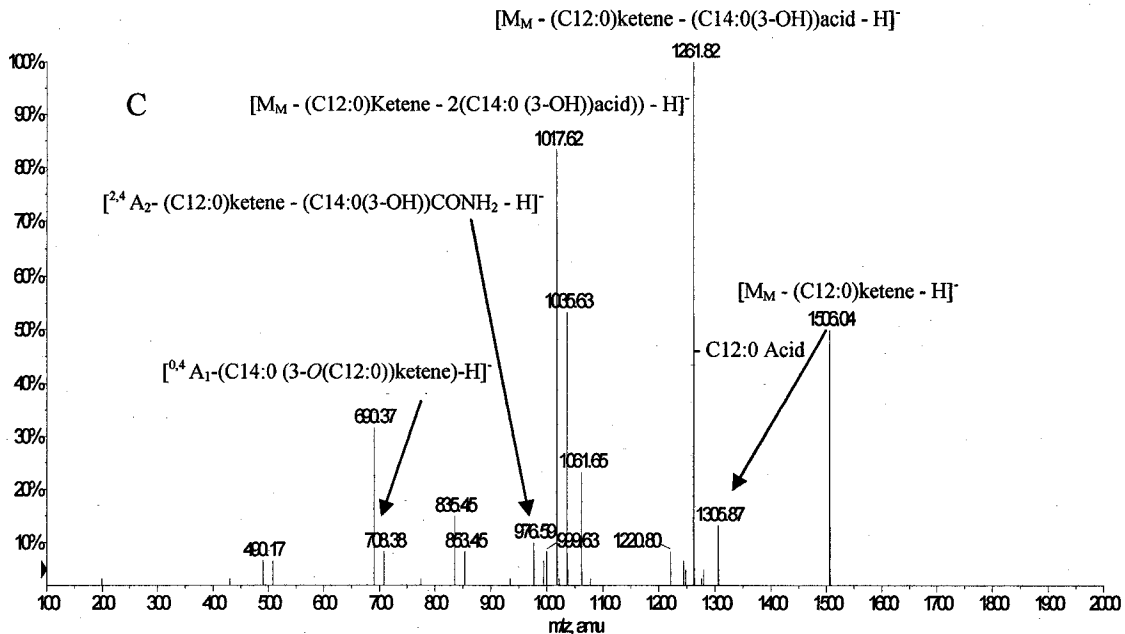
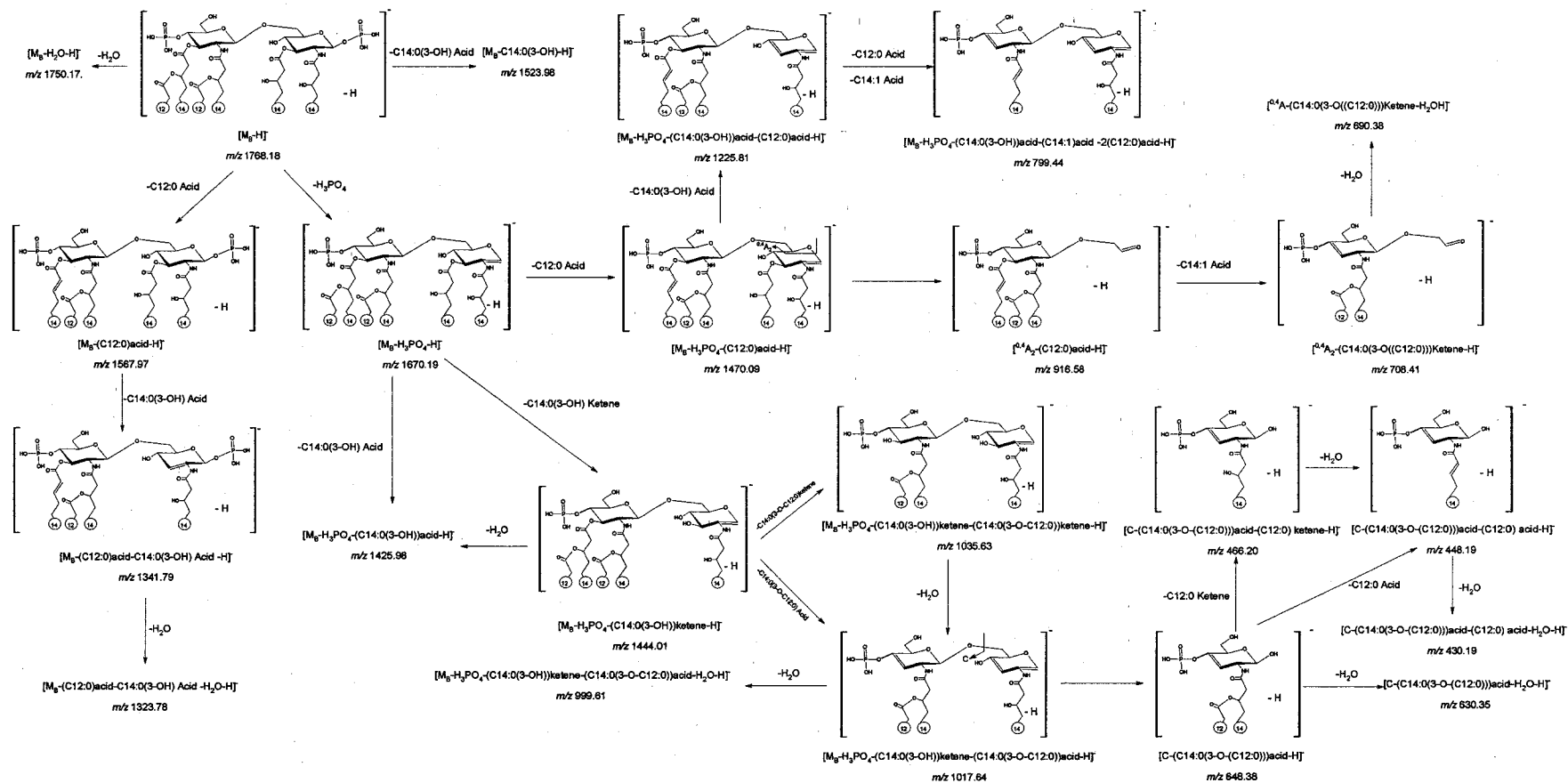


Figure 3-11: Negative ion CID-MS/MS of the ions: $[M_M - (C12:0)ketene - H]^-$ at m/z 1768.18 (A); $[M_B - (C12:0)ketene - 2H]^{2-}$ at m/z 792.50 (B); $[M_M - (C12:0)ketene - H]^-$ at m/z 1506.04 (C); $[M_M - (C14:0(3-OH))Ketene - H]^-$ at m/z 1462.05 (D).



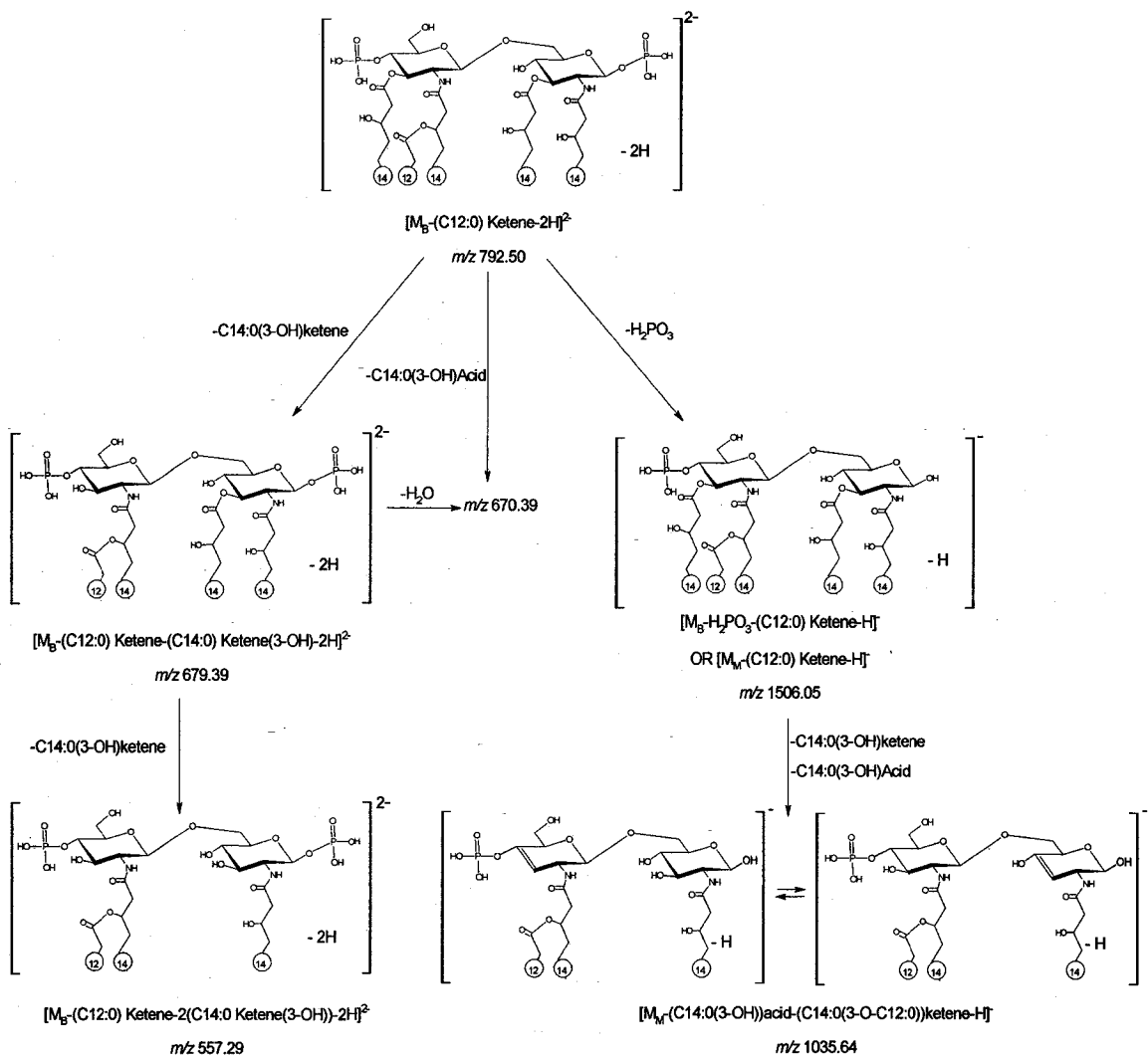


Figure 3-13: Fragmentation pattern of the doubly-charged precursor ion $[M_B-(C12:0) \text{ Ketene-}2H]^{2-}$ observed at $m/z \ 792.50$. Both singly and doubly-charged fragment ions were formed confirming the proposed structure of this precursor.

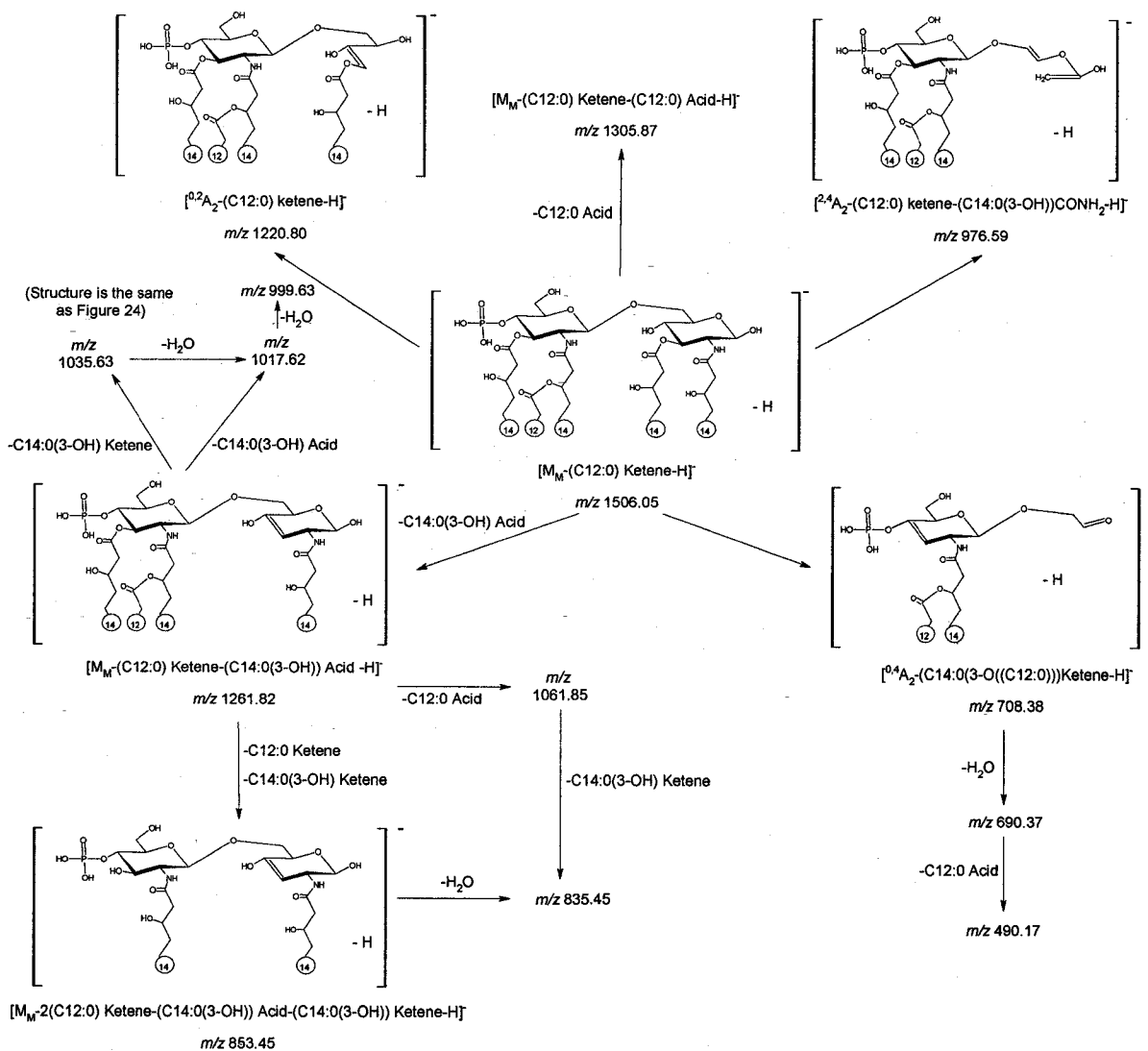


Figure 3-14: Fragmentation routes of the precursor ion $[M_M-(C12:0)Ketene-H]^-$ at m/z 1506.05

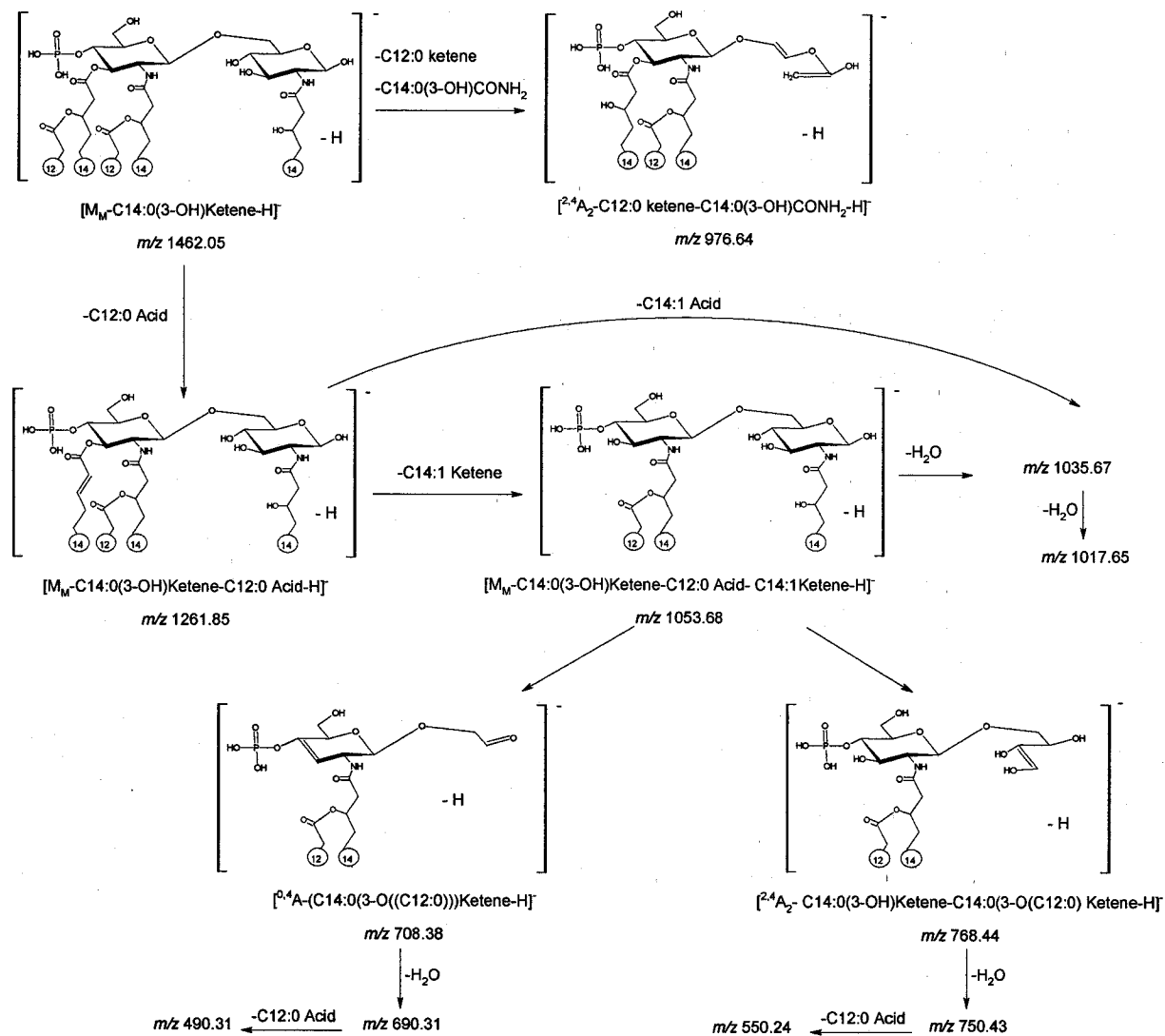


Figure 3-15: Fragmentation pattern of the precursor ion $[M_M-C14:0(3-OH) ketene - H]^-$ at m/z 1462.05.

3.5. Summary:

The chemical structure of lipid A, isolated by mild acid hydrolysis from *Aeromonas salmonicida* lipopolysaccharide, was investigated using electrospray ionization QqTOF hybrid tandem mass spectrometry and showed a great degree of microheterogeneity (El-Aneed & Banoub, 2005). The chemical structure of the main constituent of this heterogeneous mixture was identified as a D-(1→6) linked D-glucosamine disaccharide substituted by two phosphate groups, one being bound to the non-reducing end at position O-4' and the other to position O-1 of the reducing end of the D-glucosamine disaccharide. The location of the fatty acids linked to the disaccharide backbone was established by identifying diagnostic ions in the conventional QqToF-MS scan. Low-energy collision tandem mass spectrometry analysis of the selected precursor diagnostic ions confirmed, unambiguously, their proposed molecular structures. It was established that myristyloxylauric (C14:0(3-O(12:0))) acid residues were both N-2' and O-3' linked to the non-reducing end of the D-GlcN residue, whereas two 3-hydroxy myristic (C14:0(3-OH)) acid chains acylated the remaining positions of the reducing end (El-Aneed & Banoub, 2005). The MS and MS/MS data obtained allowed us to determine the complex molecular structure of lipid A. In addition, the fragmentation patterns were clearly illustrated and established for this biologically-active structure.

CHAPTER 4: Mass Spectrometric Analysis of the Core Oligosaccharide of Wild-Type *Aeromonas salmonicida*

4.1. Background:

In the previous chapter the molecular structure and the fragmentation pattern of the hydrophobic lipid A was demonstrated. The other LPS portion, a hydrophilic polysaccharide, may be further subdivided into the O-specific chain and the core oligosaccharide. The core oligosaccharide is relatively conserved in its structure and composition compared to the O-chain and can be divided into inner and outer subdomains (see Figure 1-10). The inner core oligosaccharides include unique residues characteristic of LPS, namely Kdo (α -3-deoxy-D-manno-oct-2-ulosonic acid) and Hep (L-glycero-D-manno-heptose).

Both O-antigenic carbohydrate chains and core oligosaccharides have been used for biomedical applications such as vaccine and antibody design. It has been shown in the last decade that antibodies directed against the core region of bacterial lipopolysaccharides are of significant clinical interest for their potential of neutralizing or enhancing the manifold biological effects of endotoxins (Di Padova *et al.*, 1993) and their potential use as fish vaccines in aquaculture ventures (Banoub *et al.*, 1989).

The molecular structure of the inner-core region usually contains a α -Kdop-(2 \rightarrow 8)- α -Kdop-(2 \rightarrow 4)- α -Kdop-(2 \rightarrow) trisaccharide as in the structure of the LPS of *Klebsiella pneumoniae* ssp. *Pneumoniae* (Suskind *et al.*, 1995). The LPS of *Chlamydia trachomatis* was shown to contain the disaccharides α -Kdop-(2 \rightarrow 4)- α -Kdop-(2 \rightarrow) and α -

Kdop-(2→8)- α -Kdop-(2→ which were identified by GC-MS (Holst *et al.*, 1992). A feature of some inner core regions of lipopolysaccharides such as the core oligosaccharide of *Yersinia ruckerii*, Serotype II, is the presence of at least one residue of Kdo (Bateman *et al.*, 1996).

The inability to detect Kdo in LPS from the genera *Vibrio* and *Aeromonas* was first pointed out in 1971 (Jackson & Redmond, 1971) and subsequently by Jann *et al.* and by Hisatsune *et al.* for *V. cholerae* (Hisatsune *et al.*, 1982; Jann *et al.*, 1973). Accordingly, it was commonly believed by all researchers that Kdo was absent from the LPS of all members of the *Vibrionaceae* family of gram-negative bacteria, and its absence, as established by the thiobarbiturate-based colorimetric assay (the Weissbach reaction), was used as a characteristic for taxonomic classification (Jann *et al.*, 1973). Nevertheless, the first demonstration of the presence of one residue of Kdo or Kdo-like substance in LPS of the *Vibrionaceae*, family was reported in early 1980s (Banoub *et al.*, 1983), in direct contrast to the generally accepted view of the absence of this compound.

Phosphorylated Kdo units have been isolated from and detected in a number of lipopolysaccharide preparations. Kdo derivatives phosphorylated in position O-5 were released from the lipopolysaccharide of *V. cholerae* Ogawa and Inaba after strong acid hydrolysis. The phosphorylated Kdo was identified by gas-liquid chromatography and mass spectrometry, after reduction and permethylation, as Kdo-5-phosphate (Brade, 1985). Phosphorylated Kdo units have been isolated from various LPS preparations obtained from different types of gram-negative bacteria. It has been shown by Szabo's research group that Kdo derivatives, phosphorylated in position 4, behave differently from the other positional isomers. It was found that at 100°C, they eliminate their

phosphate group with extreme facility in acidic, neutral or alkaline media (Chaby & Szabo, 1975). The olefinic acid presumably formed as the first product produces a derivative of furoic acid by ring closure involving (C-2)-(O-5)-(C-5), (Figure 4-1). Carof and coworkers have shown that in the LPS-2 of *Bordetella pertussis* endotoxin, the Kdo unit was substituted at O-5 by the inner core oligosaccharide portion and also carried a phosphate substituent on the O-4 position. They established that, following mild hydrolysis of the glycosidic bond of the Kdo unit, the phosphate group was easily released and eliminated. They noticed that no furoic acid derivative was produced and the product formed was still attached to the core oligosaccharide portion and could not be identified (Carof *et al.*, 1987). Auzanneau *et al* have shown that mild acid hydrolysis of a Kdo unit which was methylated at O-5 and phosphorylated at position O-4 produced a mixture of type-specific 4,8- and 4,7-anhydro-Kdo units. They proposed that this was most probably the case for a lot of other “Kdo-less” endotoxins or thiobarbiturate negative endotoxins, in which the Kdo terminal reducing end group could not be determined by conventional analysis (Auzanneau *et al.*, 1991).

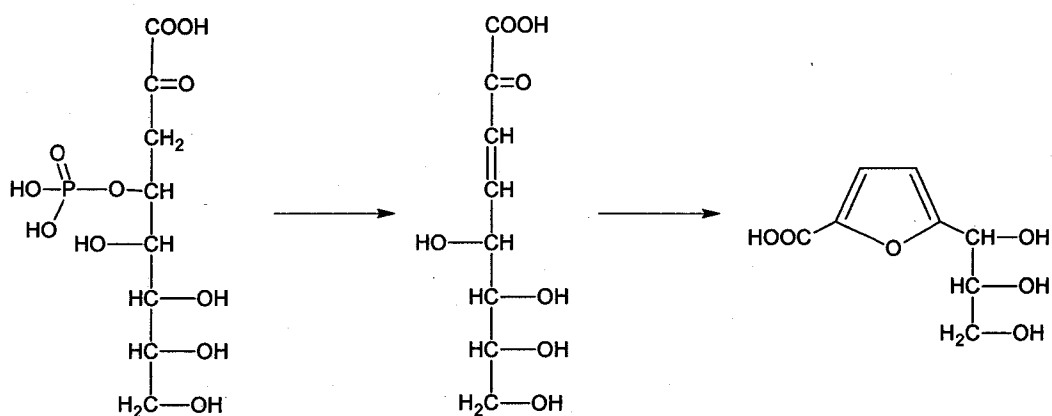


Figure 4-1: Facile elimination of O-4 phosphorylated Kdo to produce a furoic acid derivative by ring closure involving (C-2)-(O-5)-(C-5).

To date, there is no evidence for the occurrence of a phosphorylated Kdo unit within the LPS of *A. salmonicida*. This phosphate group, if present, will be sensitive to acid hydrolysis. Following treatment of the LPS with 1% acetic acid at 100°C for 90 min to glycosidically cleave the lipid A from the rough core oligosaccharide, the O-4 phosphate group is instantaneously eliminated as phosphoric acid to form the core oligosaccharide containing the C-3-C-4 olefinic D-arabino-3-en-2-ulonic acid open chain reducing end (Figure 4-2). This latter oligosaccharide, containing the straight chain olefinic acid at the reducing end of this molecule, undergoes an intramolecular addition reaction between the alcoholic function at C-7 or C-8 to the olefinic double bond, to produce the isomer pairs of 4,8- and 4,7-anhydro derivatives of the enolizable α -keto-acids **3A** and **4A** (Figure 4-3).

In the following sections, the fragmentation pathways of the smooth wild-type core region of *A. salmonicida* have been established for the first time. In addition, this analysis confirmed precisely the molecular structure of the core oligosaccharide, illustrated a decade ago (Shaw *et al.*, 1992). This biological extract is now shown to be a homogeneous mixture of the native core oligosaccharide **2B** (Figure 4-2) and the degraded oligosaccharide containing the isomeric pairs of 4,8- and 4,7- anhydro- α -keto acid derivatives **3A**, **4A** (Figure 4-3), and the open olefinic chain **2A** (Figure 4-2). This was accomplished using a combination of ESI and MALDI mass spectrometry with a QqToF-MS hybrid instrument and low energy collision induced dissociation (CID)-QqToF-MS/MS analyses. The ESI-QqToF-MS/MS analyses and sequencing of the core

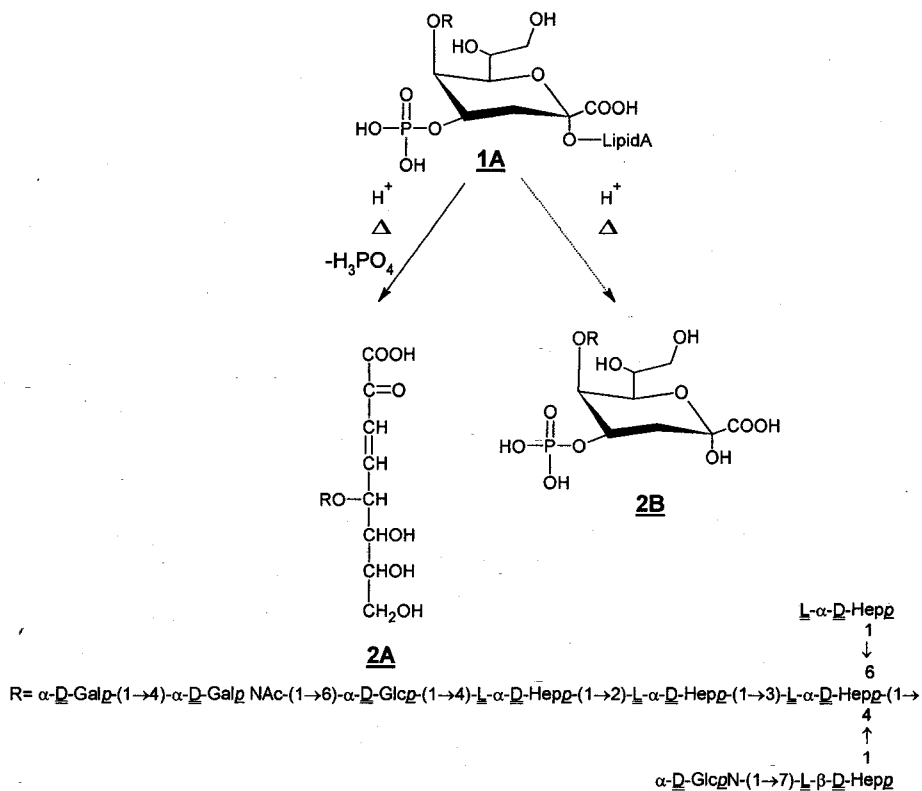
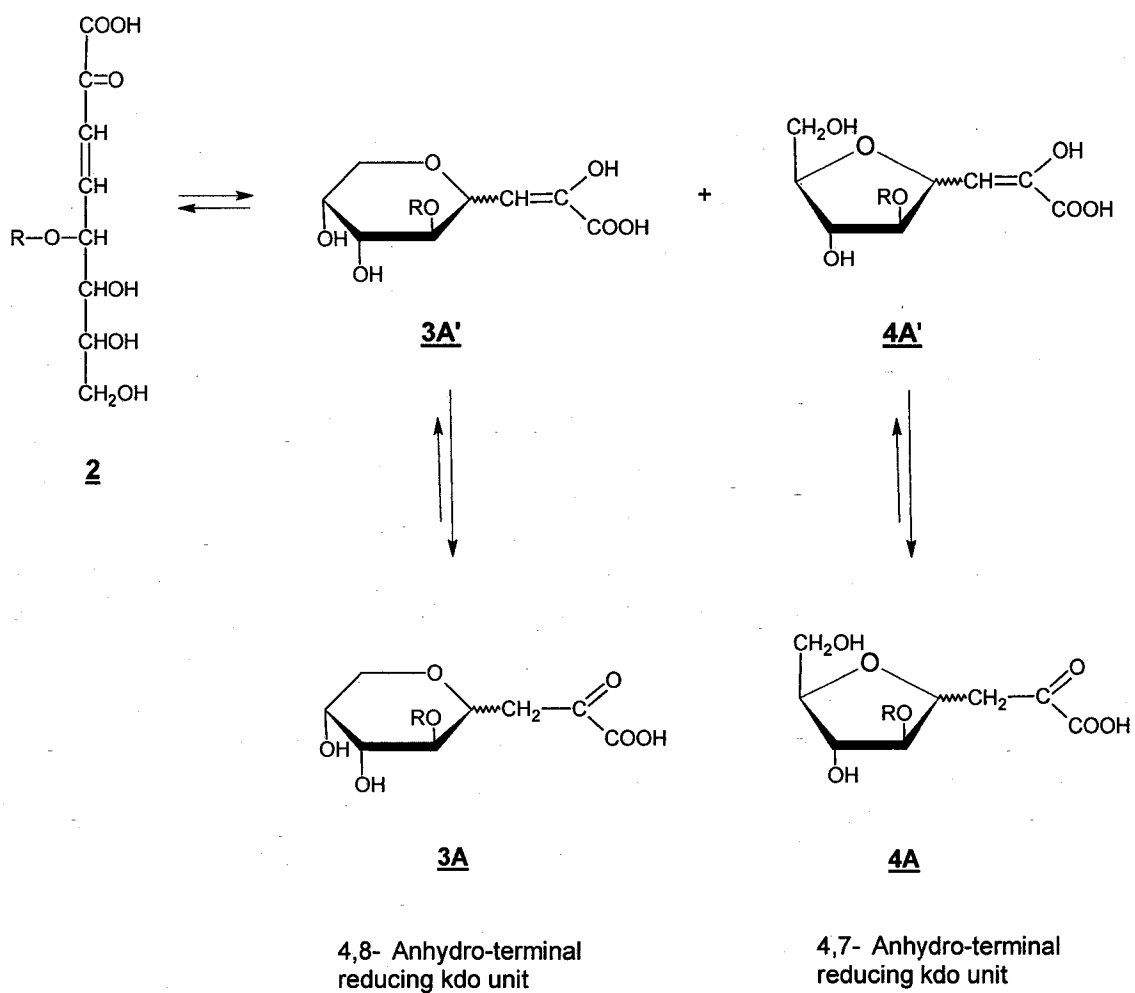


Figure 4-2: Products formed after treatment of the LPS of *A. salmonicida* (Structure 1A) with 1% acetic acid at 100°C for 90 minutes. Two products are formed, the core bearing the intact O-4-phosphorylated Kdo (2B) and the the C-3-C-4 olefinic D-arabino-3-en-2-ulonic acid open chain (2A).



R = core oligosaccharide glycosyl portion

Figure 4-3: Formation of the dephosphorylated core oligosaccharide containing the diastereomeric mixture of the 5-*O*-glycosylated 4,8-anhydro- and 4,7-anhydro derivatives of the enolizable α -keto-acid.

oligosaccharide containing the intact *O*-4 phosphorylated Kdo residue, and, the remainder of the homogenous mixture of the dephosphorylated core oligosaccharide, allowed the exact identification of a series of diagnostic protonated molecular ions. The stereospecific fragmentation routes obtained during the tandem mass spectrometric analyses are also illustrated.

Furthermore, concrete MS/MS evidence of the presence of the intact *O*-4 phosphorylated and *O*-5 glycosylated reducing end terminal Kdo residue **2B** and the 4,8- and 4,7-anhydro derivatives **3A** and **4A** of the enolizable α -keto acids, in this cleaved core oligosaccharide homogeneous mixture is presented. Similarly, the low energy CID-MS/MS experiments performed on the permethylated samples precisely confirmed the structure of the degraded core oligosaccharides, containing the isomers 4,8- and 4,7-anhydro α -keto acid dephosphorylated Kdo terminal reducing end residue. Also, notable was the complete permethylation of the *O*-5 glycosylated *D*-arabino-3-en-2-ulonic acid, open terminal chain, **2A**, providing direct evidence for the presence of this open chain unit.

4.2. MS analysis of the homogenous mixture of the core oligosaccharide:

4.2.1. Negative-ion mode QqToF-MS analysis:

The homogeneous mixture of the core oligosaccharides obtained after cleavage from the lipid A was analyzed by electrospray mass spectrometry in the negative ion mode. The ESI-QqToF-MS, measured with a declustering potential (DP)= -100V (Figure 4-4), showed the presence of an unforeseen ion at m/z 982.2939. This ion was assigned as the deprotonated molecule $[M_{P_{O_4}-2H}]^{2-}$ of the intact *O*-4 phosphorylated and *O*-5

substituted α -D-*manno*-octulosonic acid Kdo in the pyranose form **2B**. This native core oligosaccharide containing the intact O-4 phosphorylated Kdo molecule, was assigned the empirical formula of $C_{69}H_{117}N_2O_{60}P$, corresponding to an observed and calculated monoisotopic mass of 1966.60 Da, and 1966.61 Da, respectively.

The deprotonated molecules $[M-2H]^{2-}$ at m/z 933.3015 and $[M-H]^-$ at m/z 1867.6866 were also observed. This species is consistent with a core oligosaccharide composed of nine glycone units, having an empirical formula of $C_{69}H_{116}N_2O_{56}$, observed M_r 1868.69 Da, calculated M_r 1868.63 Da. It should be noted that the same structure of the core oligosaccharide containing the 4,8-anhydro- α -keto acid derivatives **3A** (or **3A'**) has the same molecular mass. The same could be corroborated for compounds **2A** and **4A**, meaning that when recording a conventional mass spectrum of a series of underivatized diastereoisomers with a one stage instrument (one analyzer), it is not possible to know the exact structure of the population of all the ions produced, as these have the same masses.

The rationale behind the formation of the intact $[M_{PO_4}-2H]^{2-}$ O-4 phosphorylated Kdo deprotonated molecule, is that the treatment of the LPS with 1% acetic acid at 100° C for 90 minutes, is not long enough to promote the complete elimination of the C-3-C4 phosphoric acid to form the open chain **2A** olefinic compound D-*arabino*-4-O-phosphate-3-en-2-octulonic acid. Some O-4 phosphorylated Kdo units remain attached intact to the core oligosaccharide region. MS in the negative ion mode was, however, sensitive enough to detect this minor ion and due to the presence of the phosphate group, this ion was dominant in the spectrum under the experimental conditions.

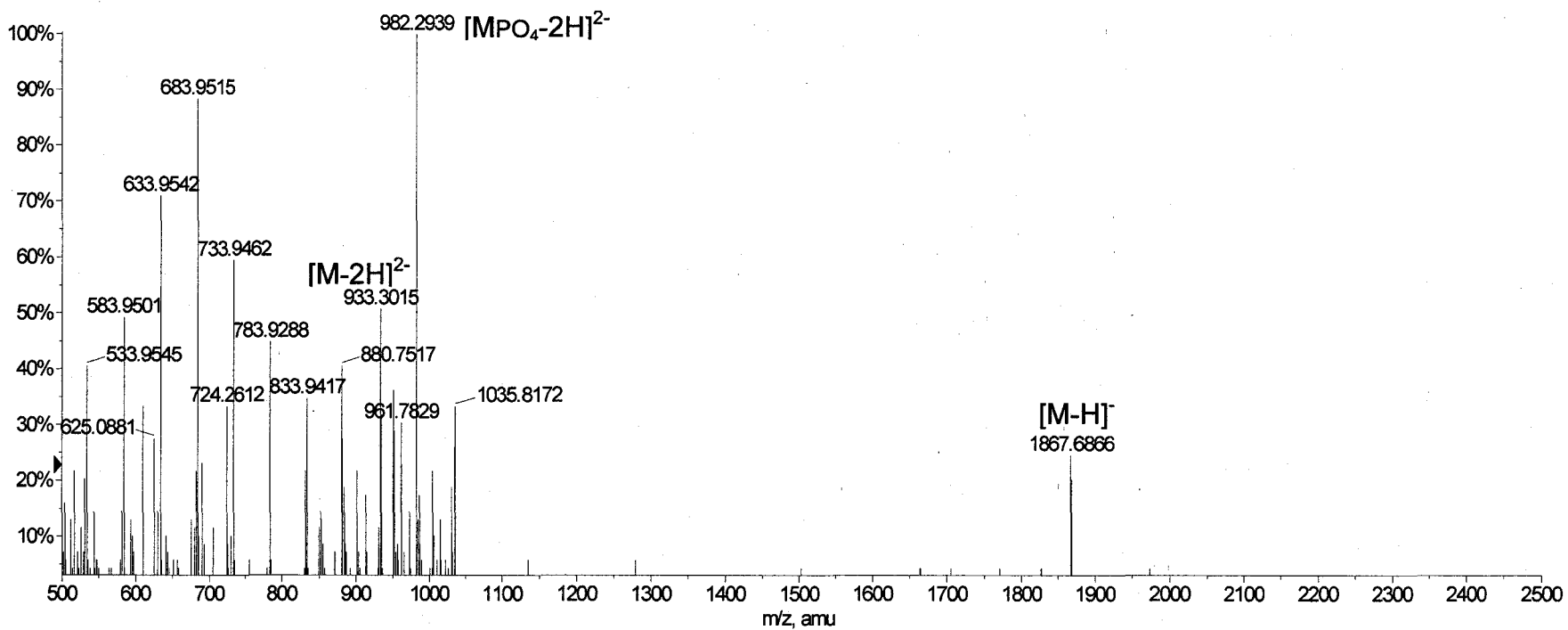


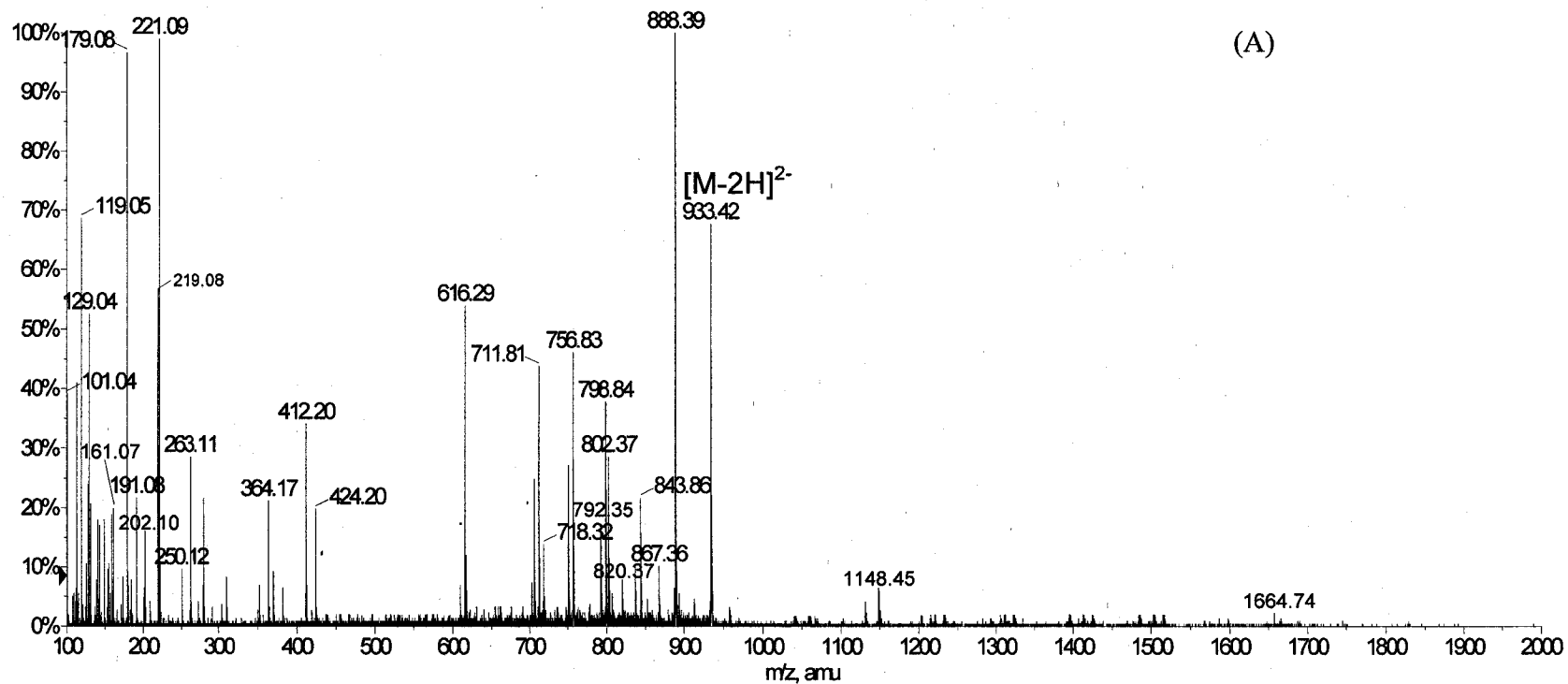
Figure 4.4: Negative ion mode ESI-MS spectrum of the homogeneous core oligosaccharide mixture using a declustering potential (DP) of -100V

4.2.2. Negative-ion mode MS-MS analysis:

Structural information on the glycone sequence of oligosaccharides was obtained using tandem mass spectrometry. The unique dissociation patterns of the precursor ions provided diagnostic product ions, which facilitate the glycone sequences, and may be helpful in the discrimination of the various isomeric structures of the product ions.

The low energy ESI-CID-QqToF-MS/MS (CE=40eV) of the precursor deprotonated molecules $[M-2H]^{2-}$ at m/z 933.3015 is shown in Figures 4-5 and 4-6. The proposed fragmentation routes obtained were rationalized by using the scheme for systematic nomenclature of carbohydrate fragmentation using FAB MS/MS proposed by Domon and Costello to describe the putative fragmentation process (Domon & Costello, 1988a; Domon & Costello, 1988b).

The product ion scan of the deprotonated molecule $[M-2H]^{2-}$ at m/z 933.3015 appears to contain several diagnostic dissociation patterns. As can be seen in Figures 4-5 and 4-6, several different major series of diagnostic product ions, namely: the [A]⁻, [B]⁻ and [C]⁻ series, in which charge retention occurs on the non-reducing part of this core oligosaccharide; and the [X]⁻, [Y]⁻ and [Z]⁻ series in which charge retention occurs at the reducing end, were observed. Notably, the presence of the major abundant product ions at m/z 888.39 as the $[^{0,3}X_6]^{2-}$ product ion; m/z 798.84 assigned to the $[^{0,3}X_5-H_2O]^{2-}$ product ion; m/z 756.83 assigned as the $[M-2H-(GlcN1\rightarrow 7Hep)]^{2-}$ product ion; m/z 711.81 assigned as the $[^{0,3}X_6-(GlcN1\rightarrow 7Hep)]^{2-}$; m/z 616.29 assigned as the $[^{1,4}A_4-H]^-$ product ion, and m/z 412.20 assigned as the $[^{2,5}A_6-B_5]^-$ product ion was observed. Some of the diagnostic product ions belonging to the [Z]⁻ series are illustrated in Figures 4-5 and 4-6.



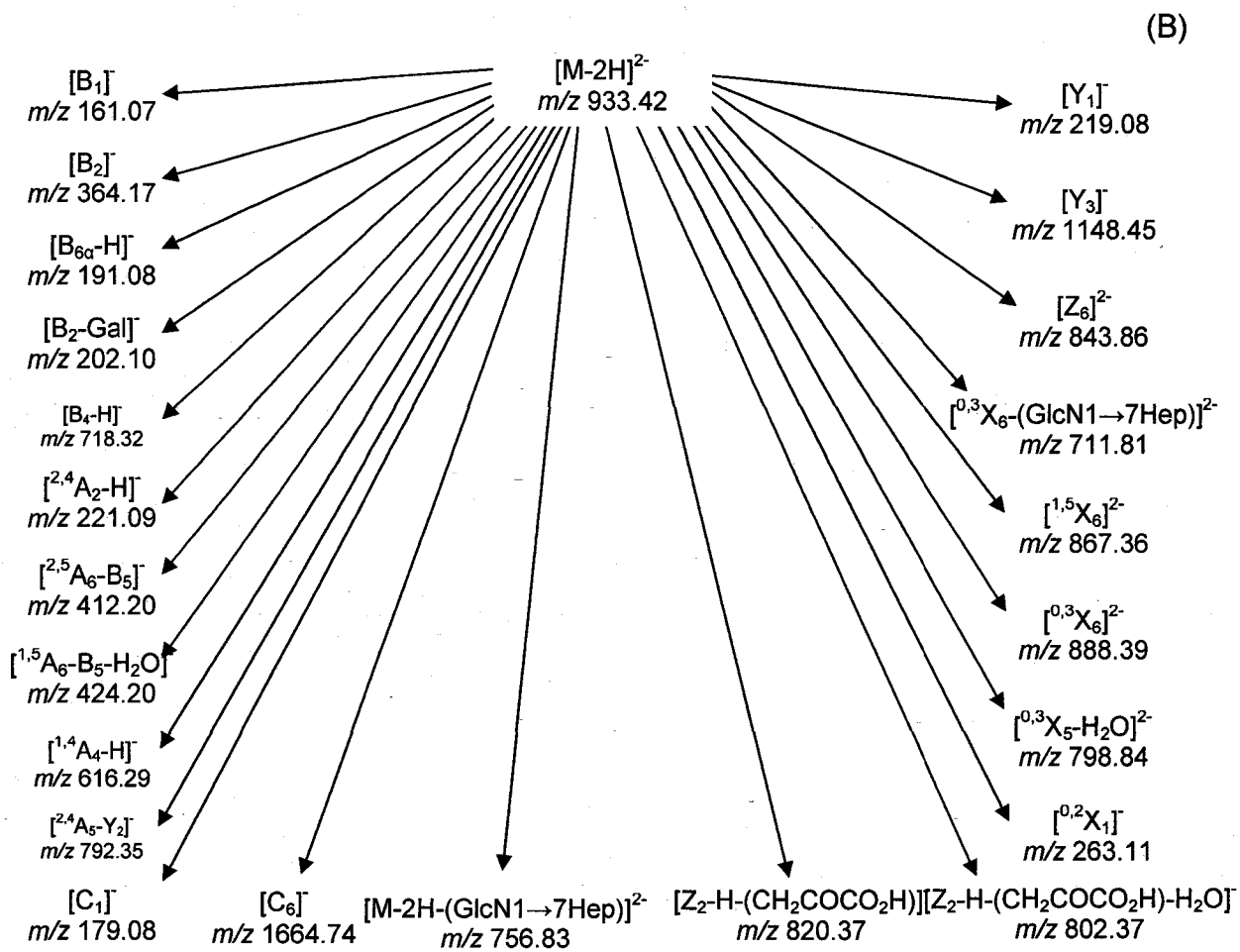


Figure 4-5: (A) ESI-MS/MS spectrum of the precursor ion $[M-2H]^{2-}$ at m/z 933.30.
 (B) The proposed fragmentation routes and the product ions of $[M-2H]^{2-}$.

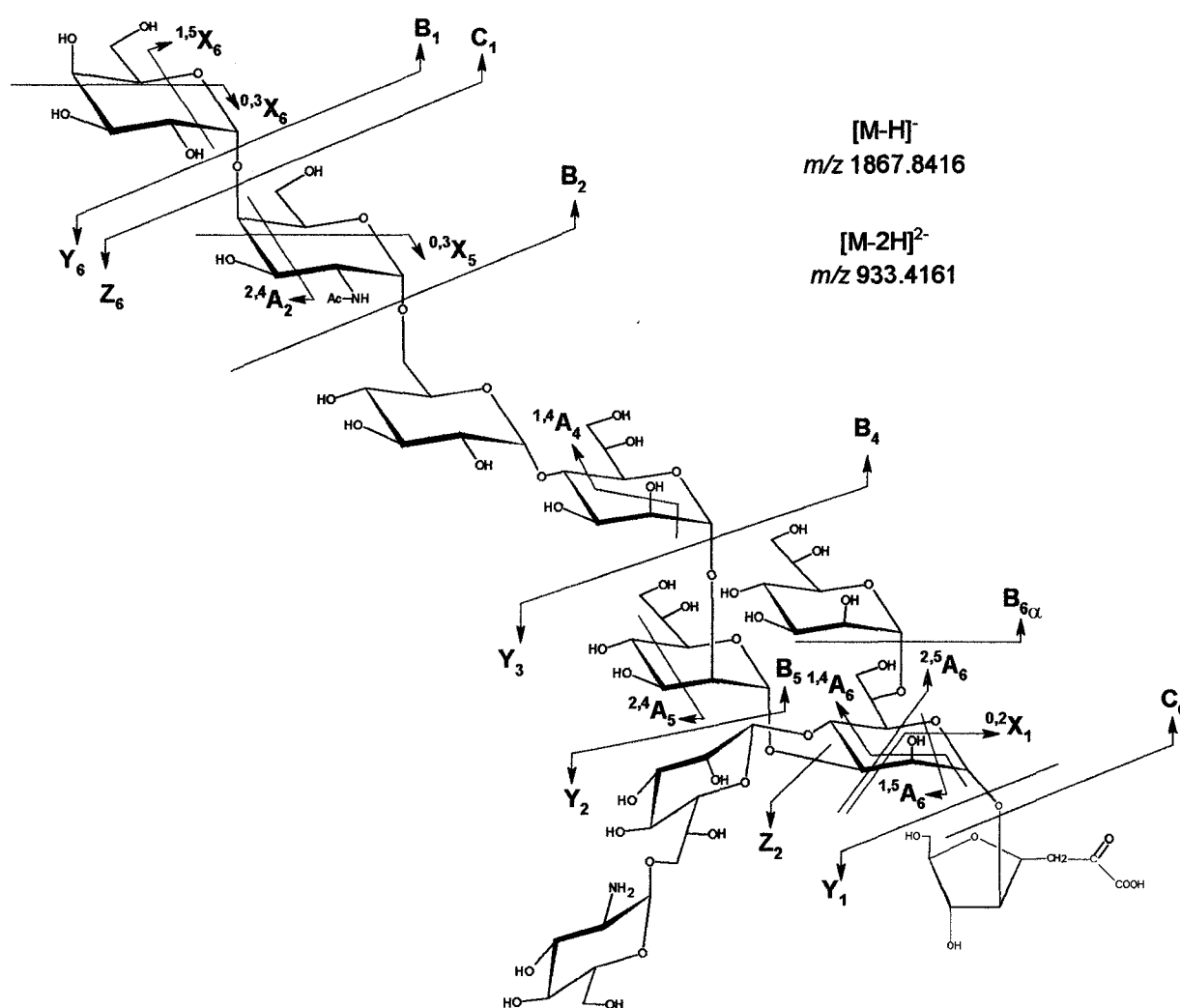


Figure 4-6: Schematic representation of the fragmentation pattern of the core oligosaccharide of *A. salmonicida* recorded in the negative ion mode. ESI-MS/MS common fragmentation routes of both the $[M-H]^-$ and $[M-2H]^{2-}$ at m/z 1867.68 and 933.30, respectively are shown in red. Fragmentation patterns exclusive to the $[M-H]^-$ and $[M-2H]^{2-}$ are shown in blue and green, respectively.

The product ion scan of the precursor deprotonated molecule $[M-H]^-$ at m/z 1867.63 shown in Figure 4-7A, afforded less dissociation than the deprotonated precursor ion $[M-2H]^{2-}$. The formation of the product ions are illustrated in Figure 4-7B and Figure 4-6, all of which are straightforward dissociations of the precursor ions. Some of the diagnostic product ions obtained from the $[X]^-$, $[Y]^-$ and $[Z]^-$ series and two diagnostic product ions at m/z 820.37 and 802.36, assigned as $[Z_2-H-CH_2COCO_2H]^-$ and $[Z_2-H-CH_2COCO_2H-H_2O]^-$, are illustrated in Figure 4-8, and confirms, without doubt, the ubiquitous presence of the 4,7-anhydro- α -keto acid (terminal reducing end).

It should be noted that, for simplicity, derivative **4A** from the obtained homogeneous mixture of oligosaccharide has been chosen to illustrate all of the ESI-CID-QqToF-MS/MS fragmentations described in this rationale. The same fragmentation routes are expected to be identical for the olefinic open chain derivative **2A** and the anomeric mixtures **3A**, **3A'** and **4A'**.

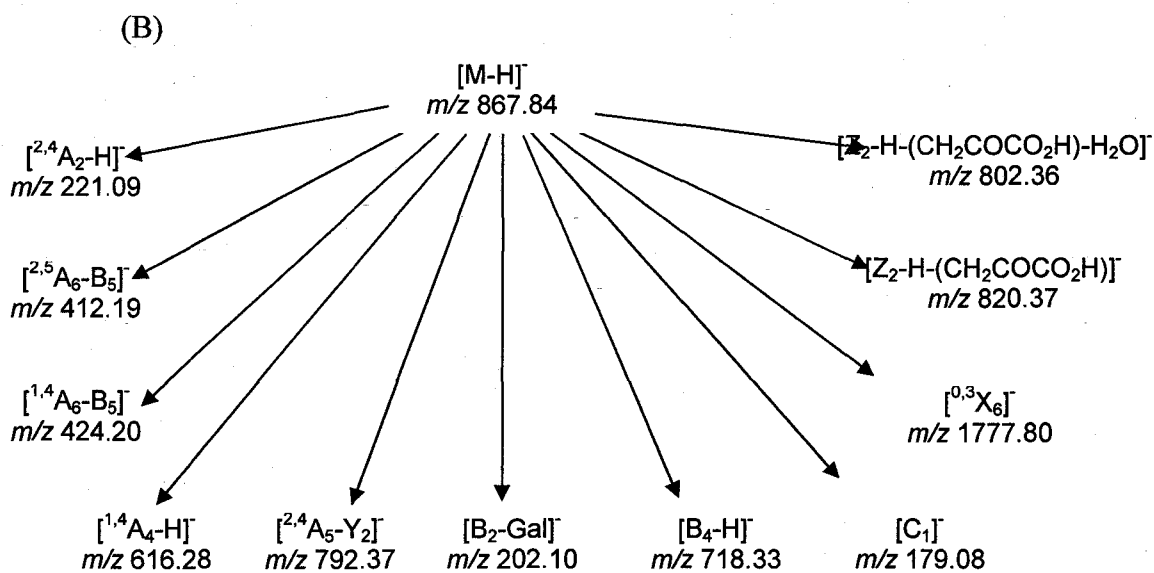
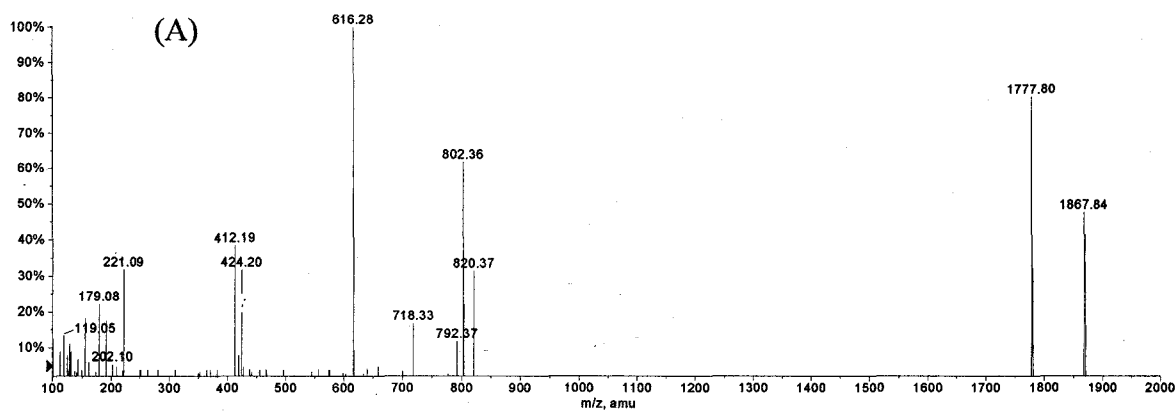


Figure 4-7: (A) ESI-MS/MS spectrum of the precursor ion $[M-2H]^-$ at m/z 1867.84. (B) The proposed fragmentation routes and the product ions of $[M-2H]^-$.

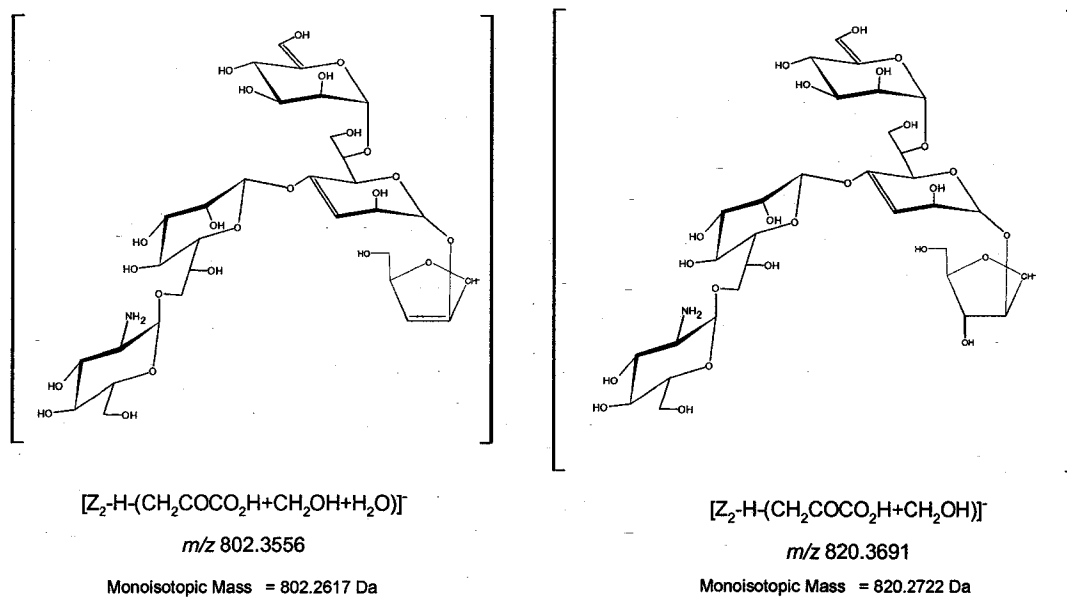


Figure 4-8A

Figure 4-8: Diagnostic Z-type product ions resulting from the low energy CID-MS/MS of both the $[M-2H]^{2-}$ and $[M-H]^-$ precursor ions are illustrated.

4.2.3. MS/MS evidence for the presence of phosphorylated Kdo unit within the core oligosaccharide:

The previous section has confirmed the sequence of the LPS core region isolated from *A. salmonicida* and provided indirect evidence for the presence of an O-4 phosphorylated Kdo reducing end unit. The presence of this phosphate group can be established by evaluating the fragmentation pattern of the ion $[M_{PO_4-2H}]^{2-}$ observed at m/z 982.29 in the single-stage MS-ToF experiment (see Figure 4-4).

The product ion scan of the precursor deprotonated molecule $[M_{PO_4-2H}]^{2-}$ selected from the intact phosphorylated Kdo at m/z 982.2939 is shown in Figure 4-9. The most striking aspect of this product ion scan is that when it was recorded with a collision energy of 40 eV and a CID gas pressure = 4, the formation of only the doubly and singly charged species of the dephosphorylated form of this oligosaccharide containing the 4,7-anhydro- α -keto acid was observed. Thus the $[M_{PO_4-2H}]^{2-}$ ion at m/z 982.2939 dissociated by the elimination of phosphoric acid to afford the $[M-2H]^{2-}$ and $[M-H]^-$ product ions at m/z 933.33 and 1867.71, respectively. This instantaneous elimination from C-3-C-4 affords the deprotonated molecules obtained from the olefinic *D-arabino*-3-en-2-ulonic acid open chain reducing end.

This finding is in agreement with the phosphorous content analysis (FisKe & Subbarow, 1925), performed kindly by Dr. P. Davis, Department of Biochemistry, Memorial University of Newfoundland, of the cleaved lipid A and the complete LPS that indicated a phosphate content of 2 mol/mol for lipid A and 3 mol/mol for LPS.

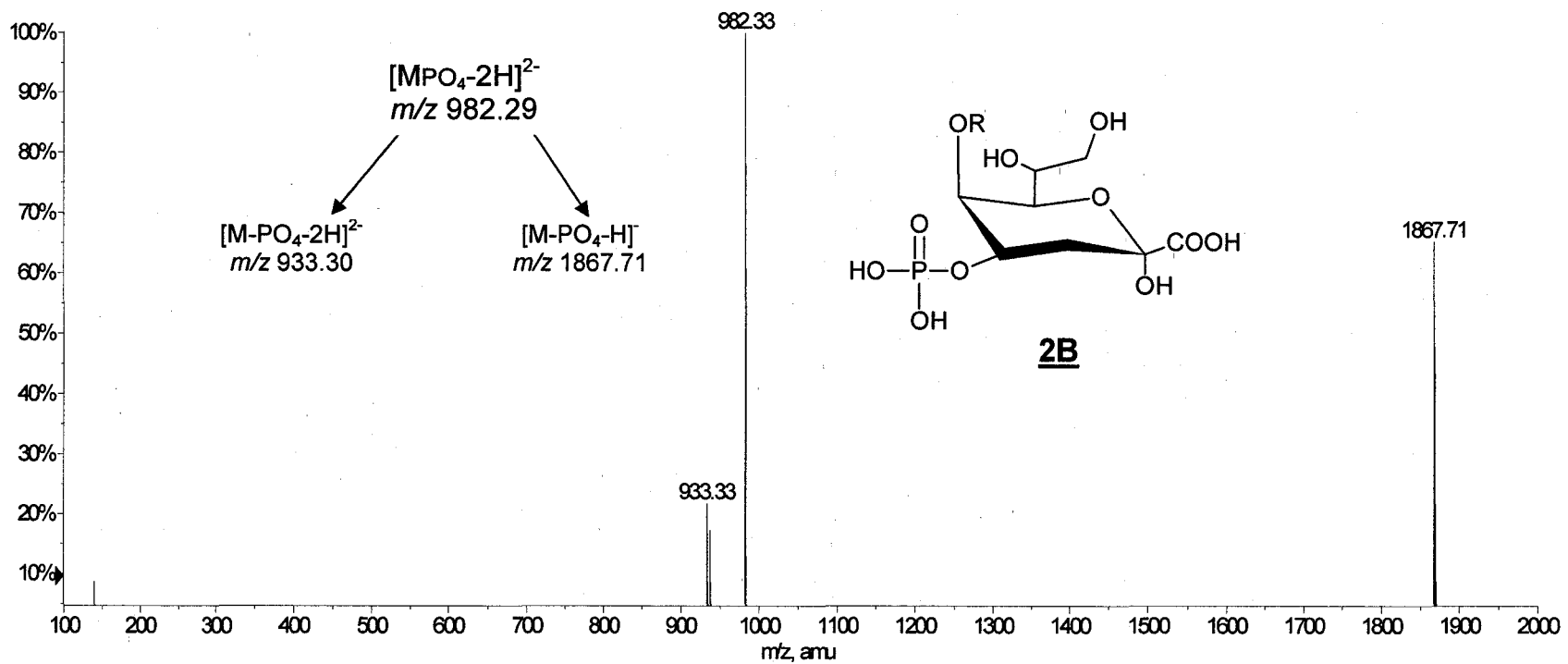


Figure 4-9: ESI-MS/MS spectrum and the proposed product ions of the precursor ion $[MPO_4-2H]^{2-}$ at m/z 982.29

This is due to the fact that acid hydrolysis would cleave a significant portion of the phosphate group; the presence and the location of which being on the Kdo was only established by MS and MS/MS analysis. The negative ion mode analysis was of great importance as it facilitates the production of the doubly charged species $[M_{P04-2H}]^{2-}$.

4.2.4. Positive-ion mode MS and MS/MS analysis:

The homogeneous mixture of degraded core oligosaccharide was dissolved in a mixture of water/methanol/formic acid and electrosprayed in the positive ion mode. The ESI-QqToF-MS, measured with declustering potential (DP)=80V, is shown in Figure 4-10. The protonated molecules $[M+2H]^{2+}$ at m/z 935.3332 and $[M+H]^+$ at m/z 1869.6236 were observed. It should be stated that increasing the DP values (up to 150), in both the negative- and positive-ion MS analysis modes, enhanced the formation of the singly charged species in comparison to other ions.

The product ion scan and the fragmentation pattern of the di-protonated molecule $[M+2H]^{2+}$ at m/z 935.33 is shown in Figures 4-11 and 4-12. The fragmentation to afford the series of diagnostic product ions is self explanatory, and these were shown to be straightforward dissociations mainly occurring from the terminal reducing end of the molecule. A diagnostic product ion $[Y_6+2H]^{2+}$ was observed at m/z 854.37 from the non-reducing end of the core oligosaccharide (Figure 4-12).

The product ion scan of the protonated molecule $[M+H]^+$ at m/z 1869.62, shown in Figure 4-13, indicated a series of diagnostic product ions (Figure 4-12 and Figure 4-13). Once more the genesis of the product ions is self explanatory and does not need to be further discussed.

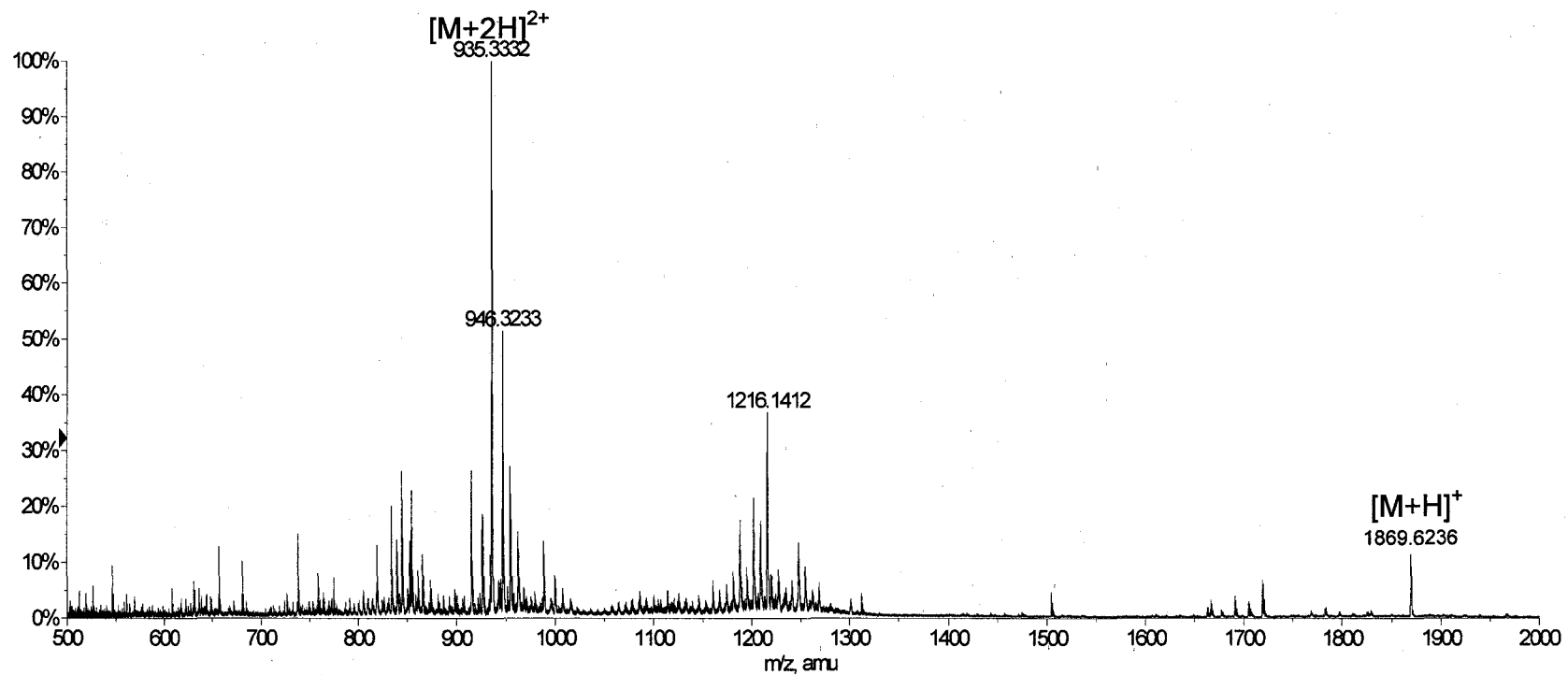


Figure 4-10: Positive ion mode ESI-MS spectra of the homogeneous core oligosaccharide mixture using a declustering potential (DP) of 80V.

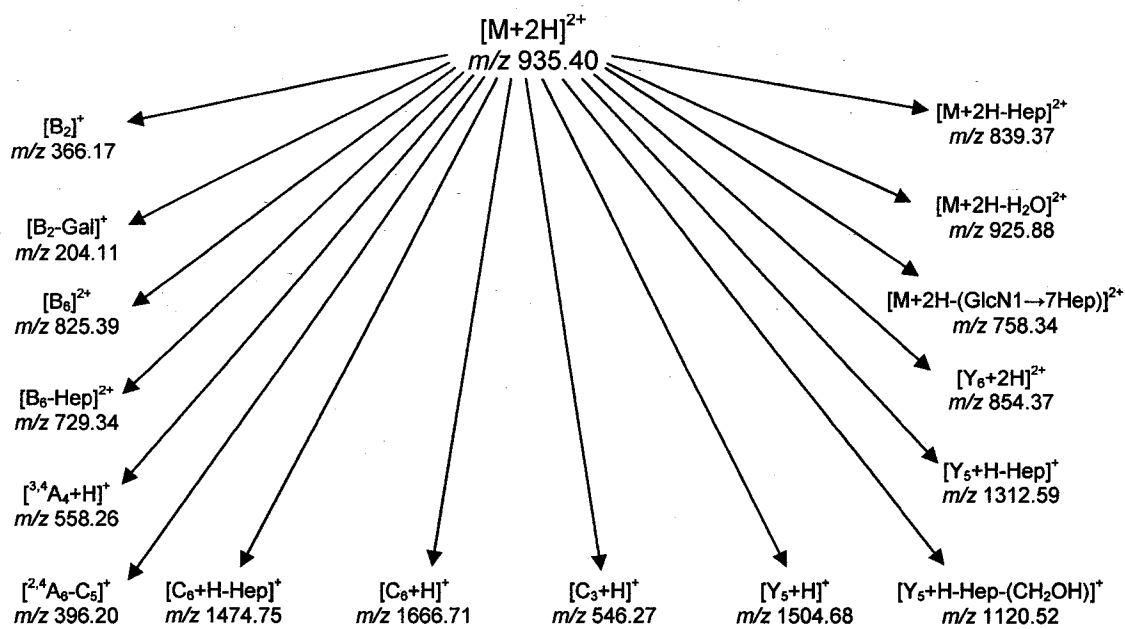
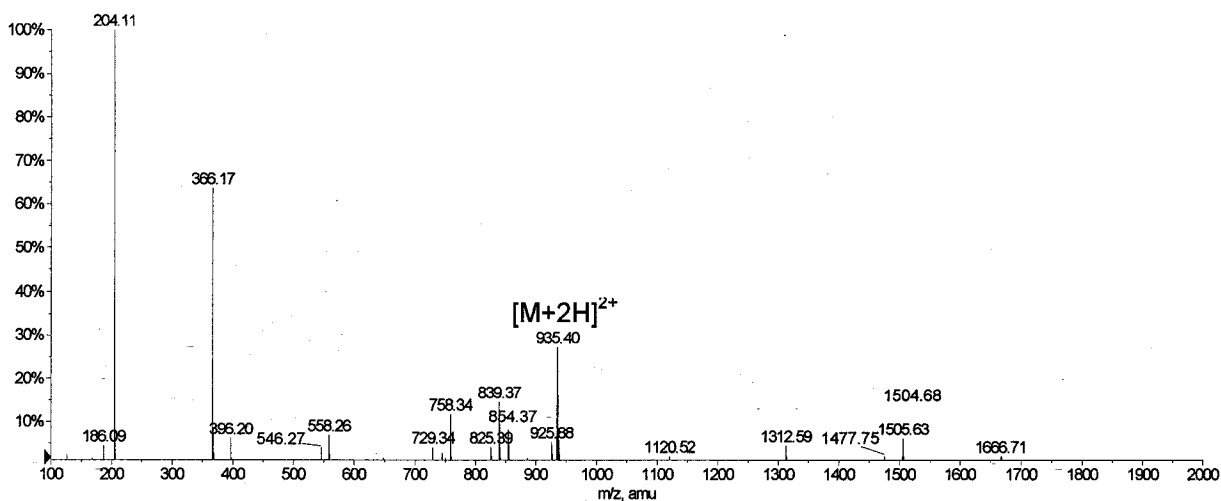


Figure 4-11: Positive ion mode ESI-MS spectra of the homogeneous core oligosaccharide mixture using a declustering potential (DP) of 80V. The proposed fragmentation routes and product ions are also shown.

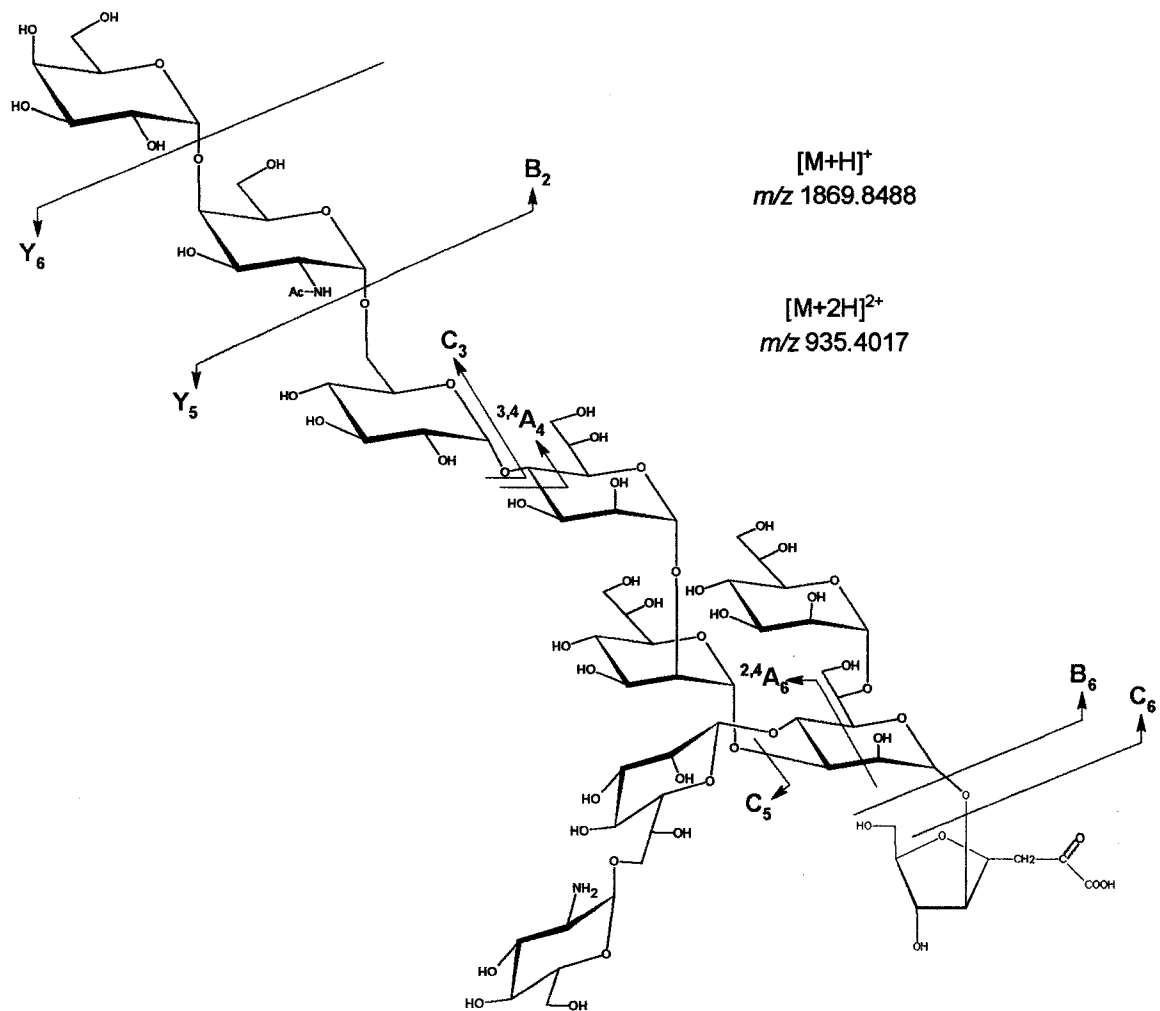


Figure 4-12: Fragmentation pattern of the core oligosaccharide of the wild-type *A. salmonicida* recorded in the positive ion mode. ESI-MS/MS common fragmentation routes of both the $[M+H]^+$ and $[M+2H]^{2+}$ at m/z 1869.62 and 935.33, respectively are shown in red. Fragmentation routes exclusive of $[M+2H]^{2+}$ are shown in green.

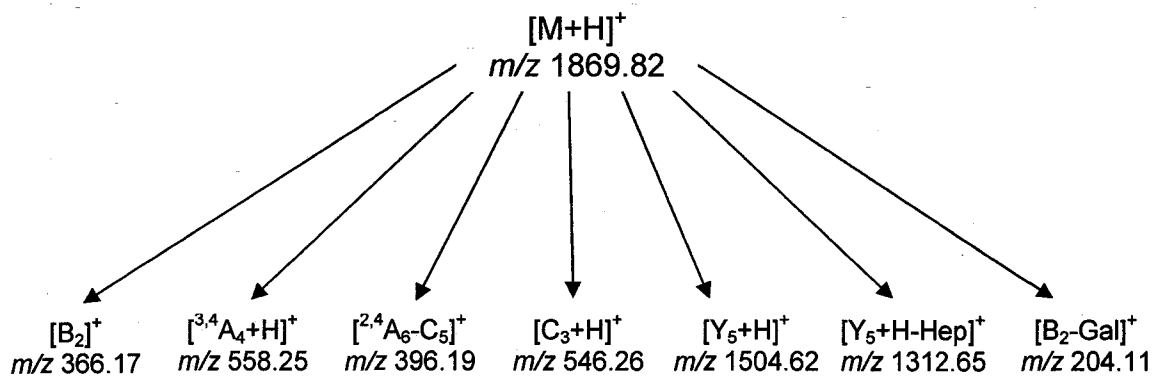
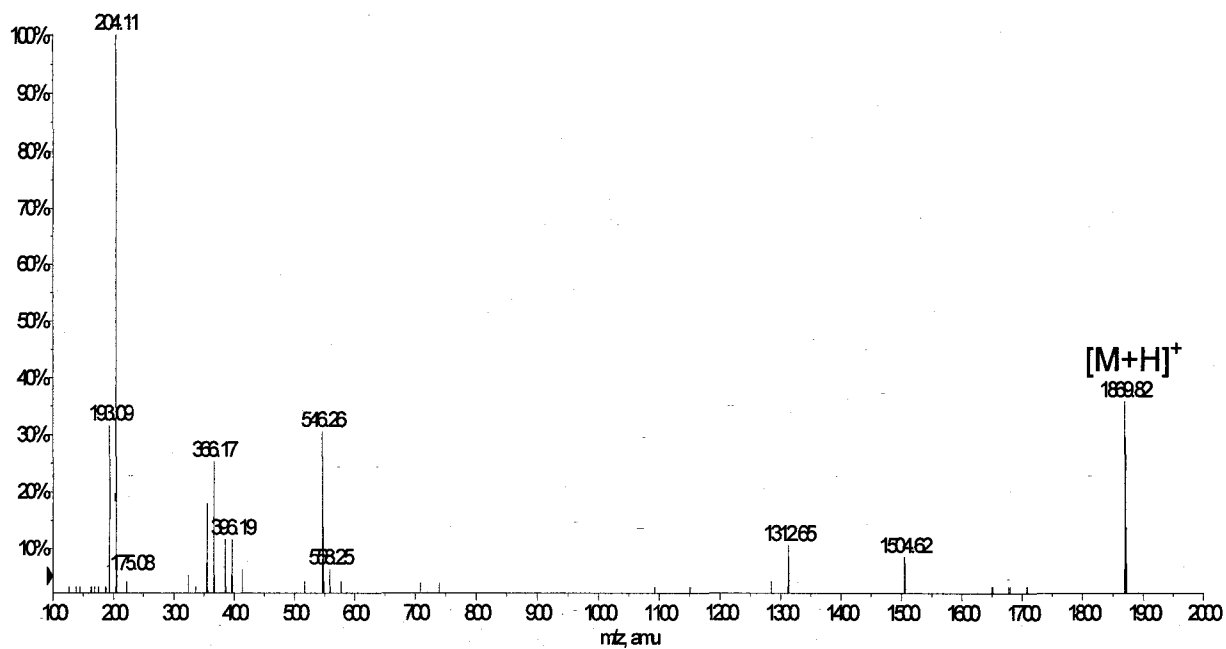


Figure 4-13: ESI-MS/MS spectrum of the precursor $[M+H]^+$ at m/z 1869.62 and the proposed fragmentation routes of the product ions.

It is interesting to note the absence of the $[M_{PO_4+2H}]^{2+}$ and the $[M_{PO_4+H}]^+$ species in the positive mode ESI-MS. This was not surprising considering that under the experimental conditions the negative charges were most likely localized on the phosphate group. This clearly illustrates that the core bearing intact *O*-4 phosphorylated Kdo is a minor constituent within this complex mixture.

4.3. MS analysis of the permethylated core oligosaccharide:

4.3.1. QqToF-MS:

The permethylated core oligosaccharide mixture, dissolved in methanol, was electrosprayed in the positive ion mode. The ESI-QqToF-MS is shown in Figure 4-14A and indicates the presence of a multitude of protonated $[M_n+H]^+$ in addition to the diprotonated molecules $[M_n+2H]^{2+}$ and the sodiated cluster $[M_n+H+Na]^{2+}$. The observed molecular masses of the obtained series were compared to the calculated molecular masses of the expected products, and these are presented in Table 4-1.

The formation of the $[M_{NHMe}+H]^+$ ion at m/z 2374.2003, which is consistent with an empirical formula $C_{105}H_{189}N_2O_{56}$ resulting from the incorporation of 36 methyl groups was observed. This is due to the presence of the free amino group on the D-glucosamine residue, which tends to form NHMe in addition to NMe_2 (Banoub *et al.*, 1984). The $[M+H]^+$ ion at m/z 2388.2289, which is consistent with an empirical formula of $C_{106}H_{191}N_2O_{56}$, results from the incorporation of 37 methyl groups. The remaining $[M_n+H]^+$ ions of this series is indicated in Table 4-1. The incorporation of 38 methyl groups to form the $[M_1+2H]^{2+}$ ion involves the formation of the enol form of the 4,7-anhydro- α -keto acid derivative **4A'**. The incorporation of 39 methyl groups to form the

$[M_2+2H]^{2+}$ was, however, attributed to an extra C-methylation of the H-3 olefinic proton in the enol form of the 4,7-anhydro derivative **4A'**. The QqToF-MS of this permethylated homogeneous mixture reflects the complexity of the composition, and the number of diastereomers of these oligosaccharide series. This was not quite as evident from the conventional ESI-QqToF-MS of the underivatized homogeneous oligosaccharides mixture.

The incorporation of 40 methyl groups to form the $[M_3+2H]^{2+}$ was attributed, once more, to an extra C-methylation on C-5 of the 4,7-anhydro-derivative **4A'**. The incorporation of 41 methyl groups to form the $[M_4+2H]^{2+}$ can be attributed to enolization of the carbonyl group at C-2 followed by oxidation at C-4, methylation, and addition of a molecule of methanol on C-3-C-2, most probably occurring in the methylation reaction and subsequent work up. The incorporation of 42 methyl groups results in a final substitution reaction with the hydrogen located at C-5 (See Table 4-1).

To investigate whether it was possible to enhance the formation of the mono-charged series of protonated molecules, another ionization method was utilized, namely, MALDI-MS. The spectrum of the permethylated heterogeneous mixture of the core oligosaccharide was recorded using 2,5-dihydroxybenzoic acid (DHB) as a matrix. The spectrum showed only the expected series of the singly charged protonated molecules shown in Figure 4-14B and Table 4-1.

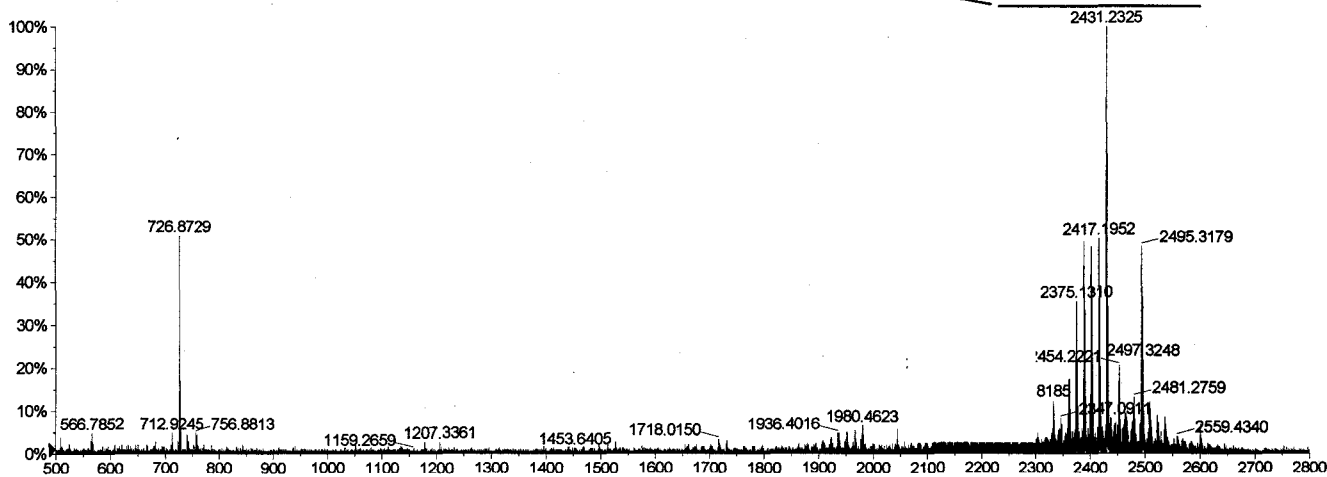
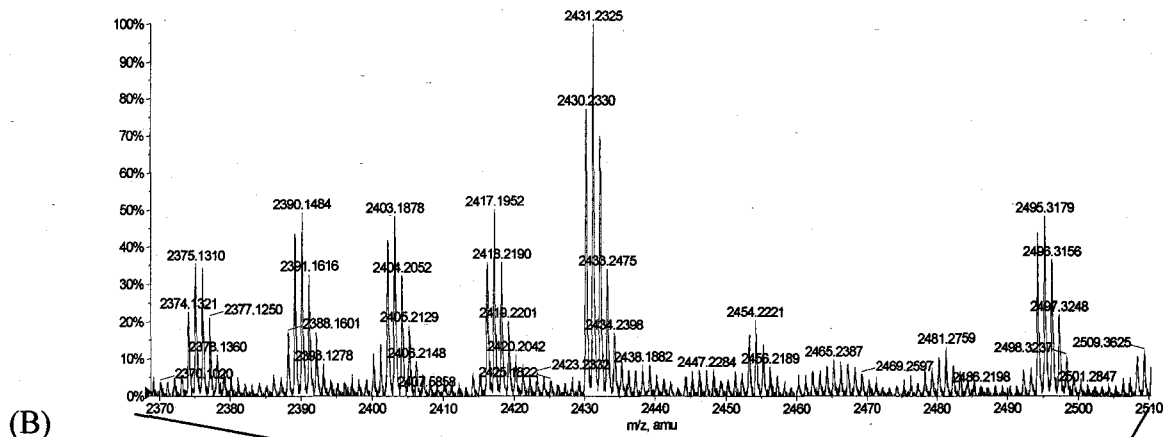
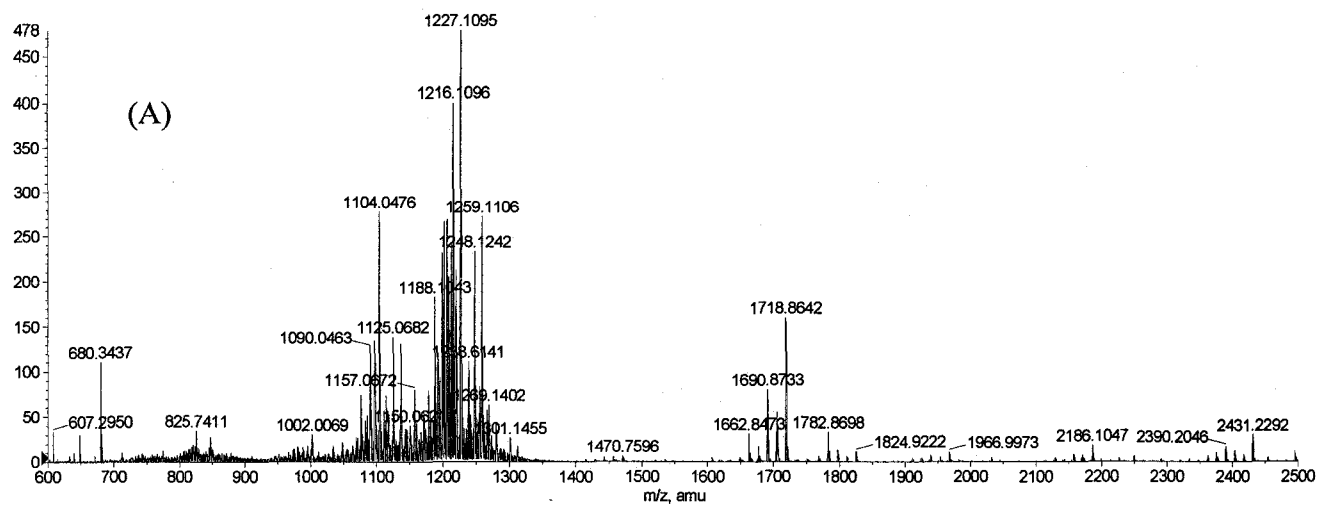


Figure 4-14: Positive ion mode ESI-MS (A) and MALDI-MS (B) spectra of the permethylated homogeneous core oligosaccharide mixture dissolved in methanol with the addition of trace amounts of formic acid. MALDI-MS produced a major shift towards the formation of diprotonated ions and sodiated clusters.

Table 4-1: Protonated molecular ions derived from the ESI-MS of the permethylated homogenous mixture of the core oligosaccharides of *A. salmonicida*.

Protonated Molecules	Incorporation of Me groups	Molecular Formula	Calculated <i>m/z</i>	Observed <i>m/z</i>	Difference (ppm)
$[M_{\text{NHMe}}+\text{H}]^+$	36	$\text{C}_{105}\text{H}_{189}\text{N}_2\text{O}_{56}$	2374.2003	2374.2129	-5.3071
$[\text{M}+\text{H}]^+$	37	$\text{C}_{106}\text{H}_{191}\text{N}_2\text{O}_{56}$	2388.2160	2388.2289	-5.4015
$[\text{M}_1+\text{H}]^+$	38	$\text{C}_{107}\text{H}_{193}\text{N}_2\text{O}_{56}$	2402.2316	2402.2429	-4.7040
$[\text{M}_2+\text{H}]^+$	39	$\text{C}_{108}\text{H}_{195}\text{N}_2\text{O}_{56}$	2416.2473	2416.2315	6.5391
$[\text{M}_3+\text{H}]^+$	40	$\text{C}_{109}\text{H}_{197}\text{N}_2\text{O}_{56}$	2430.2629	2430.2330	12.3032
$[\text{M}_4+\text{H}]^+$	41	$\text{C}_{110}\text{H}_{203}\text{N}_2\text{O}_{58}$	2480.2997	2480.2581	16.7722
$[\text{M}_5+\text{H}]^+$	42	$\text{C}_{111}\text{H}_{205}\text{N}_2\text{O}_{58}$	2494.3075	2494.2429	25.8990
$[\text{M}_{\text{NHMe}}+2\text{H}]^{2+}$	36	$\text{C}_{105}\text{H}_{190}\text{N}_2\text{O}_{56}$	1187.6041	1187.6019	1.8525
$[\text{M}+2\text{H}]^{2+}$	37	$\text{C}_{106}\text{H}_{192}\text{N}_2\text{O}_{56}$	1194.6119	1194.6071	4.0180
$[\text{M}_1+2\text{H}]^{2+}$	38	$\text{C}_{107}\text{H}_{194}\text{N}_2\text{O}_{56}$	1201.6197	1201.6137	4.9933
$[\text{M}_2+2\text{H}]^{2+}$	39	$\text{C}_{108}\text{H}_{196}\text{N}_2\text{O}_{56}$	1208.6276	1208.6037	19.7745
$[\text{M}_3+2\text{H}]^{2+}$	40	$\text{C}_{109}\text{H}_{198}\text{N}_2\text{O}_{56}$	1215.6354	1215.6116	19.5782
$[\text{M}_4+2\text{H}]^{2+}$	41	$\text{C}_{110}\text{H}_{204}\text{N}_2\text{O}_{58}$	1240.6438	1240.6341	7.8185
$[\text{M}_5+2\text{H}]^{2+}$	42	$\text{C}_{111}\text{H}_{206}\text{N}_2\text{O}_{58}$	1247.6537	1247.6269	21.4803
$[\text{M}+\text{H}+\text{Na}]^{2+}$	37	$\text{C}_{106}\text{H}_{191}\text{N}_2\text{NaO}_{56}$	1205.6029	1205.6041	-0.9954
$[\text{M}_1+\text{H}+\text{Na}]^{2+}$	38	$\text{C}_{107}\text{H}_{193}\text{N}_2\text{NaO}_{56}$	1212.6107	1212.6083	1.9792
$[\text{M}_3+\text{H}+\text{Na}]^{2+}$	39	$\text{C}_{109}\text{H}_{197}\text{N}_2\text{NaO}_{56}$	1226.6263	1226.6114	12.1471
$[\text{M}_5+\text{H}+\text{Na}]^{2+}$	42	$\text{C}_{111}\text{H}_{205}\text{N}_2\text{NaO}_{58}$	1258.6238	1258.6122	9.2164

4.3.2. MS/MS analysis of the permethylated core oligosaccharide:

The product ion series of the $[M+2H]^{2+}$, $[M_1+2H]^{2+}$, $[M_2+2H]^{2+}$, $[M_3+2H]^{2+}$, $[M_4+2H]^{2+}$ and $[M_5+2H]^{2+}$ ions at m/z 1194.61, 1201.61, 1208.60, 1215.63, 1240.6341 and 1247.63, respectively, were recorded with a CE varying from 40 -60 eV and CID gas pressure=4, and it was noted that all tandem mass spectra showed some degree of similarity. The tentative pathways of the dissociation of these selected precursor ions are presented in Figure 4-15.

As an illustration, the ESI-CID-QqToF-MS/MS of the di-protonated molecule $[M+2H]^{2+}$ at m/z 1194.61 is shown in Figure 4-16. In this tandem mass spectrum, the fragmentation routes are governed from both the non-reducing and reducing terminal ends of the molecule (Figures 4-15 and 4-16).

It should be noted that for all the CID-MS/MS of this series of precursor ions: $[M_{\text{NHMe}}+2H]^{2+}$, $[M+2H]^{2+}$, $[M_1+2H]^{2+}$, $[M_2+2H]^{2+}$, $[M_3+2H]^{2+}$, $[M_4+2H]^{2+}$ and $[M_5+2H]^{2+}$ have in common the same m/z values for the diagnostic product ions derived from the $[B]^+$ and $[C]^+$ series, as shown in Figures 4-15 and 4-16 (detailed analysis is shown in Appendix II). In addition, the presence of the diagnostic product ion $[^{0,2}X_{1\beta}-Z_1-2H+H]^+$ at m/z 1718,90 in some of the CID-MS/MS of the precursor series $[M_{\text{NHMe}}+2H]^{2+}$, $[M+2H]^{2+}$, $[M_1+2H]^{2+}$, $[M_2+2H]^{2+}$ and $[M_3+2H]^{2+}$ is noteworthy. The presence of this product ion indicates that the incremental increase of 14 Da, as speculated, is localized on the (degraded Kdo) 4,6-anhydro-keto acid $[Z_1]$ portion of the permethylated core oligosaccharide.

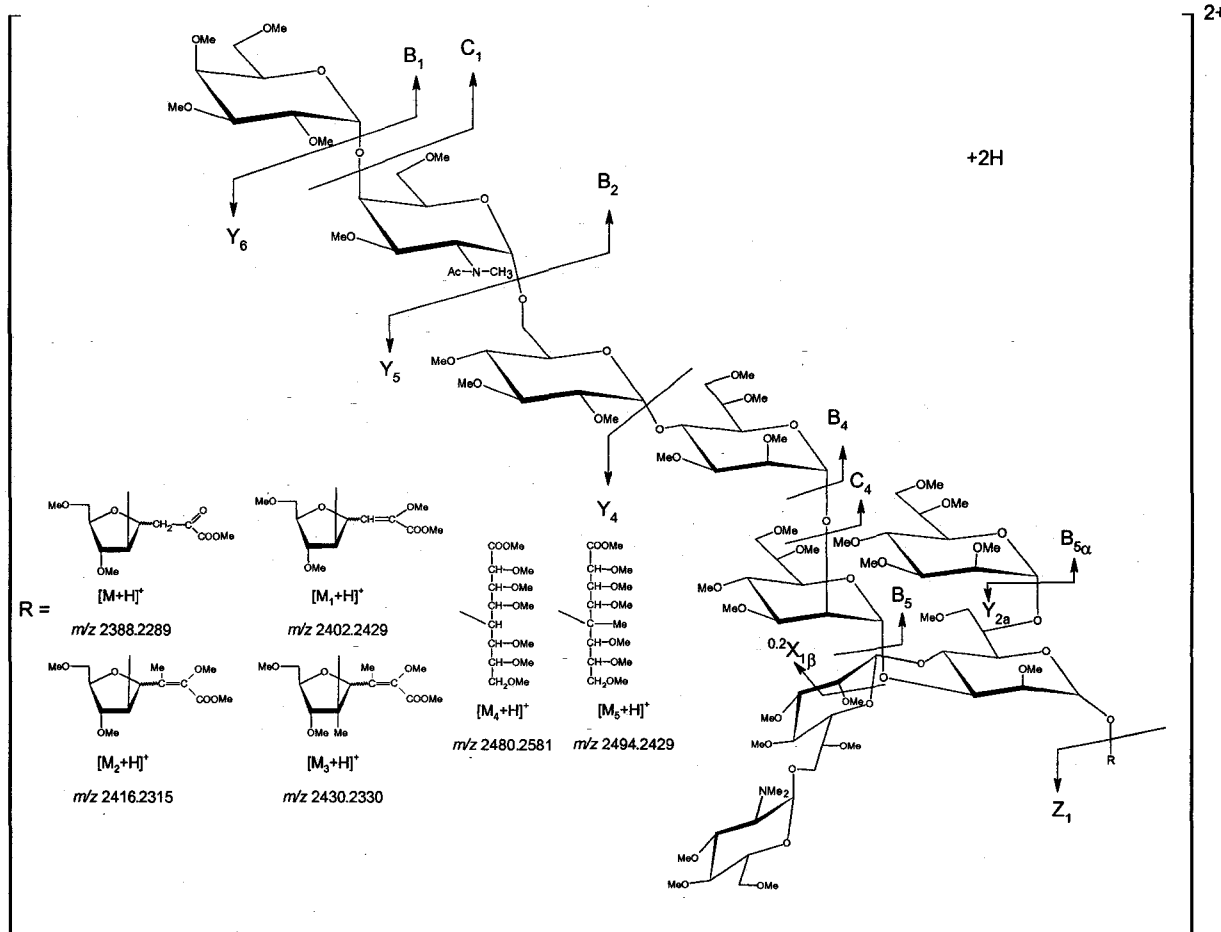


Figure 4-15: Schematic representation of the fragmentation patterns of the permethylated homogeneous mixture of core oligosaccharides recorded in the positive ion mode. ESI-MS/MS are illustrated for the $[M+2H]^{2+}$, $[M_1+2H]^{2+}$, $[M_2+2H]^{2+}$, $[M_3+2H]^{2+}$, $[M_4+2H]^{2+}$ and $[M_5+2H]^{2+}$ structures indicating the multiple methylated species of the 4,7-anhydro- α -keto acid derivatives 4A and 4A'.

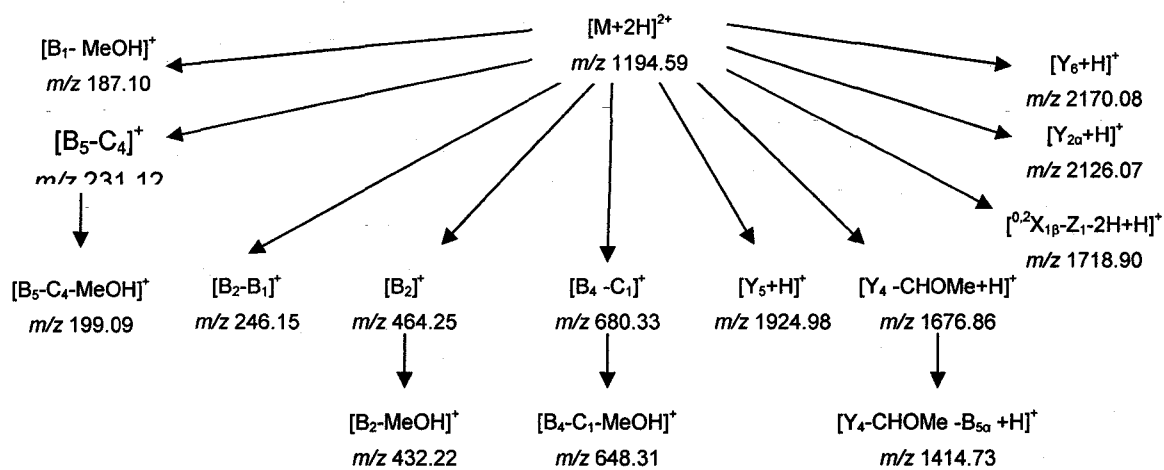
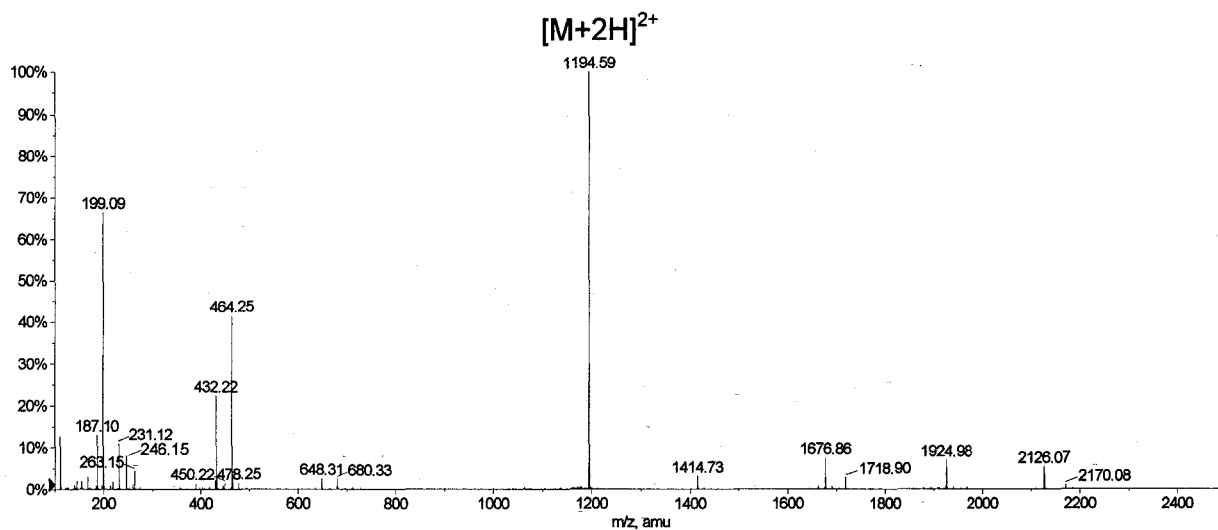


Figure 4-16: ESI-MS/MS spectra of the permethylated precursor ions $[M+2H]^{2+}$ at m/z 1194.61 and the proposed fragmentation routes and product ions of this precursor.

In the special case of the CID-MS/MS of the precursor $[M_3+2H]^{2+}$ ion, the intensity of the product ion at m/z 1718.90 was increased considerably. This was explained by the different genesis of two isobaric product ions, which resulted from two different consecutive mechanisms. One fragmentation mechanism produced the $[^{0,2}X_{1\beta}-Z_1-2H+H]^+$, whereas the other product ion $[Y_4-CHOMe+H]^+$ was formed by a $[Y_4]$ cleavage, followed by a loss of a hydroxyl methyl group and protonation. This latter product ion loses the $[B_{5\alpha}]$ terminal heptose group, to afford the $[Y_4-CHOMe-B_{5\alpha}+H]^+$ product ion at m/z 1456.75 (shown in Appendix II; Figure II-3).

However, for the $[Y]^+$ series, namely the $[Y_4+B_{5\alpha}-CHOMe+H]^+$, $[Y_4-CHOMe+H]^+$, $[Y_5+H]^+$, $[Y_{2\alpha}+H]^+$ and $[Y_6+H]^+$, the obtained diagnostic product ions resulted from an incremental addition of 14 Daltons, produced by the introduction of an extra methyl group, as shown in Table 4-2.

The product ion scans of the precursor di-protonated molecules $[M_4+2H]^{2+}$ and $[M_5+2H]^{2+}$ at m/z 1240.63 and 1247.63, respectively, are somewhat different from those obtained above. The ESI-MS/MS spectrum of the $[M_5+2H]^{2+}$ ion and the tentative dissociation pathways obtained during this ESI-CID-QqToF-MS/MS are presented in Figure 4-17. In this tandem mass spectrum, more product ions containing the fully permethylated open Kdo chain were formed (Figure 4-17 and Table 4-2). In Table 4-1, it was indicated that the precursor ion $[M_5+2H]^{2+}$ resulted from the incorporation of 42 methyl groups which, as stated earlier, seems to arise from an overmethylation during the Hakamori methylation (1964) of the cleaved heterogeneous core oligosaccharide containing the olefinic open chain. This occurred by the enolization of the carbonyl group at C-2, followed by oxidation of C-4, methylation, addition of a molecule of

methanol on C-2-C-3 and, finally, substitution reaction on the hydrogen of C-5 with a methyl group, most probably occurring in the methylation reaction and subsequent work up.

The ESI-CID-QqToF-MS/MS of the singly charged protonated molecule of this permethylated series was also affected. The product ion scans of the protonated molecules $[M_{\text{NHMe}}+\text{H}]^+$, $[\text{M}+\text{H}]^+$, $[\text{M}_1+\text{H}]^+$, $[\text{M}_2+\text{H}]^+$, $[\text{M}_3+\text{H}]^+$, $[\text{M}_4+\text{H}]^+$ and $[\text{M}_5+\text{H}]^+$ respectively at m/z 2374.21, 2388.23, 2402.24, 2416.23, 2430.23, 2480.26 and 2494.24 were also measured with a CE = 80 eV and CID gas pressure = 8. Unfortunately these series of product ion scans did not produce diagnostic high mass product ions, but rather low mass product ions such as $[\text{GlcN1}\rightarrow\text{7Hep}]^+$ at m/z 464.15, $[\text{B}_2\text{-MeOH}]^+$ at m/z 432.14, $[\text{Hep}]^+$ at m/z 199.05 and $[\text{B}_1\text{-MeOH}]^+$ at m/z 187.06. These MS/MS indicate that the peripheral region and the side branch glycones of the precursor protonated molecule are easily fragmented.

To investigate whether it was possible to enhance the fragmentation of these mono-charged series of protonated molecules, MALDI tandem mass spectrometric analyses were performed. These tandem mass spectra were identical to those obtained by ESI-CID-QqToF-MS/MS of the same precursor ion series, producing $[\text{GlcN1}\rightarrow\text{7Hep}]^+$ at m/z 464.1585 and $[\text{B}_2\text{-MeOH}]^+$ at m/z 432.1360. These results confirm the ease of fragmentation of the peripheral region glycones and suggest that the singly charged protonated molecules are resilient to the experimental gas phase dissociation conditions of both ESI- and MALDI-CID-MS/MS analysis. ESI-MS/MS and MALDI-MS/MS are shown in Appendix III.

Table 4-2: Diagnostic product ions of the [Y]⁺ series resulting from incremental addition of 14 Da, indicating the multiple methylated species of the 4,7-anhydro- α -keto acid derivatives **4A** and **4A'**.

Protonated Molecules	Diagnostic Product Ions				
	$[Y_4-B_{5\alpha}-CHOMe+H]^+$	$[Y_4-CHOMe+H]^+$	$[Y_5+H]^+$	$[Y_{2a}+H]^+$	$[Y_6+H]^+$
$[M_{NHMe}+2H]^{2+}$	1400.71	1662.85	1910.97	2112.06	2156.13
$[M+2H]^{2+}$	1414.72	1676.86	1924.97	2126.07	2170.07
$[M_1+2H]^{2+}$	1482.74	1690.88	1938.99	2140.11	2184.10
$[M_2+2H]^{2+}$	1442.72	1704.86	1952.99	2154.08	2198.10
$[M_3+2H]^{2+}$	1456.74	1718.87	1967.00	2168.09	2112.10
$[M_4+2H]^{2+}$	1506.73	1768.89	2016.99	2118.10	2262.12
$[M_5+2H]^{2+}$	1520.86	1782.89	2013.01	2232.10	-

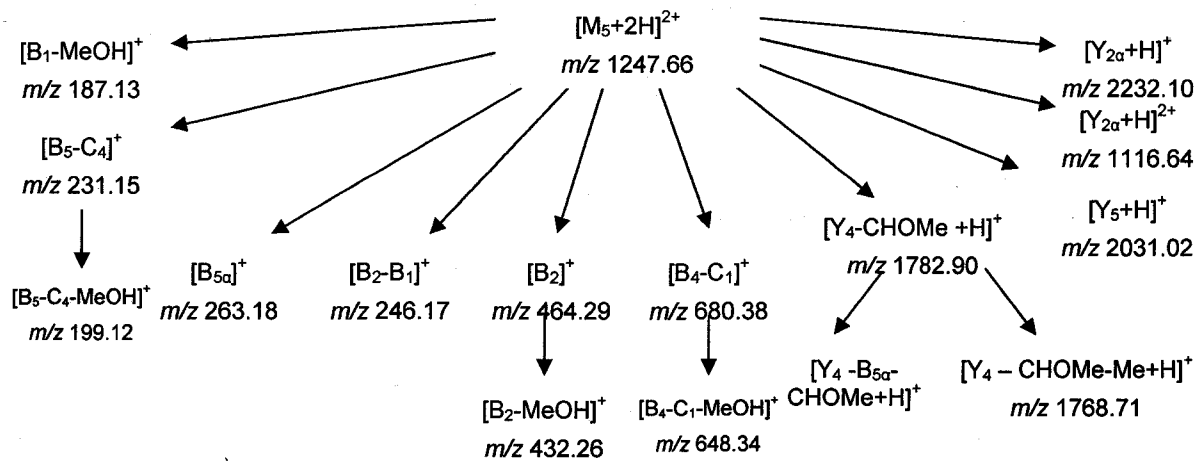
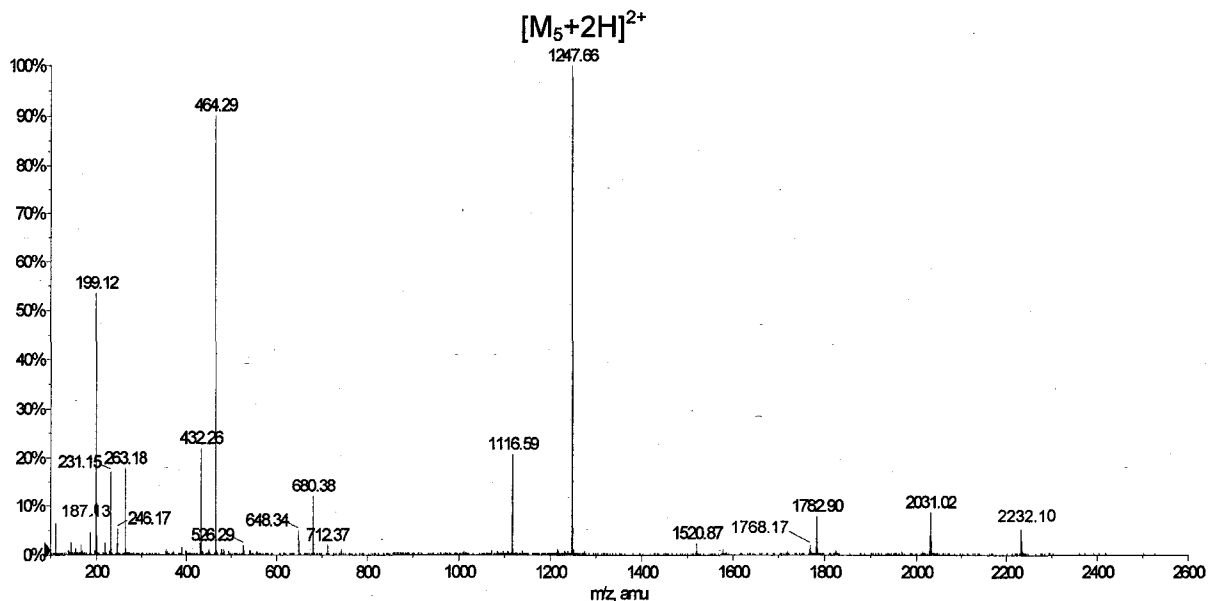
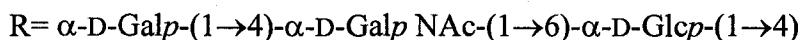
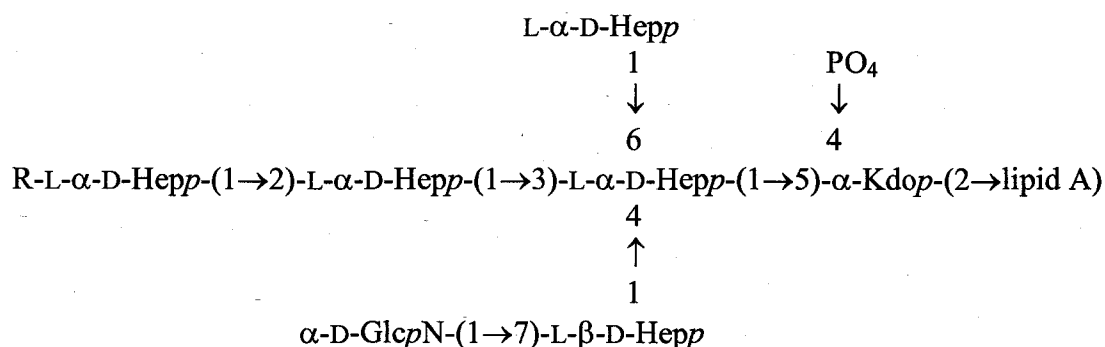


Figure 4-17: ESI-MS/MS spectra of the permethylated precursor ions $[M_5+2H]^+$ at m/z 1247.63 and the proposed fragmentation routes and product ions of this precursor.

4.4. Summary:

The molecular structure of the wild-strain of the lipopolysaccharide core of *Aeromonas salmonicida* has been sequenced using tandem mass spectrometry, illustrating for the first time the mass spectrometric fingerprints of this biologically-active extract (Banoub *et al.*, 2004b). In addition, the core oligosaccharide was determined to contain an *O*-4 phosphorylated and *O*-5 substituted Kdo reducing group, and its structure is proposed as the following:



After the core oligosaccharide of the LPS was released from the lipid A portion by conventional treatment with 1% acetic acid, the existence of a homogeneous mixture composed of the native core oligosaccharide containing the Kdo with its *O*-4 phosphate group intact, and a degraded core oligosaccharide mixture, which eliminated the *O*-4 phosphate group with extreme facility were demonstrated. The precise molecular structure and glycone sequence of the homogeneous mixture of phosphorylated and dephosphorylated core oligosaccharides was determined by ESI mass spectrometry and tandem mass spectrometric analysis. CID-MS/MS of the homogeneous mixture of permethylated core oligosaccharides afforded a series of diagnostic product ions which

confirmed the established sequence of the glycones to be determined. MALDI tandem mass spectrometry reconfirmed the molecular structure of the dephosphorylated homogeneous permethylated mixture of the core oligosaccharides containing the structural isomers 4,8- and 4,7-anhydro- α -keto acids.

CHAPTER 5: Mass Spectrometric Analysis of the Core Oligosaccharide of Mutant *Areomonas salmonicida*

5.1. Background:

The core oligosaccharide isolated from the mutant *A. salmonicida* is composed of four sugar residues (i.e. the inner core) and is shown in Figure 5-1. MS analysis of the inner core supports the observations associated with the presence of a phosphorylated Kdo unit at the reducing end of this poly-sugar. It illustrates the presence of the C-3-C-4 olefinic *D-arabino*-3-en-2-ulonic acid open chain reducing end (Figure 5-1) and the isomers 4,8- and 4,7-anhydro- α -keto acids derivatives as shown in Figure 4-3.

The MS fingerprint identification has a similar impact as in the case of the wild-type core. That is to say, for identification or quantification purposes, which can be essential for any biochemical study that includes this biologically-active inner core. One of the interesting findings in the MS analysis of the mutant inner-core is the absence of a $[M_{PO_4-H}]^-$ species. This is not surprising as this extract was acid treated accidentally for 2 hours while the wild-type core was hydrolyzed for merely 90 min. The identification of the open chain reducing end (Figure 5-1), however, provided strong evidence for the presence of the *O*-4 phosphorylated Kdo unit.

The ESI-QqTOF-MS/MS analyses of the permethylated inner core also allowed the exact identification of the series of diagnostic protonated molecular ions and, similar to the core isolated from the wild-type bacterium, pseudomolecular ions formed by addition of extra methyl groups were identified. The stereo-specific fragmentation routes

obtained during the tandem mass spectrometric analyses also permitted the precise sequencing of this dephosphorylated rough core oligosaccharide.

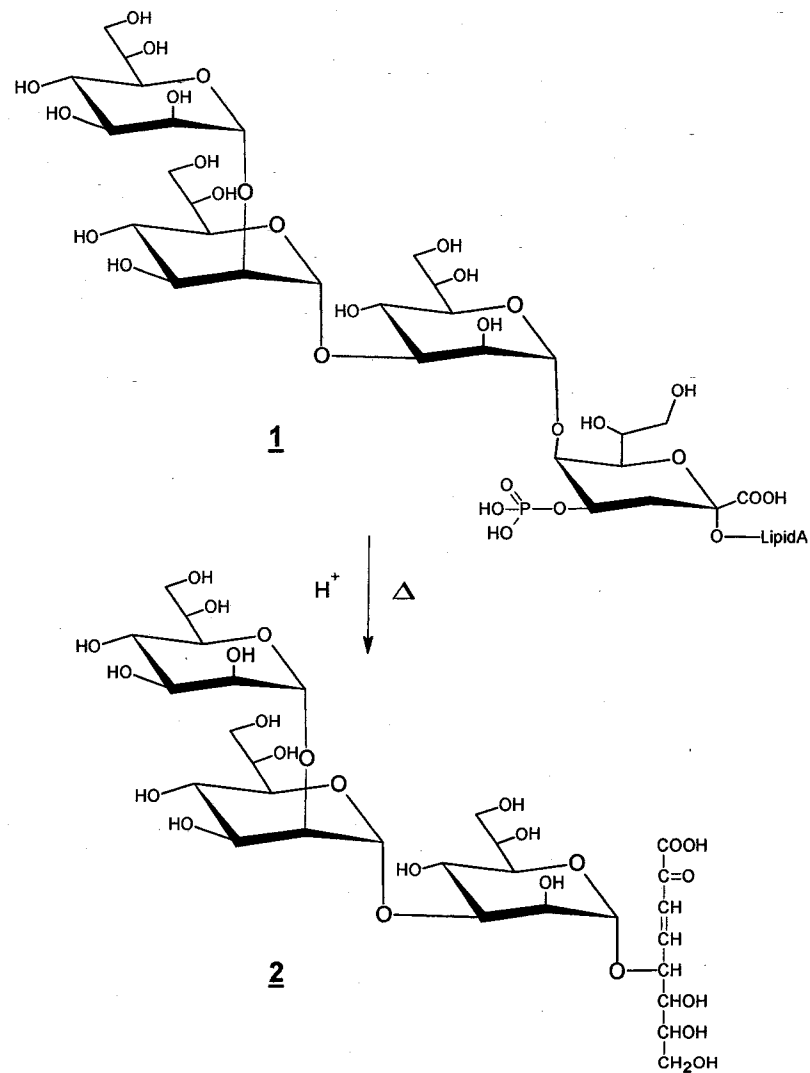


Figure 5-1: The molecular structure of the core oligosaccharide of the mutant form *A. salmonicida* lipopolysaccharide, containing an *O*-4 phosphorylated Kdo residue.

5.2. MS analysis of the homogenous mixture of the inner-core oligosaccharide:

5.2.1. Negative-ion mode MS analysis:

The native core oligosaccharide of the mutant form of *A. salmonicida*, after cleavage from the lipid A, was analyzed by electrospray mass spectrometry in the negative ion mode. The ESI-QqTOF-MS at DP=15 showed abundant [M-H]⁻ molecules at *m/z* 794.8839 (see Figure 5-2). The presence of this deprotonated molecule confirms the newly revised structure which consists of L- α -D-Hep(1 \rightarrow 2) L- α -D-Hep(1 \rightarrow 3) L- α -D-Hep(1 \rightarrow 5)Kdo(4,7-anhydro-derivative 4A) (Figures 5-1 and 4-3).

The same structure of the core oligosaccharide terminated at the reducing end by the 5-*O*-glycosylated, 4,8-anhydro- α -keto acid derivative 3A (or 3A') has the same molecular mass. The same can be corroborated for compounds 2 and 4A' (Figures 5-1 and 4-3). The prevalence of the 4,7-anhydro- α -keto acid derivative of the degraded core oligosaccharide is expected, as the preference for a furanose structure has been illustrated (Susskind *et al.*, 1998).

5.2.2. Negative-ion mode ESI-QqToF-MS/MS analysis:

Structural information, such as sequence patterns of branched oligosaccharides or differentiation of isomeric hexosyl units, has been obtained using tandem mass spectrometry. The unique dissociation patterns of the precursor ions provide diagnostic product ions which facilitate differentiation of isomeric species.

The low energy CID-QqTOF-MS/MS (CE=15 eV) of the precursor deprotonated molecular ion [M-H]⁻ at *m/z* 794.88 is shown in Figure 5-3. The proposed fragmentation

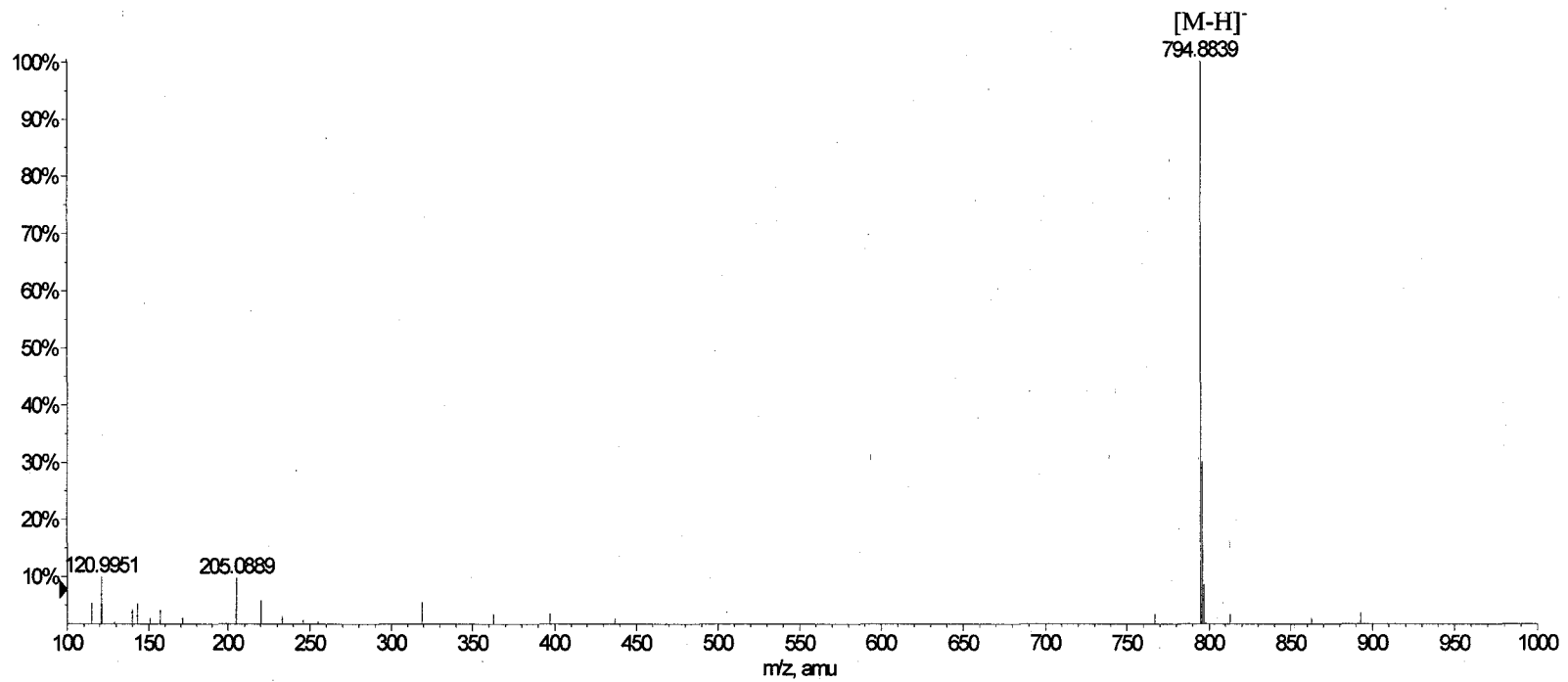


Figure 5-2: Negative ion mode, full scan, ESI-QqTOF-MS of core oligosaccharide of mutant *A. salmonicida* at DP=15.

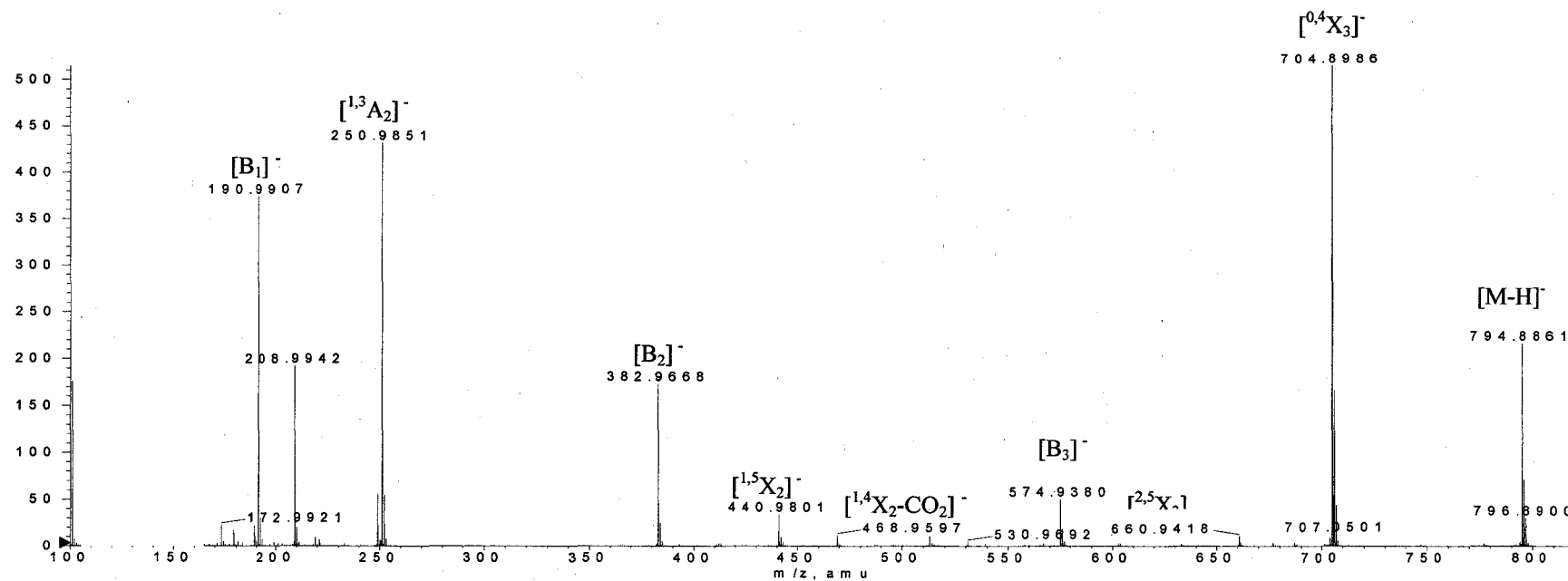


Figure 5-3: Product ion scan of m/z 794.88. Peaks are labelled according to the proposed fragmentation routes.

routes obtained have been rationalized by using the scheme for systematic nomenclature for carbohydrate fragmentation using FAB MS/MS proposed by Domon and Costello to describe putative fragmentation processes (Domon & Costello, 1988a; Domon & Costello, 1988b) and is shown in Figure 5-4.

The product ion scan of the ion at m/z 794.88 afforded three different major series of diagnostic product ions, namely, the $[X]^-$, $[B]^-$ and $[A]^-$ series. The charge retention occurs in the case of the $[B]^-$ and $[A]^-$ ions on the non-reducing part of this core oligosaccharide. Thus, the major abundant product ions $[B_3]^-$, $[B_2]^-$ and $[B_1]^-$ at m/z 574.93, 382.96 and 190.99, respectively, were observed. It was also noticed that the $[^{1,3}A_2]^-$ product ion at m/z 250.98 loses a molecule of ketene (42 Da) to afford the $[^{1,3}A_2-CH_2CO]^-$ product ion at m/z 208.99 (Figure 5-4A and 5-4B).

Additional diagnostic ions, namely $[Y]^-$ and $[X]^-$ ions, in which charge retention is localized on the reducing end were also formed. The major product ion $[^{0,4}X_3]^-$ at m/z 704.89 was formed; resulting from the elimination of monoglyceraldehyde $C_3H_7O_3$ (90.0 Da) from the non-reducing terminal *L-glycero-D-manno*-heptosyl residue of this core oligosaccharide (Figure 5-3 and Figure 5-4A and 5-4B). Cleavages of the C-1 and C-4 bonds in the *O*-2-substituted *L-glycero-D-manno*-heptosyl residue afforded the $[^{1,4}X_2]^-$ product ion at m/z 512.92 which loses a molecule of CO_2 to afford the $[^{1,4}X_2-CO_2]^-$ product ion at m/z 468.95. There are other product ions which are depicted in Figure 5-4B.

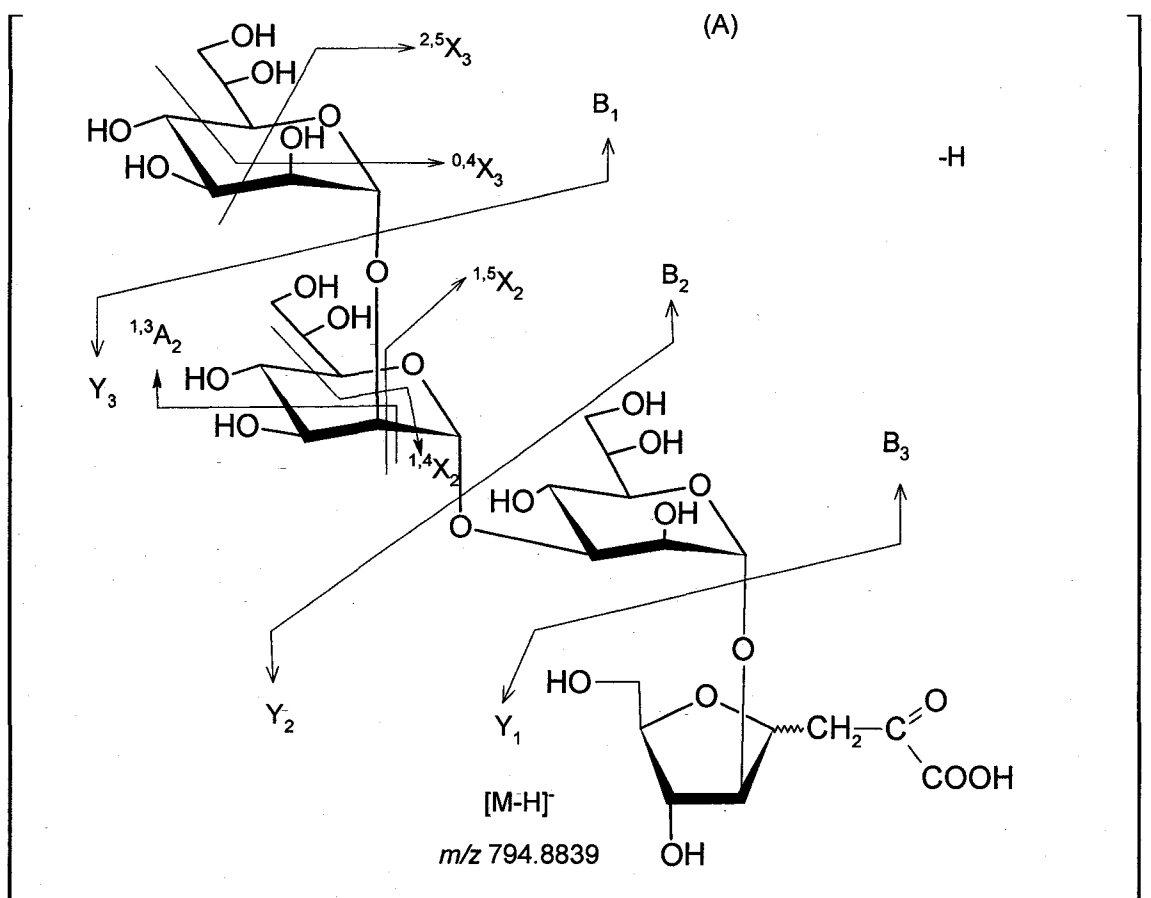
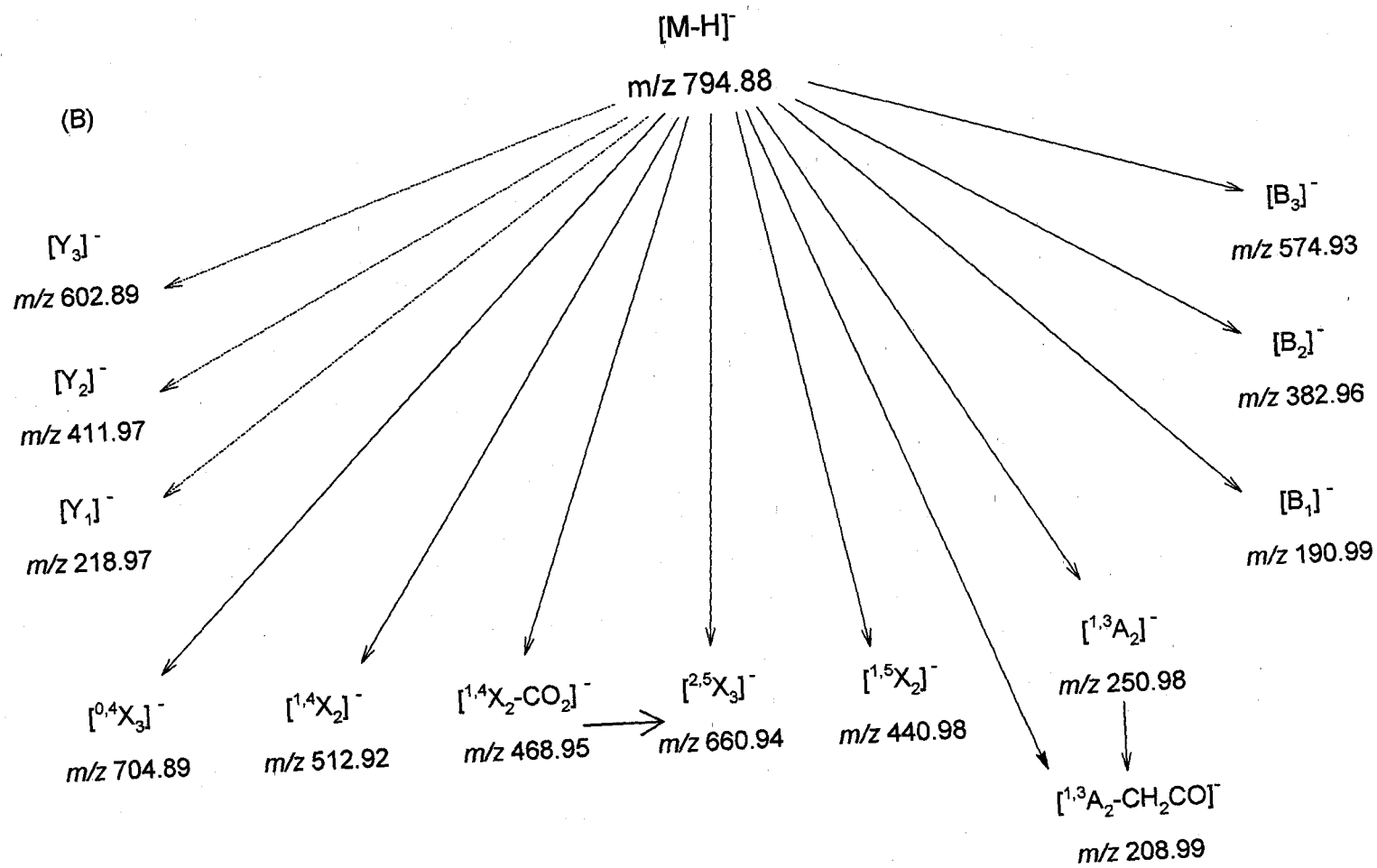


Figure 5-4: (A) Proposed major fragmentation patterns of the deprotonated molecule $[M-H]^-$ at m/z 794.88 (A). Types of product ions observed in this CID-MS/MS analysis (B) (next page); Dotted lines indicate a low relative abundance (<10%).



The very low abundance of the “Y-type” product ion series was noted. In this case, the charge retention also occurred on the portion containing the open olefinic chain and the anhydro derivatives present in **2**, **3A**, **3A'** and **4A'** on, typically, what is supposed to be the reducing end of this core oligosaccharide. Thus, the presence of the small abundant diagnostic product ions $[Y_3]^-$ and $[Y_2]^-$ containing the respective 4,7-anhydro-derivative **4A** of the terminal degraded reducing end of Kdo at m/z 602.89 and 411.97 was observed. In addition, the $[Y_1]^-$ product ion at m/z 218.97 was also present in low abundance. In the CID-QqTOF-MS/MS of the $[M-H]^-$ ion at m/z 794.88, aside from the low abundances of the Y series product ion, no product ion resulting from internal fragmentations of the anomeric mixtures of the 4,8-anhydro- and 4,7-anhydro-derivatives of the reducing end terminal degraded Kdo residue was observed. This is not really surprising, considering the fact that the degraded 4,7-anhydro-Kdo-derivative is a C-linked glycoside attached to the C-3 of the aglyconic $CH_2-CO-CO_2H$ chain rather than an O-linked glycoside. Consequently, the fragmentation will occur in a different manner during MS/MS analysis; an observation that was also noted in the previous chapter, concerning the wild-type core oligosaccharide.

The MS fingerprints data obtained from the product ion scan of the $[M-H]^-$ corroborates the majority of the glycosyl sequences and establishes, without a doubt, the presence of the 4,7-anhydro-derivative of the degraded Kdo which was formed from the 4-O-phosphorylated, 5-O-glycosylated reducing end Kdo residue which.

5.3. MS analysis of the permethylated core oligosaccharide:

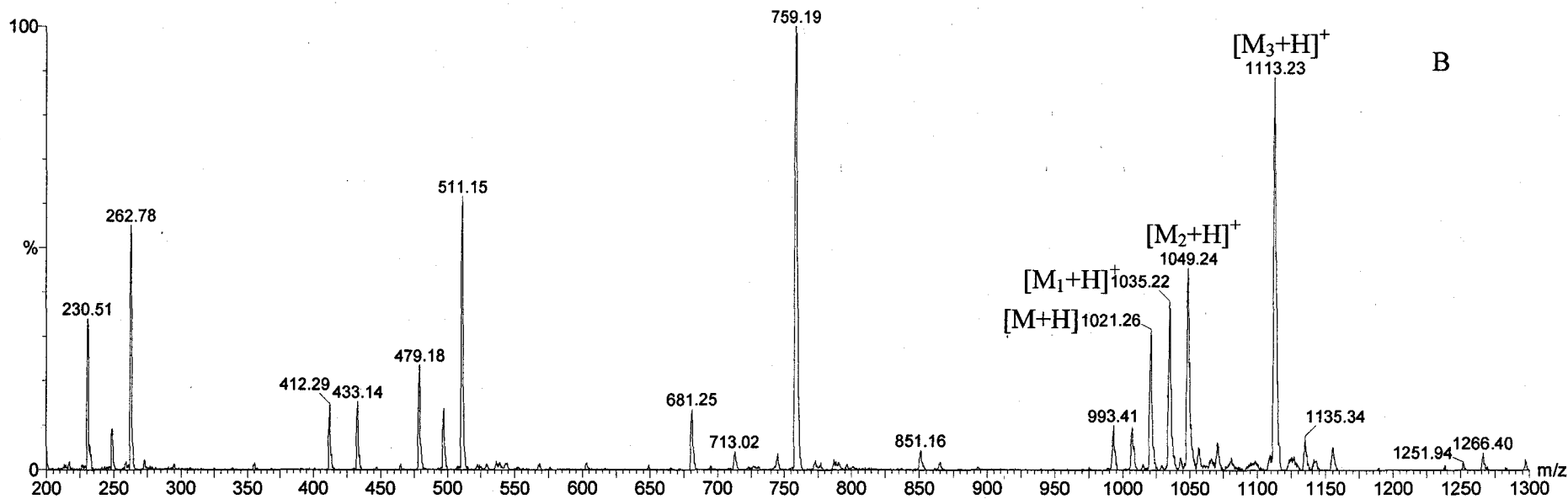
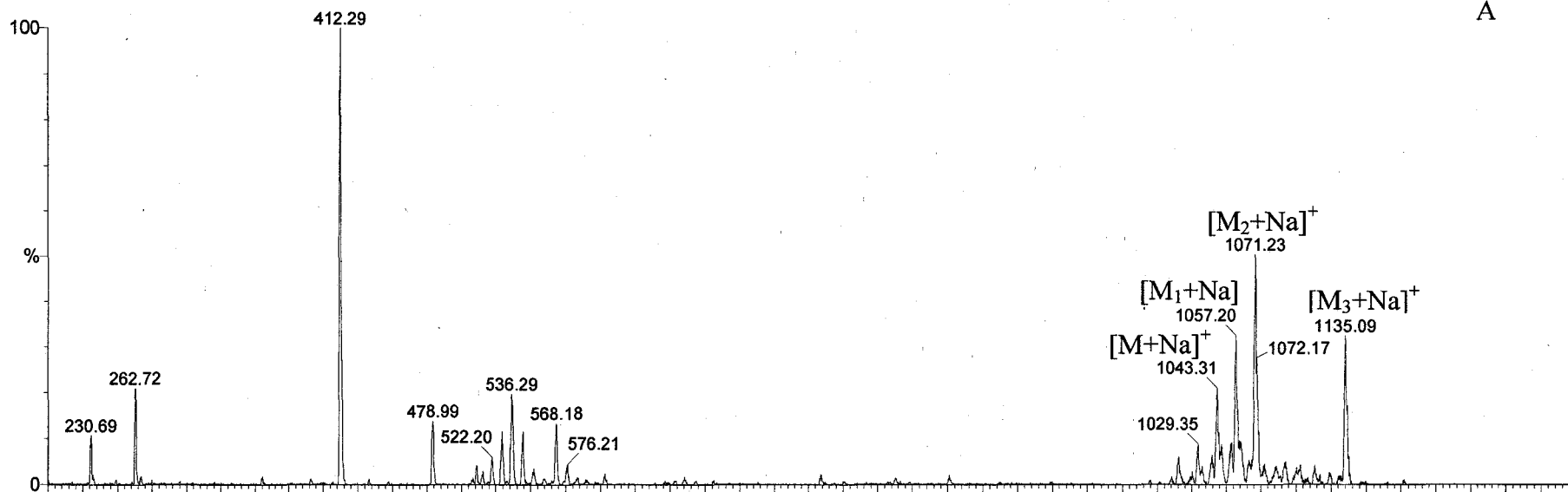
5.3.1. ESI-QqToF-MS:

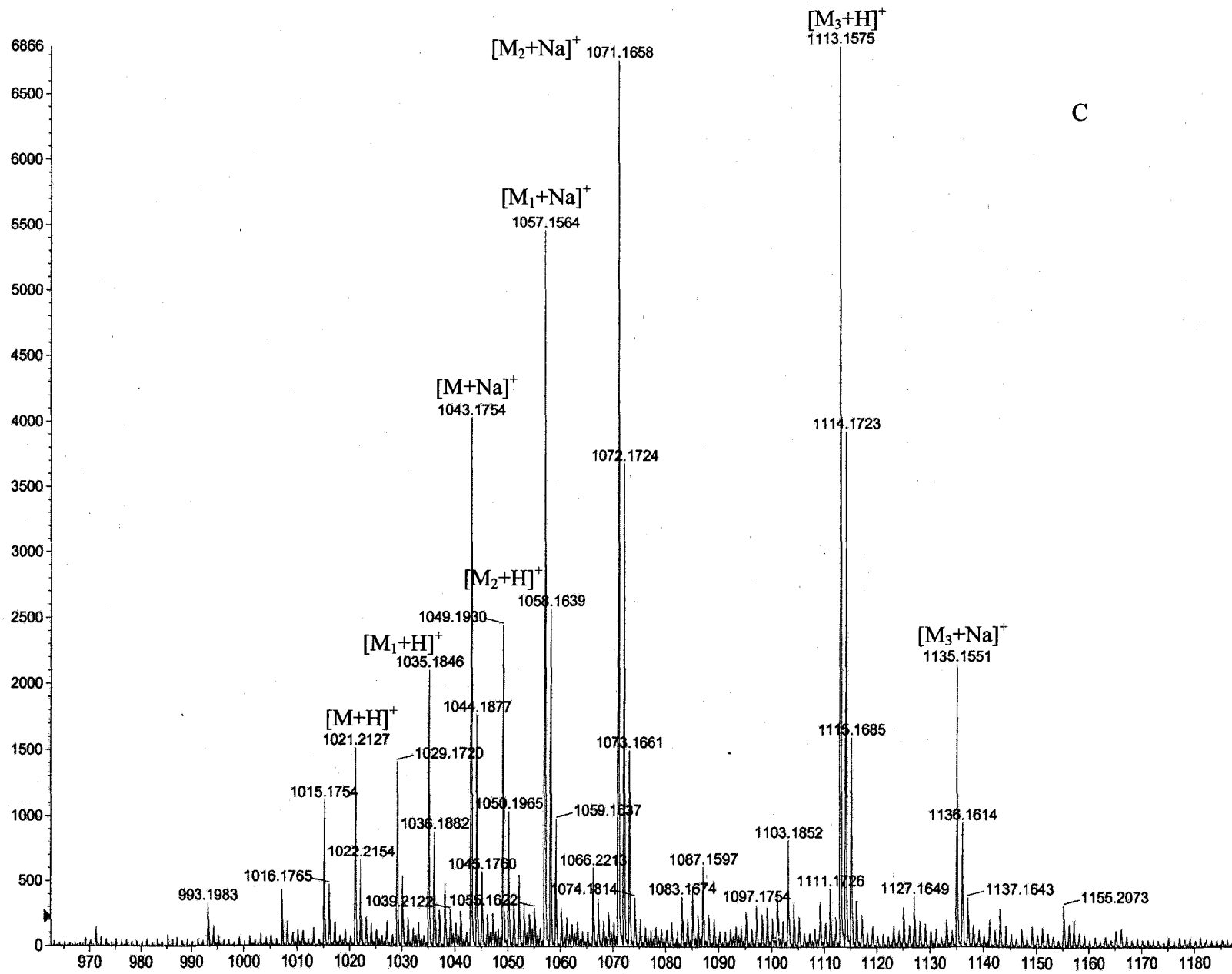
The permethylated, cleaved oligosaccharide was electrosprayed in the positive ion mode in a quadrupole-hexapole-quadrupole MS/MS instrument using methanol as the mobile phase. The ESI-MS is shown in Figure 5-5A and indicates the presence of various sodiated molecules. The first sodiated molecular ion $[M+Na]^+$ at m/z 1043.1754 resulting from the incorporation of 16 methyl groups and cationization with a sodium atom in the 4,7-anhydro-derivative **4A**, was identified. The presence of the $[M_1+Na]^+$ at m/z 1057.1564 was consistent with the incorporation of 17 methyl groups and cationization with a sodium atom of the enol form of the 4,7-anhydro-derivative **4A'**.

In addition, another pseudo-molecular ion of this sodiated cluster was identified as the $[M_2+Na]^+$ at m/z 1071.1658, which results from the incorporation of 18 methyl groups and cationization with a sodium ion in the enol form of the 4,7-anhydro- α -keto acid derivative. The incorporation of an extra methyl group (from M_1) was attributed to a C-methylation of the H-3 olefinic proton in the enol form of the 4,7-anhydro-derivative. It has already been suggested by Dell and coworkers that C-methylations of Kdo residues are possible and were encountered during the FAB-MS of permethylated core oligosaccharide containing "normal," non-phosphorylated and *O*-glycosylated reducing pyranose Kdo residue (Dell *et al.*, 1990). Finally, another pseudo-molecular sodiated $[M_3+Na]^+$ ion was observed at m/z 1135.1561 which resembles the ion $[M_4+H]^+$ of the wild-type bacterium (Figure 4-15).

It should be noted that, for the sake of simplicity, the m/z values reported for all the permethylated, protonated molecules and sodiated molecule clusters reported in the

above and following sections, are those obtained with the ESI-QqTOF-MS hybrid instrument (Figure 5-5C). The m/z reported on Figures 5-5A and 5-5B are those obtained with the quadrupole-hexapole-quadrupole instrument. The permethylated, cleaved core oligosaccharide was once more electrosprayed in methanol containing traces of formic acid. The ESI-MS in Figure 5-5C showed the presence of the protonated molecule $[M+H]^+$ at m/z 1021.2127 of the permethylated 4,7-anhydro-derivative. The $[M_1+H]^+$ at m/z 1035.1846 was obtained from the incorporation of 17 methyl groups in the enol form of the 4,7-anhydro- α -keto acid derivative. The $[M_2+H]^+$ at m/z 1049.1980 was attributed to the incorporation of 18 methyl groups resulting in permethylation of the enol form of the 4,7-anhydro- α -keto acid derivative followed by C-methylation. Once more, the $[M_3+H]^+$ at m/z 1113.1575 Da was also noted. The permethylated cleaved core oligosaccharide was electrosprayed in methanol alone in the QqToF-MS hybrid instrument and the spectra did not change whether it was electrosprayed in methanol alone or methanol containing traces of formic acid (Figure 5-5C).





C

Figure 5-5: (A) Positive ion mode full scan MS of permethylated core oligosaccharide of mutant *A. salmonicida* by ESI-QhQ MS. (B) Positive ion mode full scan MS of permethylated core oligosaccharide of mutant *A. salmonicida* treated with traces of formic acid by ESI-QhQ MS. (C) Positive ion mode full scan MS of permethylated core oligosaccharide of mutant *A. salmonicida* by ESI-QqTOF MS.

5.3.2. Positive-ion mode MS/MS analysis:

The low energy collision CID-QqTOF-MS/MS analyses were repeated with the hybrid instrument. The product ion scans of the protonated molecule $[M+H]^+$ at m/z 1021.52, recorded at collision energy (CE)=10, is shown in Figure 5-6. The proposed fragmentation routes obtained from these product ion scans are indicated in Figure 5-7 and 5-8.

The product ion scans of m/z 1021.52 gave no product ions resulting from charge retention of this so-called terminal reducing end; that is, no $[Y]^+$ type product ions were observed. However, all the diagnostic product ions formed during MS/MS fragmentation were identified, with charge retention on the non-reducing part of this permethylated core oligosaccharide. All of the expected product ions belonging to the $[B]^+$ series were observed in high abundance. Thus, the major diagnostic product ions $[B_3]^+$, $[B_2]^+$ and $[B_1]^+$ at m/z 759.39, 511.28 and 263.16, respectively, were observed (Figure 5-7 and 5-8). In addition, product ions resulting from elimination of methanol molecules were also observed. The product ion $[B_3-\text{MeOH}]^+$ was observed at m/z 727.39 (Figure 5-8) as well as the product ions $[B_2-\text{MeOH}]^+$, $[B_2-2\text{MeOH}]^+$ and $[B_3-3\text{MeOH}]^+$ at m/z 479.26, 447.23 and 415.20, respectively. Finally, the product ions $[B_1-\text{MeOH}]^+$, $[B_1-2\text{MeOH}]^+$ and $[B_1-3\text{MeOH}]^+$ at m/z 231.13, 199.10 and 167.08, respectively, were also formed. In this context, it should be noted that the series of product ions $[B_a-b\text{MeOH}]^+$, in which $a=1-3$ and $b=1-3$, could be formed by either consecutive fragmentation via the B-route followed by the loss of methanol, or by a concerted fragmentation mechanism occurring at the same time. In these MS/MS experiments, it simply means that they are both lost at the same time and within the same reaction region in the tandem mass spectrometer. Thus, it

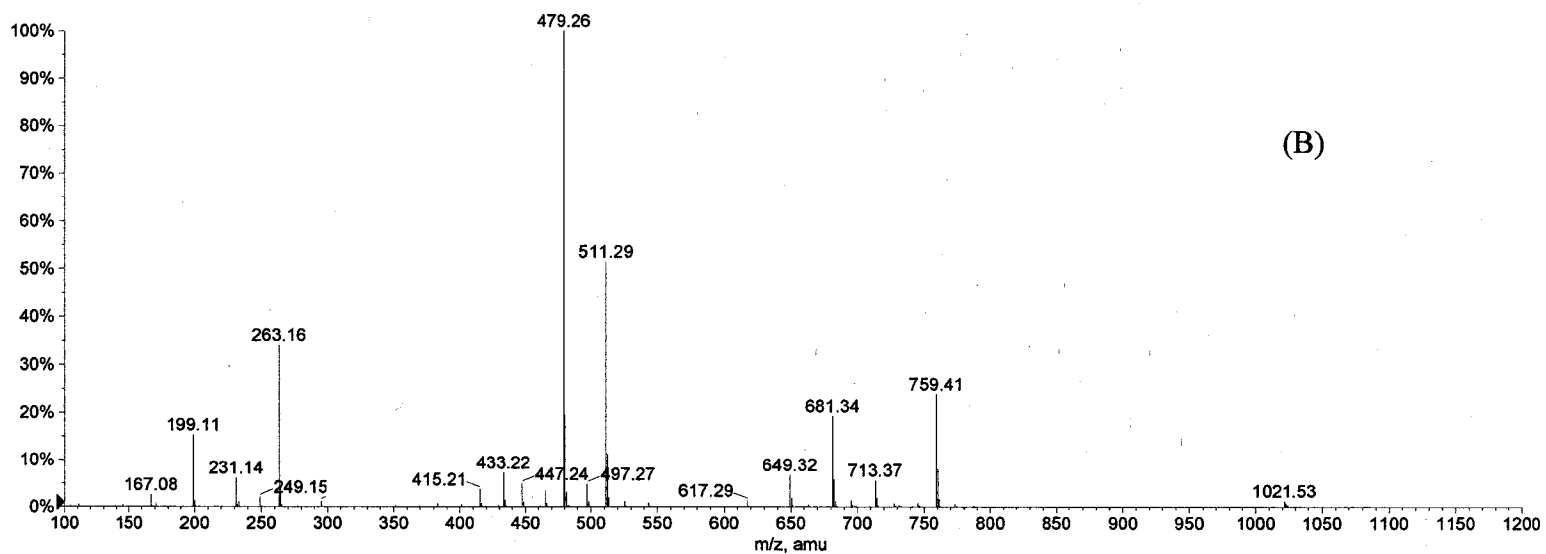
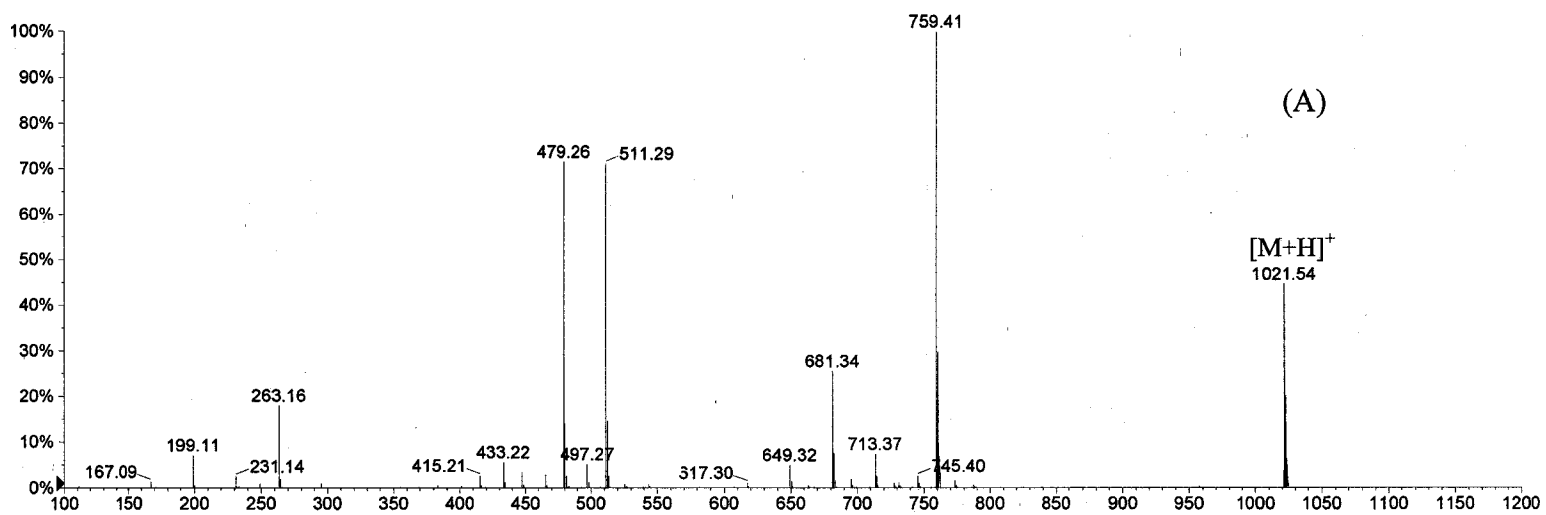


Figure 5-6: Product ion scan of m/z 1021.52 by ESI-QqTOF MS/MS using low energy CID at two different collision energies (A: 10eV and B: 15eV).

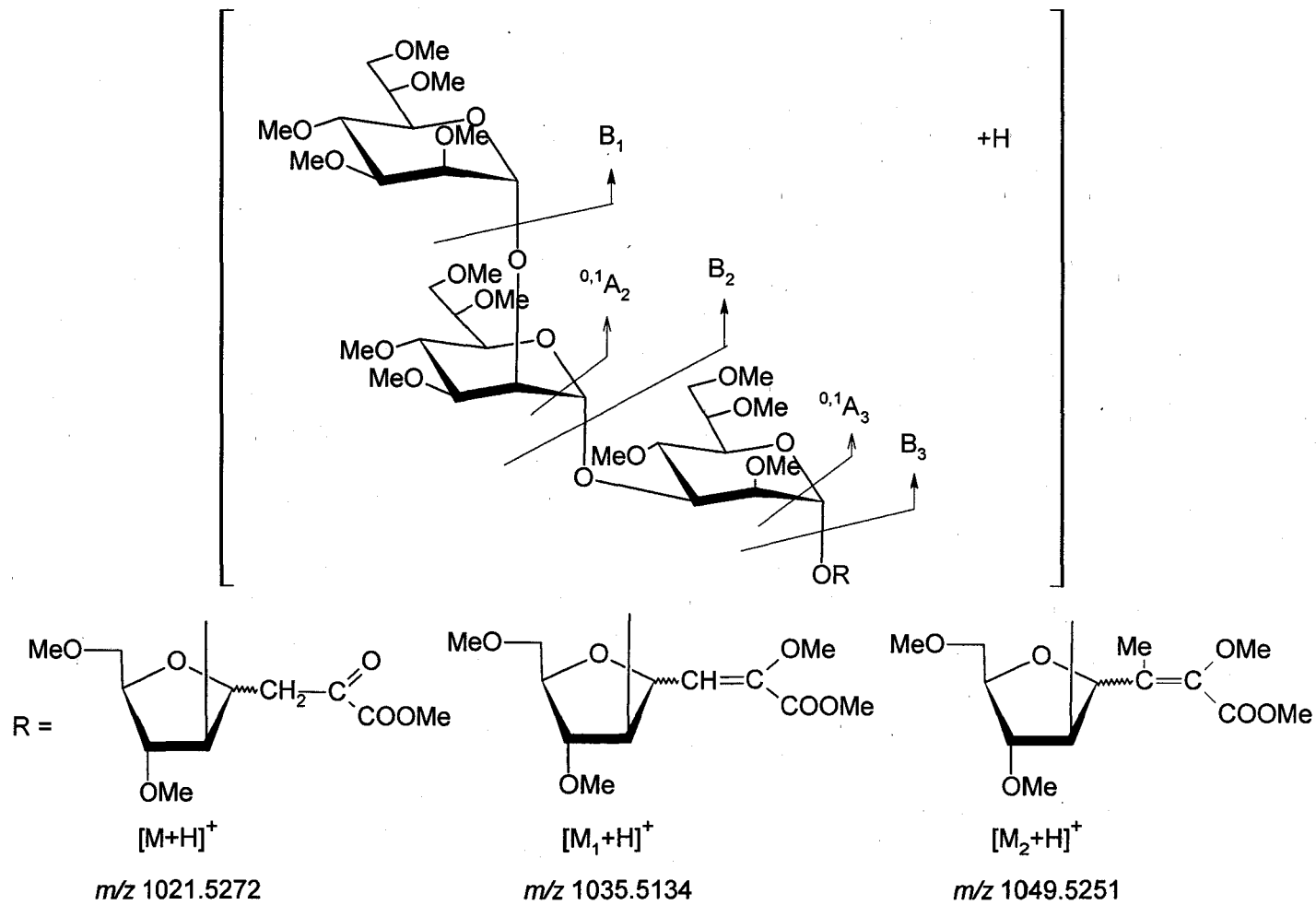


Figure 5-7: Proposed major fragmentation patterns of the permethylated protonated molecules [M+H]^+ at m/z 1021.52, $\text{[M}_1\text{+H]}^+$ at m/z 1035.5134 and $\text{[M}_2\text{+H]}^+$ at m/z 1049.5251.

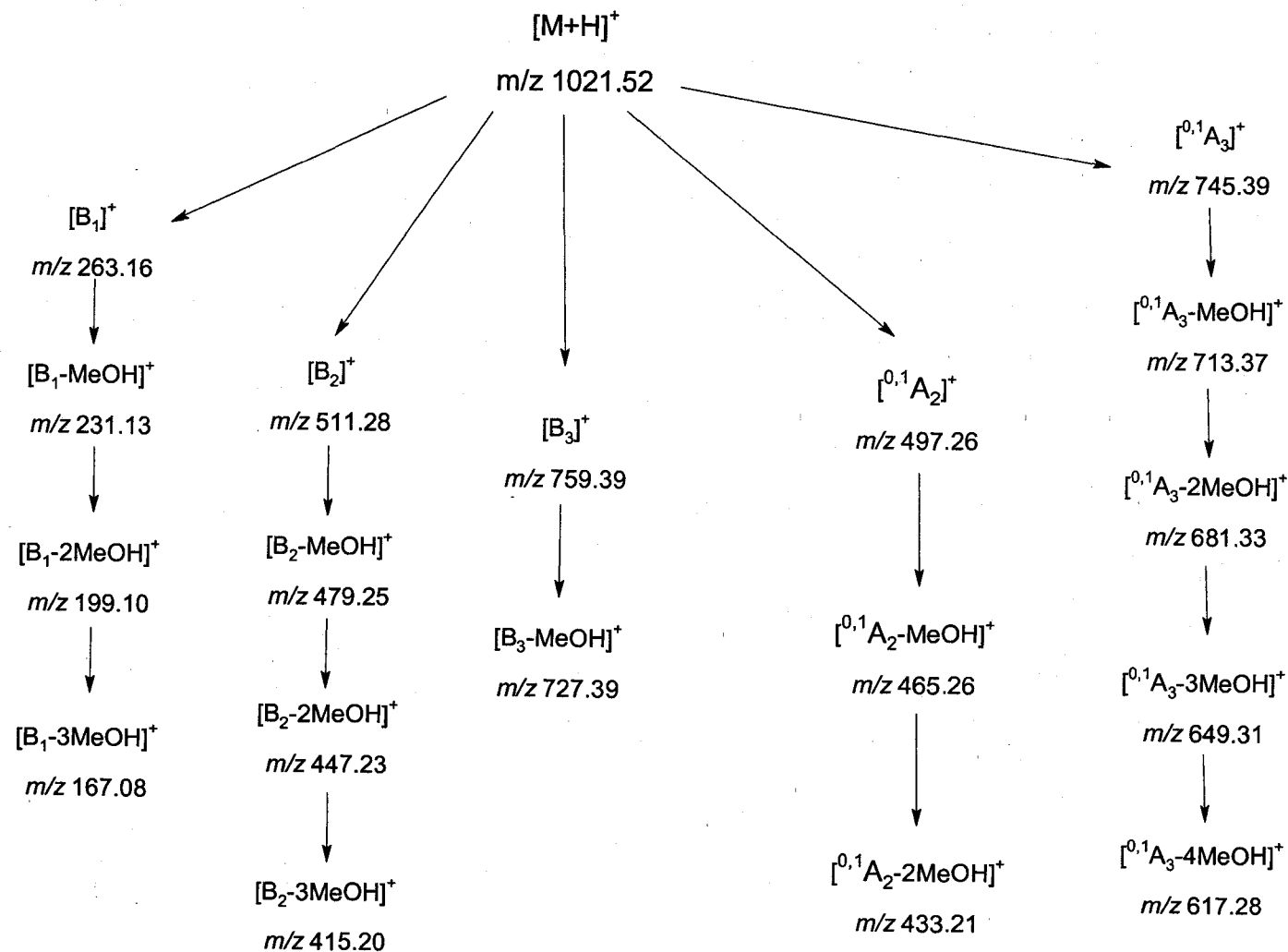


Figure 5-8: Types of product ions observed in the CID-MS/MS analysis of the permethylated protonated molecule $[M+H]^+$ at m/z 1021.52.

is difficult to deduce the order of fragmentation involving consecutive or concerted losses under MS/MS conditions.

Another $[A]^+$ type diagnostic product ion resulting from the fragmentation of the terminal non-reducing end of this dephosphorylated core oligosaccharide was also observed. Thus, the $[^{0,1}A_2]^+$ product ion at m/z 497.26 was identified (Figures 5-7 and 5-8). The methanol eliminated product ions $[^{0,1}A_2\text{-MeOH}]^+$ and $[^{0,1}A_2\text{-2MeOH}]^+$ at m/z 465.26 and 433.21, respectively, were identified. Finally, the $[^{0,1}A_3]^+$ product ion was also observed at 745.39. This product ion gave a series of elimination product ions $[^{0,1}A_3\text{-}b\text{MeOH}]^+$, in which $b=1-4$ at m/z 713.37, 681.3371, 649.31 and 617.28, respectively (Figure 5-8).

The product ion scan of the protonated molecule $[M_1+H]^+$ at m/z 1035.52 was measured with different collision energies (10 and 15 eV). This protonated molecule corresponds to the incorporation of 17 methyl groups on the enol form of the 4,7-anhydro- α -keto acid derivative **4A'**. Please note that the obtained product ion scans in this CID-QqTOF-MS/MS are identical to those obtained for the product ion scan of $[M+H]^+$ at m/z 1021.52 (Figure 5-8). This could be explained by the fact that the MS/MS fragmentation of the $[M_1+H]^+$ at m/z 1035.51 was governed by the loss of 276 Da, corresponding to the non-observed $[Y_1]$ portion containing the permethylated, enol form of the 4,7-anhydro-derivative of the degraded Kdo reducing end group (Figure 5-7).

Similarly, the product ion scans of the protonated molecule $[M_2+H]^+$ at m/z 1049.53, corresponding to the incorporation of 18 methyl groups on the enol form of the 4,7-anhydro-derivative **4A**, were recorded at different collision energies of 10 and 15 volts. Once more, the obtained CID-QqTOF-MS/MS afforded the same series of product

ions obtained for the protonated molecule $[M+H]^+$ at m/z 1021.52. Again, the MS/MS fragmentation of the $[M_2+H]^+$ at m/z 1049.52 was governed by the loss of 290 Da, which corresponds to the non-observed $[Y_1]$ portion containing the permethylated enolizable 4,7-anhydro-derivative. The CID-MS/MS spectra of the $[M_1+H]^+$ and $[M_2+H]^+$ are shown in Appendix IV.

The product ion scan of the $[M_3+H]^+$ at m/z 1113.1562 was recorded and is shown in Figure 5-9. This tandem mass spectrum was completely different from those obtained for $[M+H]^+$, $[M_1+H]^+$ and $[M_2+H]^+$ and seemed to arise from a complicated mechanism occurring during the Hakomori permethylation of the cleaved core oligosaccharide containing the open olefinic chain having the *D-arabino*-oct-3-en-2-ulonic acid terminal residue (as shown for the wild-type core LPS, Figure 4-15). The fragmentation routes of the product ion scan of $[M_3+H]^+$ at m/z 1113.15, are proposed in Figures 5-10 and 5-11.

As can be seen in this scan, the fragmentation routes are governed from both ends of the molecule. Indeed, the presence of the major product ions $[Y_3+H]^+$, $[Y_2+H]^+$ and $[Y_1+H]^+$ at m/z 851.12, 603.06 and 355.02, respectively, confirms the proposed structure. Additional diagnostic ions were observed such as the $[Y_1+H-MeOH]^+$ product ion at m/z 323.02 which results from the elimination of one molecule of methanol from the $[Y_1+H]^+$ product ion. These result from the permethylated alditol chain derived from the reducing end Kdo residue. A minor series of ions were formed from the non-reducing end of the core oligosaccharide. The low intensity $[B_1]^+$, $[B_2]^+$ and $[B_3]^+$ product ions were observed at m/z 263.06, 511.12 and 759.39, respectively. Similar to the $[M+H]^+$, $[M_1+H]^+$, and $[M_2+H]^+$ series, product ions resulting from elimination of methanol, as expected, were also noted for the $[B]^+$ series. Thus, the $[B_1-MeOH]^+$ and $[B_1-2MeOH]^+$ were observed at

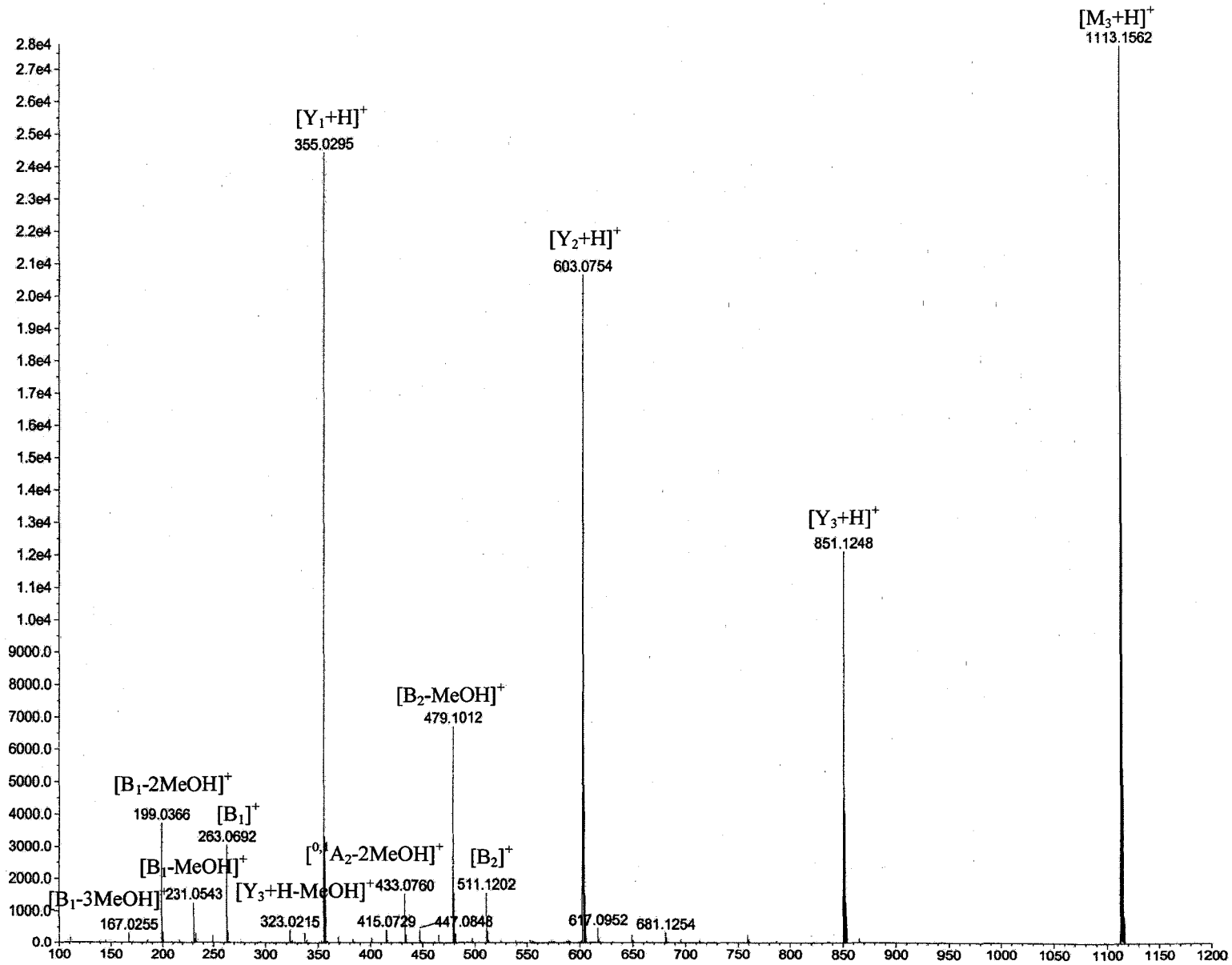


Figure 5-9: Product ion scan of m/z 1113.15 by ESI-QqTOF MS/MS using low energy CID.

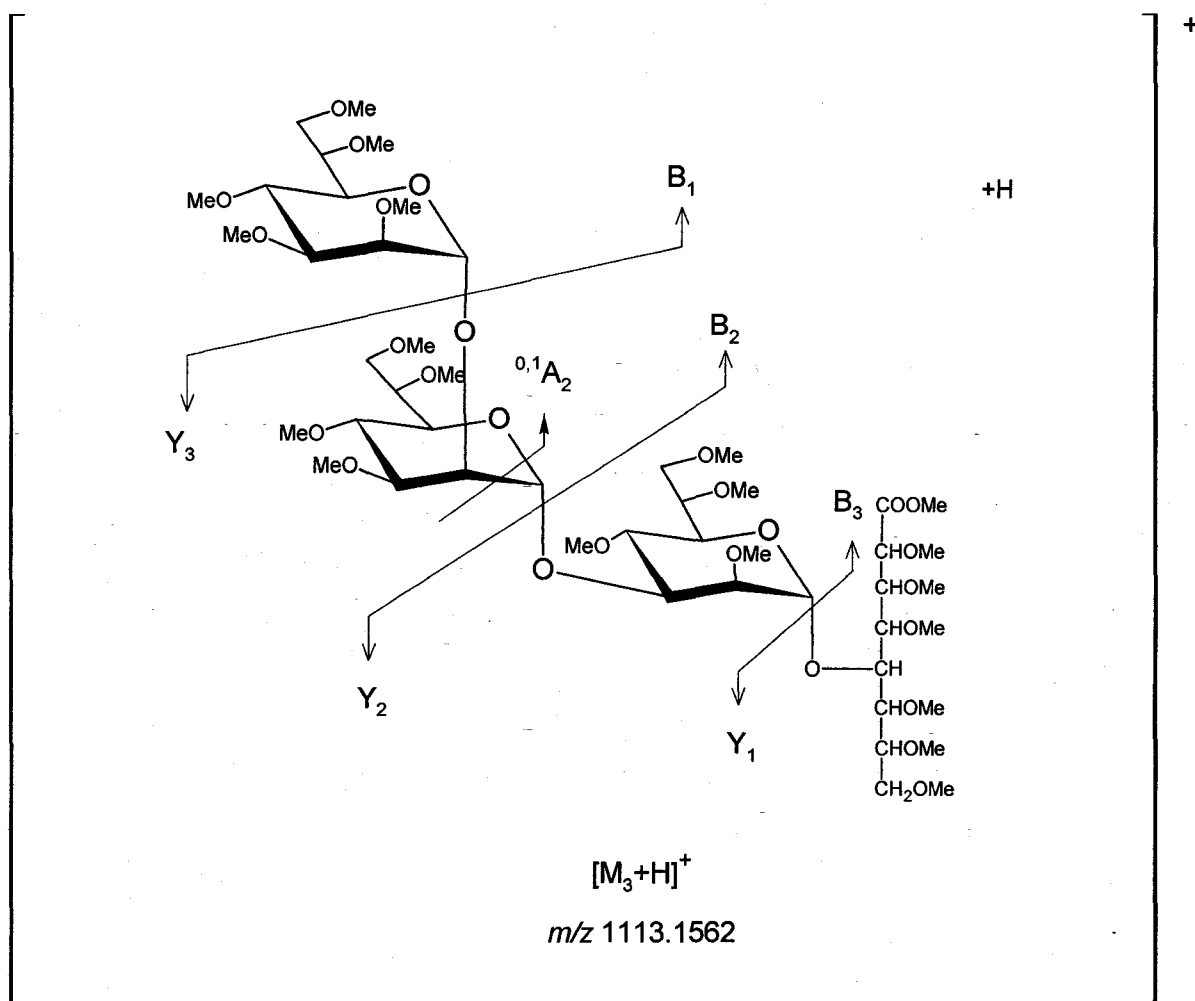


Figure 5-10: Proposed major fragmentation patterns of the permethylated protonated molecule $[M_3+H]^+$ at m/z 1113.1562.

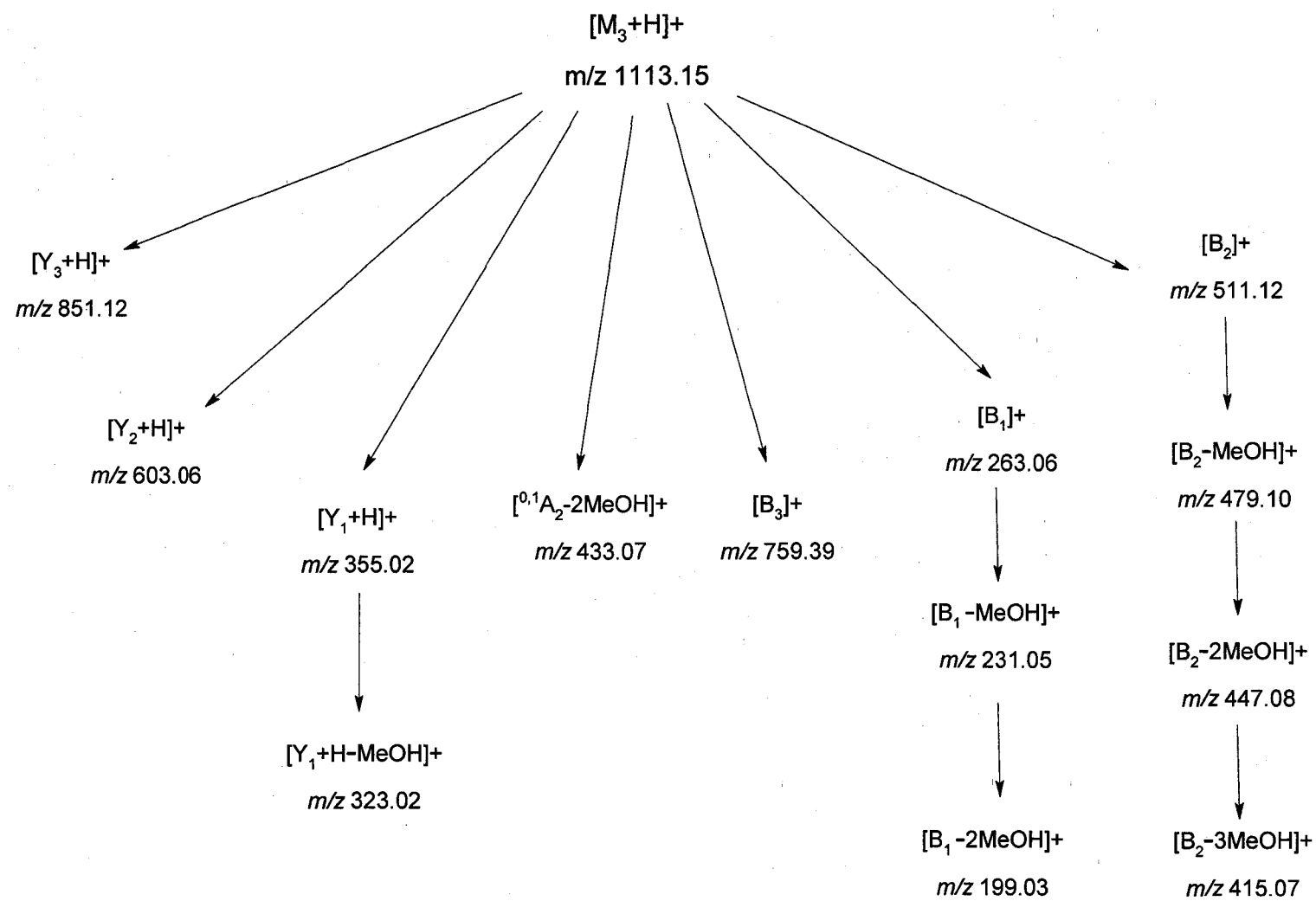
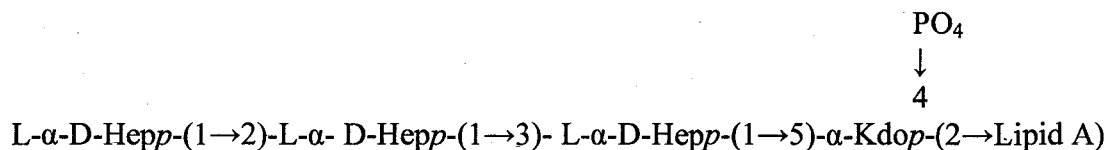


Figure 5-11: Types of product ions observed in the CID-MS/MS analysis of the permethylated protonated molecule $[M_3+H]^+$ at m/z 1113.1562.

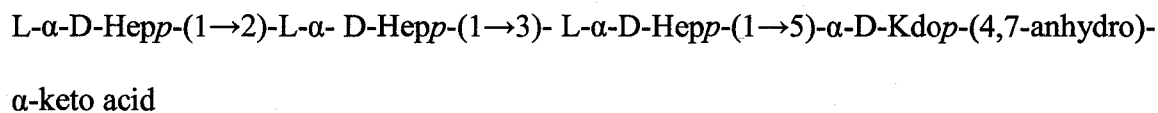
m/z 231.05 and 199.03, respectively. The product ions $[B_2\text{-MeOH}]^+$, $[B_2\text{-2MeOH}]^+$ and $[B_3\text{-MeOH}]^+$ at m/z 479.10, 447.08 and 415.07, respectively, were also formed.

5.4. Summary:

The molecular structure of the mutant form of the lipopolysaccharide of *Aeromonas salmonicida* was determined to contain an *O*-4 phosphorylated and *O*-5 substituted Kdo reducing group, and is proposed as the following:



It was established that during the cleavage of this LPS with 1% acetic acid, to release the core oligosaccharide from the lipid A portion, a degraded core oligosaccharide was obtained which eliminated its phosphate group with extreme facility. The molecular structure and the fragmentation patterns of this dephosphorylated core was deduced by electrospray mass spectrometry and is proposed as the following:



Low energy collision ESI-QqTOF-MS/MS analysis of the dephosphorylated core oligosaccharide confirmed the presence of the *O*-5 glycosylated 4,8- and 4,7-anhydro derivatives of the enolizable α -keto-acids. The CID tandem mass spectrometric analysis of the heterogeneous mixture of the permethylated core oligosaccharide established the methylation reaction on the isomeric 4,8- and 4,7-anhydro α -keto-acids and the complete

permethylation and addition reaction of the *O*-5 glycosylated open chain reducing end terminal D-*arabino*-3-en-2-ulonic acid. The stereo-specific fragmentation routes obtained during the tandem mass spectrometric analysis permitted the sequencing of this dephosphorylated rough core oligosaccharide of the mutant LPS of *A. salmonicida*.

CHAPTER 6: Mass Spectrometric Fingerprints of Synthetic Cholesteryl Neoglycolipids: The Presence of a Unique C-Glycoside

6.1. Background:

Liposomes are widely used as drug delivery systems; Cationic liposomes, for example, are one of the most prevalent non-viral gene delivery systems used in gene therapy (El-Aneed, 2004). Their safety, simplicity of preparation and high encapsulation capacity of foreign genetic materials make them excellent candidates as alternatives to the immunogenic viral vectors which have been traditionally superior in terms of their gene transfer ability (Katsube *et al.*, 2004; Lundstrom & Boulikas, 2003).

One major limitation of the usage of liposomal formulations is their tendency to aggregate, as well as their rapid clearance in the circulatory system. Many modifications have been introduced to counter and prevent these drawbacks. Liposomes-drug complexes bearing polyethylene glycol (i.e. PEG-liposomes) were, for example, introduced (Klibanov *et al.*, 1991; Klibanov *et al.*, 1990) and have proven to significantly prolong the half life of liposomal formulations via steric stabilization. More recently, synthetic neoglycolipids were tested as an alternative to PEG-liposomes, providing better formulations in terms of stability and therapeutic outcomes (Perouzel *et al.*, 2003; Xu *et al.*, 2002).

Structural conformation and purity of synthetic neoglycolipids can be investigated with the aid of mass spectrometry (Pohlentz *et al.*, 1994; Routier *et al.*, 1999). In addition to structural studies, quality control and quality assurance of liposomal formulations are

pharmaceutical necessities for the production of any therapeutically relevant liposomal-based drug carrier. Mass spectrometric analysis and fingerprint identification (through CID-MS/MS analysis) of different liposomal components can, with a great degree of sensitivity, assist in monitoring various steps in the production process as well as during any pharmacokinetic study (Khan *et al.*, 2003; Ng *et al.*, 2004).

In the following sections, it is reported, for the first time, the fragmentation pattern and the unique “*in situ*” formation of a steroidal C-glycoside species both within the ESI interface and in the collision cell during CID-MS/MS analysis of novel amphiphilic neoglycolipid cholesteryl derivatives. This C-glycosylation reaction results from an ion-molecule reaction between the sugar oxonium ion and the neutral cholest-3,5-diene molecule. This finding is of great interest to the field of carbohydrate chemistry, as the occurrence of a C-glycosylation is, by far, more difficult than that of normal O- or N-glycosylation reactions.

C-Glycoside chemistry has grown over the years and numerous published materials focus on the various methodologies of C-glycoside synthesis (Postema, 1995). In addition, many C-glycoside analogues have been used for their therapeutic values such as anti-cancer vaccines (Kuberan *et al.*, 2003; Peri *et al.*, 2001) and for protection against malaria as well as melanoma metastases (Schmiege *et al.*, 2003). The formation of aryl C-glycoside within the mass spectrometry is a novel finding that needs to be explored and may allow interesting simple gas-phase C-glycoside reactions in contrast to tedious conventional bench-top chemistry.

In this chapter, a new series of cholesteryl neoglycolipids bearing various carbohydrate moieties were synthesized and these are presented in Figure 2-1. The low-

energy CID-MS/MS analyses of these series of novel synthetic neoglycolipids were performed and, subsequently, the fingerprint fragment ions were identified; which were common among different structures.

6.2. QqToF-MS Analysis:

Regardless of the structure of the tested neoglycolipid, abundant protonated $[M+H]^+$ species were observed during ESI-QqToF-MS analysis; and in most cases, the sodiated $[M+Na]^+$ along with the corresponding $[M+K]^+$ adduct ions were also formed. The formation of the protonated singly-charged ion was enhanced by the addition of formic acid, whereas the series of fragment ions obtained in the ESI-MS were the same (i.e. with or without acid). QqToF-MS experiments also revealed the presence of a series of 1,2 sugar oxonium ions, namely $[GlcNAc]^+$ at m/z 204.08, $[GlcNH_2]^+$ at m/z 162.07, $[GlcNHCOCD_3]^+$ at m/z 207.10, $[Fuc]^+$ at 147.06, $[GlcNAloc]^+$ at m/z 246.07, $[LacNAc]^+$ at m/z 366.11, and the corresponding per-*O*-acetylated species of GlcNAloc and LacNAc at m/z 372.12 and 618.20 respectively. Figure 6-1 represents the QqToF-MS spectra of four neoglycolipids bearing $GlcNHCOCD_3$, GlcNAloc, $GlcNH_2$ and GlcNAc (exact structures are shown within the figure) and illustrates the formation of the expected sugar $[Oxonium]^+$ ions. The complete ESI-MS spectra of all the remaining compounds are shown in Appendix V and VI. In addition, the cholesteryl cation that bears a positive charge, speculated to be localized on C-3', was formed, possibly via intact C-C covalent bond cleavage and was assigned as the $[Cholestene]^+$ ion observed at m/z 369.35.

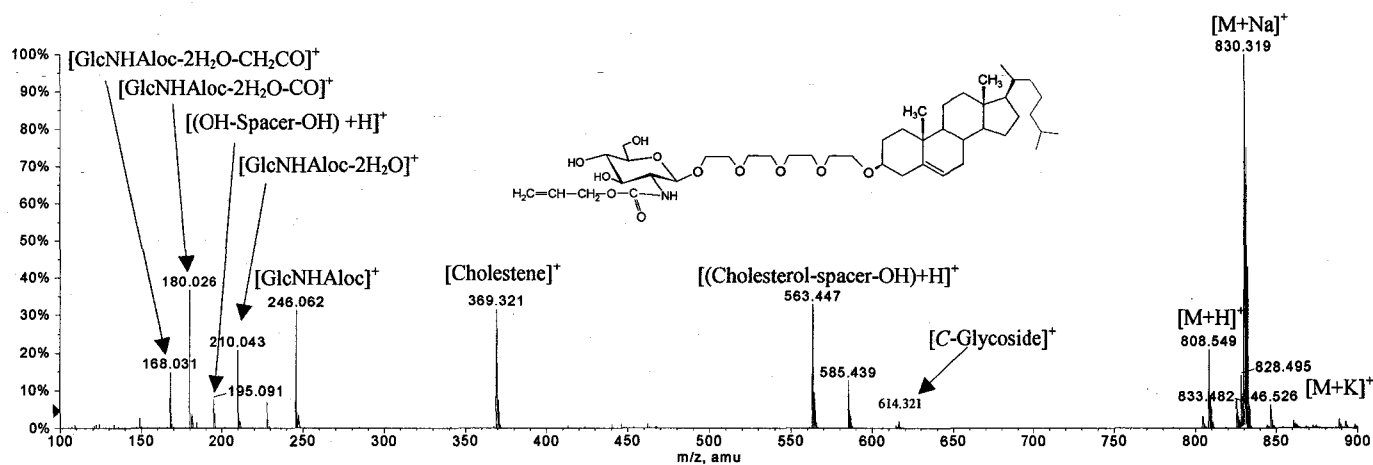
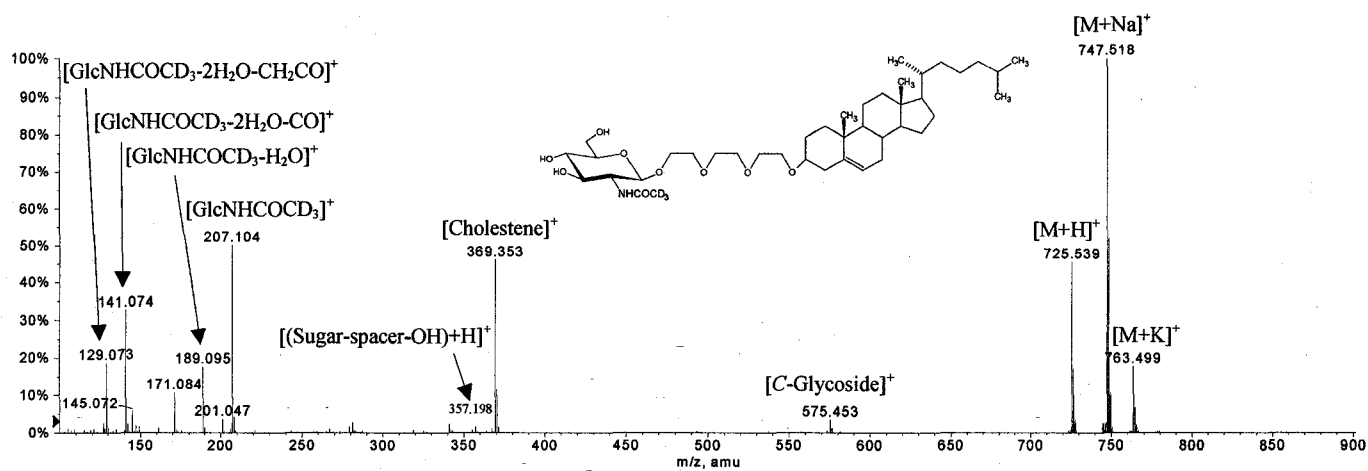


Figure 6-1: Four examples of positive QqToF-MS scans of different amphiphilic neoglycolipids (structure shown within the figure).

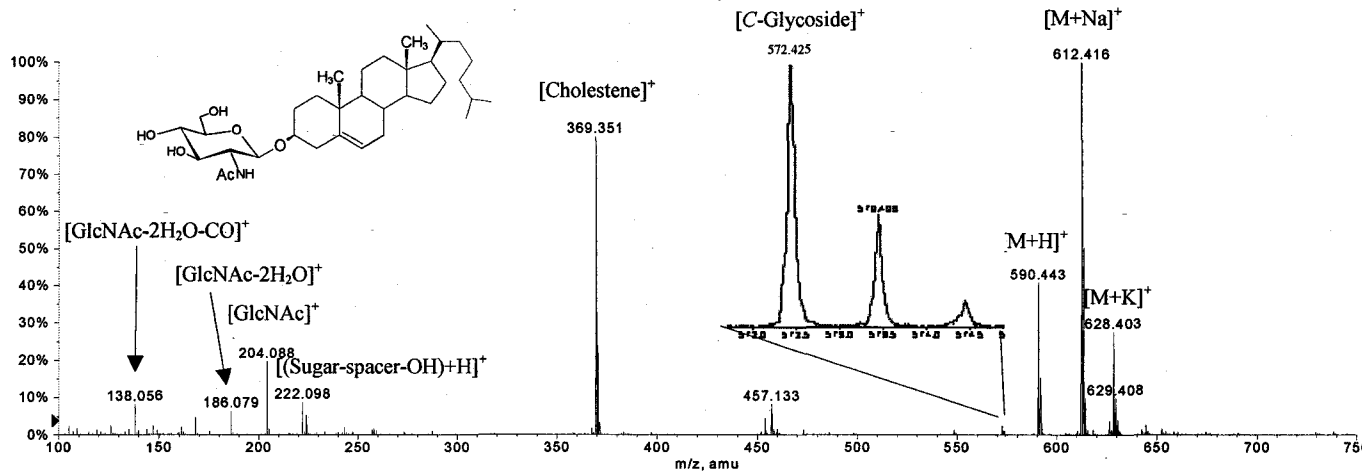
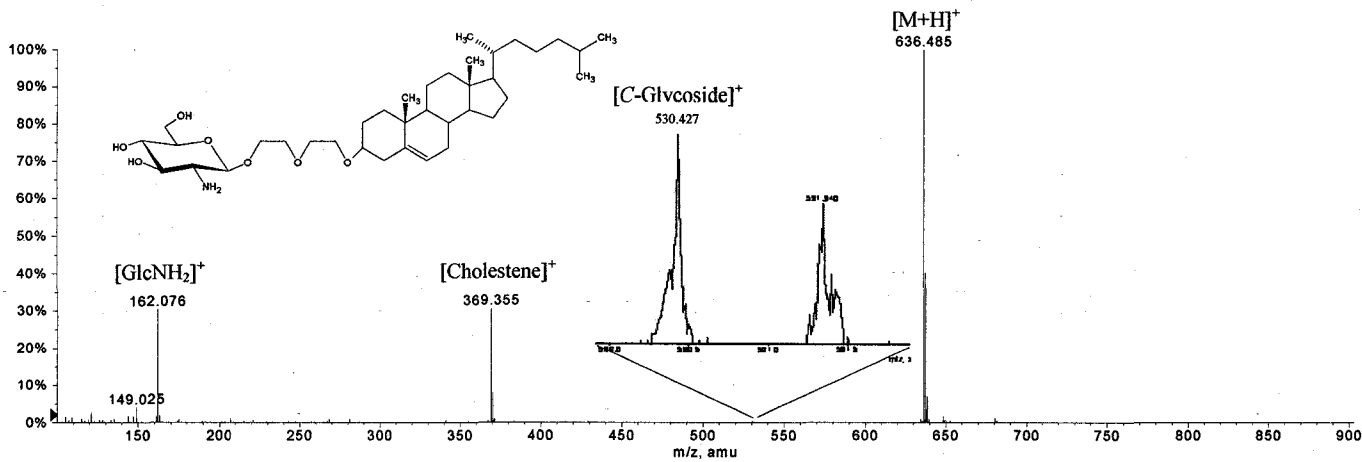


Figure 6-2 is a general schematic representation of the fragment ions observed during ESI-QqToF analysis of these series of neoglycolipids. In this schematic representation, and for the sake of simplicity, the sugar oxonium portion was illustrated as a glucosamine derivative. As can be seen from Figures 6-1 and 6-2, these neoglycolipids can fragment at either of the spacer's ends producing the two diagnostic fragment ions designated as [(Sugar-spacer-OH)+H]⁺ and/or [(Cholesterol-spacer-OH)+H]⁺. Obviously, the length of the "Spacer-OH" corresponds with high accuracy to the tested neoglycolipids. Evidently, there were no "Spacer-OH" in the simple neoglycolipids with O-glycoside linkages and these were observed as protonated reducing sugars bearing the anomeric hydroxyl group. The occurrence of the [(Sugar-spacer-OH)+H]⁺ species was more frequently formed during the analysis than the [(Cholesterol-spacer-OH)+H]⁺ ion and was present in most of the studied neoglycolipids. The genesis of the [(Sugar-spacer-OH)+H]⁺ fragment ion was confirmed using four identical neoglycolipids that bear GlcNAc and a spacer of (CH₂CH₂O)₃ which includes deuterated CH₂ at varying positions of the chain. As expected the non-deuterated species produced the [(Sugar-spacer-OH)+H]⁺ fragment ion at *m/z* 354.17 while the *m/z* value for the corresponding deuterated species was 356.18 (see Figure 6-3). Similarly, the presence of GlcNHCOCD₃ instead of GlcNAc resulted, as expected, in a shift in the *m/z* value of the [(Sugar-spacer-OH)+H]⁺ ion from *m/z* 354.17 Th to *m/z* 357.19 Th (see Figure 6-3).

Additional elimination products, originating from the sugar [Oxonium]⁺ ions, were also observed. These can be summarized as ions formed by the expected loss of one or two water molecules designated as [Oxonium-H₂O]⁺ and [Oxonium-2H₂O]⁺. The subsequent elimination of CO and CH₂CO from these product ions was also noted,

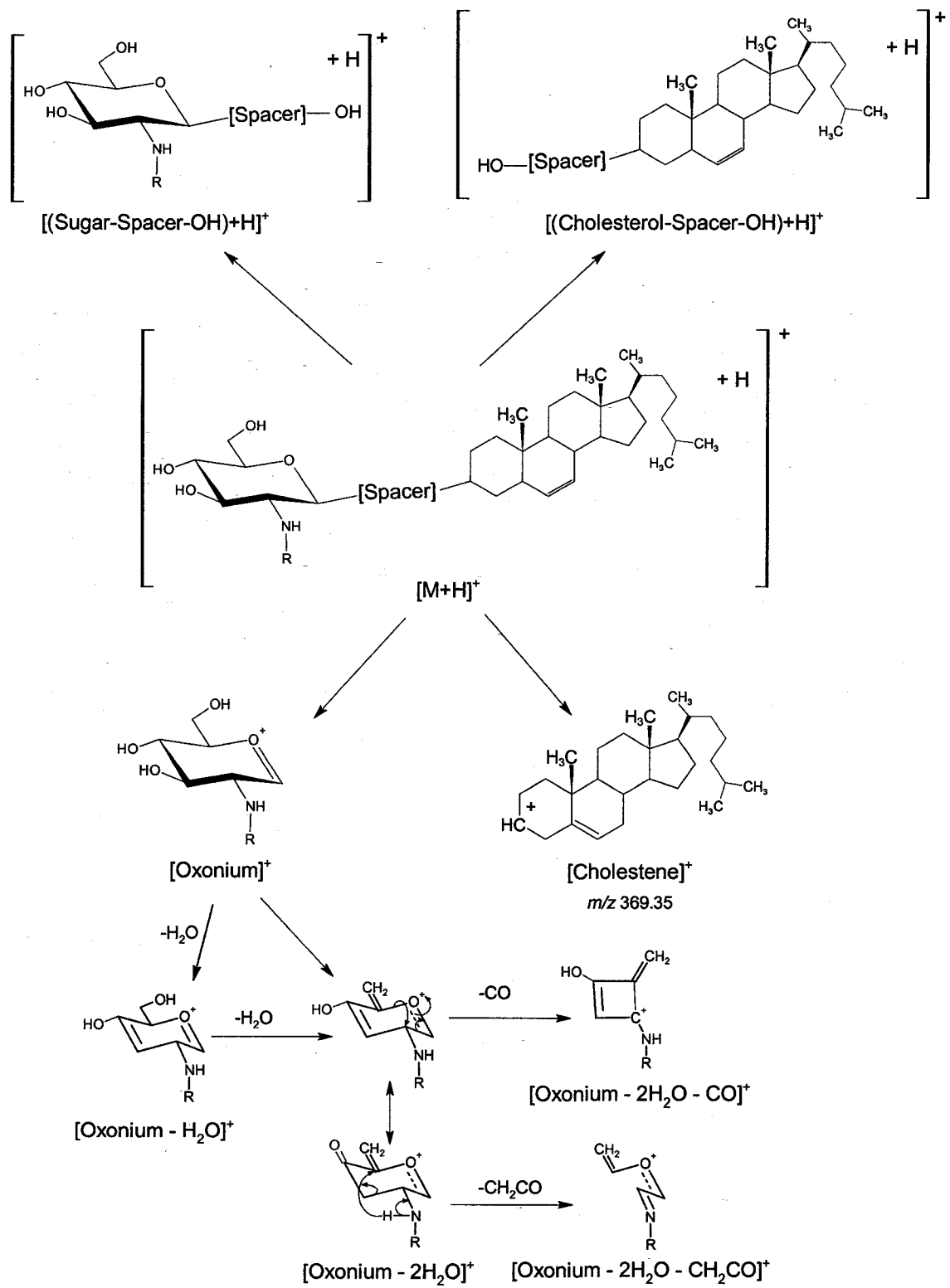
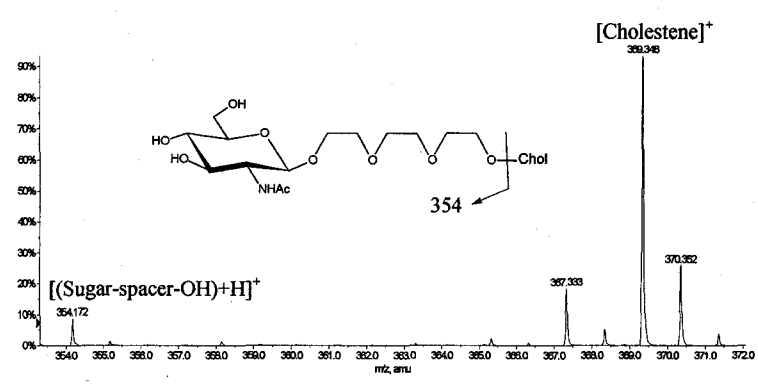
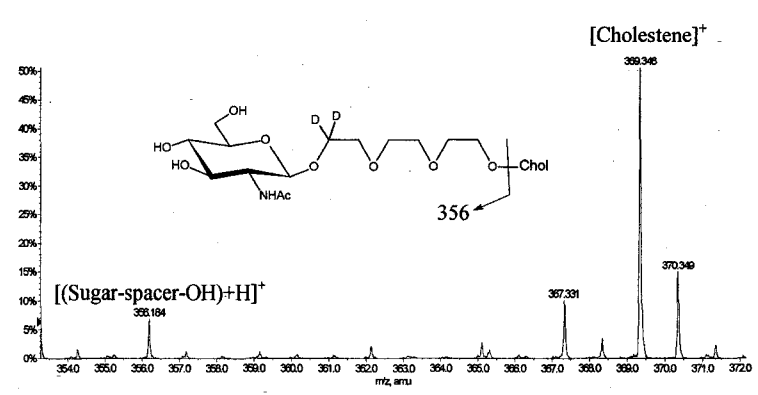
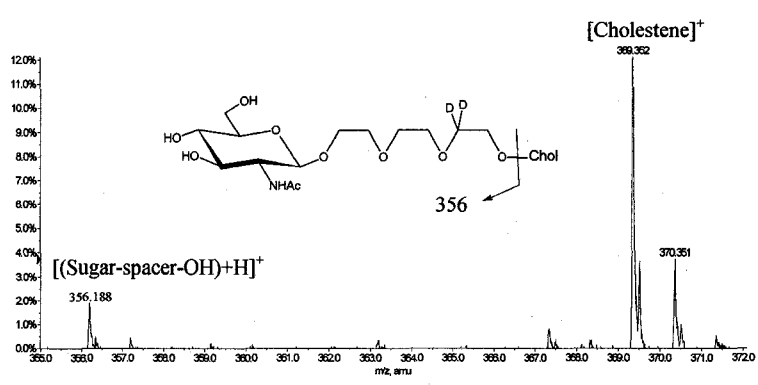


Figure 6-2: General schematic representation of the common fragmentation pattern of the cholesteryl neoglycolipids observed in ToF-MS analysis. The sugar portion is illustrated as glucosamine derivative where R = H, COCH₃, COCD₃, or COOCH₂CH=CH₂.



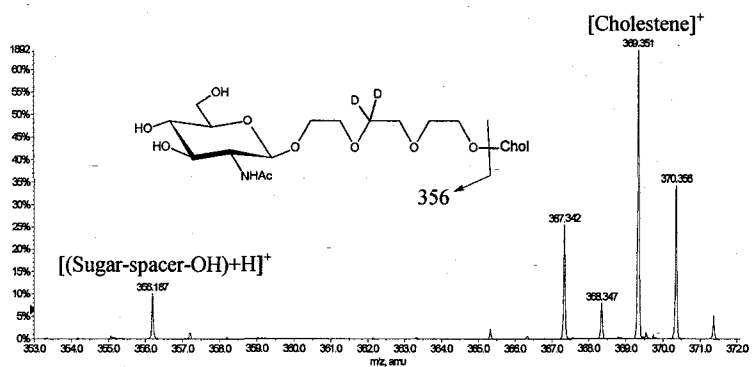
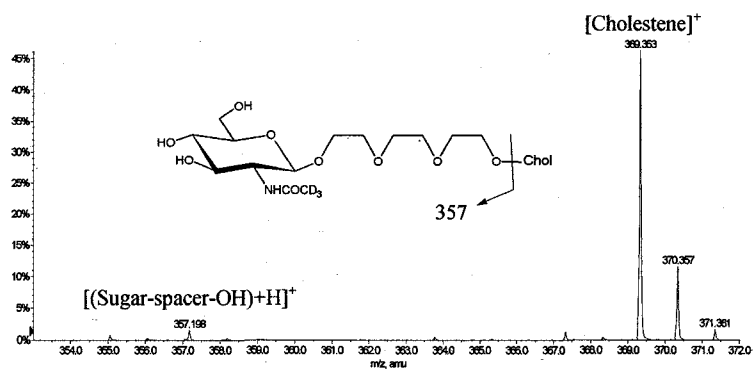


Figure 6-3: Confirmation of the genesis of the ions designated as [(Sugar-spacer-OH)+H]⁺ using deuterated neoglycolipid species.

forming the ions assigned as $[\text{Oxonium-2H}_2\text{O-CO}]^+$ and $[\text{Oxonium-2H}_2\text{O-CH}_2\text{CO}]^+$. Figure 6-1 and Figure 6-2 show the proposed mechanism of these losses. Such elimination products were absent in the case of the sugar $[\text{Oxonium}]^+$ ions of the pre-*O*-acetylated neoglycolipids. Instead, elimination products that correspond to $[\text{Oxonium-OAc}]^+$, $[\text{Oxonium-2OAc}]^+$ and $[\text{Oxonium-3OAc}]^+$ were observed (see Appendix VI). The confirmation of the proposed structure of the various ions observed in the QqToF-MS was accomplished by CID-MS/MS analysis, as described below.

6.3. CID-MS/MS analysis:

The discussion in this section will be divided based on the presence or absence of the acetylated hydroxyl groups within the sugar portion (i.e. protected vs non-protected species).

6.3.1. CID-MS/MS analysis of the precursor protonated molecules of the non-protected neoglycolipids:

Table 6-1 summarizes the fragment ions observed in the CID-MS/MS analysis of the precursor protonated species $[\text{M}+\text{H}]^+$ of some of the amphiphilic neoglycolipids. In this table, a comparison was made between 9 neoglycolipids which bear different sugars; either a linker with different lengths of polyethoxy spacer or a simple *O*-glycoside linkage. The coding of the compounds in this table was based on the assigned number in Figure 2-1 and the nature of the spacer.

As can be seen from Table 6-1, a general fragmentation pattern which is in agreement with Figure 6-2 was observed. Fragment ions, representing $[\text{Cholestene}]^+$,

Fragment Ion	1(CH ₂ CH ₂ O) ₂	1O-glycoside	2(CH ₂ CH ₂ O) ₃	2O-glycoside	3(CH ₂ CH ₂ O) ₃	4(CH ₂ CH ₂ O) ₃	5(CH ₂ CH ₂ O) ₄	6O-glycoside	6(CH ₂ CH ₂ O) ₄
[M+H] ⁺	636.47 C ₃₇ H ₆₆ NO ₇	548.43 C ₃₃ H ₅₈ NO ₅	722.54 C ₄₁ H ₇₂ NO ₉	590.46 C ₃₅ H ₆₀ NO ₆	725.53 C ₄₁ H ₆₉ D ₃ NO ₉	884.60 C ₄₇ H ₈₂ NO ₁₄	709.49 C ₄₁ H ₇₅ O ₉	632.47 C ₃₇ H ₆₂ NO ₇	808.58 C ₄₅ H ₃₄ NO ₁₁
[Cholestene] ⁺	369.36 C ₇₇ H ₄₅	369.35 C ₇₇ H ₄₅	369.38 C ₇₇ H ₄₅	369.36 C ₇₇ H ₄₅	369.36 C ₇₇ H ₄₅	—	369.34 C ₇₇ H ₄₅	369.35 C ₇₇ H ₄₅	369.33 C ₇₇ H ₄₅
[(Sugar-spacer-OH)+H] ⁺	268.15 C ₁₀ H ₂₁ NO ₇	180.08 C ₆ H ₁₄ NO ₅	354.21 C ₁₄ H ₂₈ NO ₉	222.09 C ₈ H ₁₆ NO ₆	357.20 C ₁₄ H ₂₅ D ₃ NO ₉	516.18 C ₂₀ H ₃₈ NO ₁₄	341.17 C ₁₄ H ₂₉ O ₉	264.10 C ₁₀ H ₁₇ NO ₇	440.16 C ₁₈ H ₇₈ NO ₁₁
[(Cholesterol-spacer-OH)+H] ⁺	—	—	—	—	—	—	563.45 C ₃₅ H ₆₃ O ₅	—	563.47 C ₃₅ H ₆₃ O ₅
[C-Glycoside] ⁺	530.42 C ₃₃ H ₅₆ NO ₄	530.43 C ₃₃ H ₅₆ NO ₄	572.46 C ₃₅ H ₅₈ NO ₅	572.44 C ₃₅ H ₅₈ NO ₅	575.45 C ₃₅ H ₅₅ D ₃ NO ₅	734.49 C ₄₁ H ₆₈ NO ₁₀	—	614.46 C ₃₇ H ₆₀ NO ₆	614.33 C ₃₇ H ₆₀ NO ₆
[Oxonium] ⁺	162.09 C ₆ H ₁₂ NO ₄	162.07 C ₆ H ₁₂ NO ₄	204.11 C ₈ H ₁₄ NO ₅	204.08 C ₈ H ₁₄ NO ₅	207.11 C ₈ H ₁₁ D ₃ NO ₅	366.11 C ₁₄ H ₂₄ NO ₁₀	147.01 C ₆ H ₁₁ O ₄	246.09 C ₁₀ H ₁₆ NO ₆	246.07 C ₁₀ H ₁₆ NO ₆
[Oxonium-H ₂ O] ⁺	144.08 C ₆ H ₁₀ NO ₃	144.06 C ₆ H ₁₀ NO ₃	186.10 C ₈ H ₁₂ NO ₄	186.07 C ₈ H ₁₂ NO ₄	189.10 C ₈ H ₉ D ₃ NO ₄	—	—	228.09 C ₁₀ H ₁₄ NO ₅	228.08 C ₁₀ H ₁₄ NO ₅
[Oxonium-2H ₂ O] ⁺	—	—	168.10 C ₈ H ₁₀ NO ₃	168.06 C ₈ H ₁₀ NO ₃	171.09 C ₈ H ₇ D ₃ NO ₃	—	—	210.07 C ₁₀ H ₁₂ NO ₄	210.05 C ₁₀ H ₁₂ NO ₄
[Oxonium-2H ₂ O-CO] ⁺	—	—	138.07 C ₇ H ₈ NO ₂	138.05 C ₇ H ₈ NO ₂	141.09 C ₇ H ₅ D ₃ NO ₂	—	—	180.06 C ₉ H ₁₀ NO ₃	180.04 C ₉ H ₁₀ NO ₃
[Oxonium-2H ₂ O-CH ₂ CO] ⁺	—	—	126.08 C ₆ H ₈ NO ₂	126.05 C ₆ H ₈ NO ₂	129.08 C ₆ H ₅ D ₃ NO ₂	—	—	168.06 C ₈ H ₁₀ NO ₃	168.05 C ₈ H ₁₀ NO ₃
[(OH-Spacer-OH)+H] ⁺	—	—	—	—	—	—	195.11 C ₈ H ₁₉ O ₅	—	195.09 C ₈ H ₁₉ O ₅

Table 6-1: list of characteristic ions observed within MS/MS analysis of 9 protonated molecules $[M+H]^+$ of the neoglycolipids bearing non-protected sugar species. Each neoglycolipid was designated based on the sugar portion (Figure 2-1) and the nature of the spacer.

[Oxonium]⁺, [(Sugar-spacer-OH)+H]⁺ and [(Cholesterol-spacer-OH)+H]⁺ were identified. Figure 6-4 shows the CID-MS/MS spectra of three neoglycolipids bearing LacNAc and GlcNAc sugar moieties. The [(Sugar-spacer-OH)+H]⁺ fragment ion was simply [(Sugar-OH)+H]⁺ when the sugar was attached to the cholesterol portion through *O*-glycoside (see Figure 6-4A). As expected, elimination product ions derived from the sugar [Oxonium]⁺ species were also observed and were similar to those obtained via conventional single stage QqToF-MS analysis (Figure 6-2). The general fragmentation pattern observed in the CID-MS/MS spectra (Table 6-1) suggested that the ions obtained in the one-stage QqToF-MS (Figure 6-1) are indeed fragments that originate from the protonated species of these neoglycolipids, rather than being separate species. This was supported by the fact that the “in source” fragmentation was significantly repressed when manipulating the mass spectrometry parameters, namely reducing the Declustering Potential (DP). It was also observed that the presence of the [(Cholesterol-spacer-OH)+H]⁺ and [(OH-Spacer-OH) +H]⁺ fragment ions were only associated with the neoglycolipids bearing a polyethoxy spacer of (CH₂CH₂O)₄ (Table 6-1, Fig 6-4B). The CID-MS/MS spectra of all the neoglycolipids are presented in Appendix VII.

In addition to the expected fragment ions, an unforeseen peak, whose mass was compatible with that of a *C*-glycoside species, presumably formed by nucleophilic attack of the neutral cholest-3,5-diene molecule on the sugar [oxonium]⁺ ion formed during the CID-MS/MS process. The formation of the unique [*C*-Glycoside]⁺ ion was observed during the CID-MS/MS only when the neoglycolipids contained a 1,2-participating group, with the exception of L-fucose. In fact, this ion was also present in the conventional one-stage ESI-QqToF-MS; careful examination of the spectra shows that the

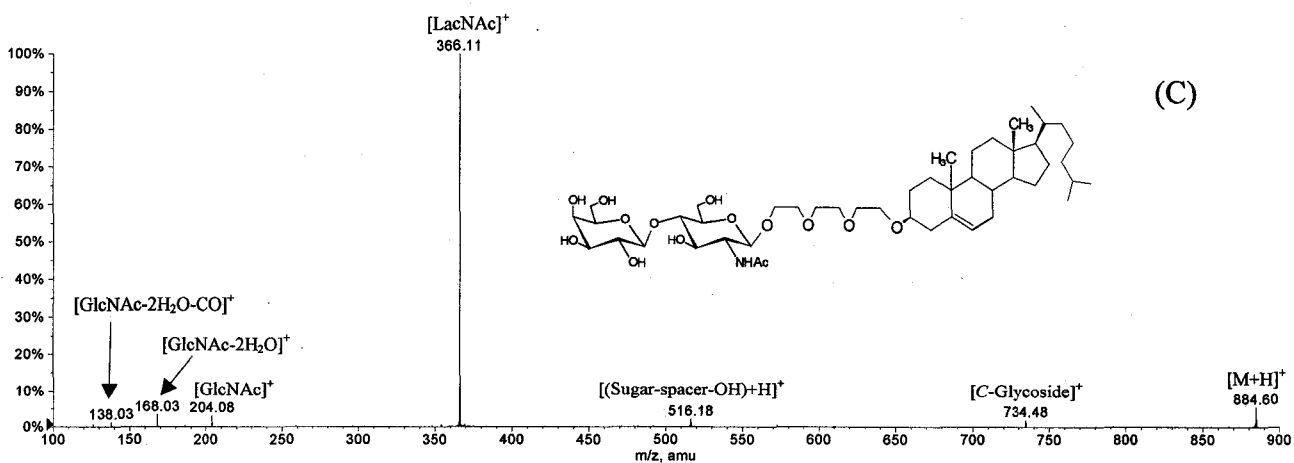
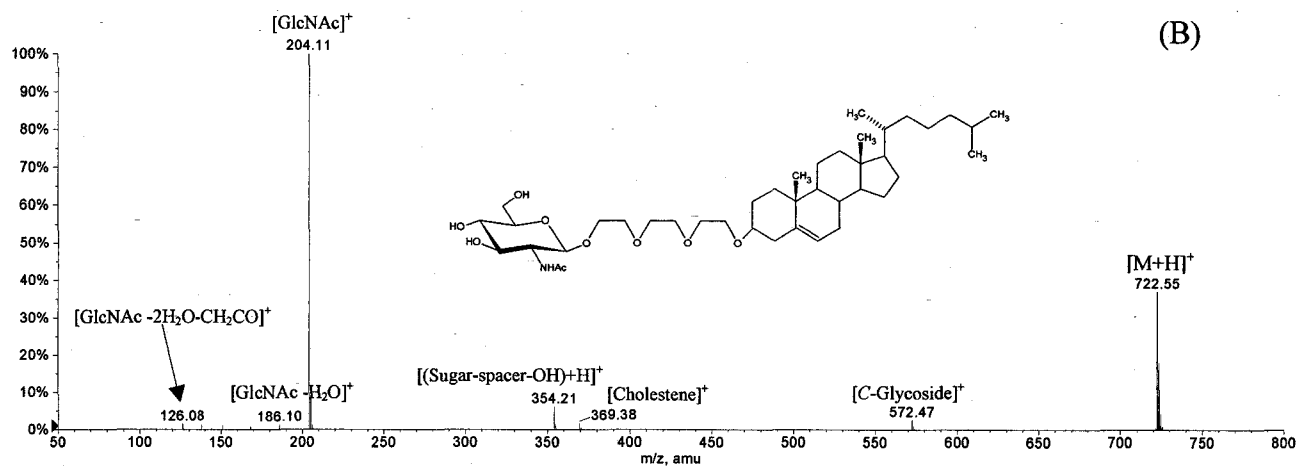
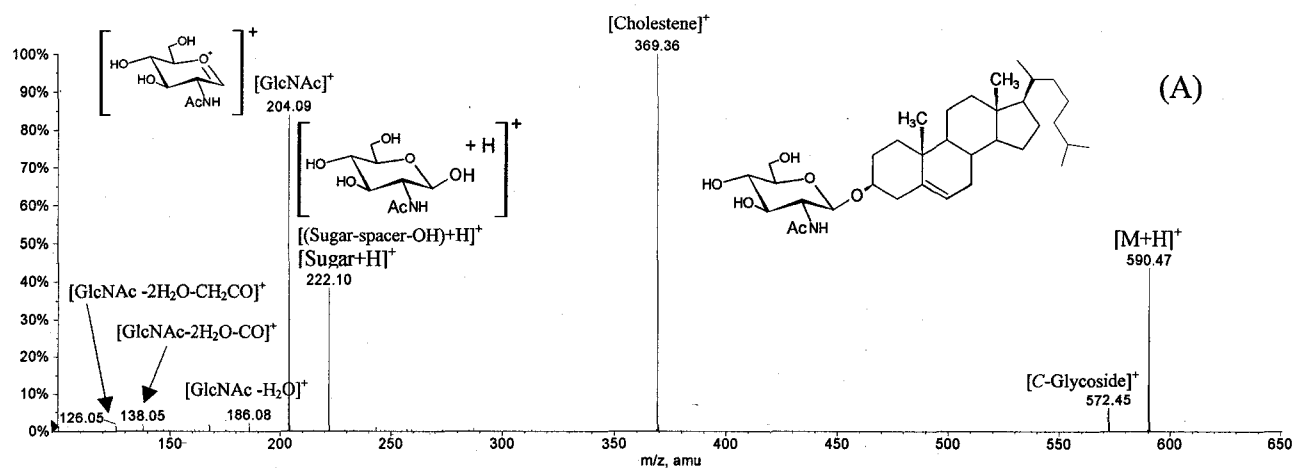


Figure 6-4: MS/ MS experiments of neoglycolipids bearing (A) GlcNAc linked to the cholesterol portion via *O*-Glycoside; (B) GlcNAc linked to the cholesterol portion via $(\text{CH}_2\text{CH}_2\text{O})_3$ spacer; and (C) LacNAc linked to the cholesterol portion via $(\text{CH}_2\text{CH}_2\text{O})_3$ spacer.

[C-Glycoside]⁺ ion was also formed during ESI ionization and it was not simply an “impurity” as was speculated initially when examining the QqToF-MS spectra (refer to Figure 6-1). It was hypothesized that this ion results from a unique ion-molecule reaction between the sugar portion as an oxonium ion and a neutral cholesterol species. Further discussion on the structure and formation of this ion using the various neoglycolipids evaluated in this study will be presented in the following sections.

Finally, the presence of LacNAc (β -D-Galp-(1→4)-D-GlcpNAc) resulted in the formation of additional sugar fragment ions beside the ones presented in Table 6-1 (Figure 6-4C). These ions were formed from the diagnostic [LacNAc]⁺ ion observed at m/z 366.11 (i.e. [Oxonium]⁺) and include the [GlcNAc]⁺ ion at m/z 204.08, the [GlcNAc-2H₂O]⁺ ion at m/z 186.04, and the [GlcNAc-2H₂O-CO]⁺ ion at m/z 138.03 (all derived from the reducing end of the disaccharide). The presence of these additional fragments is expected and they serve as diagnostic product ions confirming the structure of this neoglycolipid.

To verify the authenticity of the fragment ions assigned based on the conventional single-stage QqToF-MS analysis and on the CID-MS/MS experiments of the precursor protonated species [M+H]⁺, additional CID-MS/MS were obtained by increasing the “in source” fragmentation (also called “*in nozzle*” fragmentation) which can be enhanced and optimized for each tested species through manipulation of the Declustering Potential (DP) and the Focusing Potential (FP) values within the ionization source (i.e. optimum potentials for each precursor ion, in terms of ion count and S/N ratio).

Figure 6-5 represents the CID-MS/MS spectra of the neoglycolipid structure 6 (Figure 2-1) bearing (CH₂CH₂O)₄ as a spacer (Figure 6-5A) as well as the CID-MS/MS of

the [(Cholesterol-spacer-OH)+H]⁺ (Figure 6-5B) and the [(OH-Spacer-OH)+H]⁺ fragment ions (Figure 6-5C). As can be seen in Figure 6-5A, the CID-MS/MS analysis of the [M+H]⁺ ion followed the same pattern as discussed earlier and shown in Figure 6-2 and Table 6-1. However, the CID-MS/MS of the [(Cholesterol-spacer-OH)+H]⁺ species at 563.47 produced two major product ions corresponding to [Cholestene]⁺ at *m/z* 369.33 and the [(HO-(CH₂CH₂O)₃-OH)+H]⁺ at *m/z* 195.09. Similarly, the CID-MS/MS of the [(HO-(CH₂CH₂O)₃-OH)+H]⁺ ion at 195.09 produced product ions corresponding to the proposed structure of this ion (see Figure 6-4C). It showed distinctive, consecutive losses of water molecules followed by elimination of an acetylene species (CH≡CH). These findings established the universal fragmentation pattern illustrated in Figure 6-2.

6.3.1.1. The formation of [C-Glycoside]⁺:

As shown in Table 6-1 and Figure 6-4, [C-Glycoside]⁺ species were observed first during the MS/MS experiment within the collision cell of the tandem mass spectrometer. However, this ion was also present in the one stage ESI-QqToF experiment (see Figure 6-1). The formation of this unique ion cannot be explained based on the molecular structure of these novel synthetic neoglycolipids (Figure 2-1). To confirm the proposed structure of this ion, CID-MS/MS was performed on the isolated C-glycoside and showed that this ion can undergo two concerted cleavages which occur simultaneously from the precursor [C-glycoside]⁺ ion. The first involves the elimination of the axial H-2 hydrogen of the sugar moiety, with consecutive rupture and migration of the anomeric C-1-C-3' bond and the consequent formation of the neutral fragment 2-*N*-acetyl-2-deoxy-D-glucal. This is followed by formation of the C-3'-C-4' double bond and migration of the

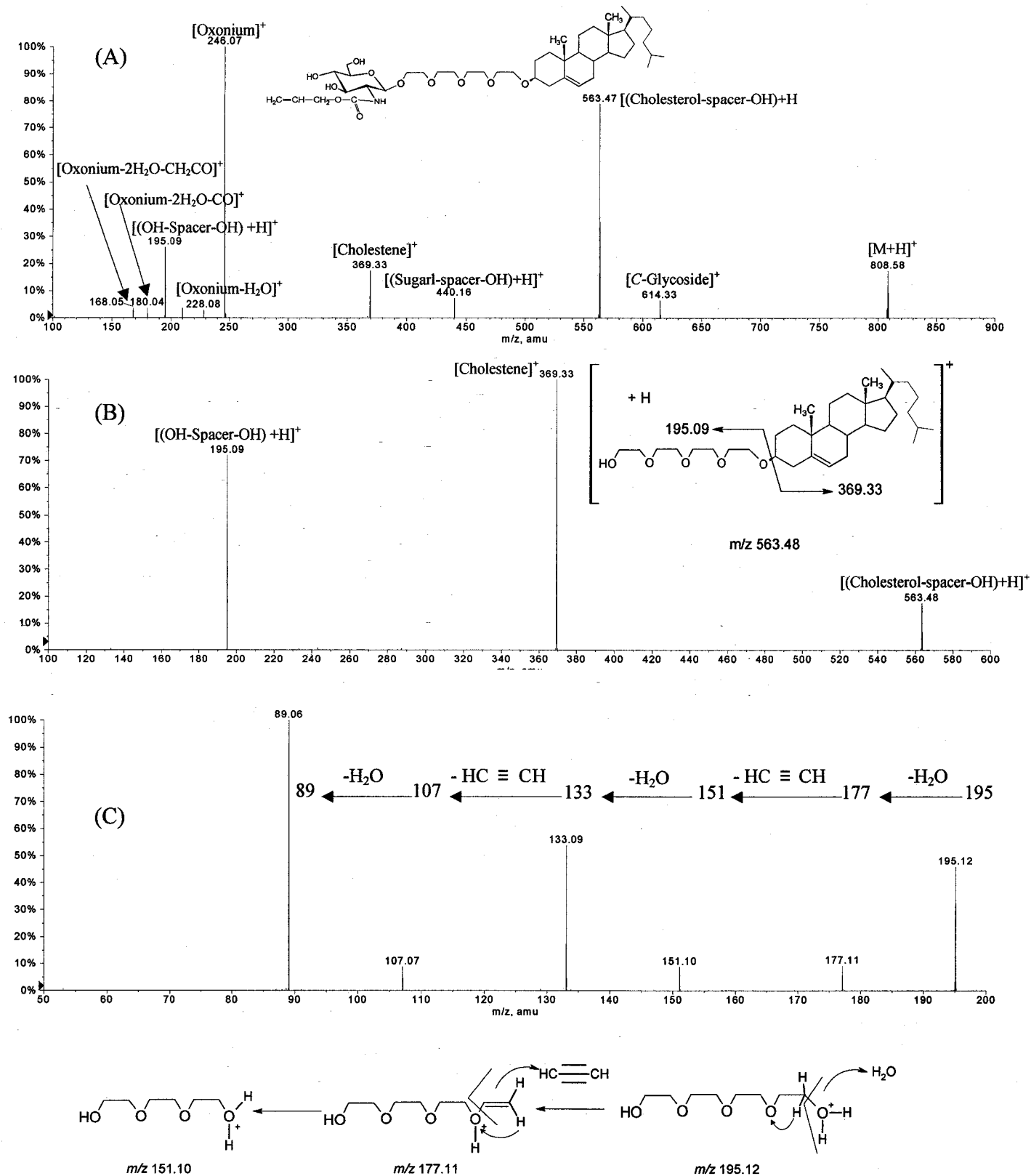


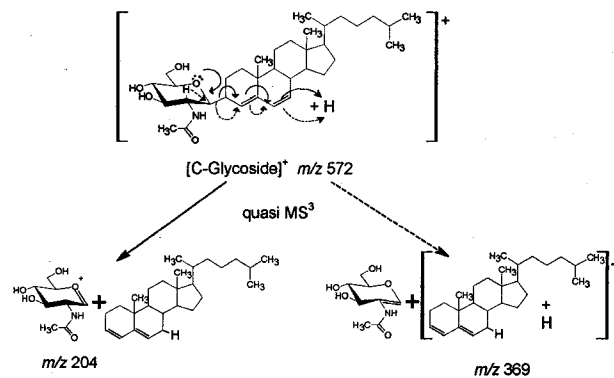
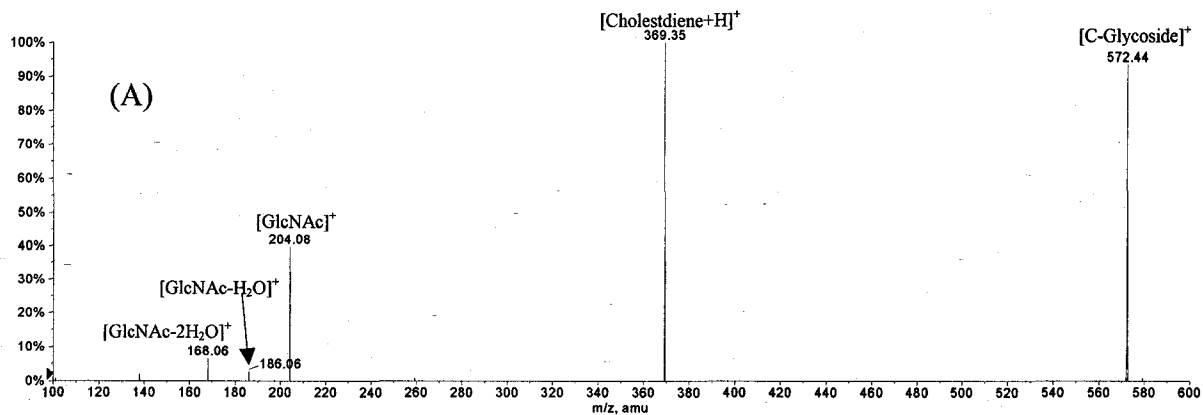
Figure 6-5: (A) MS/MS scan of neoglycolipid bearing GlcNAloc linked to the cholesterol portion via $(\text{CH}_2\text{CH}_2\text{O})_4$ spacer. (B) MS/MS of the fragment ion designated as $[(\text{Cholesterol-spacer-OH})+\text{H}]^+$. (C) MS/MS of the fragment ion designated as $[(\text{OH-Spacer-OH})+\text{H}]^+$.

endocyclic C-4'-C-5' double bond, to afford the protonated cholest-3,5-diene molecule assigned as [Cholestadiene+H]⁺ at *m/z* 369.35. The second mechanism suggests the participation of the lone pair of electrons on the sugar ring oxygen to afford the stable sugar 1,2-oxonium ion [Oxonium]⁺, with identical rupture of the anomeric C-1-C-3' bond and migration of the double bonds, to produce the neutral cholest-3,5-diene molecule.

Figure 6-6 shows the CID-MS/MS of two [C-Glycoside]⁺ ions that contain LacNAc and GlcNAloc (extracted from the neoglycolipids **4** and **2**, containing the (OCH₂CH₂)₃ spacer or simple *O*-glycoside, respectively) and illustrates clearly the presence of [Cholestadiene+H]⁺ at *m/z* 369.35, [LacNAc]⁺ at *m/z* 366.13 and [GlcNAc]⁺ at *m/z* 204.08. Elimination products of the sugar [Oxonium]⁺ were also present in this MS/MS analysis. This MS/MS analysis authenticated the proposed structure of the [C-Glycoside]⁺ ion. A list of all the [C-glycoside]⁺ species, their sources and the diagnostic product ions is shown in Table 6-2.

Table 6-2: Tabulated CID-MS/MS results of the [C-Glycoside]⁺ ions

<i>m/z</i> value of the C-glycoside species	Source	Diagnostic product ions [Cholestene] ⁺ , [Oxonium] ⁺
530.42	Compounds 1	369.35, 162.07
572.43	Compounds 2	369.35, 204.08
575.44	Compound 3	369.35, 207.10
734.48	Compound 4	369.35, 366.13
614.44	Compounds 6	369.35, 246.09



To explain the rationale beyond the formation of the $[C\text{-glycoside}]^+$ ion, it was proposed that a unique ion-molecule reaction occurs in the collision cell and within the ESI interface of the turbo ion spray source. It was postulated that the parent $[M+H]^+$ ion of the complete neoglycolipid molecule undergoes covalent bond cleavages producing the sugar $[\text{Oxonium}]^+$ ion as well as the neutral cholestene. The latter can then attack through the electrophilic center of the nucleophilic cyclic sugar $[\text{Oxonium}]^+$ species producing the ion designated as the $[C\text{-Glycoside}]^+$. The presence of the amino group at position C-2 of the sugar residue enhances the formation of a more “reactive” 1,2 cyclic oxonium aziridinium species with a “strong” electrophilic position that is prone to nucleophilic attack from the neutral cholestene species to afford for the formation of the corresponding *C*-glycoside (see Figure 6-7A & 6-7B for details). In the event that the glycosyl moiety of the neoglycolipid did not bear a participating group at position C-2, the $[C\text{-Glycoside}]^+$ was absent as in the case of neoglycolipid bearing the Fuc sugar (Table 6-1). Despite the presence of the $[\text{Fuc}]^+$ oxonium ion at m/z 147.01 during ESI ionization, this ion failed to react with the neutral cholestene species since it lacks the participating group at position C-2 and as a result it can not form the corresponding ion $[C\text{-Glycoside}]^+$ (Figure 6-7C). As can be seen from Figure 6-7 and Figure 6-6, it was opted to illustrate that the $[C\text{-Glycoside}]^+$ ions were produced by the formation of a C-1-C-3' covalent bond between the sugar and the cholesteryl portions. However, the presence of another $[C\text{-Glycoside}]^+$ species that carries the C-1-C-5' covalent bond can not be excluded by the same mechanism, although it is improbable due to the potential steric hindrance of this latter *C*-glycoside. Needless to say, there is no way to tell for sure whether the formed *C*-

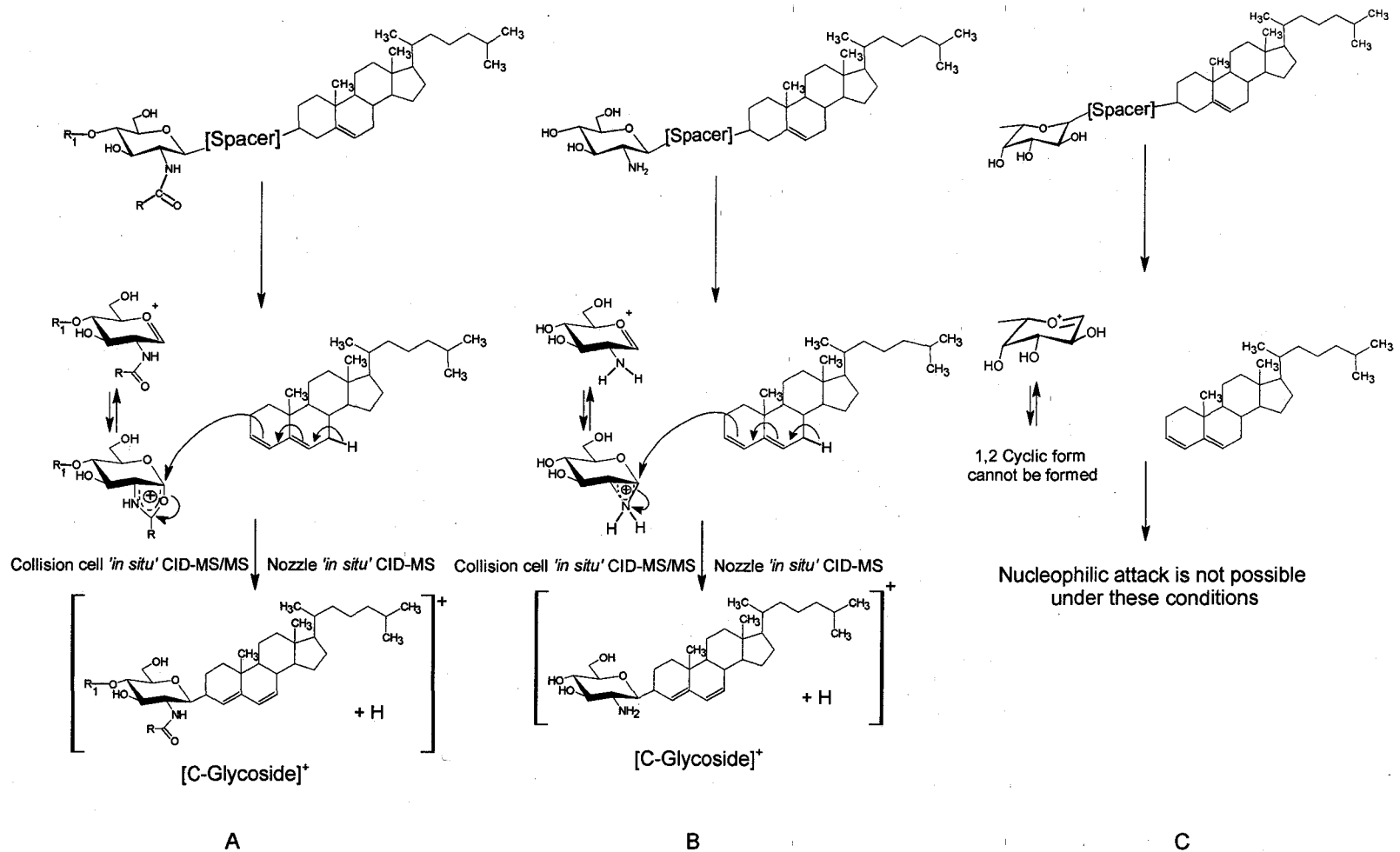


Figure 6-7: Schematic representation of the mechanistic process that leads to the formation of the $[C\text{-Glycoside}]^+$ ion within the ESI interface and during CID-MS/MS analysis. A) The sugar portion is a derivative *N*-acyl glucosamine where $R=\text{CH}_3$, CD_3 , or $\text{COOCH}_2\text{CH}=\text{CH}_2$; $R_1=\text{H}$, or $\beta\text{-D-Gal}$. B) The sugar portion is a GlcNH_2 species. C) The sugar portion is Fuc species.

glycoside possesses the β -D-configuration, the α -D-configuration, or an anomeric mixture of both. Nevertheless, the attributed β -D-configuration is, without doubt, the preferred configuration as it is known that it more kinetically and thermodynamically stable (Banoub *et al.*, 1992).

In addition to the absence of the $[C\text{-Glycoside}]^+$ in the case of the Fuc derived neoglycolipids, this ion was also absent in the low energy CID-MS/MS analysis of the sodiated adducts $[M+Na]^+$ of the neoglycolipid series evaluated in this study. For illustration purpose, Figure 6-8 represents the fragmentation pattern of the product ion scan of the $[M+Na]^+$, isolated from the neoglycolipid designated as 3, containing the spacer $(CH_2CH_2O)_3$. The fact that both $[Oxonium]^+$ and $[Cholestene]^+$ ions were absent in the MS/MS of the $[M+Na]^+$, suggests that this adduct breaks in different fashion than the one observed with $[M+H]^+$ and does not form the reactive species that can result in the formation of the C-glycoside bond. All the fragment ions were actually sodiated species and included a fragment ion that is generated from inner sugar breakage, namely $^{0,2}X$. Such inner sugar fragments are common and widely observed in glycoconjugate analysis (Banoub *et al.*, 2004b; El-Aneed & Banoub, 2005), and it was observed in our study of the $[M+H]^+$, namely the ion designated $[Oxonium-2H_2O-CH_2CO]^+$ (see Figure 6-2).

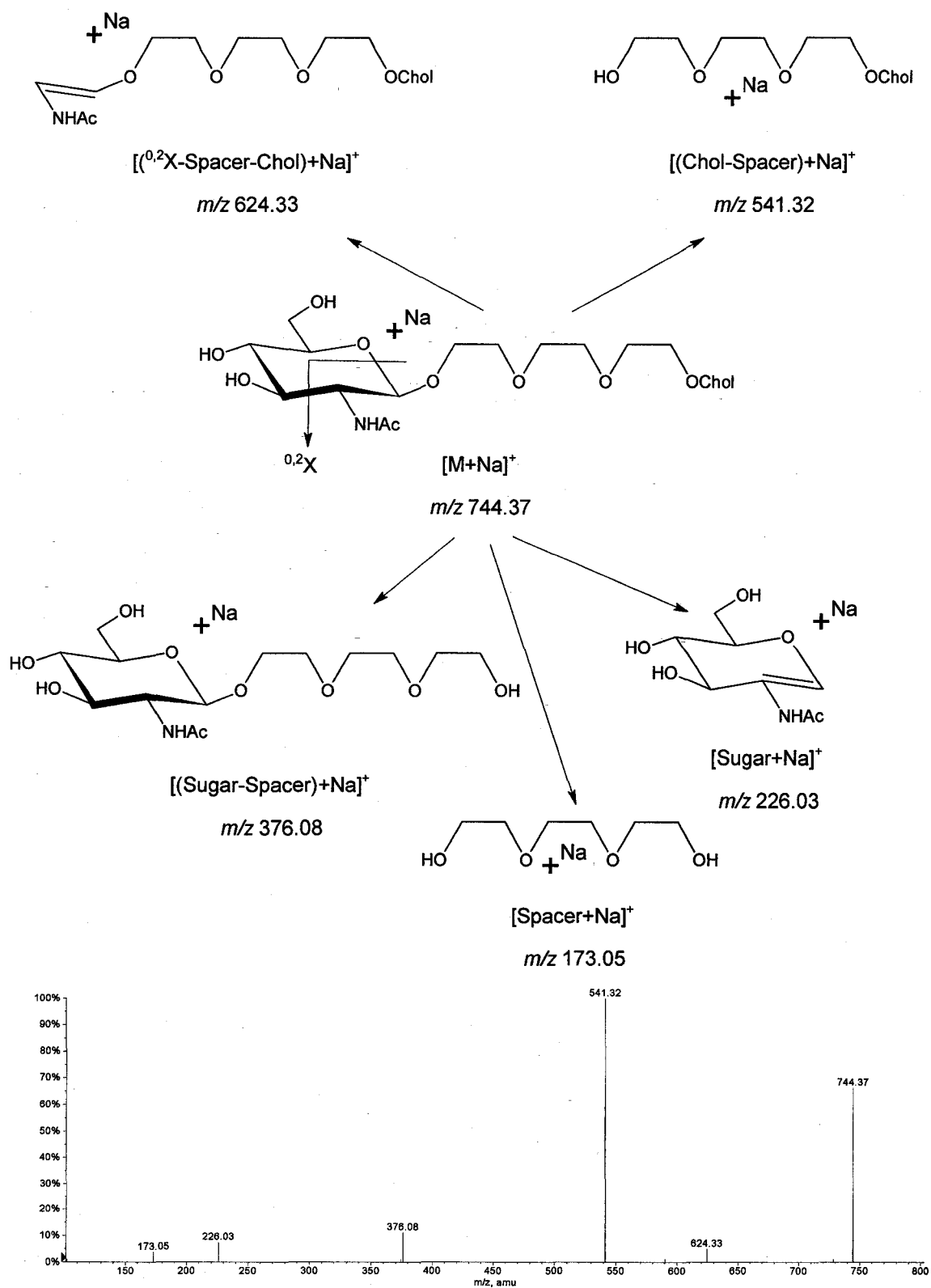


Figure 6-8: The proposed fragmentation pattern of the $[\text{M}+\text{Na}]^+$ of the neoglycolipid bearing GlcNAc with a $(\text{CH}_2\text{CH}_2\text{O})_3$ spacer.

6.3.1.2. The influence of Declustering Potential (DP) and Focusing potential (FP) on the formation of C-Glycoside:

Both DP and FP are electrical voltages that have the greatest effects on the extent of the fragmentation within the orifice-skimmer region of the ESI source of the QStar XL hybrid tandem mass spectrometer. C-Glycoside ion formation was significantly correlated with the DP (Spearman's correlation coefficient, p-value=0.009), (Figure 6-9A) but not with the FP (p-value=0.54) (Figure 6-9B). Therefore, the FP value was kept constant (FP=220) while studying the influence of the DP on ion formation. The pattern between the ion count (intensity) and the DP values was similar for the formation of the C-glycoside species and the sugar [oxonium]⁺ ions (2 samples Kolmogorov-Smirnov Test, p-value=0.34), but showed significance differences when the formation of the C-glycoside was compared to that of other ions such as [M+H]⁺ and [(Sugar-spacer-OH)+H]⁺ (p-value= 8.082e-08 and < 2.2e-16, respectively).

As shown in Figure 6-10, the [C-Glycoside]⁺ ion formation (with respect to DP values) followed the exact pattern of the sugar [oxonium]⁺ species. This supports the theory that the formation of the [C-Glycoside]⁺ species was a product of a reaction between the sugar [oxonium]⁺ ion and the neutral fragment cholesta-3,5-diene. Please note that when comparing different species the ion count values were normalized to the maximum reading.

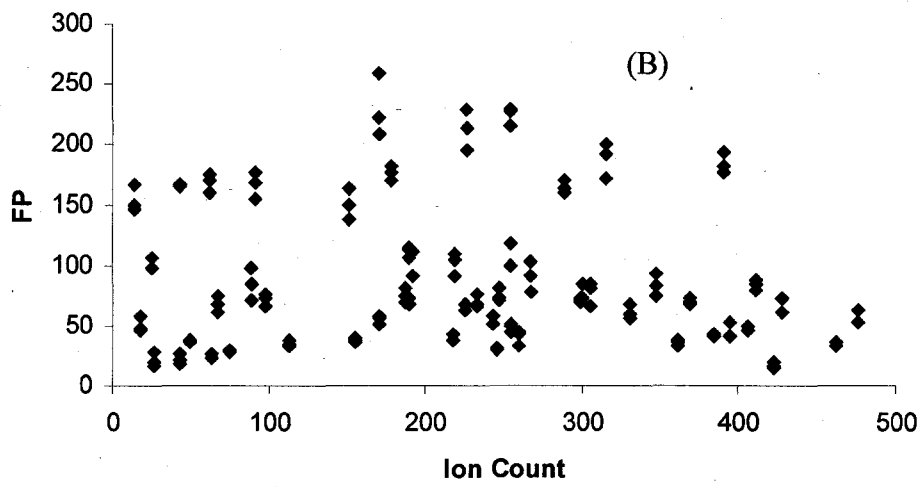
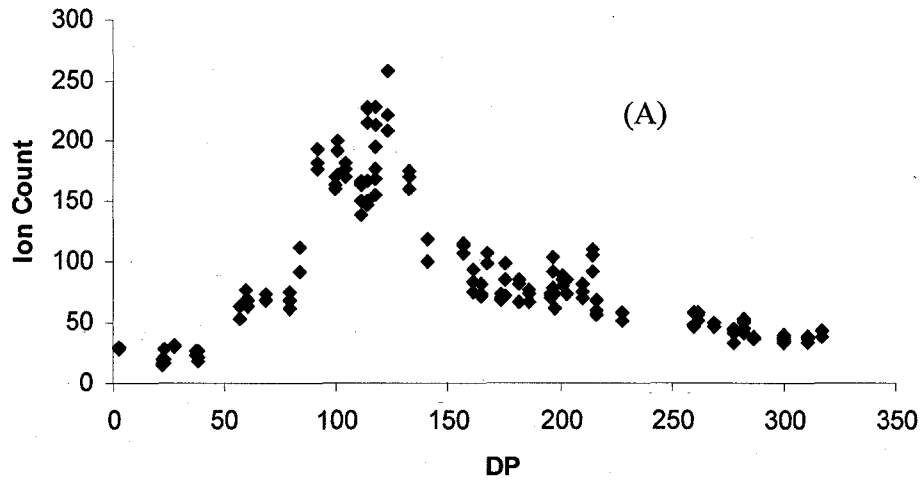


Figure 6-9: The relationship between $[C\text{-glycoside}]^+$ ion count and (A) DP values; (B) FP values.

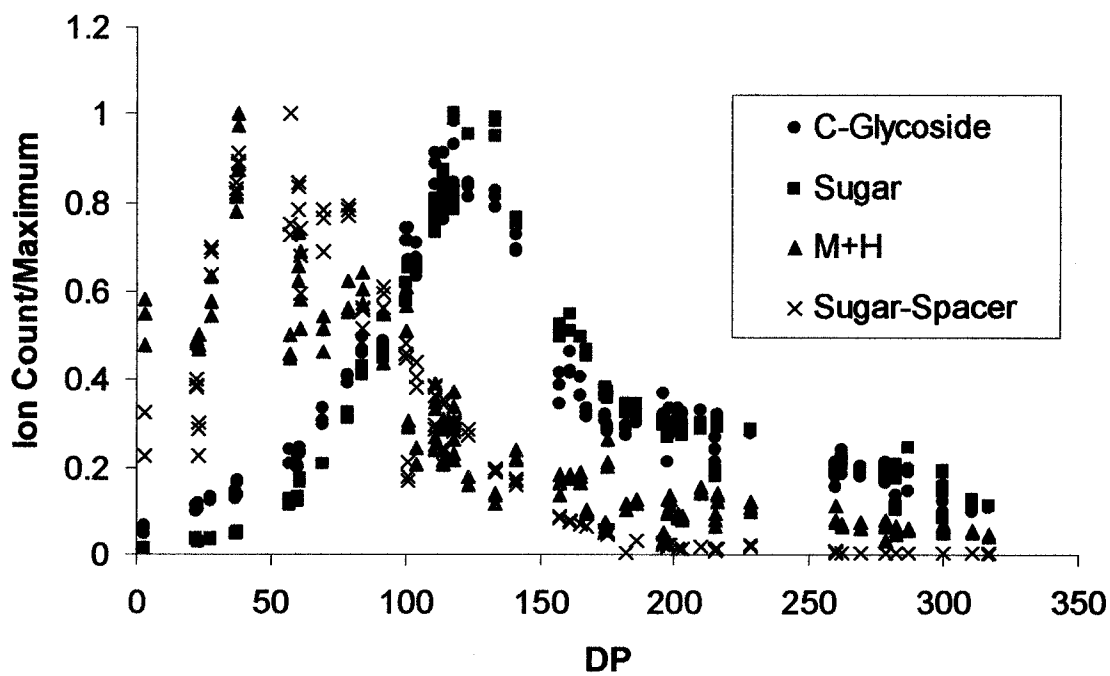


Figure 6-10: The influence of DP on the formation of $[C\text{-glycoside}]^+$, $[\text{Oxonium}]^+$, $[M+H]^+$, and $[(\text{Sugar-spacer})+H]^+$ ions within the ESI interface of the Q-Star Machine.

6.3.2. CID-MS/MS analysis of the precursor protonated molecules of the protected per-*O*-acetylated neoglycolipids:

The per-*O*-acetylated neoglycolipids were used, as it was anticipated that the formation of the more reactive 1,2-cyclic oxonium ion would enhance the rate of the ion-molecule reaction. This may result in more efficient formation of the *C*-glycoside in the ESI source and in the collision cell of the hybrid tandem mass spectrometer. Table 6-3 summarizes the fragmentation pattern of the protonated molecules $[M+H]^+$ of the per-*O*-acetylated neoglycolipids. The presence of the diagnostic fingerprint ions namely $[Cholestene]^+$, $[(Sugar-spacer-OH)+H]^+$, and $[Oxonium]^+$ were observed. Similar to the non-protected neoglycolipids, the presence of $[(Cholesterol-spacer-OH)+H]^+$ was only associated with the neoglycolipid bearing $(CH_2CHO)_4$ spacer. As expected, the elimination products originating from the $[Oxonium]^+$ ions were a result of one, two or three losses of acetic acid groups (see Table 6-3). Additional elimination products of the $[Oxonium]^+$ are also formed and are presented in detail below.

The most interesting finding was, however, that the $[C-Glycoside]^+$ ion was absent in the case of these per-*O*-acetylated sugar derivatives (See Table 6-3). This observation contradicts expectations, as the per-*O*-acetylated sugars are routinely used for *C*-glycosylation reactions in synthetic chemistry (Postema, 1995). In fact, the per-*O*-acetylated neoglycolipids are not used for liposomal preparations and they were synthesized in order to enhance to formation of *C*-glycoside. However, the fact that this reaction occurs in the gas phase can introduce many new factors which are different from the conditions that rule solid and solution chemistry. One possible explanation is the overall reactivity of the per-*O*-acetylated-sugar oxonium ions. These oxonium ions,

Fragment Ion	4(CH ₂ CH ₂ O) ₃	6(CH ₂ CH ₂ O) ₄	6O-glycoside
[M+H] ⁺	1136.66 C ₅₉ H ₉₄ NO ₂₀	943.62 C ₅₁ H ₈₄ NO ₁₄	758.51 C ₄₃ H ₆₈ NO ₁₀
[Cholestene] ⁺	369.34 C ₇₇ H ₄₅	—	369.37 C ₇₇ H ₄₅
[(Cholesterol-spacer-OH)+H] ⁺	—	563.47 C ₃₅ H ₆₃ O ₅	—
[(Sugar-spacer-OH)+H] ⁺	768.29 C ₃₂ H ₅₀ NO ₂₀	566.25 C ₂₄ H ₄₀ NO ₁₄	390.16 C ₁₆ H ₂₄ NO ₁₀
[C-Glycoside] ⁺	—	—	—
[Oxonium] ⁺	618.20 C ₂₆ H ₃₆ NO ₁₆	372.12 C ₁₆ H ₂₂ NO ₉	372.14 C ₁₆ H ₂₂ NO ₉
[Oxonium-OAc] ⁺	558.18 C ₂₄ H ₃₂ NO ₁₄	—	312.10 C ₁₄ H ₁₈ NO ₇
[Oxonium-2OAc] ⁺	498.15 C ₂₂ H ₂₈ NO ₁₂	252.08 C ₁₂ H ₁₄ NO ₅	252.09 C ₁₂ H ₁₄ NO ₅
[Oxonium-3OAc] ⁺	438.09 C ₂₀ H ₂₄ NO ₁₀	192.06	192.07 C ₁₀ H ₁₀ NO ₃

Table 6-3: list of characteristic ions observed within MS/MS analysis protonated molecules of the neoglycolipids bearing protected sugar species. Each neoglycolipid was designated based on the sugar portion (Scheme 1) and the nature of the spacer.

being extremely reactive due to the presence of OAc groups, preferentially eliminate molecules of acetic acid and ketene, by concerted mechanisms, destabilizing the 1,2-cyclic oxonium ion. Therefore, this oxonium ion has no time to form the cyclic reactive species which can react with the nucleophilic cholesta-3,5-diene molecule in the collision cell. Although this speculation can provide some explanation for the absence of the [C-Glycoside]⁺, other possible mechanisms such as steric hindrance cannot be excluded. Other possibilities may also unfold in the future with advances in the field of gas-phase chemistry.

CID-MS/MS, once more, confirmed the assigned structure of the product ions shown in Table 6-3. Figure 6-11 represents a comparison of the CID-MS/MS of the [Oxonium]⁺ ions that corresponds to neoglycolipids bearing the 2-*N*-allyloxycarbonylamino-2-deoxy group (GlcNAloc), or the per-*O*-acetylated GlcNAloc sugar species with the (CH₂CH₂O)₄ spacer. This figure shows the discrepancy in the fragmentation patterns as the per-*O*-acetylated [Oxonium]⁺ ion produces unique ions that are directly related to the presence of acetyl groups. As can be seen from Figure 6-11A, the non-protected [GlcNAloc]⁺ produced 6 fragment ions that are in accordance with Figure 6-2 and Table 6-1. The protected per-*O*-acetylated [GlcNAloc]⁺ ion, however, produced 15 fragment ions (Figure 6-11B). This fact supports the speculation regarding the overall reactivity of the per-*O*-acetylated oxonium ion in comparison to the non-protected oxonium.

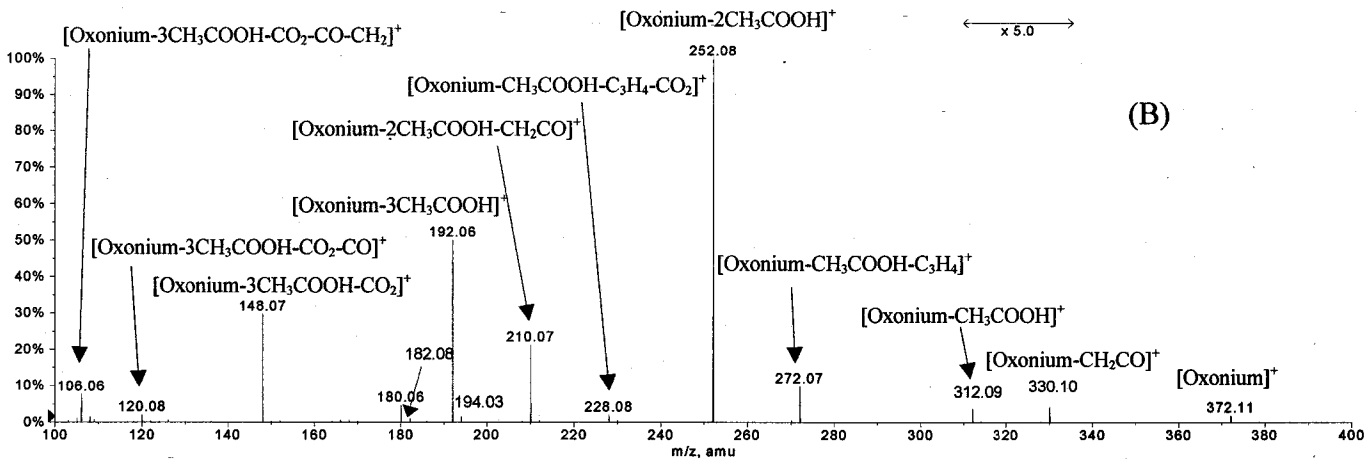
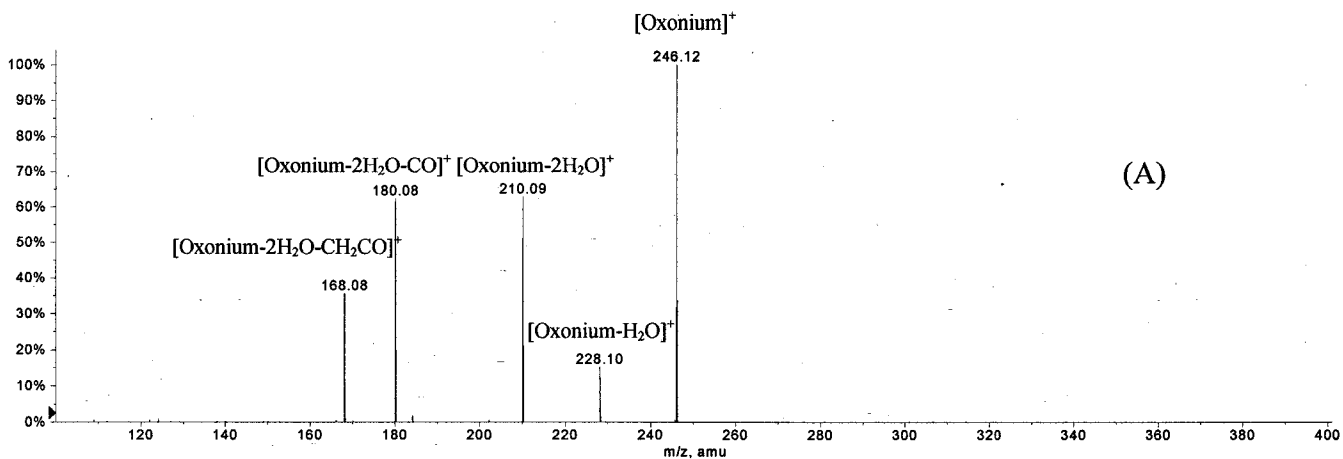


Figure 6-11: CID-MS/MS of the [Oxonium]⁺ ions extracted from neoglycolipid that bear GlcNAloc sugar species (A) and the per-*O*-acetylated GlcNAloc (B).

The fragmentation pattern of the protected per-*O*-acetylated [GlcNAloc]⁺ ion is schematically presented in Figure 6-12. The protected [GlcNAloc]⁺ at *m/z* 372.13 can lose a molecule of either acetic acid or ketene producing the minor fragment ions designated as [Oxonium-CH₃COOH]⁺ at *m/z* 312.11 and [Oxonium-CH₂CO]⁺ at *m/z* 330.12. The former product ion can further eliminate a molecule of C₃H₄ from the allyloxycarbonyl side chain and produce the ion [Oxonium-CH₃COOH-C₃H₄]⁺ at 272.08 which bears the carboxylic acid group. The structure of this ion was confirmed by the distinctive loss of 44 Da (i.e. CO₂), producing the ion observed at *m/z* 228.09. The [Oxonium-CH₃COOH]⁺ product ion can lose an additional molecule of acetic acid, resulting in the formation of the major ion [Oxonium-2CH₃COOH]⁺ at *m/z* 252.09. This major ion can produce three additional product ions, the first of which is produced by eliminating of a molecule of C₃H₅O from the allyloxycarbonyl chain producing the species assigned as [Oxonium-2CH₃COOH-C₃H₅O]⁺ at *m/z* 194.03. The second involves a neutral loss of a ketene group to yield the [Oxonium-2CH₃COOH-CH₂CO+H]⁺ ion at *m/z* 210.06 which bears a ketone group at position 4 of the sugar. This ketone group can then be eliminated as a molecule of CO through inner-ring contraction, forming the transitional minor ion species observed at 182.06, which then eliminates a molecule of H₂, producing the resonantly-stabilized ion observed at *m/z* 180.06. Finally, the [Oxonium-2CH₃COOH]⁺ can undergo a final breakage by eliminating an additional molecule of acetic acid, with relocation of the double bonds, producing the stabilized ion designated as [Oxonium-3CH₃COOH]⁺ at *m/z* 192.05. Due to the presence of an amino group at position C-2, the [Oxonium-3CH₃COOH]⁺ ion can also exist in 1,2-cyclic form that can lose the internal CO₂ accompanied by structural rearrangement, to yield the

[Oxonium-2CH₃COOH-CO₂]⁺ ion at *m/z* 148.07. The latter ion can finally undergo subsequent breakages losing CO followed by CH₂ resulting in the formation of the product ions observed at *m/z* 120.08 and 106.06, respectively.

It should be noted that the fragmentation pattern and the proposed origin of the various ions, shown in Figure 6-12, were authenticated by performing multiple MS/MS experiments (can be referred to as *quasi MSⁿ*). For example, the [Oxonium]⁺ ion was a daughter of the [M+H]⁺ (see Table 6-2) and the MS/MS experiment of this ion can be considered a *quasi MS³*. Therefore, the CID analysis of the [Oxonium-CH₃COOH]⁺ fragment ion at *m/z* 312.11 can be argued to be MS⁴ and has proven that both [Oxonium-CH₃COOH-C₃H₄]⁺ at *m/z* 272.08 and [Oxonium-CH₃COOH-C₃H₄-CO]⁺ at *m/z* 228.09 originate from this ion (see Figure 6-12). Similarly the CID analysis of the [Oxonium-CH₃COOH-C₃H₄]⁺ ion at *m/z* 272.08 (MS⁵) showed that 228.08 was a product of this ion. Such *quasi MSⁿ* experiments are very powerful for structural studies and Banoub's research group were the first to conduct and describe such a series of *quasi MSⁿ* using ESI-CID-QqToF-MS/MS in which the novel fragmentation routes of morphine opiate receptor antagonists were established (Joly *et al.*, 2005). The multiple MSⁿ spectra that established the fragmentation pattern presented in Figure 6-12 are shown in Table 6-4.

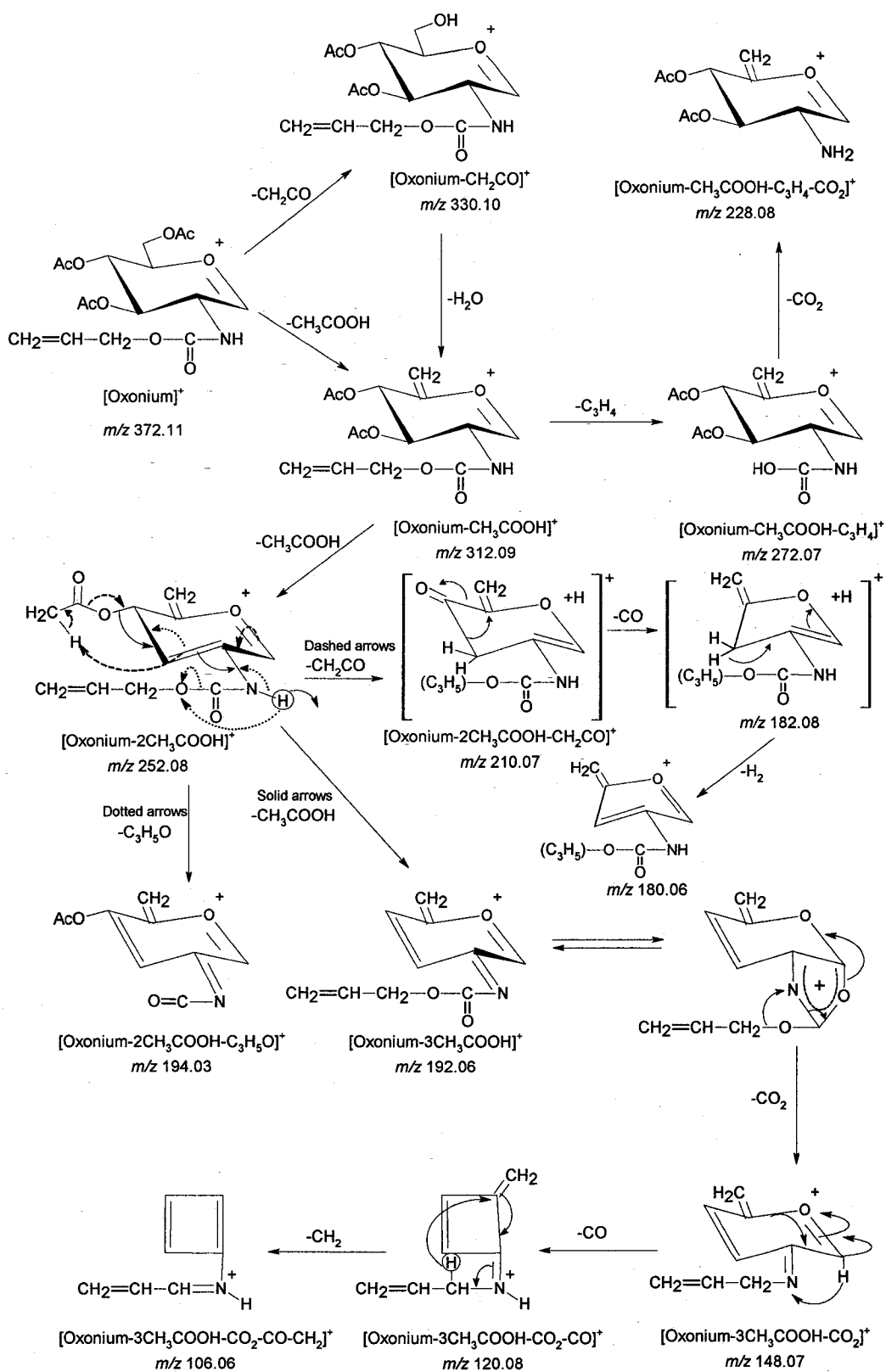


Figure 6-12: The fragmentation pattern of the protected $[\text{GlcNAloc}]^+$.

Table 6-4: Tabulated CID-MS/MS results that established Figure 6-12.

Precursor Ion	Product ions
312	272, 228, 252
272	228
252	210, 194, 192, 148, 120, 106
210	182, 180
192	148, 120, 106
180	No diagnostic ions

6.4. Summary:

The fragmentation patterns of 18 novel amphiphilic neoglycolipid cholesteryl derivatives were evaluated. These compounds can be used to increase liposomal stability and efficiency. These neoglycolipids bear different sugar moieties namely, D-glucosamine, *N*-acetyl-D-glucosamine, *N*-trideuterioacetyl-D-glucosamine, *N*-acetyl-lactosamine, L-fucose, *N*-allyloxycarbonyl-D-glucosamine, and some of their per-*O*-acetylated derivatives. Regardless of the structure of the tested neoglycolipid, QqToF-MS analysis using ESI source showed abundant protonated $[M+H]^+$ species. It has also been identified by both QqToF-MS and low-energy collision tandem mass spectrometry (CID-MS/MS) of the $[M+H]^+$ ion, the presence of specific common fingerprint fragment ions namely, $[Cholestene]^+$, sugar $[oxonium]^+$, $[(Sugar-spacer-OH)+H]^+$, $[oxonium-H_2O]^+$ and $[(Cholesterol-spacer-OH)+H]^+$.

In addition, a unique ion, which could not be rationally explained by the expected fragmentation of these amphiphilic molecules, was observed. This ion was compatible with that of a *C*-glycoside species formed by a chemical reaction between the sugar portion and the cholesterol. MS/MS analysis of this unique $[C-glycoside]^+$, confirmed the authenticity of the proposed structure of this ion. The presence of an amino group at position C-2 and free hydroxyl groups of the sugar motif is crucial for the formation of a “reactive” sugar oxonium ion that can form the $[C-glycoside]^+$ species.

In summary, the fragmentation patterns of the tested series of neoglycolipid cholesteryl derivatives was precisely established and their structure as well as the formation of a *C*-glycoside with the ESI source under atmospheric pressure and in the

collision cell during MS/MS analysis was authenticated (Banoub *et al.*, 2005a; El Aneed *et al.*, 2006).

CHAPTER 7: Conclusions and Summary

Advancements in biological mass spectrometry have significantly grown over the past few decades; over 5000 abstracts, for example, were presented in the 54th ASMS (American Society for Mass Spectrometry) annual conference in 2006. MS has the advantages of limited sample consumption and relatively short analysis time. One of the most significant mass spectrometric research areas is concerned with the identification of mass spectrometric fingerprints of natural and synthetic compounds (Es-Safi *et al.*, 2005; Li *et al.*, 2006). ESI-MSⁿ using FTMS instrumentation, for example, elucidated the fragmentation patterns and the molecular structures of synthetic indole derivatives (Cao *et al.*, 2005), as well as natural core oligosaccharide extract isolated from the bacteria *Proteus* (Kondakova *et al.*, 2005).

Natural and synthetic glycoconjugates are evaluated in this document and their fragmentation patterns are presented for the first time. These compounds are divided into two major groups, the naturally-occurring LPS-derived oligosaccharides and the synthetic neoglycolipids. While the latter is a liposome-stabilizing and targeting agent, the former is isolated from the outer membrane of the fish pathogen *A. salmonicida*, a candidate for vaccine development either as liposomal formulations (Nakhla *et al.*, 1994) or as protein-hapten conjugates (Banoub *et al.*, 1989). The LPS portions include the lipid A, the inner core and the complete core oligosaccharide. The data presented are additional steps which will help in understanding the mechanisms that govern sugar MS analysis; this will eventually lead to the development of robust and efficient sequencing algorithms (Joshi *et*

al., 2004; Tang *et al.*, 2005) that can, similar to MS protein and peptide sequencing programs, be incorporated into the software of future commercial MS instruments.

7.1. Mass spectrometric analysis of LPS oligosaccharide:

7.1.1. Lipid A:

ESI-MS is commonly used for the characterization of lipid A molecules (Boue & Cole, 2000; Chan & Reinhold, 1994; Corsaro *et al.*, 2004b; Corsaro *et al.*, 2002) which have been proven to be universally composed of two D-GlcN sugar moieties forming a β -D-(1 \rightarrow 6)-D-GlcN disaccharide. This disaccharide is substituted by two phosphate groups, one being attached at position O-4' of the non-reducing end sugar and the other at the anomeric OH of the disaccharide reducing end (C-1 position). Fatty acid chains acylate the various free positions of the D-GlcN disaccharide-backbone, resulting in the formation of O- and N- linked fatty acid esters (see Figure 3-1). It has been reported in the literature that the phosphate group can also be substituted by other functional groups such as phosphate or phosphorylethanolamine (Kulshin *et al.*, 1992; Masoud *et al.*, 1994). A glycosyl residue such as 4-amino-4-deoxy-L-arabinose, has been identified to be attached at position O-4' of the phosphate group (Reitschel *et al.*, 1984). More recently, the presence of lipid A containing α -D-mannose sugars instead of phosphate residues was reported (Schwudke *et al.*, 2003).

Lipid A extracts are not merely composed of a single entity and are in reality a mixture of many structurally- related components (Chan & Reinhold, 1994; Corsaro *et al.*, 2004b; Hsu & Turk, 2000; Krasikova *et al.*, 2001; Zarrouk *et al.*, 1997). Due to this complex nature of lipid A, ESI coupled to tandem MS/MS is an excellent tool to illustrate

the precise molecular structure of this biologically active extract. Tandem mass spectrometry was used to analyze the lipid A which was the major compound in a mixture of various structurally related components, without the need for any tedious separating techniques. It was demonstrated that lipid A, isolated by acid hydrolysis from the *A. salmonicida* LPS, had two phosphate groups at position *O*-1 and *O*-4'. In addition, both D-GlcN units of the β -D-(1 \rightarrow 6) disaccharide were *O*- and *N*- substituted with various fatty acids which were identified to be C12:0 and C14 (3-OH). The distribution of the fatty acids on the molecule was established through the presence of the distinctive ions in the QqToF-MS, namely the [Y]⁻ and [C]⁻ derived ions (see Figure 3-2 and 3-3), as well as from the product ions originating from inner sugar fragments, observed in the MS/MS analysis. Furthermore, MS/MS analysis of the [Y]⁻ and [C]⁻ ions clearly confirmed the presence of two C14:0 (3-OH) fatty acids on the reducing end group, and two C14:0(3-O(12:0)) on the non-reducing end group of the disaccharide (Figure 3-9). This was also evident by the generation of product ions associated with distinctive losses of these fatty chains, either as neutral ketene or as a free fatty acid (Figure 3-8).

In summary, the high-resolution hybrid QqToF-MS/MS instrument was used resourcefully to “separate” the major lipid A components and to locate the fatty acid and phosphate groups on their proper positions on the D-GlcN disaccharide. In addition, the mass spectrometric fingerprints of this biological compound were identified and established (Table 3-1 and Table 3-2). This allows the precise molecular structure of the major lipid A component to be elucidated from the other modified lipid A compounds of this complex mixture.

7.1.2. The core oligosaccharide:

There has been considerable confusion during the last few decades concerning the presence (or absence) of Kdo in lipopolysaccharides isolated from bacteria of the *Vibrionaceae* family (Hisatsune *et al.*, 1982; Kondo *et al.*, 1992). Difficulty in measuring the Kdo in the case of the LPS of *A. salmonicida* indicates the presence of a phosphate group attached through *O*-4 and glycosylated through *O*-5. Thus, the determination of the Kdo by the Weissbach thiobarbiturate colorimetric reaction could not measure the formation of malonaldehyde released by periodate oxidation.

The wild-type core oligosaccharide of *A. salmonicida* was isolated from the lipid A portion with 1 % acetic acid at 100° C for 90 minutes and a homogeneous mixture of oligosaccharides was obtained. This mixture was composed of the native core oligosaccharide containing the intact 4-*O*-phosphorylated reducing Kdo residue **2B** (Figure 4-2), in addition to the core oligosaccharide containing the C-3-C-4 olefinic D-arabino-3-en-2-ulonic acid open chain reducing end **2A** (Figure 4-2), obtained from the elimination of the *O*-4 phosphate group as phosphoric acid from the C-3-C-4 position. This degraded core oligosaccharide underwent an intramolecular addition reaction between the alcoholic function at *O*-7 or *O*-8 to the olefinic double bond, to produce a mixture of isomeric pairs of the 4,8- and 4,7-anhydro derivatives **3A** and **4A** of the enolizable α -keto acids (Figure 4-3).

The ESI-QqToF-MS/MS has assisted in the complete structural characterization of the core oligosaccharide containing an *O*-4 phosphorylated and *O*-5 glycosylated Kdo reducing end group. This work contributes an extra step in a unique approach for the

elucidation of more sophisticated natural bacterial oligosaccharides. The ESI-CID-QqToF of the precursor ion $[M_{PO_4} - 2H]^{2-}$ at m/z 982.29, obtained from **2B** (Figure 4-9) illustrated the diagnostic elimination of phosphoric acid to afford the $[M-2H]^{2-}$ and $[M-H]^-$ respectively at m/z 933.33 and 1867.71. The mechanism of the elimination of the PO_4 group from the *O*-4 phosphate and *O*-5 glycosylated Kdo terminal reducing end group **2B** was explained by a three-stepwise mechanism to afford the 4,8 – and 4,7-anhydro- α -keto acid derivatives **3A** and **4A** (Figures 4-2 4-3).

The characteristic molecular ion fingerprint obtained from the CID-QqToF-MS/MS of the five diprotonated permethylated molecules $[M+2H]^{2+}$, $[M_1+2H]^{2+}$, $[M_2+2H]^{2+}$, $[M_3+2H]^{2+}$, and $[M_4+2H]^{2+}$ allowed the facile identification of the cleaved core oligosaccharide mixture containing the anomeric 4,8-anhydro-and 4,7-anhydro degraded Kdo derivatives (Figures 4-15, 4-16, 4-17 and Table 4-2). The ESI- and MALDI-QqToF-MS/MS of the singly protonated molecules $[M+H]^+$, $[M_1+H]^+$, $[M_2+H]^+$, $[M_3+H]^+$, $[M_4+H]^+$ and $[M_5+H]^+$ gave tandem mass spectra containing a series of products of limited diagnostic value (Appendix III).

Similarly, the rough-type core oligosaccharide (representing the inner-core) was investigated and the mass spectrometric fingerprints were identified (Figure 5-4). The ESI-QqToF-MS/MS has assisted in the complete structural characterization of a core oligosaccharide from a mutant form of *A. salmonicida* lipopolysaccharide containing an *O*-5 phosphorylated, *O*-4 substituted Kdo reducing end group.

Finally, it should be mentioned that this type of homogeneous core oligosaccharide containing an *O*-4-phosphorylated and *O*-5 substituted Kdo in the lipopolysaccharide, can be representative of all wild type *A. salmonicida* (Banoub et al.,

1983), *A. hydrophila* (Auzanneau et al., 1991; Carof et al., 1987), and *V. anguillarum* (Kondo et al., 1992) lipopolysaccharides, which were previously studied. Accordingly, many of these published core oligosaccharide structures were presented without the presence of any Kdo residue at all, due to the limited technology available at that time. These molecular structures will have to be revised to incorporate the presence of the *O*-4 phosphorylated and *O*-5 substituted Kdo reducing end. Obviously, MS can be of great assistance in the rapid screening of core oligosaccharides obtained from different strains in order to investigate the presence of the structures currently established for other strains (including *A. salmonicida*) and to report new structural findings. In fact, minimum changes on the structural level can alter bond breakages and fragment formation.

7.2. Synthetic neoglycolipids:

7.2.1. Mass spectrometric fingerprints:

Synthetic neoglycolipids that bear a mono- or disaccharide glycosyl moiety (hydrophilic) and a cholesterol moiety (hydrophobic), which are linked by a polyethoxy spacer, were evaluated using QqToF-MS/MS hybrid instrumentation (ESI and CID-MS/MS analysis). The results demonstrated clearly that, both in the ESI source and within the collision cell of the mass spectrometer, the neoglycolipids follow a universal fragmentation pattern, producing a series of daughter ions which correspond precisely to the theoretical structure of these amphiphilic molecules (Figure 6-2 and Table 6-1).

Breakage can occur at either of the spacers ends, producing most of the fragments observed in the ESI-qQ-ToF and MS/MS analysis. In addition, elimination products that are generated from the sugar portion were also observed and include product ions which

are related to inner sugar fragmentation, such as the [Oxonium-2H₂O-CH₂CO]⁺ ion (see Figure 6-2). The genesis of these product ions was further confirmed by MS/MS analysis as shown in Figures 6-5.

This newly-established universal fragmentation pattern (Table 6-1) can be utilized to easily predict the fragmentation of new compounds that have the same general structural backbone. In addition, single or multiple ion monitor reactions can be performed for any quantitative studies of liposomes bearing these novel neoglycolipids as stabilizing components.

7.2.2. C-glycosylation reaction:

In addition to the establishment of the mass spectrometric fingerprints of these compounds, the most interesting finding was the presentation of concrete evidence for the formation of an unprecedented C-glycosylation reaction during the ESI-MS and MS/MS analysis (Figures 6-6 and 6-7). Such a reaction does not occur easily and requires reasonable efforts on a bench-top in a chemistry lab. It occurred, however, in a timeframe of milliseconds within the mass spectrometer. Ion-molecule reactions within mass spectrometry are old phenomena which were first noticed as early as 1913 (Thomson, 1913). They are mainly observed and monitored within ion trap (IT) mass analyzers (quadrupole IT and Fourier Transform MS) (Cerda *et al.*, 2002; Ottens *et al.*, 2005; Vidasky *et al.*, 1994; Wojcik & Markowski, 2005). It was suggested, for example, that poly-(ethylene/propylene glycol) under collisionally activated dissociation using FT-ICR MS/MS resulted in misleading rearrangements (Cerda *et al.*, 2002; Vidasky *et al.*, 1994). Both triple- and penta-quadrupoles were also used to evaluate ion-molecule reactions

(Chen *et al.*, 2005; Meurer *et al.*, 2005). Banoub's and Eberlin's research groups were the first to show that such reactions can occur under atmospheric pressure in the ESI source (Banoub *et al.*, 2005a; El Aneed *et al.*, 2006; Meurer & Eberlin, 2006).

In this investigation, a quadrupole time of flight mass spectrometer was used and illustrated the occurrence of a unique *C*-glycosylation reaction in the collision cell as well as under atmospheric pressure in the ESI source. The production of a *C*-glycoside occurs from a reaction between the positively charged *N*-sugar oxonium ion and a neutral cholesterol species. When studying these compounds in the negative ion mode, this reaction fails to occur, supporting the mechanism presented in Figure 6-7. The presence of an amino group at position C-2 and the free OH groups on the C-3, C-4 and C-6 positions are both critical for the formation of the *C*-Glycoside ion. This reaction is very distinctive, since the formation of the *C*-glycoside is very difficult in comparison to *O*- or *N*-glycosylation.

McLafferty's group has suggested that poly(ethylene/propylene glycol) under collisionally activated dissociation using FT-ICR MS/MS or other energetic methods, leads to misleading rearrangements (Cerda *et al.*, 2002; Vidasky *et al.*, 1994). It has been also reported that MS/MS analysis of underivatized and per-*O*- methylated trisaccharides, with either high- or low-energy CID using FAB ionization, resulted in losses of the internal residue of 1→6 substituted monosaccharide (Brüll *et al.*, 1997). This phenomenon of 'internal residue loss', which was characterized as an "internal rearrangement" process catalyzed by a proton, was not observed in the CID-MS/MS analysis of sodium-cationized oligosaccharides containing *N*-acetyl-D-glucosamine (Brull *et al.*, 1998). Claeys and collaborators evaluated the CID-MS/MS of *O*-flavonoid *O*-

eutinosides and *O*-neohesperidosides, illustrating internal glucose residue loss. They proposed mobilization of the proton from the aglycone to the disaccharide portion (Ma *et al.*, 2000). It should be noted that in the previous cases, these rearrangements reinstate the final formation of either *O*-ether or *O*-glycosidic linkages.

By comparison to the rearrangements in the aforementioned studies, the work, presented in this rationale, includes a quite different series of amphiphilic molecules containing an amino sugar and cholesteryl moieties separated by a polyethylene spacer. Also the formation of the final compounds is not an *O*-glycoside but a *C*-Glycoside, the formation of which, represents a formidable synthetic task to be achieved in a MS instrument.

It was therefore proposed that the mechanism of formation of the [C-glycoside]⁺ product ion which occurs in the collision cell of the tandem mass spectrometer, arises from the nucleophilic attack of the neutral fragment cholest-3,5-diene molecule on the activated intermediate product [GlcNAc]⁺ oxonium ion. We postulated that these latter were formed in the collision cell by fragmentation of the precursor protonated molecule. Thus, the formation of this *C*-glycoside occurs from the net result of breakage of two original covalent bonds separated by the polyethoxy chain spacer in the precursor protonated neoglycolipid. This [C-glycoside]⁺ reforms by a product ion-molecule reaction to produce a new C-1-C-3' covalent bond.

During the CID-MS/MS of the protonated neoglycolipid molecules, the *N*-acetyl-2-deoxy-D-glucosaminyl and the cholesteryl moieties, are both *O*-linked, and are separated by a variable length polyethoxy spacer arm. Therefore, the formation of the *C*-glycoside was not related to any specific conformation in the gas phase. This formation

of a C-C linkage by this type of ion-molecule reaction is quite unusual and rather unique, and could not involve, under any circumstances, a C-O intra-molecular rearrangement.

It should be also noted that most gas-phase ion-molecule reactions involve reactive atoms such as oxygen, nitrogen, and sulphur (Eberlin, 2006). The formation of carbon-carbon bonds (in non-sugar structures) were, however, observed previously; for example, the formation of a characteristic cyclic product, resulting from a selective reaction between ethyl vinyl ether and hydroxycarbonyl compounds has been previously demonstrated (Kenttamaa & Cooks, 1989).

In summary, the exact structure and the fragmentation patterns of these synthetic neoglycolipids were precisely established, including the elucidation of a unique “*in situ*” C-glycosylation reaction. This fact will be further explored in the future with the aid of state-of-the-art desorption electrospray ionization (DESI), and mass spectrometry may eventually serve as a reaction vessel, capable of generating the final products within a very short timeframe.

7.3. Future directions:

The intact LPS molecule of *A. salmonicida* will be studied by ESI- and MALDI-tandem mass spectrometry. This large biomaterial will be evaluated in its native form or after chemical manipulation to enhance the MS analysis; e.g. deacetylation of the fatty acids from the lipid A and permethylation (Robinson *et al.*, 2005).

Both liposomes and protein carriers were used to formulate *A. salmonicida* oligosaccharide vaccines (Banoub *et al.*, 1989; Nakhla *et al.*, 1994). Neoglycolipid-stabilized liposomes and BSA will be used as liposomal and protein carriers, respectively,

of the core oligosaccharide so that fish can be challenged with these formulations. It was shown recently that 83.5% of carp (*Cyprinus carpio*) immunized with liposomally-entrapped *A. salmonicida* antigens survived infections compared to 62.5% for non-immunized carp (Irie *et al.*, 2005). It should also be mentioned that the native structure of these oligosaccharides can serve as the basis for synthetic analogs that retain activity, reduce side effects and ease the design of pharmaceutical formulations (Asai, 2004; Baldrige & Crane, 1999).

In addition to vaccine-related work associated with LPS, one of the most exciting findings, when evaluating neoglycolipids, is related to the formation of the *C*-glycoside species during ESI-MS and MS/MS analysis. The formation of this ion will be evaluated using mass analyzers which “trap” ions, namely IT-MS and FT-MS. Various structures will be co-infused (with deuterated species) and the formation of the corresponding *C*-glycoside will be monitored. In addition, various neoglycolipids that bear glucosamine derivatives that are blocked at one or two variable positions will be synthesized and tested for the formation of the [*C*-Glycoside]⁺ so that additional explanation for the absence of this species within the per-*O*-acetylated neoglycolipids can be established.

7.4. Closing remarks:

The fragmentation pattern and the mass spectrometric fingerprints of natural *A. salmonicida* LPS and synthetic cholesteryl neoglycolipids are discussed and established. Complex oligosaccharide mixtures are evaluated by MS revealing the formation of ions, formed by glycosidic cleavages where bond ruptures occur between different sugar units and involve hydrogen migration. In addition, cross-ring fragmentations were also

observed, providing concrete information with respect to the sequence and type of linkages between monosaccharides and various non-sugar substituents. The MS data can assist in predicting the fragmentation patterns of similar structures and may serve as the basis for any quantitative or qualitative studies involving the series of glycoconjugates evaluated in this project.

References:

- Ada G., and Isaacs D. (2003). Carbohydrate-protein conjugate vaccines. *Clin Microbiol Infect* **9**: 79-85.
- Alving C. R., Verma J. N., Rao M., Krzych U., Amselem S., Green S. M., and Wassef N. M. (1992). Liposomes containing lipid A as a potent non-toxic adjuvant. *Res Immunol* **143**: 197-8.
- Archibald A. R., Baddiley J., and Blumsom N. L. (1968). The teichoic acids. *Adv Enzymol Relat Areas Mol Biol* **30**: 223-53.
- Arigita C., Luijkx T., Jiskoot W., Poelen M., Hennink W. E., Crommelin D. J., Ley P., Els C., and Kersten G. F. (2005). Well-defined and potent liposomal meningococcal B vaccines adjuvated with LPS derivatives. *Vaccine* **23**: 5091-8.
- Asai Y. (2004). Development of an injectable formulation for the novel lipid A analog E5531 using a 'pH-jump method'. *Yakugaku Zasshi* **124**: 965-72.
- Aston F. W. (1942). "Mass Spectra and isotopes," Longmans, Green and Co, New York.
- Austin B., and Austin D. A. (1999). "Bacterial fish pathogens. Disease of farmed and wild fish," Cornwall.
- Auzanneau F. I., Charon D., and Szabo L. (1991). Phosphorylated sugars. Part. 27. Synthesis and reaction in acidic medium of 5-O-substituted methyl 3-deoxy- α -D-manno-2-octulopyranosidonic acid 4-phosphate. *J Chem Soc Perkin Trans I*: 509-517.
- Avery O. T., and Goebel W. F. (1929). Chemo-immunological studies on conjugated carbohydrate proteins. II. Immunological specificity of sugar protein antigen. *J Exp Med* **50**: 533-550.
- Balazy M. (2004). Eicosanomics: targeted lipidomics of eicosanoids in biological systems. *Prostaglandins Other Lipid Mediat* **73**: 173-80.
- Baldrige J. R., and Crane R. T. (1999). Monophosphoryl lipid A (MPL) formulations for the next generation of vaccines. *Methods* **19**: 103-7.
- Baldrige J. R., Yorgensen Y., Ward J. R., and Ulrich J. T. (2000). Monophosphoryl lipid A enhances mucosal and systemic immunity to vaccine antigens following intranasal administration. *Vaccine* **18**: 2416-25.
- Baldwin M. A. (2005). Mass spectrometers for the analysis of biomolecules. *Methods Enzymol* **402**: 3-48.

Banemann A., Deppisch H., and Gross R. (1998). The lipopolysaccharide of *Bordetella bronchiseptica* acts as a protective shield against antimicrobial peptides. *Infect Immun* **66**: 5607-12.

Bangham A. D., Standish M. M., and Watkins J. C. (1965a). Diffusion of univalent ions across the lamellae of swollen phospholipids. *J Mol Biol* **13**: 238-52.

Bangham A. D., Standish M. M., and Weissmann G. (1965b). The action of steroids and streptolysin S on the permeability of phospholipid structures to cations. *J Mol Biol* **13**: 253-9.

Banoub J., Boullanger P., and Lafont D. (1992). Synthesis of oligosaccharides of 2-amino-2-deoxy sugars. *Chem. Rev.* **92**: 1167-1195.

Banoub J., Boullanger P., Lafont D., Cohen A., El Aneed A., and Rowlands E. (2005a). In situ formation of C-glycosides during electrospray ionization tandem mass spectrometry of a series of synthetic amphiphilic cholesteryl polyethoxy neoglycolipids containing N-acetyl-D-glucosamine. *J Am Soc Mass Spectrom* **16**: 565-70.

Banoub J., Cohen A., Mansour A., and Thibault P. (2004a). Characterization and de novo sequencing of Atlantic salmon vitellogenin protein by electrospray tandem and matrix-assisted laser desorption/ionization mass spectrometry. *Eur J Mass Spectrom (Chichester, Eng)* **10**: 121-34.

Banoub J., El Aneed A., Cohen A., and Martin P. (2004b). Characterization of the O-4 phosphorylated and O-5 substituted Kdo reducing end group and sequencing of the core oligosaccharide of *Aeromonas salmonicida* ssp *salmonicida* lipopolysaccharide using tandem mass spectrometry. *Eur J Mass Spectrom (Chichester, Eng)* **10**: 715-30.

Banoub J., Michon F., Shaw D. H., and Roy R. (1984). E.I. and C.I. mass-spectral identification of some derivatives of 7-O-(2-amino-2-deoxy- α -glucopyranosyl)-glycero-manno-heptose, obtained from lipopolysaccharides representative of the Vibrionaceae family. *Carbohydr Res* **128**: 203-216.

Banoub J., Thibault P., Mansour A., Cohen A., Heeley D. H., and Jackman D. (2003). Characterisation of the intact rainbow trout vitellogenin protein and analysis of its derived tryptic and cyanogen bromide peptides by matrix-assisted laser desorption/ionisation time-of-flight-mass spectrometry and electrospray ionisation quadrupole/time-of-flight mass spectrometry. *Eur J Mass Spectrom (Chichester, Eng)* **9**: 509-24.

Banoub J. H., Newton R. P., Esmans E., Ewing D. F., and Mackenzie G. (2005b). Recent developments in mass spectrometry for the characterization of nucleosides, nucleotides, oligonucleotides, and nucleic acids. *Chem Rev* **105**: 1869-915.

Banoub J. H., Shaw D. H., and Michon F. (1983). Hydrolytic release, and identification by g.l.c.-m.s., of 3-deoxy-D-manno-2-octulosonic acid in the lipopolysaccharides isolated from bacteria of the Vibrionaceae. *Carbohydr Res* **123**: 117-22.

Banoub J. H., Shaw D. H., Nakhla N. A., and Hodder H. J. (1989). Synthesis of glycoconjugates derived from various lipopolysaccharides of the Vibrionaceae family. *Eur J Biochem* **179**: 651-7.

Banoub J. H., Shaw D. H., Pang H., Krepinsky J. J., Nakhla N. A., and Patel T. (1990). Structural elucidation of the O-specific antigen of *Yersinia ruckerii* by fast atom bombardment mass spectrometry (FAB-MS). *Biomed Environ Mass Spectrom* **19**: 787-90.

Barber M., Bordoli R. S., Sedgwick R. D., and Tyler A. (1981). Fast atom bombardment of solids as an ion source in mass spectrometry. *Nature* **293**: 270-275.

Bardonnet P. L., Faivre V., Pirot F., Boullanger P., and Falson F. (2005). Cholesteryl oligoethyleneglycol glycosides: fluidizing effect of their embedment into phospholipid bilayers. *Biochem Biophys Res Commun* **329**: 1186-92.

Bateman K. P., Banoub J. H., and Thibault P. (1996). Probing the microheterogeneity of O-specific chains from *Yersinia ruckeri* using capillary zone electrophoresis/electrospray mass spectrometry. *Electrophoresis* **17**: 1818-28.

Beckey H. D. (1969). Field desorption mass spectrometry: a technique for the study of thermally unstable substances of low volatility. *Int J Mass Spectrom Ion Phys* **2**: 500-503.

Belland R. J., and Trust T. J. (1988). DNA:DNA reassociation analysis of *Aeromonas salmonicida*. *J Gen Microbiol* **134**: 307-15.

Bennett-Guerrero E., McIntosh T. J., Barclay G. R., Snyder D. S., Gibbs R. J., Mythen M. G., and Poxton I. R. (2000). Preparation and preclinical evaluation of a novel liposomal complete-core lipopolysaccharide vaccine. *Infect Immun* **68**: 6202-8.

Beveridge T. J., and Davies J. A. (1983). Cellular responses of *Bacillus subtilis* and *Escherichia coli* to the Gram stain. *J Bacteriol* **156**: 846-58.

Biroccio A., Urbani A., Massoud R., di Ilio C., Sacchetta P., Bernardini S., Cortese C., and Federici G. (2005). A quantitative method for the analysis of glycosylated and glutathionylated hemoglobin by matrix-assisted laser desorption ionization-time of flight mass spectrometry. *Anal Biochem* **336**: 279-88.

Boue S. M., and Cole R. B. (2000). Confirmation of the structure of lipid A from *Enterobacter agglomerans* by electrospray ionization tandem mass spectrometry. *J Mass Spectrom* **35**: 361-8.

Boullanger P., Chevalier Y., Croizier M. C., Lafont D., and Sancho M. R. (1995a). Synthesis and surface-active properties of some alkyl 2-amino-2-deoxy- β -D-glucopyranosides. *Carbohydr Res* **278**: 91-101.

Boullanger P., Chevalier Y., Croizier M. C., Lafont D., and Sancho M. R. (1995b). Synthesis and surface active properties of some alkyl 2-amino-2-deoxy- β -D-glucopyranosides. *Carbohydr Res* **278**: 91-101.

Bowden R. A., Cloeckert A., Zygmunt M. S., and Dubray G. (1995). Outer-membrane protein- and rough lipopolysaccharide-specific monoclonal antibodies protect mice against *Brucella ovis*. *J Med Microbiol* **43**: 344-7.

Brade H. (1985). Occurrence of 2-keto-deoxyoctonic acid 5-phosphate in lipopolysaccharides of *Vibrio cholerae* Ogawa and Inaba. *J Bacteriol* **161**: 795-8.

Brandenburg K., Matsuura M., Heine H., Muller M., Kiso M., Ishida H., Koch M. H., and Seydel U. (2002). Biophysical characterization of triacyl monosaccharide lipid a partial structures in relation to bioactivity. *Biophys J* **83**: 322-33.

Brandenburg K., Richter W., Koch M. H., Meyer H. W., and Seydel U. (1998). Characterization of the nonlamellar cubic and HII structures of lipid A from *Salmonella enterica* serovar Minnesota by X-ray diffraction and freeze-fracture electron microscopy. *Chem Phys Lipids* **91**: 53-69.

Breaux G. A., Green-Church K. B., France A., and Limbach P. A. (2000). Surfactant-aided, matrix-assisted laser desorption/ionization mass spectrometry of hydrophobic and hydrophilic peptides. *Anal Chem* **72**: 1169-74.

Brecker L. (2003). Nuclear magnetic resonance of lipid A--the influence of solvents on spin relaxation and spectral quality. *Chem Phys Lipids* **125**: 27-39.

Brown R. S., and Lennon J. J. (1995). Mass resolution improvement by incorporation of pulsed ion extraction in a matrix-assisted laser desorption/ionization linear time-of-flight mass spectrometer. *Anal Chem* **67**: 1998-2003.

Brüll L., Heerma W., Thomas-Oates J. E., Haverkamp J., Kováčik V., and Kovac P. (1997). Loss of Internal 1 \rightarrow 6 Substituted Monosaccharide residues and per-O-methylated trisaccharides. *J Am Soc Mass Spectrom* **8**: 43-49.

Brull L. P., Kovacik V., Thomas-Oates J. E., Heerma W., and Haverkamp J. (1998). Sodium-cationized oligosaccharides do not appear to undergo 'internal residue loss' rearrangement processes on tandem mass spectrometry. *Rapid Commun Mass Spectrom* **12**: 1520-32.

- Cao S., Liu H., Xu W., Liao X., and Zhao Y. (2005). Characterizing the electrospray ionization mass spectral fragmentation pattern of indole derivatives synthesized from 2-keto glycosides. *J Mass Spectrom* **40**: 452-7.
- Carof M., Lebbar S., and Szabo L. (1987). Detection of 3-deoxy-2-octulosonic acid in thiobarbiturate-negative endotoxins. *Carbohydr Res* **161**: c4-7.
- Caroff M., and Karibian D. (2003). Structure of bacterial lipopolysaccharides. *Carbohydr Res* **338**: 2431-47.
- Caroff M., Lebbar S., and Szabo L. (1987). Do endotoxins devoid of 3-deoxy-D-manno-2-octulosonic acid exist? *Biochem Biophys Res Commun* **143**: 845-7.
- Cerda B. A., Horn D. H. M., Breuker K., and McLafferty F. W. (2002). Sequencing of specific Copolymer Oligomers by Electron Capture-Dissociation Mass spectrometry. *J Am Chem Soc* **124**: 9287-9291.
- Chaby R., and Szabo L. (1975). 3-Deoxy-2-octulosonic acid 5-phosphate: a component of the endotoxin of *Bordetella pertussis*. *Eur J Biochem* **59**: 277-80.
- Chan S., and Reinhold V. N. (1994). Detailed structural characterization of lipid A: electrospray ionization coupled with tandem mass spectrometry. *Anal Biochem* **218**: 63-73.
- Chen H., Cooks R. G., Meurer E. C., and Eberlin M. N. (2005). Hydrogen/Chlorine exchange reactions of gaseous carbanions. *J Am Soc Mass Spectrom* **16**: 2045-51.
- Chernushevich I. V., Loboda A. V., and Thomson B. A. (2001). An introduction to quadrupole-time-of-flight mass spectrometry. *J Mass Spectrom* **36**: 849-65.
- Chernyak A., Kondo S., Wade T. K., Meeks M. D., Alzari P. M., Fournier J. M., Taylor R. K., Kovac P., and Wade W. F. (2002). Induction of protective immunity by synthetic *Vibrio cholerae* hexasaccharide derived from *V. cholerae* O1 Ogawa lipopolysaccharide bound to a protein carrier. *J Infect Dis* **185**: 950-62.
- Clauser K. R., Baker P., and Burlingame A. L. (1999). Role of accurate mass measurement (± 10 ppm) in protein identification strategies employing MS or MS/MS and database searching. *Anal Chem* **71**: 2871-82.
- Cohen A. M., Mansour A. A., and Banoub J. H. (2006). Absolute quantification of Atlantic salmon and rainbow trout vitellogenin by the 'signature peptide' approach using electrospray ionization QqToF tandem mass spectrometry. *J Mass Spectrom*: 646-658.
- Conover W. J. (1999). "Practical nonparametric statistics," John Wiley & Sons, New York.

- Cooks R. G., Ouyang Z., Takats Z., and Wiseman J. M. (2006). Detection Technologies. Ambient mass spectrometry. *Science* **311**: 1566-70.
- Corsaro M. M., Lanzetta R., Parrilli E., Parrilli M., Tutino M. L., and Ummarino S. (2004a). Influence of growth temperature on lipid and phosphate contents of surface polysaccharides from the antarctic bacterium *Pseudoalteromonas haloplanktis* TAC 125. *J Bacteriol* **186**: 29-34.
- Corsaro M. M., Piaz F. D., Lanzetta R., Naldi T., and Parrilli M. (2004b). Structure of Lipid A from *Pseudomonas corrugata* by electrospray ionization quadrupole time-of-flight tandem mass spectrometry. *Rapid Commun Mass Spectrom* **18**: 853-8.
- Corsaro M. M., Piaz F. D., Lanzetta R., and Parrilli M. (2002). Lipid A structure of *Pseudoalteromonas haloplanktis* TAC 125: use of electrospray ionization tandem mass spectrometry for the determination of fatty acid distribution. *J Mass Spectrom* **37**: 481-8.
- Dell A., Azadi P., Tiller P., Thomas-Oates J., Jennings H. J., Beurret M., and Michon F. (1990). Analysis of oligosaccharide epitopes of meningococcal lipopolysaccharides by fast-atom-bombardment mass spectrometry. *Carbohydr Res* **200**: 59-76.
- Demchenko A. V., Wolfert M. A., Santhanam B., Moore J. N., and Boons G.-J. (2003). Synthesis and biological evaluation of *Rhizobium sin-a* lipid A derivatives. *J Am Chem Soc* **125**: 6103-6112.
- Di Padova F. E., Brade H., Barclay G. R., Poxton I. R., Liehl E., Schuetze E., Kocher H. P., Ramsay G., Schreier M. H., McClelland D. B., and et al. (1993). A broadly cross-protective monoclonal antibody binding to *Escherichia coli* and *Salmonella* lipopolysaccharides. *Infect Immun* **61**: 3863-72.
- Dijkstra A. J., and Keck W. (1996). Peptidoglycan as a barrier to transenvelope transport. *J Bacteriol* **178**: 5555-62.
- Dole M., Mach L., Hines R. L., Mobley R. C., Ferguson L. D., and Alice M. B. (1968). Molecular beams of macroions. *J Chem Phys* **49**: 2240-2247.
- Domon B., and Costello C. E. (1988a). Structure elucidation of glycosphingolipids and gangliosides using high-performance tandem mass spectrometry. *Biochemistry* **27**: 1534-43.
- Domon B., and Costello C. E. (1988b). A systematic nomenclature for carbohydrate fragmentations in FAB-MS/MS spectra of glycoconjugates. *Glycoconjugate J* **5**: 397-409.
- Dongre A. R., Somogyi A., and Wysocki V. H. (1996). Surface-induced dissociation: an effective tool to probe structure, energetics and fragmentation mechanisms of protonated peptides. *J Mass Spectrom* **31**: 339-50.

Downard K. (2004). "Mass spectrometry: a foundation course," TJ International Ltd, Cornwall.

Duffels A., Green L. G., Ley S. V., and Miller A. D. (2000). Synthesis of high-mannose type neoglycolipids: active targeting of liposomes to macrophages in gene therapy. *Chemistry* **6**: 1416-30.

Eberlin M. N. (2006). Structurally diagnostic ion/molecule reactions: class and functional-group identification by mass spectrometry. *J Mass Spectrom* **41**: 141-56.

Edmondson R. D., and Russell D. H. (1996). Evaluation of Matrix-Assisted Laser Desorption Ionization-Time-of-Flight Mass Measurement Accuracy by Using Delayed Extraction. *J Am Soc Mass Spectrom* **7**: 995-1001.

El-Aneed A. (2004). An overview of current delivery systems in cancer gene therapy. *J Control Release* **94**: 1-14.

El-Aneed A., and Banoub J. (2005). Elucidation of the molecular structure of lipid A isolated from both a rough mutant and a wild strain of *Aeromonas salmonicida* lipopolysaccharides using electrospray ionization quadrupole time-of-flight tandem mass spectrometry. *Rapid Commun Mass Spectrom* **19**: 1683-95.

El Aneed A. (2003). Targeted cationic liposomes, technologies, and development. *Pharmaceu Tech* **27**: 58-62.

El Aneed A., and Banoub J. (2006). Proteomics and the Diagnosis of Hepatocellular Carcinoma: Focus on High Risk Hepatitis B and C Patients. *Anticancer Res* **In Press**.

El Aneed A., Banoub J., Boullanger P., Lafont D., and Koen-Alonso (2006). Establishment of mass spectrometric fingerprints of novel synthetic cholesteryl neoglycolipids: the presence of a unique C-glycoside species during electrospray ionization and during collision induced dissociation tandem mass spectrometry. *J Am Soc Mass Spectrom* **In Press**.

Emmett M. R., and Caprioli R. M. (1994). Micro electrospray mass spectrometry: ultra-high sensitivity analysis of peptides and proteins. *J Am Chem Soc Mass Spectrom* **5**: 605-613.

Ens W., and Standing K. G. (2005). Hybrid quadrupole/time-of-flight mass spectrometers for analysis of biomolecules. *Methods Enzymol* **402**: 49-78.

Erridge C., Stewart J., Bennett-Guerrero E., McIntosh T. J., and Poxton I. R. (2002). The biological activity of a liposomal complete core lipopolysaccharide vaccine. *J Endotoxin Res* **8**: 39-46.

Es-Safi N. E., Kerhoas L., and Ducrot P. H. (2005). Application of positive and negative electrospray ionization, collision-induced dissociation and tandem mass spectrometry to a study of the fragmentation of 6-hydroxyluteolin 7-O-glucoside and 7-O-glucosyl-(1 --> 3)-glucoside. *Rapid Commun Mass Spectrom* **19**: 2734-42.

Faivre V., Costa Mde L., Boullanger P., Baszkin A., and Rosilio V. (2003). Specific interaction of lectins with liposomes and monolayers bearing neoglycolipids. *Chem Phys Lipids* **125**: 147-59.

Fattom A., Cho Y. H., Chu C., Fuller S., Fries L., and Naso R. (1999). Epitopic overload at the site of injection may result in suppression of the immune response to combined capsular polysaccharide conjugate vaccines. *Vaccine* **17**: 126-33.

Fiske C. H., and Subbarow Y. (1925). The Colorimetric Determination of Phosphorus. *J Biol Chem* **66**: 375-400.

Fukasawa M., Shimizu Y., Shikata K., Nakata M., Sakakibara R., Yamamoto N., Hatanaka M., and Mizuochi T. (1998). Liposome oligomannose-coated with neoglycolipid, a new candidate for a safe adjuvant for induction of CD8⁺ cytotoxic T lymphocytes. *FEBS Lett* **441**: 353-6.

Fukuoka S., Brandenburg K., Muller M., Lindner B., Koch M. H., and Seydel U. (2001). Physico-chemical analysis of lipid A fractions of lipopolysaccharide from *Erwinia carotovora* in relation to bioactivity. *Biochim Biophys Acta* **1510**: 185-97.

Fulop M., Mastroeni P., Green M., and Titball R. W. (2001). Role of antibody to lipopolysaccharide in protection against low- and high-virulence strains of *Francisella tularensis*. *Vaccine* **19**: 4465-72.

Fung K. Y., Askovic S., Basile F., and Duncan M. W. (2004). A simple and inexpensive approach to interfacing high-performance liquid chromatography and matrix-assisted laser desorption/ionization-time of flight-mass spectrometry. *Proteomics* **4**: 3121-7.

Gale D. C., and Smith R. D. (1993). Small volume and low flow-rate electrospray ionization mass spectrometry of aqueous samples. *Rapid Commun Mass Spectrom* **7**: 1017-1012.

Gelhausen M., Besson F., Chierici S., Lafont D., Boullanger P., and Roux B. (1998). Lectin recognition of liposomes containing neoglycolipids, influence of their lipidic anchor and spacer length. *Colloids Surfaces B* **10**: 395-404.

Gram H. C. (1884). Über die isolierte Färbung der Schizomyceten in Schnitt- und Trockenpräparaten. *Fortschritte der Medizin* **2**: 185-189.

- Grant G. A., Frison S. L., Yeung J., Vasanthan T., and Sporns P. (2003). Comparison of MALDI-TOF mass spectrometric to enzyme colorimetric quantification of glucose from enzyme-hydrolyzed starch. *J Agric Food Chem* **51**: 6137-44.
- Grayson M. A., Ed. (2002). "Measuring mass: from positive rays to proteins," Chemical Heritage Press, Philadelphia.
- Gregoriadis G., Wills E. J., Swain C. P., and Tavill A. S. (1974). Drug-carrier potential of liposomes in cancer chemotherapy. *Lancet* **1**: 1313-6.
- Griffiths W. J., Jonsson A. P., Liu S., Rai D. K., and Wang Y. (2001). Electrospray and tandem mass spectrometry in biochemistry. *Biochem J* **355**: 545-61.
- Gross M. L. (1992). Charge-remote fragmentations: method, mechanism and applications. *Int J Mass Spectrom Ion Processes* **118-119**: 137-165.
- Gu X. X., Rudy S. F., Chu C., McCullagh L., Kim H. N., Chen J., Li J., Robbins J. B., Van Waes C., and Battey J. F. (2003). Phase I study of a lipooligosaccharide-based conjugate vaccine against nontypeable Haemophilus influenzae. *Vaccine* **21**: 2107-14.
- Gut I. G. (2004). DNA analysis by MALDI-TOF mass spectrometry. *Hum Mutat* **23**: 437-41.
- Haeffner-Cavaillon N., Caroff M., and Cavaillon J. M. (1989). Interleukin-1 induction by lipopolysaccharides: structural requirements of the 3-deoxy-D-manno-2-octulosonic acid (KDO). *Mol Immunol* **26**: 485-94.
- Hakomori S. (1964). A Rapid Permethylation Of Glycolipid, And Polysaccharide Catalyzed By Methylsulfinyl Carbanion In Dimethyl Sulfoxide. *J Biochem (Tokyo)* **55**: 205-8.
- Harvey D. J. (2003). Matrix-assisted laser desorption/ionization mass spectrometry of carbohydrates and glycoconjugates. *Int J Mass Spectrom* **226**: 1-35.
- Hashimoto M., Asai Y., Tamai R., Jinno T., Umatani K., and Ogawa T. (2003). Chemical structure and immunobiological activity of lipid A from *Prevotella intermedia* ATCC 25611 lipopolysaccharide. *FEBS Lett* **543**: 98-102.
- Hastein T., Gudding R., and Evensen O. (2005). Bacterial vaccines for fish--an update of the current situation worldwide. *Dev Biol (Basel)* **121**: 55-74.
- Heine H., Muller-Loennies S., Brade L., Lindner B., and Brade H. (2003). Endotoxic activity and chemical structure of lipopolysaccharides from *Chlamydia trachomatis* serotypes E and L2 and *Chlamydochlamydia psittaci* 6BC. *Eur J Biochem* **270**: 440-50.

- Henderson W., and McIndoe J. S. (2005). "Mass spectrometry of inorganic and organometallic compounds," John Wiley & Sons Ltd., Chichester.
- Herbert C. G., and Johnstone R. A. W. (2003). "Mass spectrometry basics," CRC Press, Boca Raton.
- Hisatsune K., Kondo S., Iguchi T., Machida M., Asou S., Inaguma M., and Yamamoto F. (1982). Sugar composition of lipopolysaccharides of family Vibrionaceae. Absence of 2-keto-3-deoxyoctonate (KDO) except in *Vibrio parahaemolyticus* O6. *Microbiol Immunol* **26**: 649-64.
- Holmes J. C., and Morrell F. A. (1957). Oscillographic mass spectrometric monitoring of gas chromatography. *Appl Spectrosc* **11**: 86-87.
- Holst O., Brade H., and Kosma P. (1992). GLC-MS of reduced, acetylated, and methylated (2----4)- and (2----8)-linked disaccharides of 3-deoxy-D-mannooctulopyranosonic acid (Kdo). *Carbohydr Res* **231**: 65-71.
- Hsu F. F., and Turk J. (2000). Charge-remote and charge-driven fragmentation processes in diacyl glycerophosphoethanolamine upon low-energy collisional activation: a mechanistic proposal. *J Am Soc Mass Spectrom* **11**: 892-9.
- Hutchens T. W., and Yip T. T. (1993). New desorption strategies for mass spectrometric analysis of macromolecules. *Rapid Commun Mass Spectrom* **7**: 576-580.
- Inghram M. G., and Gomer R. (1954). Mass spectrometric analysis of ions from the field microscope. *J Chem Phys* **22**: 1279-1280.
- Iribarne J. V., and Thomson B. A. (1976). On the evaporation of small ions from charged droplets. *J Chem Phys* **64**: 2287-2294.
- Irie T., Watarai S., Iwasaki T., and Kodama H. (2005). Protection against experimental *Aeromonas salmonicida* infection in carp by oral immunisation with bacterial antigen entrapped liposomes. *Fish Shellfish Immunol* **18**: 235-42.
- Jackson G. D., and Redmond J. W. (1971). Immunochemical studies of the O-antigens of *Vibrio cholerae*. The constitution of a lipopolysaccharide from *V. cholerae* 569B (Inaba). *FEBS Lett* **13**: 117-120.
- James A. T., and Martin A. J. P. (1952). Gas-liquid partition chromatography: the separation and microestimation of volatile fatty acids from formic acid to dodecanoic acid. *Biochem J* **50**: 679-690.
- Jann B., Jann K., and Beyaert G. O. (1973). 2-Amino-2,6-dideoxy-d-glucose (D-quinovosamine): a constituent of the lipopolysaccharides of *Vibrio cholerae*. *Eur J Biochem* **37**: 531-4.

Jennings K. R. (1968). Collision-induced decompositions of aromatic molecular ions. *Int J Mass Spectrom Ion Phys* **1**: 227-235.

Johnson R. S., Her G. R., Grabarek J., Hawiger J., and Reinhold V. N. (1990). Structural characterization of monophosphoryl lipid A homologs obtained from Salmonella minnesota Re595 lipopolysaccharide. *J Biol Chem* **265**: 8108-16.

Joly N., El-Aneed A., Martin P., Cecchelli R., and Banoub J. (2005). Structural determination of the novel fragmentation routes of morphine opiate receptor antagonists using electrospray ionization quadrupole time-of-flight tandem mass spectrometry. *Rapid Commun Mass Spectrom* **19**: 3119-30.

Joshi H. J., Harrison M. J., Schulz B. L., Cooper C. A., Packer N. H., and Karlsson N. G. (2004). Development of a mass fingerprinting tool for automated interpretation of oligosaccharide fragmentation data. *Proteomics* **4**: 1650-64.

Kallweit U., Bornsen K. O., Kresbach G. M., and Widmer H. M. (1996). Matrix compatible buffers for analysis of proteins with matrix-assisted laser desorption/ionization mass spectrometry. *Rapid Commun Mass Spectrom* **10**: 845-849.

Karas M., Bahr U., and Dulcks T. (2000a). Nano-electrospray ionization mass spectrometry: addressing analytical problems beyond routine. *Fresenius J Anal Chem* **366**: 669-76.

Karas M., Gluckmann M., and Schafer J. (2000b). Ionization in matrix-assisted laser desorption/ionization: singly charged molecular ions are the lucky survivors. *J Mass Spectrom* **35**: 1-12.

Katsube K., Bishop A. T., and Friedrich P. F. (2004). Transduction of rabbit saphenous artery: a comparison of naked DNA, liposome complexes, and adenovirus vectors. *J Orthop Res* **22**: 1290-5.

Kawai Y., Watanabe M., Matsuura M., Nishijima M., and Kawahara K. (2002). The partially degraded lipopolysaccharide of Burkholderia cepacia and ornithine-containing lipids derived from some Gram-negative bacteria are useful complex lipid adjuvants. *FEMS Immunol Med Microbiol* **34**: 173-9.

Kebarle P. (2000). A brief overview of the present status of the mechanisms involved in electrospray mass spectrometry. *J Mass Spectrom* **35**: 804-17.

Kelleher N. L., Zubarev R. A., Bush K., Furie B., Furie B. C., McLafferty F. W., and Walsh C. T. (1999). Localization of labile posttranslational modifications by electron capture dissociation: the case of gamma-carboxyglutamic acid. *Anal Chem* **71**: 4250-3.

Kelly J., Masoud H., Perry M. B., Richards J. C., and Thibault P. (1996). Separation and characterization of O-deacylated lipooligosaccharides and glycans derived from

Moraxella catarrhalis using capillary electrophoresis-electrospray mass spectrometry and tandem mass spectrometry. *Anal Biochem* **233**: 15-30.

Kemoun R., Gelhausen M., Besson F., Lafont D., Buchet R., Boullanger P., and Roux B. (1999). Interactions of egg yolk phosphatidylcholine with cholesteryl polyethoxy neoglycolipids containing N-acetyl-D-glucosamine. *J Molec Structure* **478**: 295-302.

Kenttamaa H. I., and Cooks R. G. (1989). Identification of protonated B-hydroxycarbonyl compounds by reactive collisions in tandem mass spectrometry. *J Am Chem Soc* **111**: 4122-4123.

Kerwin J. L., Wiens A. M., and Ericsson L. H. (1996). Identification of fatty acids by electrospray mass spectrometry and tandem mass spectrometry. *J Mass Spectrom* **31**: 184-92.

Khan S., Ahmad A., and Ahmad I. (2003). A sensitive and rapid liquid chromatography tandem mass spectrometry method for quantitative determination of 7-ethyl-10-hydroxycamptothecin (SN-38) in human plasma containing liposome-based SN-38 (LE-SN38). *Biomed Chromatogr* **17**: 493-9.

Kim J. H., Seo H., Han S. H., Lin J., Park M. K., Sorensen U. B., and Nahm M. H. (2005). Monoacyl lipoteichoic acid from pneumococci stimulates human cells but not mouse cells. *Infect Immun* **73**: 834-40.

Kitson F. G., Larsen B. S., and McEwen C. N. (1996). "Gas chromatography and mass spectrometry: a practical guide," Academic Press, San Diego.

Klibanov A. L., Maruyama K., Beckerleg A. M., Torchilin V. P., and Huang L. (1991). Activity of amphipathic poly(ethylene glycol) 5000 to prolong the circulation time of liposomes depends on the liposome size and is unfavorable for immunoliposome binding to target. *Biochim Biophys Acta* **1062**: 142-8.

Klibanov A. L., Maruyama K., Torchilin V. P., and Huang L. (1990). Amphipathic polyethyleneglycols effectively prolong the circulation time of liposomes. *FEBS Lett* **268**: 235-7.

Kondakova A. N., Vinogradov E. V., Knirel Y. A., and Lindner B. (2005). Application of electrospray ionization with Fourier transform ion cyclotron resonance mass spectrometry for structural screening of core oligosaccharides from lipopolysaccharides of the bacteria *Proteus*. *Rapid Commun Mass Spectrom* **19**: 2343-9.

Kondo S., Haishima Y., and Hisatsune K. (1992). Taxonomic implication of the apparent undetectability of 3-deoxy-D-manno-2-octulosonate (Kdo) in lipopolysaccharides of the representatives of the family Vibrionaceae and the occurrence of Kdo 4-phosphate in their inner-core regions. *Carbohydr Res* **231**: 55-64.

Korfmacher W. A., Ed. (2005). "Using mass spectrometry for drug metabolism studies," CRC Press, Boca Raton.

Krasikova I. N., Kapustina N. V., Svetashev V. I., Gorshkova R. P., Tomshich S. V., Nazarenko E. L., Komandrova N. A., Ivanova E. P., Gorshkova N. M., Romanenko L. A., Mikhailov V. V., and Solov'eva T. F. (2001). Chemical characterization of lipid A from some marine proteobacteria. *Biochemistry (Mosc)* **66**: 1047-54.

Krutchinsky A. N., Chernushevich I. V., Spicer V., Ens W., and Standing K. G. (1998). A collisional damping interface for an electrospray ionization TOF mass spectrometer. *J Am Soc Mass Spectrom* **9**: 569-579.

Kuberan B., Sikkander S. A., Tomiyama H., and Linhardt R. J. (2003). Synthesis of a C-glycoside analogue of sTn: an HIV- and tumor-associated antigen. *Angew Chem Int Ed Engl* **42**: 2073-5.

Kulshin V. A., Zahringer U., Lindner B., Frasch C. E., Tsai C. M., Dmitriev B. A., and Rietschel E. T. (1992). Structural characterization of the lipid A component of pathogenic *Neisseria meningitidis*. *J Bacteriol* **174**: 1793-800.

Lafont D., Boullanger P., Carvalho F., and Vottero P. (1997). A convenient access to b-glycosides of N-acetylactosamine. *Carbohydr Res* **297**: 117-126.

Lafont D., Boullanger P., Chierici S., Gelhausen M., and Roux B. (1996). Cholesteryl oligoethyleneglycols as D-glucosamine anchors into phospholipid bilayers. *New J Chem* **20**: 1093-1101.

Laiko V. V., Baldwin M. A., and Burlingame A. L. (2000). Atmospheric pressure matrix-assisted laser desorption/ionization mass spectrometry. *Anal Chem* **72**: 652-7.

Larmonier C. B., Arnould L., Larmonier N., Baumann S., Moutet M., Saint-Giorgio V., Pance A., and Jeannin J. F. (2004). Kinetics of tumor cell apoptosis and immune cell activation during the regression of tumors induced by lipid A in a rat model of colon cancer. *Int J Mol Med* **13**: 355-61.

Laurent N., Lafont D., and Boullanger P. (2006). Syntheses of alpha-D-galactosamine neoglycolipids. *Carbohydr Res* **341**: 823-35.

Li J., Martin A., Cox A. D., Moxon E. R., Richards J. C., and Thibault P. (2005). Mapping bacterial glycolipid complexity using capillary electrophoresis and electrospray mass spectrometry. *Methods Enzymol* **405**: 369-97.

Li J., Purves R. W., and Richards J. C. (2004). Coupling capillary electrophoresis and high-field asymmetric waveform ion mobility spectrometry mass spectrometry for the analysis of complex lipopolysaccharides. *Anal Chem* **76**: 4676-83.

- Li R., Zhou Y., Wu Z., and Ding L. (2006). ESI-QqTOF-MS/MS and APCI-IT-MS/MS analysis of steroid saponins from the rhizomes of *Dioscorea panthaica*. *J Mass Spectrom* **41**: 1-22.
- Louris J. N., Brodbelt-lusting J. S., Cooks R. G., Glish G. L., van Berkel G. J., and McLuckey S. A. (1990). Ion isolation and sequential stages of mass spectrometry in a quadrupole ion trap mass spectrometer. *Int J Mass Spectrom Ion Processes* **96**: 117-137.
- Lundstrom K., and Boulikas T. (2003). Viral and non-viral vectors in gene therapy: technology development and clinical trials. *Technol Cancer Res Treat* **2**: 471-86.
- Ma X., Saksena R., Chernyak A., and Kovac P. (2003). Neoglycoconjugates from synthetic tetra- and hexasaccharides that mimic the terminus of the O-PS of *Vibrio cholerae* O:1, serotype Inaba. *Org Biomol Chem* **1**: 775-84.
- Ma Y. L., Vedernikova I., Van den Heuvel H., and Claeys M. (2000). Internal glucose residue loss in protonated O-diglycosyl flavonoids upon low-energy collision-induced dissociation. *J Am Soc Mass Spectrom* **11**: 136-44.
- Mamyrin B. A., and Shmikk D. V. (1979). The linear mass reflectron. *Sov Phys JETP* **49**: 762-764.
- March R. E., and Hughes R. J. (1989). "Quadrupole storage mass spectrometry," John Wiley & Sons, Inc, New York.
- Masoud H., Perry M. B., and Richards J. C. (1994). Characterization of the lipopolysaccharide of *Moraxella catarrhalis*. Structural analysis of the lipid A from *M. catarrhalis* serotype A lipopolysaccharide. *Eur J Biochem* **220**: 209-16.
- McLafferty F. W., Bente P. F., Kornfeld R., Tsai S., and Howe I. (1973). Metastable ion characteristics. XXII. Collisional activation spectra of organic ions. *J Am Chem Soc* **95**: 2120-2129.
- Meeks M. D., Saksena R., Ma X., Wade T. K., Taylor R. K., Kovac P., and Wade W. F. (2004). Synthetic fragments of *Vibrio cholerae* O1 Inaba O-specific polysaccharide bound to a protein carrier are immunogenic in mice but do not induce protective antibodies. *Infect Immun* **72**: 4090-101.
- Merchant M., and Weinberger S. R. (2000). Recent advancements in surface-enhanced laser desorption/ionization-time of flight-mass spectrometry. *Electrophoresis* **21**: 1164-77.
- Meurer E. C., and Eberlin M. N. (2006). The atmospheric pressure Meerwein reaction. *J Mass Spectrom* **41**: 470-6.

- Meurer E. C., Sparrapan R., Tomazela D. M., Eberlin M. N., and Augusti R. (2005). Cyclization reactions of acylium and thioacylium ions with isocyanates and isothiocyanates: gas phase synthesis of 3,4-dihydro-2,4-dioxo-2H-1,3,5-oxadiazinium ions. *J Am Soc Mass Spectrom* **16**: 1602-7.
- Mikhail I., Yildirim H. H., Lindahl E. C., and Schweda E. K. (2005). Structural characterization of lipid A from nontypeable and type f Haemophilus influenzae: variability of fatty acid substitution. *Anal Biochem* **340**: 303-16.
- Moll H., Knirel Y. A., Helbig J. H., and Zahringer U. (1997). Identification of an alpha-D-Manp-(1-->8)-Kdo disaccharide in the inner core region and the structure of the complete core region of the Legionella pneumophila serogroup 1 lipopolysaccharide. *Carbohydr Res* **304**: 91-5.
- Morris H. R., Panico M., Barber M., Bordoli R. S., Sedgwick R. D., and Tyler A. (1981). Fast atom bombardment: a new mass spectrometric method for peptide sequence analysis. *Biochem Biophys Res Commun* **101**: 623-31.
- Morris H. R., Paxton T., Dell A., Langhorne J., Berg M., Bordoli R. S., Hoyes J., and Bateman R. H. (1996). High sensitivity collisionally-activated decomposition tandem mass spectrometry on a novel quadrupole/orthogonal-acceleration time-of-flight mass spectrometer. *Rapid Commun Mass Spectrom* **10**: 889-96.
- Munson M. S. B., and Field F. H. (1966). Chemical Ionization Mass Spectrometry. I. General Introduction. *J Am Chem Soc* **88**: 2621-2630.
- Nakhla A. N. (1995). Incorporation of the bacterial lipopolysaccharide from Aeromonas salmonicida into liposomes and the effects on antibody responses in rainbow trout (Oncorhynchus mykiss). In "Biochemistry", Memorial University of Newfoundland, St. John's.
- Nakhla A. N., Szalai A. J., Banoub J., and Keough K. M. W. (1994). Uptake and biodistribution of free and liposomally incorporated lipopolysaccharide of Aeromonas salmonicida administered via different routes to rainbow trout (Oncorhynchus mykiss). *J Liposome Res* **4**: 1029-1041.
- Neidhart J., Allen K. O., Barlow D. L., Carpenter M., Shaw D. R., Triozzi P. L., and Conry R. M. (2004). Immunization of colorectal cancer patients with recombinant baculovirus-derived KSA (Ep-CAM) formulated with monophosphoryl lipid A in liposomal emulsion, with and without granulocyte-macrophage colony-stimulating factor. *Vaccine* **22**: 773-80.
- Ng A. W., Lukic T., Pritchard P. H., and Wasan K. M. (2004). Development and characterization of liposomal disodium ascorbyl phytostanyl phosphates (FM-VP4). *Drug Dev Ind Pharm* **30**: 739-58.

- Olsthoorn M. M., Haverkamp J., and Thomas-Oates J. E. (1999). Mass spectrometric analysis of *Klebsiella pneumoniae* ssp. *pneumoniae* rough strain R20 (O1-: K20-) lipopolysaccharide preparations: identification of novel core oligosaccharide components and three 3-deoxy-D-manno-oct-2-ulopyranosonic artifacts. *J Mass Spectrom* **34**: 622-36.
- Ottens A. K., Arkin C. R., Griffin T. P., Palmer P. T., and Harrison W. W. (2005). Ion-molecule reactions in quadrupole ion trap mass spectrometry: implications for lightweight gas analysis. *Int J Mass Spectrom* **243**: 31-39.
- Paradis S. E., Dubreuil D., Rioux S., Gottschalk M., and Jacques M. (1994). High-molecular-mass lipopolysaccharides are involved in *Actinobacillus pleuropneumoniae* adherence to porcine respiratory tract cells. *Infect Immun* **62**: 3311-9.
- Park Y. S., and Huang L. (1993). Distribution within the organs of a reticuloendothelial system of liposomes containing lipid A. *J Drug Target* **1**: 325-30.
- Pasa-Tolic L., Masselon C., Barry R. C., Shen Y., and Smith R. D. (2004). Proteomic analyses using an accurate mass and time tag strategy. *Biotechniques* **37**: 621-4, 626-33, 636 passim.
- Peri F., Cipolla L., Rescigno M., La Ferla B., and Nicotra F. (2001). Synthesis and biological evaluation of an anticancer vaccine containing the C-glycoside analogue of the Tn epitope. *Bioconjug Chem* **12**: 325-8.
- Peri F., Maranzi C., Barath M., Granucci F., Urbano M., and Nicotra F. (2006). Synthesis and biological evaluation of novel lipid A antagonists. *Bioorg Med Chem* **14**: 190-9.
- Perouzel E., Jorgensen M. R., Keller M., and Miller A. D. (2003). Synthesis and formulation of neoglycolipids for the functionalization of liposomes and lipoplexes. *Bioconjug Chem* **14**: 884-98.
- Persing D. H., Coler R. N., Lacy M. J., Johnson D. A., Baldrige J. R., Hershberg R. M., and Reed S. G. (2002). Taking toll: lipid A mimetics as adjuvants and immunomodulators. *Trends Microbiol* **10**: S32-7.
- Pohlentz G., and Drees B. (2000). Neoglycolipids derived from phosphatidylethanolamine serve as probes in cell culture studies on glycolipid metabolism. *Biol Chem* **381**: 29-34.
- Pohlentz G., Schlemm S., Klima B., and Egge H. (1994). Fast atom bombardment mass spectrometry of N-acetylated neoglycolipids of the 1-deoxy-1-phosphatidylethanolamino-lactitol-type. *Chem Phys Lipids* **70**: 83-94.
- Postema M. H. D. (1995). "C-Glycoside Synthesis," CRC Press, Boca Raton, Florida.

Pramanik B. N., Ganguly A. K., and Gross M. L., Eds. (2002). "Applied electrospray mass spectrometry," Marcel Dekker, Inc., New York.

Prince G. A., Denamur F., Deschamps M., Garcon N., Prieels J. P., Slaoui M., Thiriart C., and Porter D. D. (2001). Monophosphoryl lipid A adjuvant reverses a principal histologic parameter of formalin-inactivated respiratory syncytial virus vaccine-induced disease. *Vaccine* **19**: 2048-54.

Provan F., Bjornstad A., Pampanin D. M., Lyng E., Fontanillas R., Andersen O. K., Koppe W., and Bamber S. (2006). Mass spectrometric profiling - a diagnostic tool in fish? *Mar Environ Res* **62 Suppl**: S105-8.

Pupo E., Aguila A., Santana H., Nunez J. F., Castellanos-Serra L., and Hardy E. (1999). Mice immunization with gel electrophoresis-micropurified bacterial lipopolysaccharides. *Electrophoresis* **20**: 458-61.

Purcell A. W., and Gorman J. J. (2001). The use of post-source decay in matrix-assisted laser desorption/ionisation mass spectrometry to delineate T cell determinants. *J Immunol Methods* **249**: 17-31.

Qureshi N., Takayama K., Mascagni P., Honovich J., Wong R., and Cotter R. J. (1988). Complete structural determination of lipopolysaccharide obtained from deep rough mutant of Escherichia coli. Purification by high performance liquid chromatography and direct analysis by plasma desorption mass spectrometry. *J Biol Chem* **263**: 11971-6.

Radziejewska-Lebrecht J., Shashkov A. S., Stroobant V., Wartenberg K., Warth C., and Mayer H. (1994). The inner core region of Yersinia enterocolitica Ye75R (0:3) lipopolysaccharide. *Eur J Biochem* **221**: 343-51.

Raetz C. R., and Whitfield C. (2002). Lipopolysaccharide endotoxins. *Annu Rev Biochem* **71**: 635-700.

Reisser D., Pance A., and Jeannin J. F. (2002). Mechanisms of the antitumoral effect of lipid A. *Bioessays* **24**: 284-9.

Reitschel E., Mayer H., Wollenweber H. W., Zahringer U., Luderitz O., Westphal O., and Brade H. (1984). Bacterial lipopolysaccharide and their lipid A component. In "Bacterial endotoxine" (J. Y. Homma, S. Kanegaski, O. Luderitz, T. Shiba, and O. Westphal, Eds.), pp. 11-22, Verlag chemie, Weinheim.

Rietschel E. T., and Cavaillon J. M. (2003). Richard Pfeiffer and Alexandre Besredka: creators of the concept of endotoxin and anti-endotoxin. *Microbes Infect* **5**: 1407-14.

Robbins J. B., Schneerson R., Anderson P., and Smith D. H. (1996). The 1996 Albert Lasker Medical Research Awards. Prevention of systemic infections, especially

meningitis, caused by *Haemophilus influenzae* type b. Impact on public health and implications for other polysaccharide-based vaccines. *Jama* **276**: 1181-5.

Robinson S., Routledge A., and Thomas-Oates J. (2005). Characterisation and proposed origin of mass spectrometric ions observed 30 Th above the ionised molecules of per-O-methylated carbohydrates. *Rapid Commun Mass Spectrom* **19**: 3681-8.

Routier F. H., Nikolaev A. V., and Ferguson M. A. (1999). The preparation of neoglycoconjugates containing inter-saccharide phosphodiester linkages as potential anti-*Leishmania* vaccines. *Glycoconj J* **16**: 773-80.

Rund S., Lindner B., Brade H., and Holst O. (2000). Structural analysis of the lipopolysaccharide from *Chlamydomonas reinhardtii* strain 6BC. *Eur J Biochem* **267**: 5717-26.

Saksena R., Chernyak A., Karavanov A., and Kovac P. (2003). Conjugating low molecular mass carbohydrates to proteins. 1. Monitoring the progress of conjugation. *Methods Enzymol* **362**: 125-39.

Schaffer C., and Messner P. (2005). The structure of secondary cell wall polymers: how Gram-positive bacteria stick their cell walls together. *Microbiology* **151**: 643-51.

Schmiegel J., Yang G., Franck R. W., and Tsuji M. (2003). Superior protection against malaria and melanoma metastases by a C-glycoside analogue of the natural killer T cell ligand alpha-Galactosylceramide. *J Exp Med* **198**: 1631-41.

Schneerson R., Barrera O., Sutton A., and Robbins J. B. (1980). Preparation, characterization, and immunogenicity of *Haemophilus influenzae* type b polysaccharide-protein conjugates. *J Exp Med* **152**: 361-76.

Schwudke D., Linscheid M., Strauch E., Appel B., Zahringer U., Moll H., Muller M., Brecker L., Gronow S., and Lindner B. (2003). The obligate predatory *Bdellovibrio bacteriovorus* possesses a neutral lipid A containing alpha-D-Mannoses that replace phosphate residues: similarities and differences between the lipid As and the lipopolysaccharides of the wild type strain B. *bacteriovorus* HD100 and its host-independent derivative HI100. *J Biol Chem* **278**: 27502-12.

Seltmann G., and Holst O. (2002). "The bacterial cell wall," Springer, Berlin.

Semmes O. J., Feng Z., Adam B. L., Banez L. L., Bigbee W. L., Campos D., Cazares L. H., Chan D. W., Grizzle W. E., Izbicka E., Kagan J., Malik G., McLerran D., Moul J. W., Partin A., Prasanna P., Rosenzweig J., Sokoll L. J., Srivastava S., Srivastava S., Thompson I., Welsh M. J., White N., Winget M., Yasui Y., Zhang Z., and Zhu L. (2005). Evaluation of serum protein profiling by surface-enhanced laser desorption/ionization time-of-flight mass spectrometry for the detection of prostate cancer: I. Assessment of platform reproducibility. *Clin Chem* **51**: 102-12.

Seydel U., Lindner B., Wollenweber H. W., and Rietschel E. T. (1984). Structural studies on the lipid A component of enterobacterial lipopolysaccharides by laser desorption mass spectrometry. Location of acyl groups at the lipid A backbone. *Eur J Biochem* **145**: 505-9.

Shackleton C. H., and Straub K. M. (1982). Direct analysis of steroid conjugates: the use of secondary ion mass spectrometry. *Steroids* **40**: 35-51.

Shaw D. H., Hart M. J., and Luderitz O. (1992). Structure of the core oligosaccharide in the lipopolysaccharide isolated from *Aeromonas salmonicida* ssp. *salmonicida*. *Carbohydr Res* **231**: 83-91.

Shukla A. K., and Futrell J. H. (2000). Tandem mass spectrometry: dissociation of ions by collisional activation. *J Mass Spectrom* **35**: 1069-90.

Silipo A., Molinaro A., Cescutti P., Bedini E., Rizzo R., Parrilli M., and Lanzetta R. (2005). Complete structural characterization of the lipid A fraction of a clinical strain of *B. cepacia* genomovar I lipopolysaccharide. *Glycobiology* **15**: 561-70.

Simoes S., Moreira J. N., Fonseca C., Duzgunes N., and de Lima M. C. (2004). On the formulation of pH-sensitive liposomes with long circulation times. *Adv Drug Deliv Rev* **56**: 947-65.

Soanes C., and Stevenson A. (2005). The Oxford dictionary of English (revised version), pp. Oxford reference on line, Memorial University of Newfoundland, Oxford University press.

Stephens W. E. (1946). A pulsed mass spectrometer with time dispersion. *Phys Rev* **69**: 691.

Susskind M., Brade L., Brade H., and Holst O. (1998). Identification of a novel heptoglycan of alpha1-->2-linked D-glycero-D-manno-heptopyranose. Chemical and antigenic structure of lipopolysaccharides from *Klebsiella pneumoniae* ssp. *pneumoniae* rough strain R20 (O1:-K20-). *J Biol Chem* **273**: 7006-17.

Susskind M., Muller-Loennies S., Nimmich W., Brade H., and Holst O. (1995). Structural investigation on the carbohydrate backbone of the lipopolysaccharide from *Klebsiella pneumoniae* rough mutant R20/O1. *Carbohydr Res* **269**: C1-7.

Takats Z., Wiseman J. M., Gologan B., and Cooks R. G. (2004). Mass spectrometry sampling under ambient conditions with desorption electrospray ionization. *Science* **306**: 471-3.

Tanaka K., Waki Y., Ido Y., Akita S., Yoshida Y., and Yoshida T. (1988). *Rapid Commun Mass Spectrom* **2**.

- Tang H., Mechref Y., and Novotny M. V. (2005). Automated interpretation of MS/MS spectra of oligosaccharides. *Bioinformatics* **21 Suppl 1**: i431-9.
- Thomson J. J. (1913). "Rays of positive electricity and their applications to chemical analysis," Longmans, Greens and Co., London.
- Tipper D. J., and Strominger J. L. (1965). Mechanism of action of penicillins: a proposal based on their structural similarity to acyl-D-alanyl-D-alanine. *Proc Natl Acad Sci U S A* **54**: 1133-41.
- Torgerson D. F., Skowronski R. P., and Macfarlane R. D. (1974). New approach to the mass spectroscopy of non-volatile compounds. *Biochem Biophys Res Commun* **60**: 616-21.
- Ummarino S., Corsaro M. M., Lanzetta R., Parrilli M., and Peter-Katalinic J. (2003). Determination of phosphorylation sites in lipooligosaccharides from *Pseudoalteromonas haloplanktis* TAC 125 grown at 15 degrees C and 25 degrees C by nano-electrospray ionization quadrupole time-of-flight tandem mass spectrometry. *Rapid Commun Mass Spectrom* **17**: 2226-32.
- Vaara M. (1993). Antibiotic-supersusceptible mutants of *Escherichia coli* and *Salmonella typhimurium*. *Antimicrob Agents Chemother* **37**: 2255-60.
- Vestal M. L., and Campbell J. M. (2005). Tandem time-of-flight mass spectrometry. *Methods Enzymol* **402**: 79-108.
- Vidasky I., Chorush R. A., Longevialle P., and McLafferty F. W. (1994). Functional Group Migration in Ionized Long-Chain Compounds. *J Am Chem Soc* **116**: 5865-5872.
- Vinogradov E. V., Lindner B., Kocharova N. A., Senchenkova S. N., Shashkov A. S., Knirel Y. A., Holst O., Gremyakova T. A., Shaikhutdinova R. Z., and Anisimov A. P. (2002). The core structure of the lipopolysaccharide from the causative agent of plague, *Yersinia pestis*. *Carbohydr Res* **337**: 775-7.
- Ward J. B. (1981). Teichoic and teichuronic acids: biosynthesis, assembly, and location. *Microbiol Rev* **45**: 211-43.
- Westphal O., Αλεριτζ O., and Bister F. (1952). Über die Extraktion von Bakterien mit Phenol/Wasser. *Z Naturforsch* **76**: 148-155.
- Whitehouse C. M., Dreyer R. N., Yamashita M., and Fenn J. B. (1985). Electrospray interface for liquid chromatographs and mass spectrometers. *Anal Chem* **57**: 675-9.
- Wicken A. J., and Knox K. W. (1975). Lipoteichoic acids: a new class of bacterial antigen. *Science* **187**: 1161-7.

- Wise E. M., Jr., and Park J. T. (1965). Penicillin: its basic site of action as an inhibitor of a peptide cross-linking reaction in cell wall mucopeptide synthesis. *Proc Natl Acad Sci U S A* **54**: 75-81.
- Wojcik L., and Markowski A. (2005). Mass spectrometric study of ion/molecule reaction in methane and ammonia mixtures. *Vacuum* **78**: 235-240.
- Won E. K., Zahner M. C., Grant E. A., Gore P., and Chicoine M. R. (2003). Analysis of the antitumoral mechanisms of lipopolysaccharide against glioblastoma multiforme. *Anticancer Drugs* **14**: 457-66.
- Wu J., and Zern M. A. (1996). Modification of liposomes for liver targeting. *J Hepatol* **24**: 757-63.
- Wu T., Chen J., Murphy T. F., Green B. A., and Gu X. X. (2005). Investigation of non-typeable *Haemophilus influenzae* outer membrane protein P6 as a new carrier for lipooligosaccharide conjugate vaccines. *Vaccine* **23**: 5177-85.
- Wunschel D., Fox K. F., Fox A., Nagpal M. L., Kim K., Stewart G. C., and Shahgholi M. (1997). Quantitative analysis of neutral and acidic sugars in whole bacterial cell hydrolysates using high-performance anion-exchange liquid chromatography-electrospray ionization tandem mass spectrometry. *J Chromatogr A* **776**: 205-19.
- Xu Z., Jayaseharan J., and Marchant R. E. (2002). Synthesis and characterization of oligomaltose-grafted lipids with application to liposomes. *J Colloid Interface Sci* **252**: 57-65.
- Yamashita M., and Fenn J. B. (1984a). Electrospray ion source. Another variation on the free-jet theme. *J Phys Chem* **88**: 4451-4459.
- Yamashita M., and Fenn J. B. (1984b). Negative ion source production with electrospray ion source. *J Phys Chem* **88**: 4671-4675.
- Yost R. A., and Enke C. G. (1978). Selected ion fragmentation with a tandem quadrupole mass spectrometer. *J Am Chem Soc* **100**: 2274-2275.
- Zarrouk H., Karibian D., Bodie S., Perry M. B., Richards J. C., and Caroff M. (1997). Structural characterization of the lipids A of three *Bordetella bronchiseptica* strains: variability of fatty acid substitution. *J Bacteriol* **179**: 3756-60.
- Zdrovenko G. M., Shashkov A. S., Zdrovenko E. L., Kocharova N. A., Yakovleva L. M., Knirel Y. A., and Rudolph K. (2001). Characterization of the lipopolysaccharide and structure of the O-specific polysaccharide of the bacterium *Pseudomonas syringae* pv. *atofaciens* IMV 948. *Biochemistry (Mosc)* **66**: 369-77.

Zhang J., Yergey A., Kowalak J., and Kovac P. (1998). Studies towards neoglycoconjugates from the monosaccharide determinant of *Vibrio cholerae* O:1, serotype Ogawa using the diethyl squarate reagent. *Carbohydr Res* **313**: 15-20.

Appendix I: Lipid A

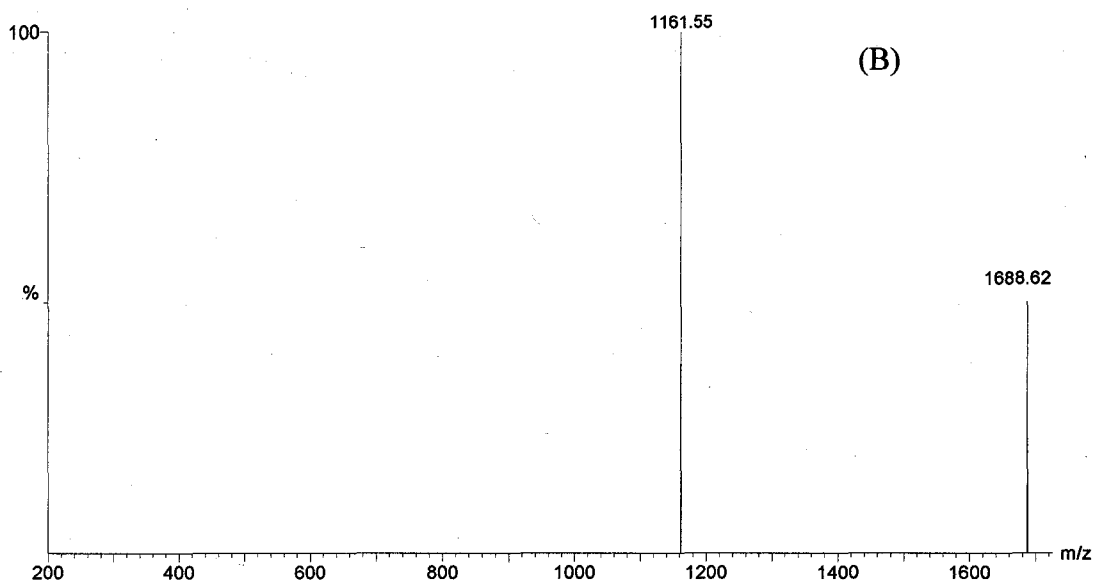
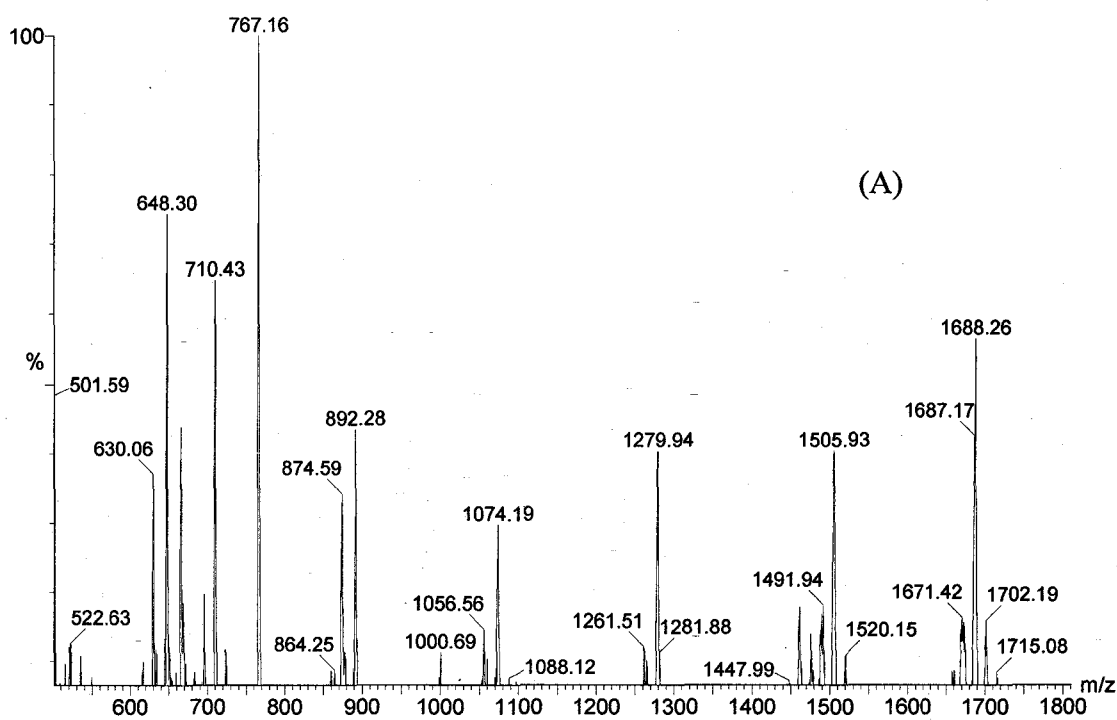


Figure I-1: Negative ESI-QhQ-MS showed the major diagnostic ions observed with QqToF instrumentation (A). However, the $[M_B-H]^-$ were not observed. This instrument failed to fragment the precursor mono-phosphorylated ion (B).

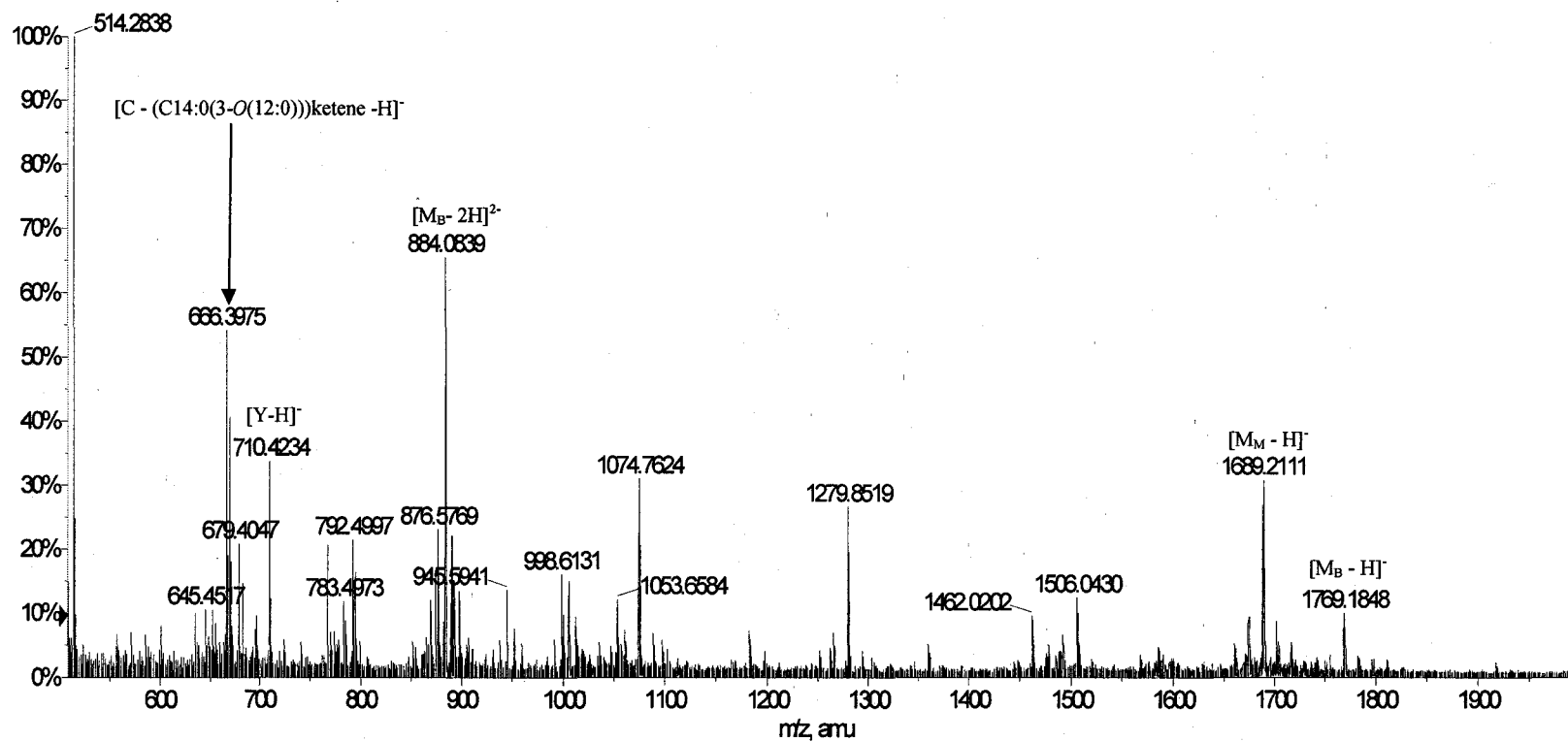


Figure I-2: Negative QqToF MS scan of the native lipid A extract from wild-type mutant *A. salmonicida* acquired at DP= - 60. The ions observed are identical to those reported for the rough mutant species (Figure 3-2). The assignment of the diagnostic ions are shown in Table 3-1.

Appendix II: The CID-MS/MS spectra and the fragmentation patterns of the doubly charged series ions presented in Table 4-1

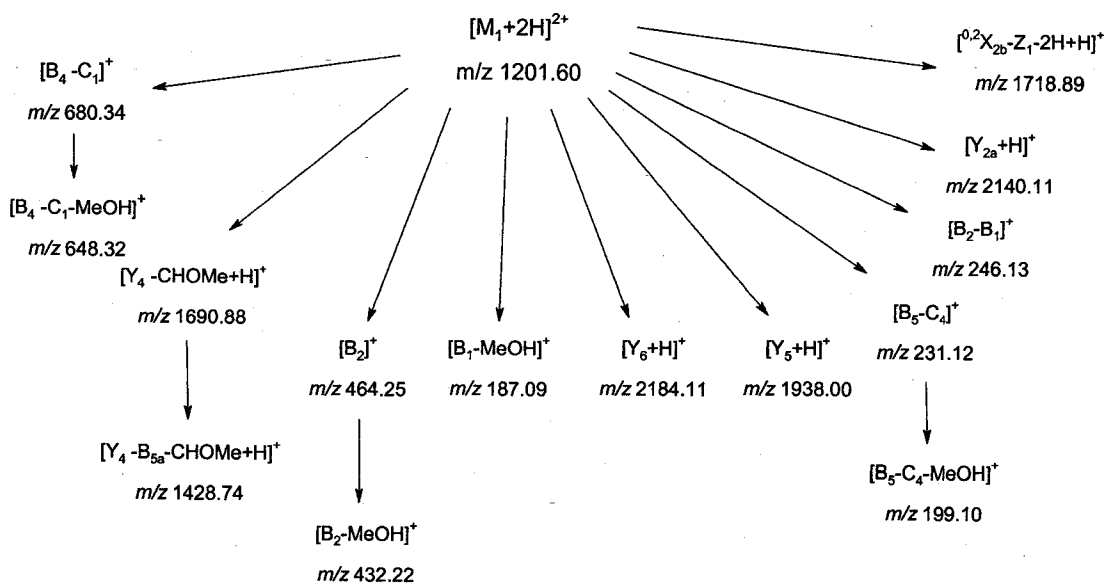
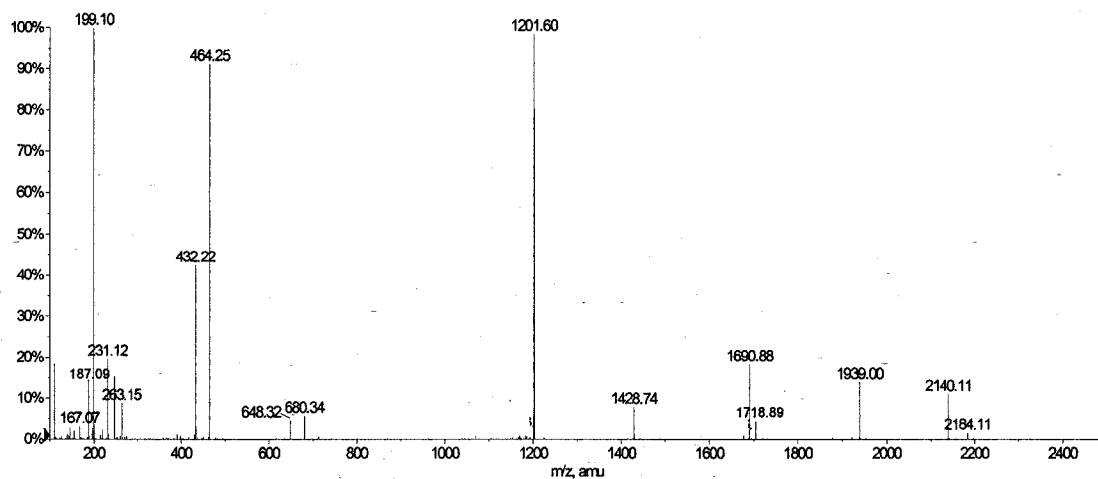


Figure II-1: ESI-MS/MS spectra of the permethylated precursor ions $[M_1+2H]^{2+}$ at m/z 1201.60 and the proposed fragmentation routes and product ions of this precursor.

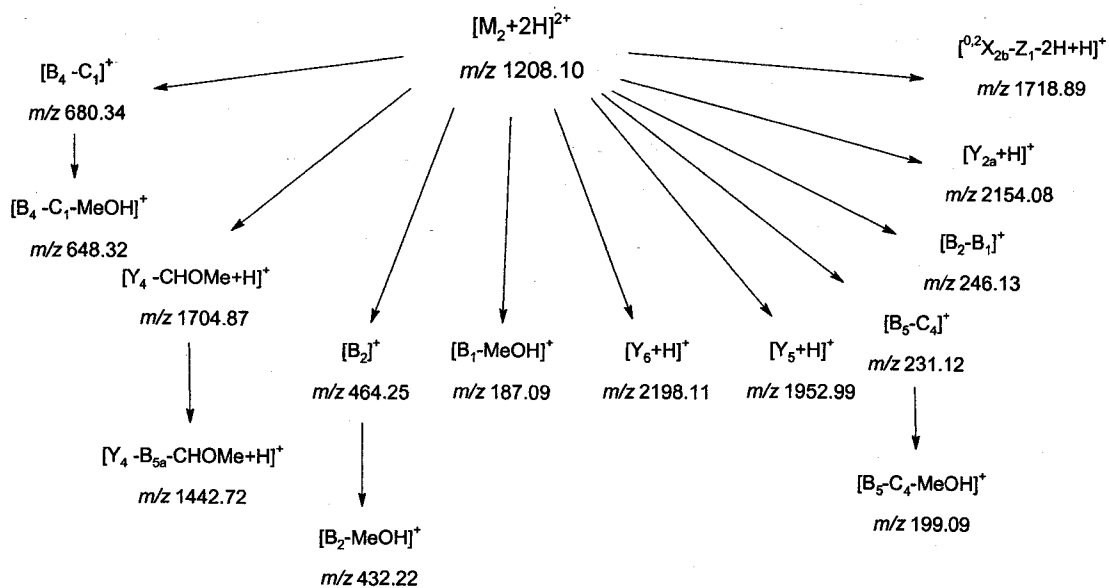
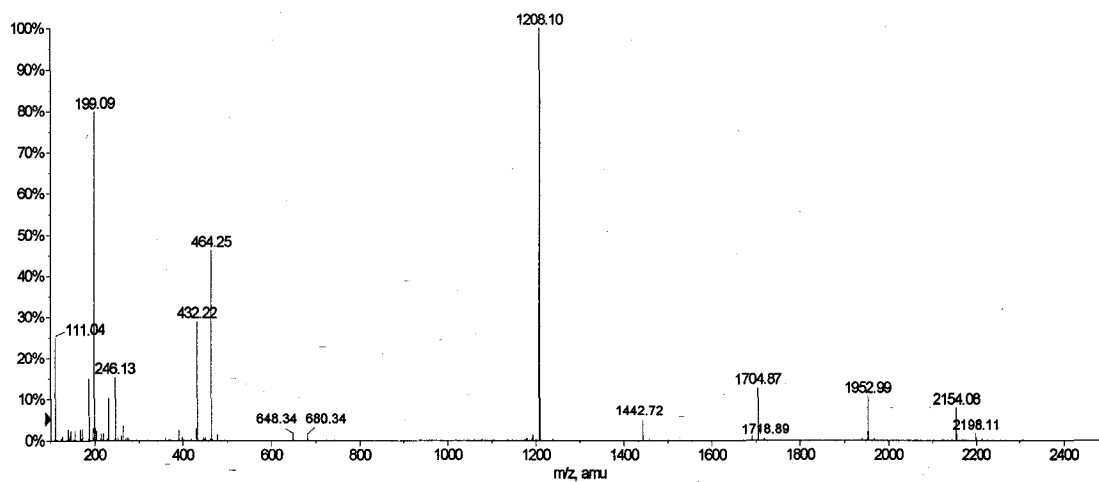


Figure II-2: ESI-MS/MS spectra of the permethylated precursor ions $[M_2+2H]^{2+}$ at m/z 1208.10 and the proposed fragmentation routes and product ions of this precursor.

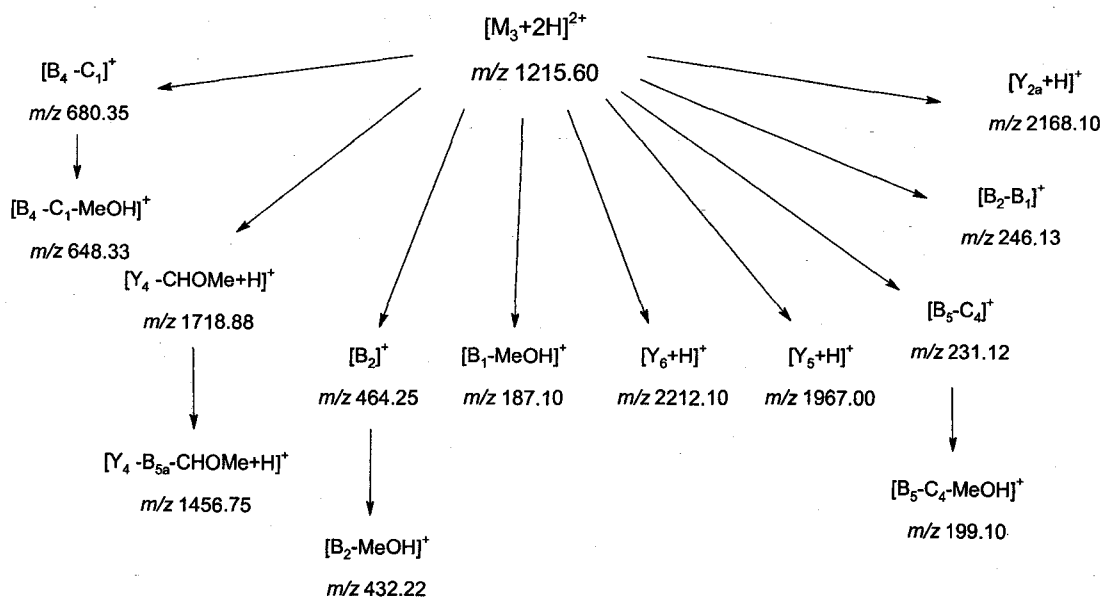
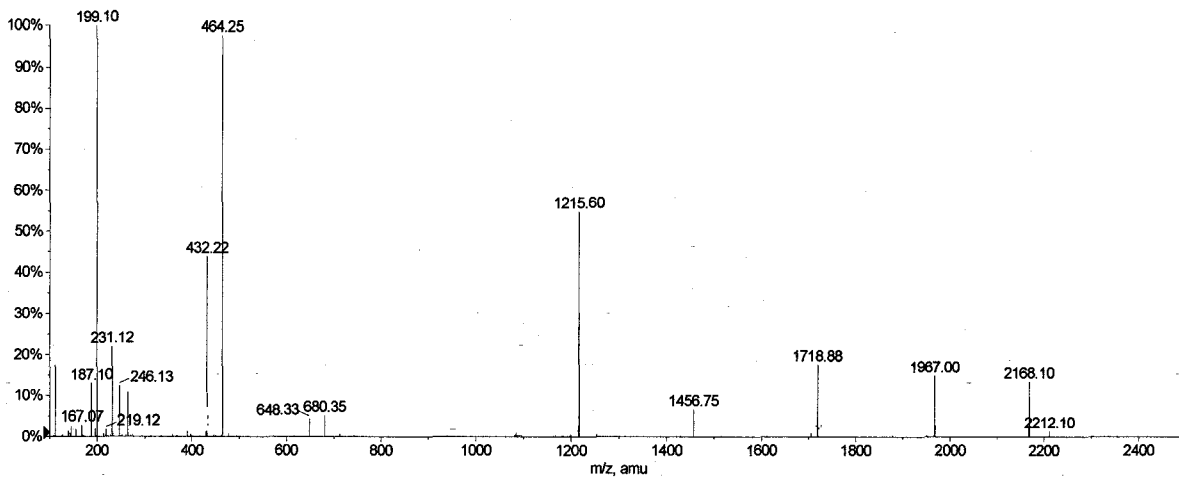


Figure II-3: ESI-MS/MS spectra of the permethylated precursor ions $[M_3+2H]^{2+}$ at m/z 1215.60 and the proposed fragmentation routes and product ions of this precursor.

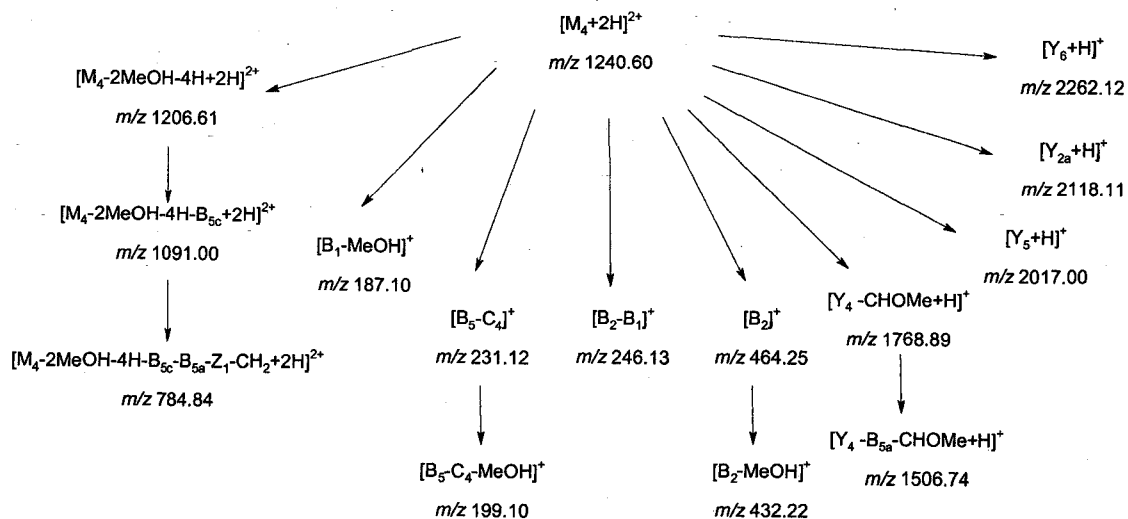
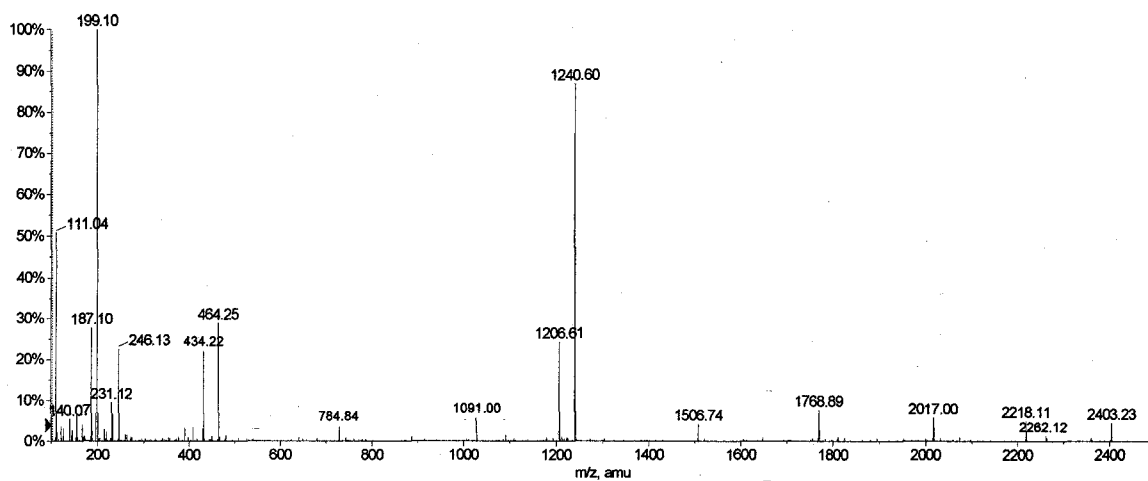


Figure II-3: ESI-MS/MS spectra of the permethylated precursor ions $[M_4+2H]^{2+}$ at m/z 1240.60 and the proposed fragmentation routes and product ions of this precursor.

Appendix III: ESI-MS/MS and MALDI-MS/MS spectra of the mono-charged series of the protonated molecules shown in Table 4-1

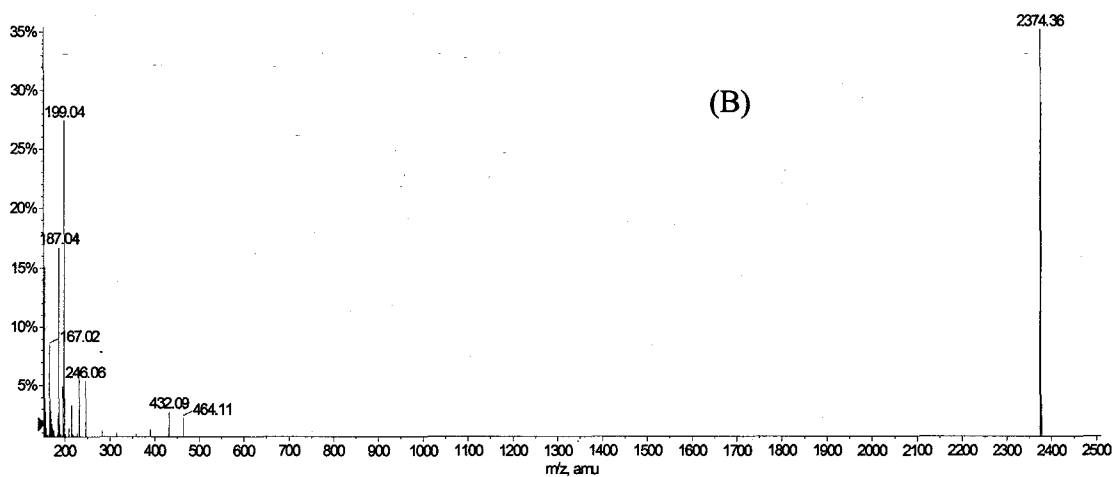
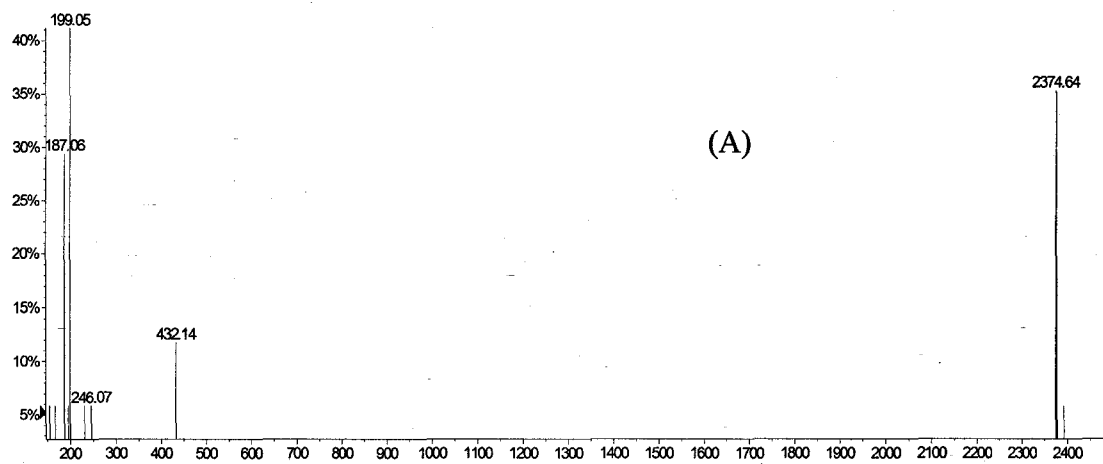


Figure III-1: MALDI-MS/MS (A) and ESI-MS/MS of the precursor $[M_{\text{NHMe}}+\text{H}]^+$ observed at 2374.2129.

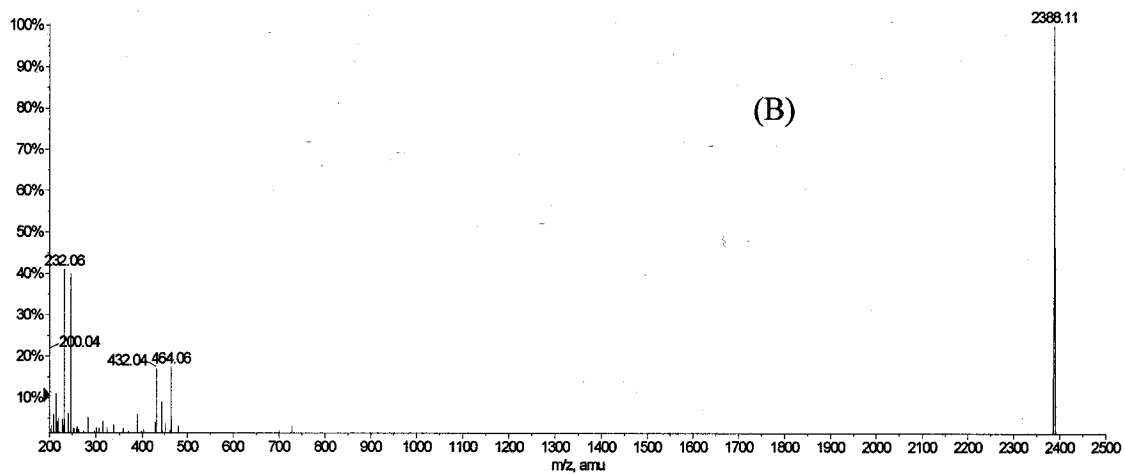
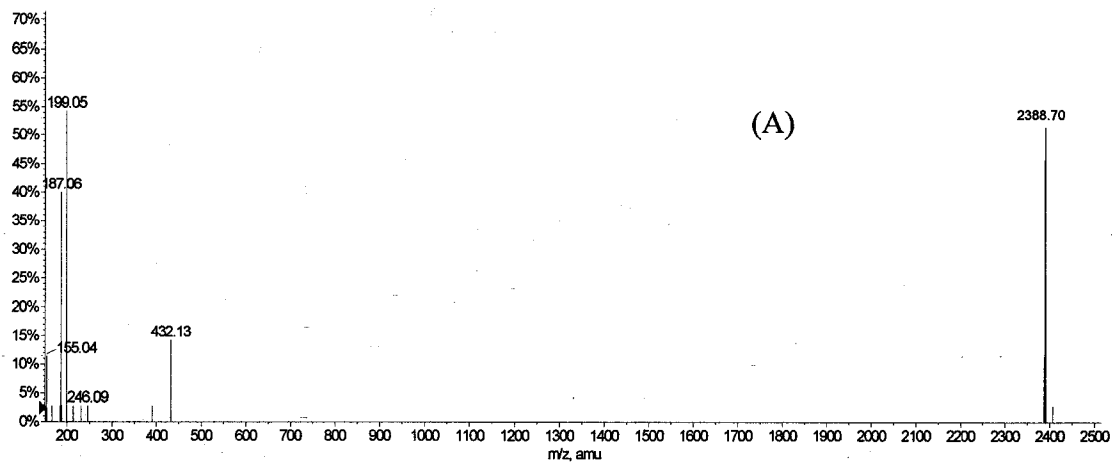


Figure III-2: MALDI-MS/MS (A) and ESI-MS/MS of the precursor $[M+H]^+$ observed at 2388.2289.

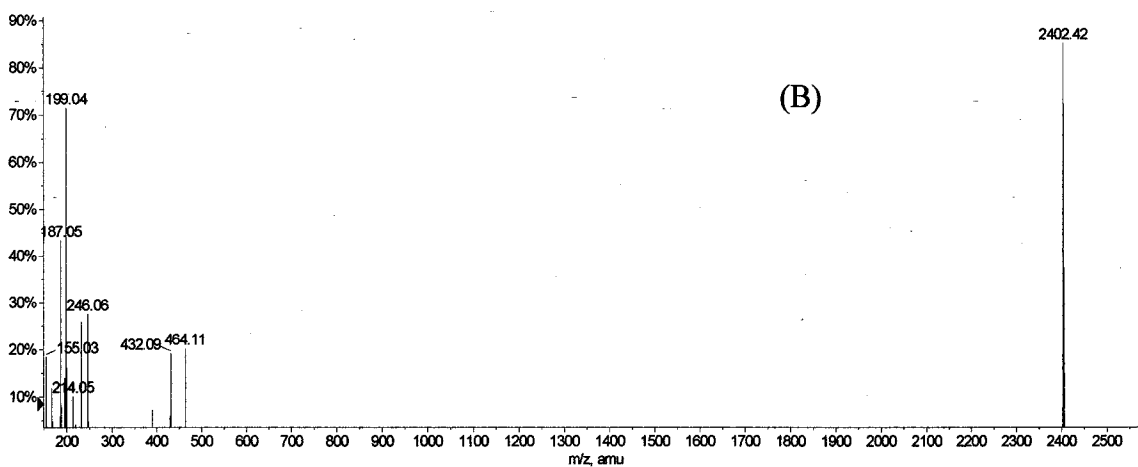
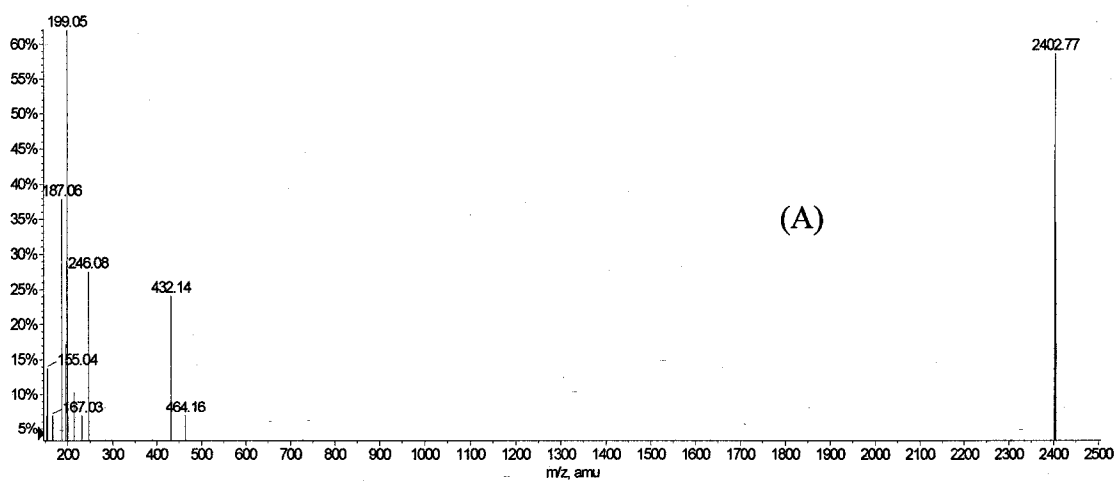


Figure III-3: MALDI-MS/MS (A) and ESI-MS/MS of the precursor $[M_1+H]^+$ observed at 2402.2429.

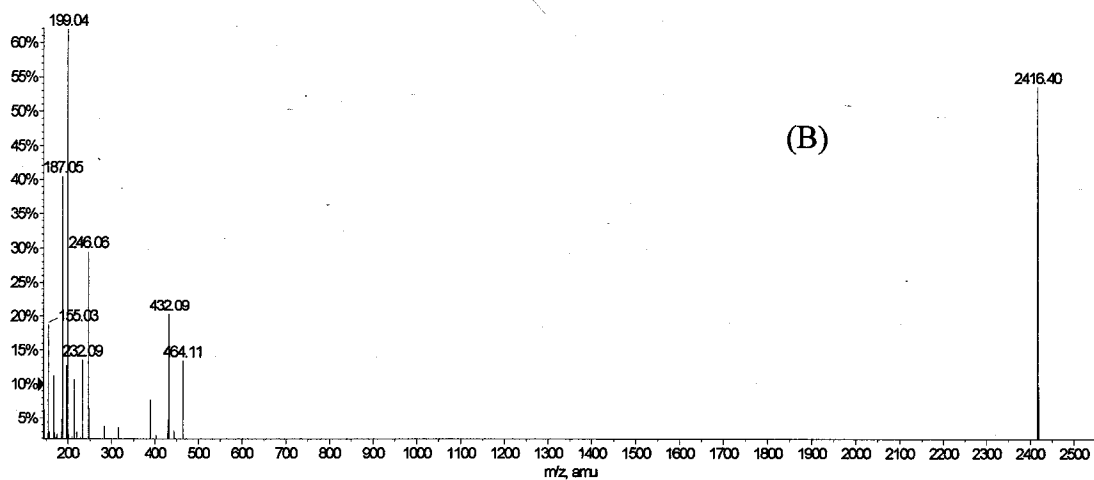
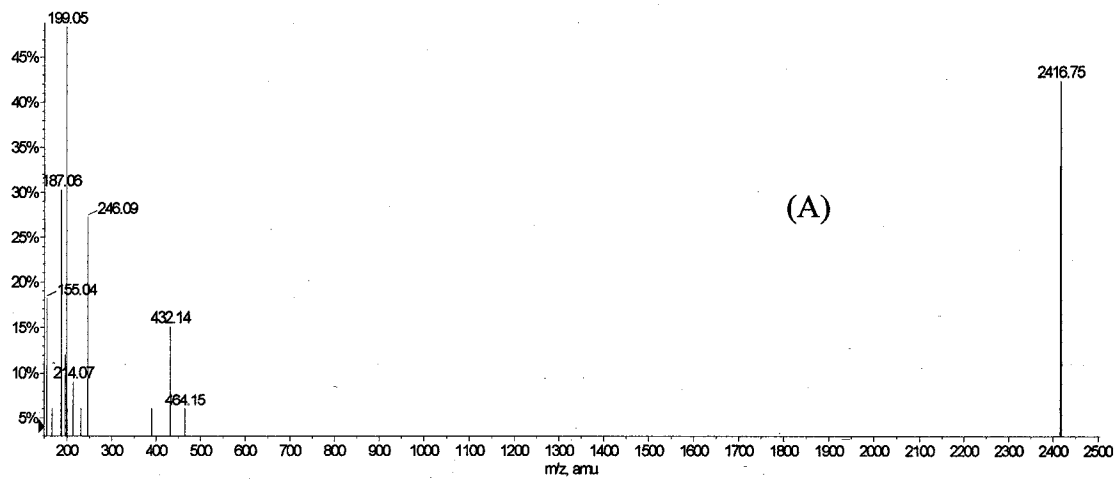


Figure III-4: MALDI-MS/MS (A) and ESI-MS/MS of the precursor $[M_2+H]^+$ observed at 2416.2315.

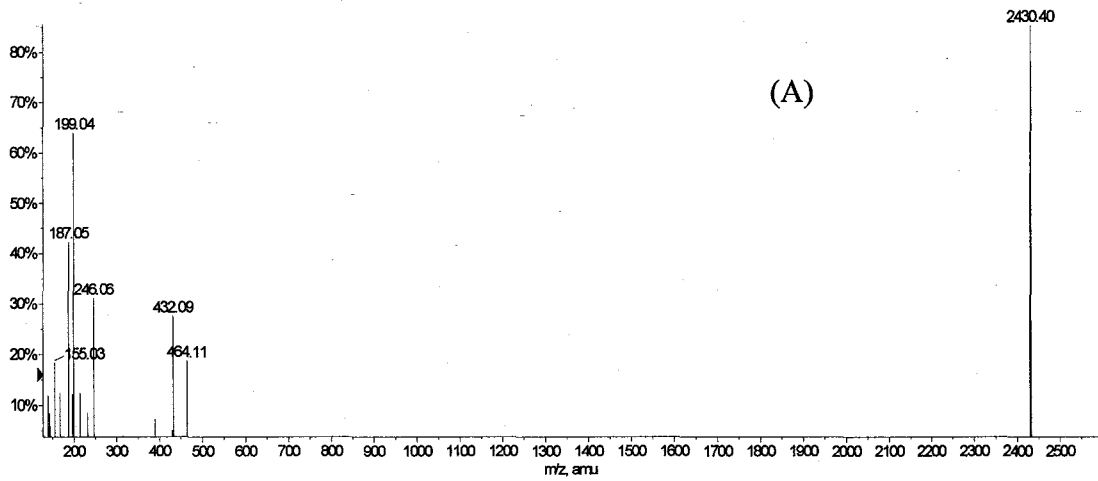
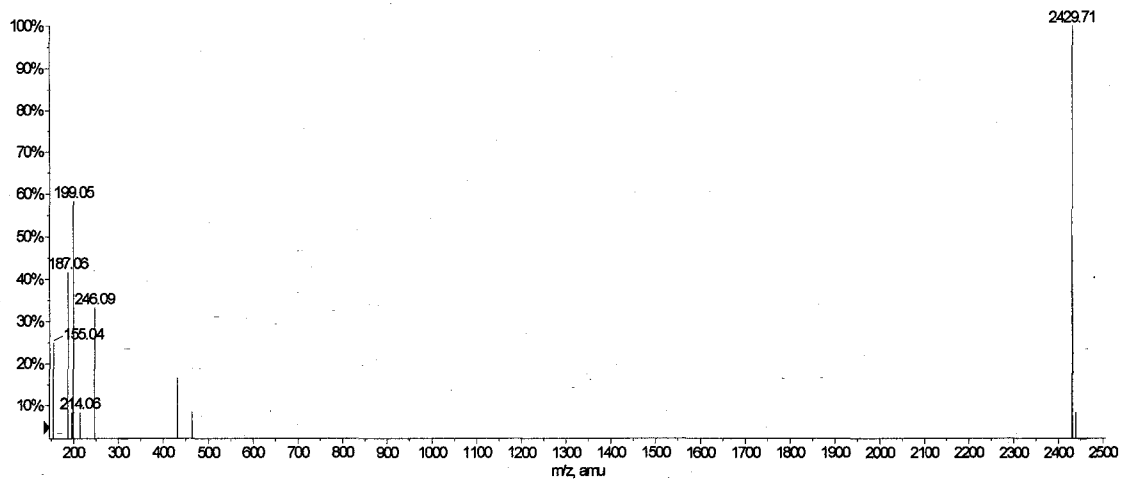


Figure III-4: MALDI-MS/MS (A) and ESI-MS/MS of the precursor $[M_3+H]^+$ observed at 2430.2330.

(B)

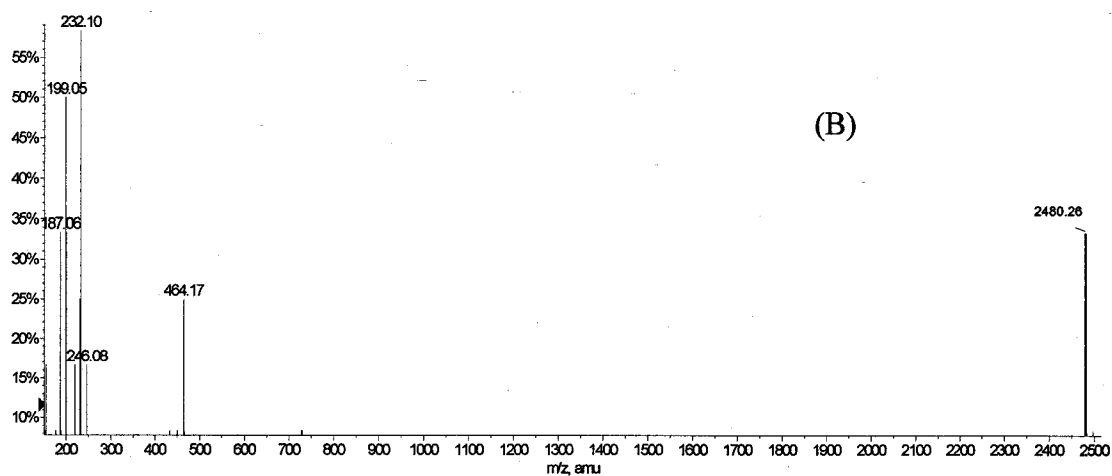
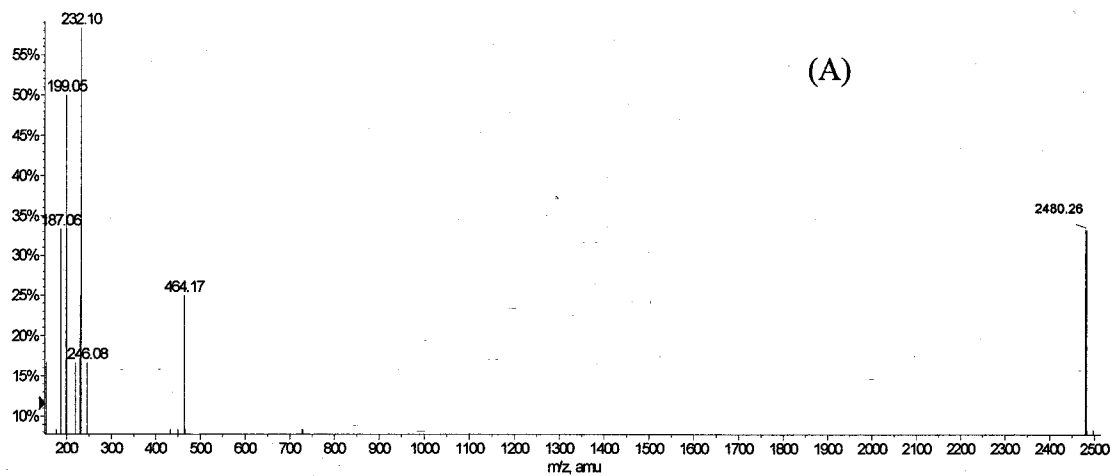


Figure III-4: MALDI-MS/MS (A) and ESI-MS/MS of the precursor $[M_4+H]^+$ observed at 2480.2581.

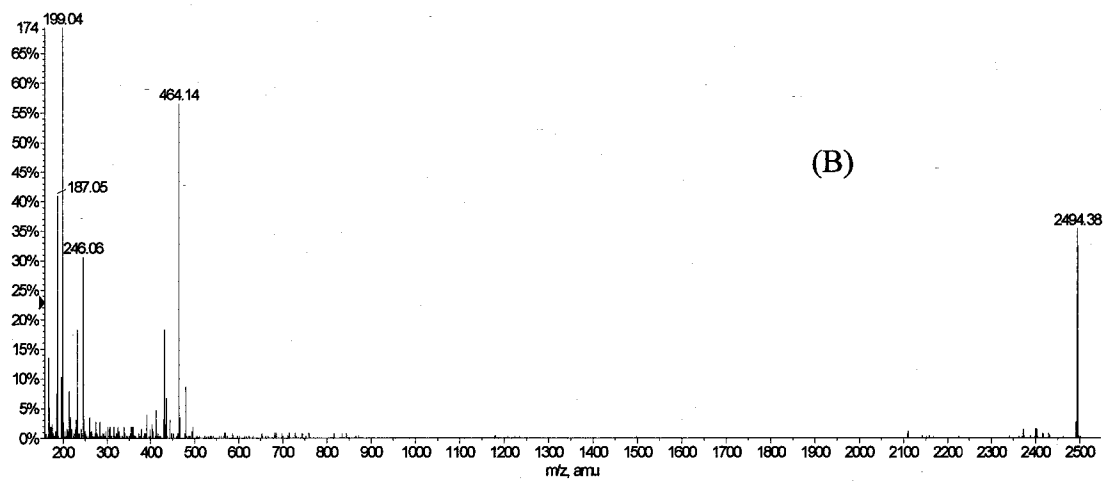
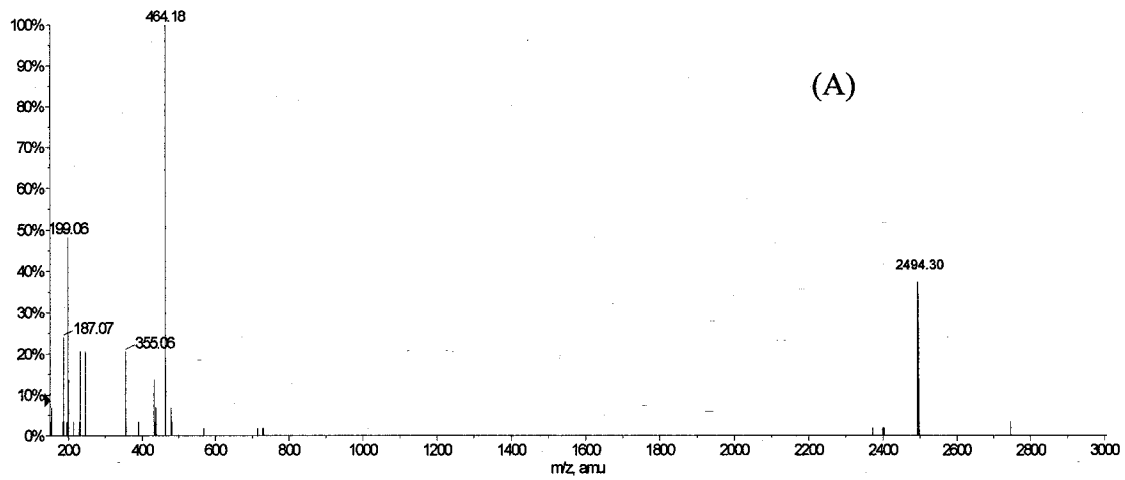


Figure III-4: MALDI-MS/MS (A) and ESI-MS/MS of the precursor $[M_5+H]^+$ observed at 2494.2429.

Appendix IV: Additional positive ESI-MS/MS spectra that established the fragmentation pattern shown in Figure 5-7

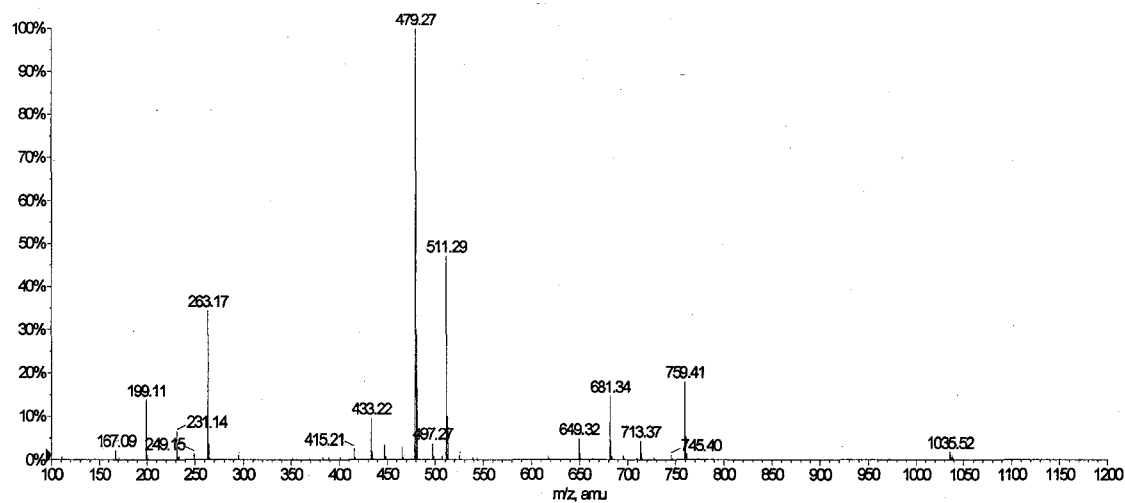
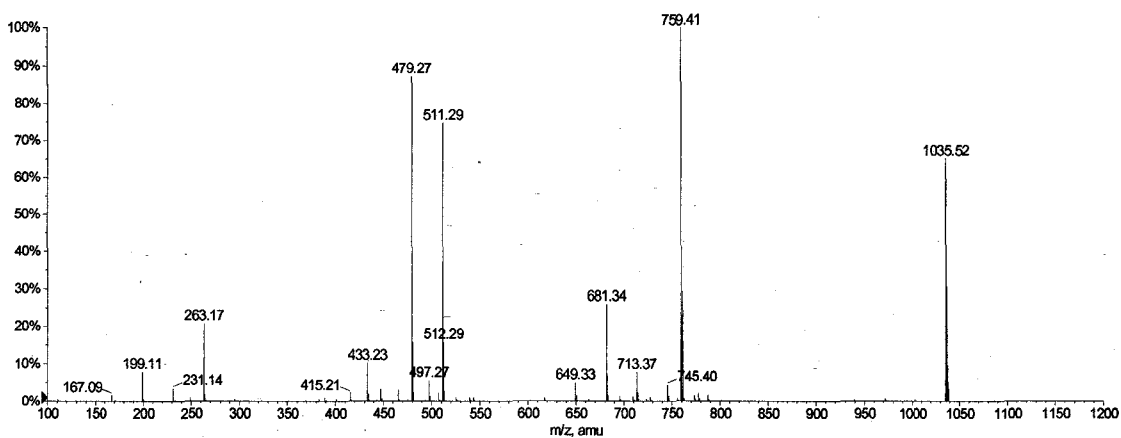


Figure IV-1: Product ion scan of m/z 1035.52 by ESI-QqTOF MS/MS using low energy CID at two different collision energies (Top: 10eV and Bottom: 15eV).

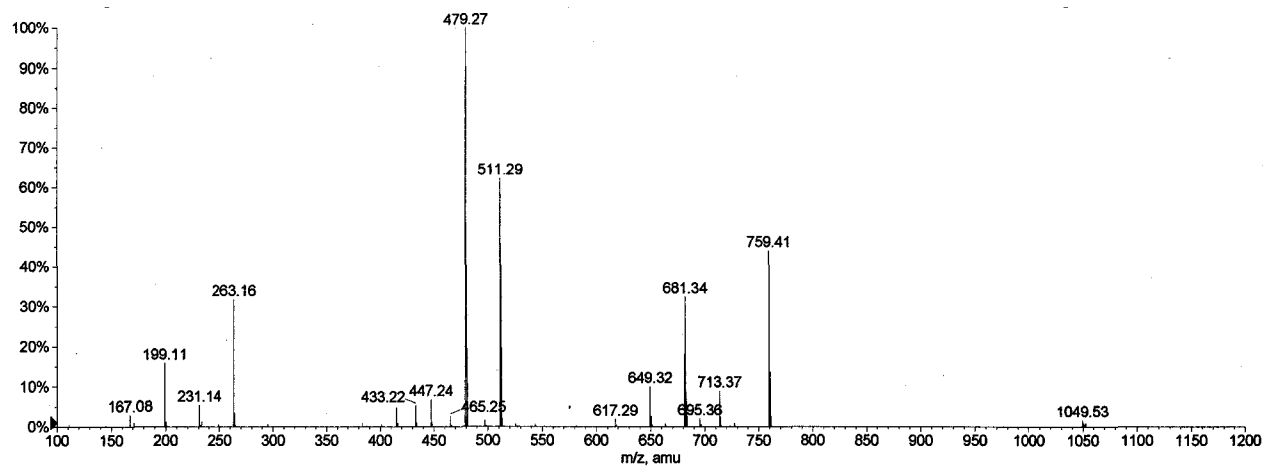
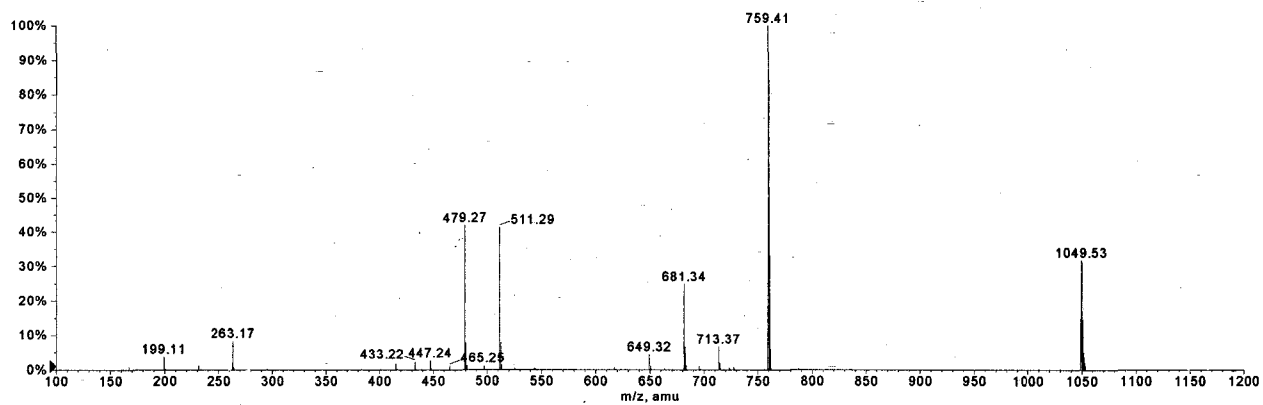


Figure IV-2: Product ion scan of m/z 1049.53 by ESI-QqTOF MS/MS using low energy CID at two different collision energies (Top: 10eV and Bottom: 15eV).

Appendix V: Positive QqToF-MS spectra of all tested neoglycolipids (except for the ones presented in Figure 6-1)

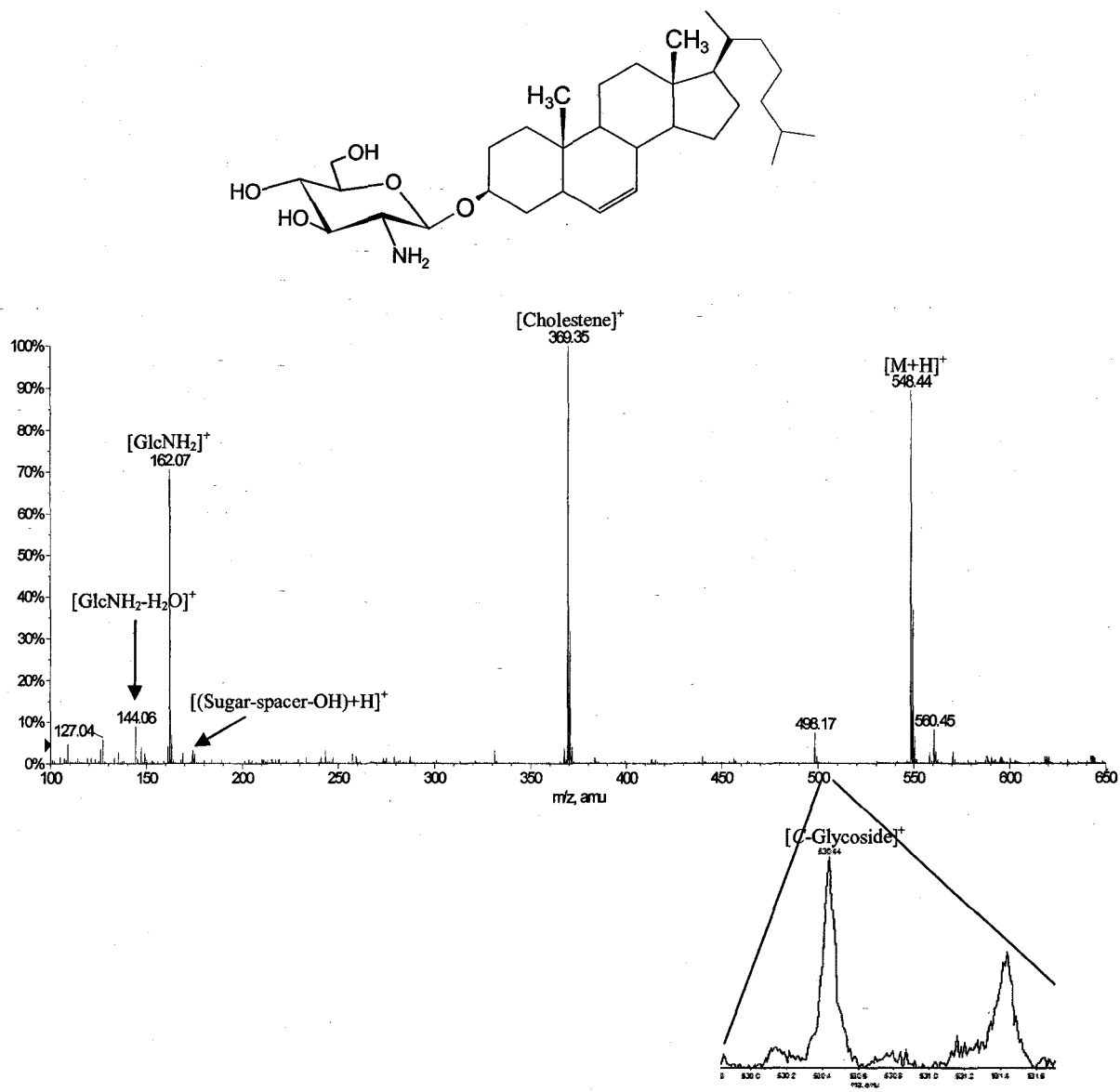


Figure V-1: ESI-QqToF spectrum of the neoglycolipid bearing GlcNH_2 with *O*-glycoside linkage (*1O*-glycoside).

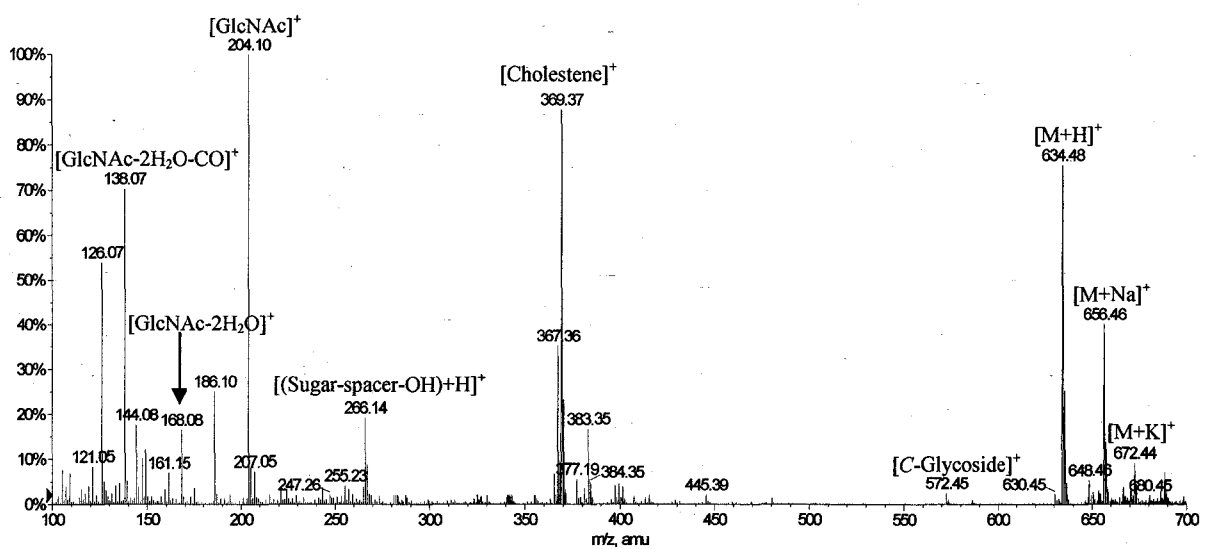
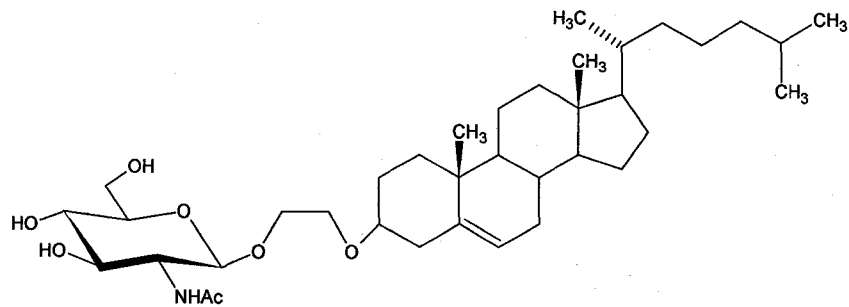


Figure V-2: ESI-QqToF spectrum of the neoglycolipid bearing GlcNAc with CH₂CH₂O spacer (2CH₂CH₂O).

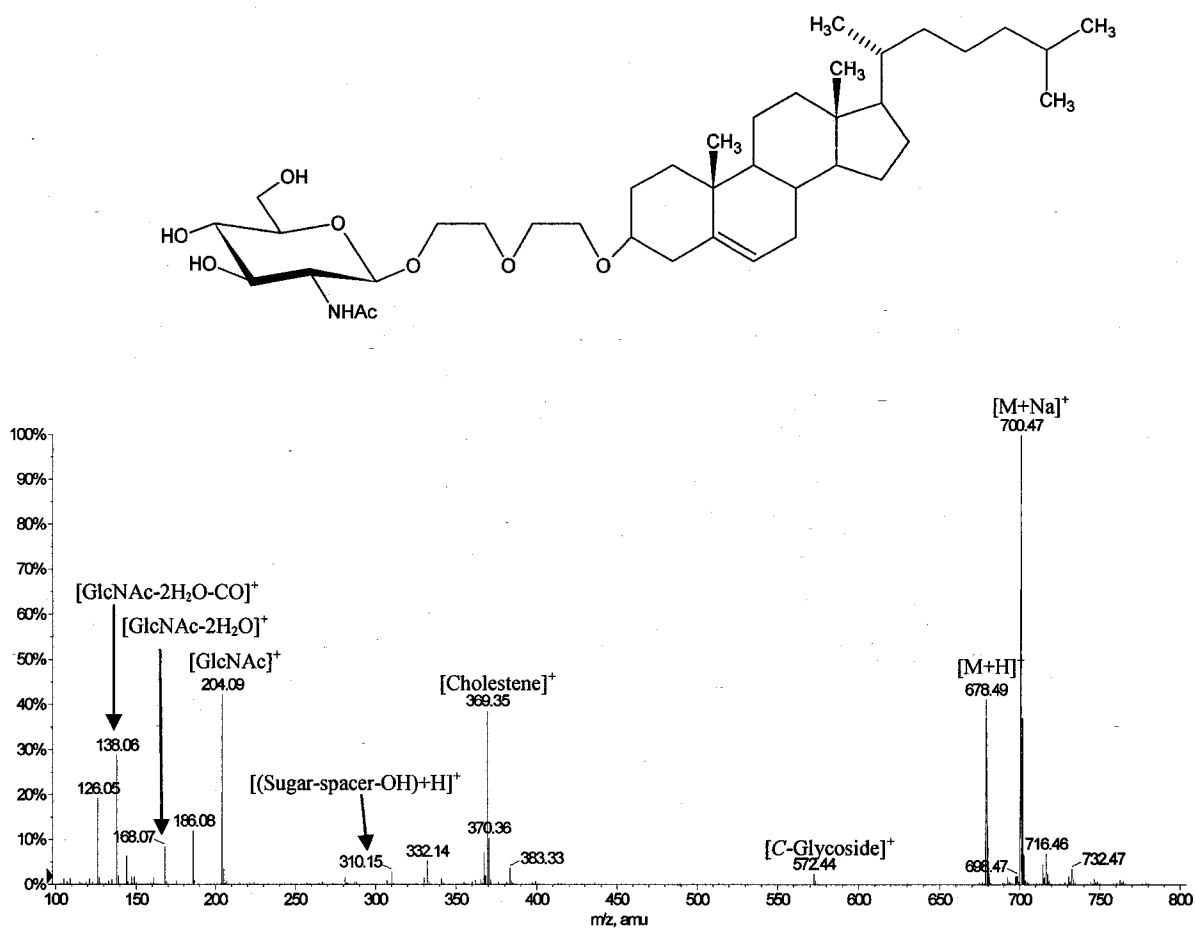


Figure V-3: ESI-QqToF spectrum of the neoglycolipid bearing GlcNAc with (CH₂CH₂O)₂ spacer (2(CH₂CH₂O)₂).

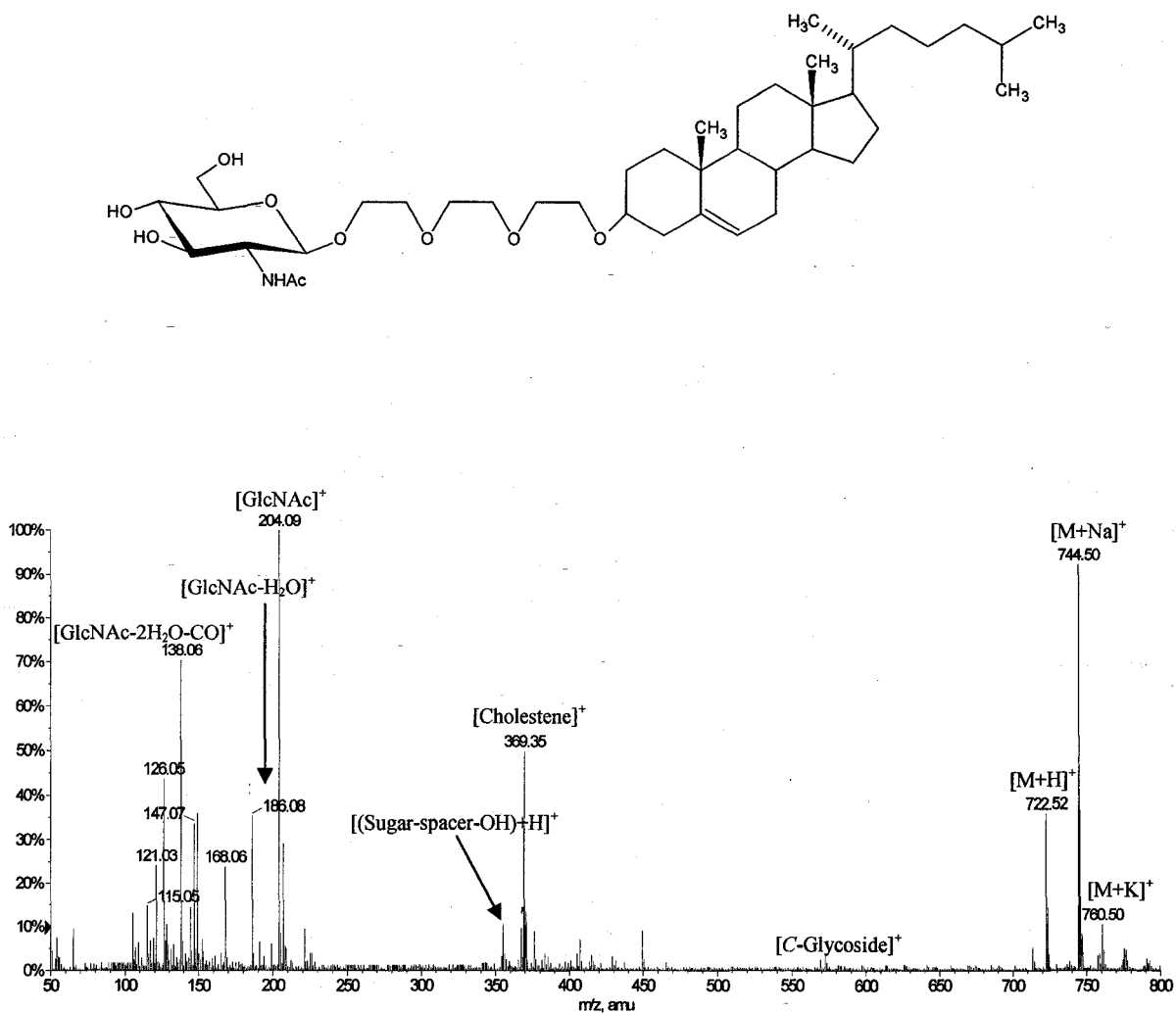


Figure V-4: ESI-QqToF spectrum of the neoglycolipid bearing GlcNAc with (CH₂CH₂O)₃ spacer (2(CH₂CH₂O)₂).

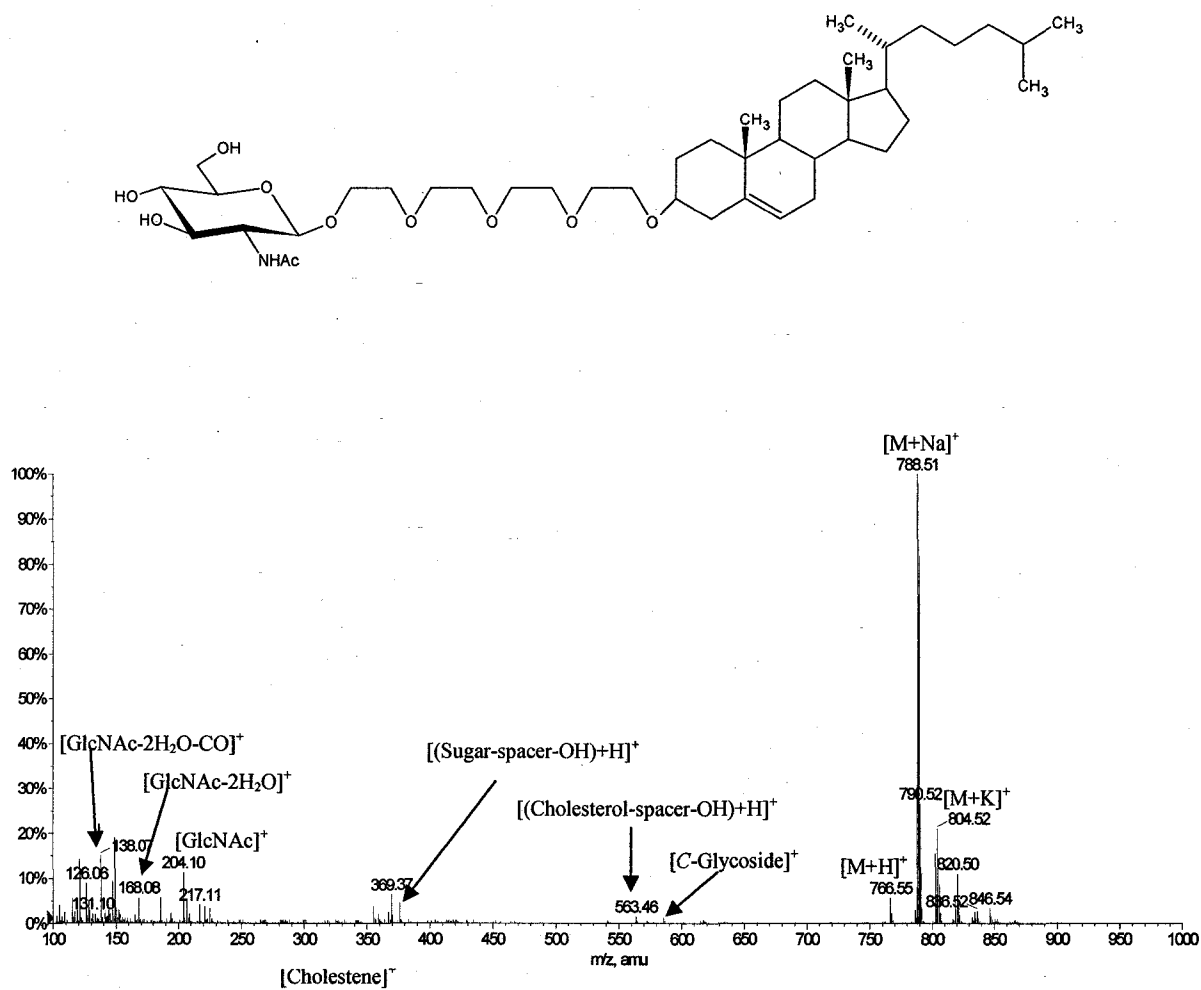


Figure V-5: ESI-QqToF spectrum of the neoglycolipid bearing GlcNAc with $(\text{CH}_2\text{CH}_2\text{O})_4$ spacer $(2(\text{CH}_2\text{CH}_2\text{O})_4)$.

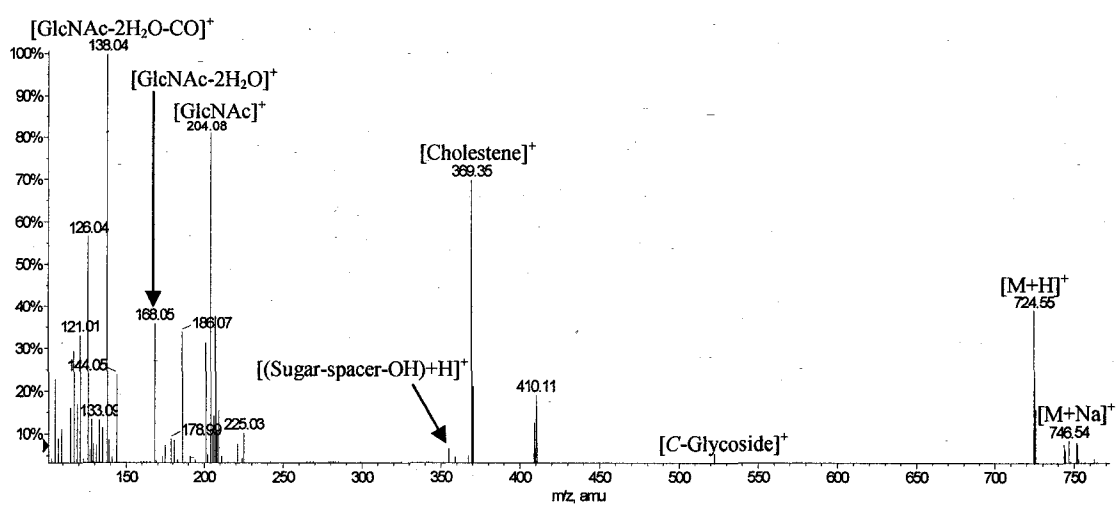
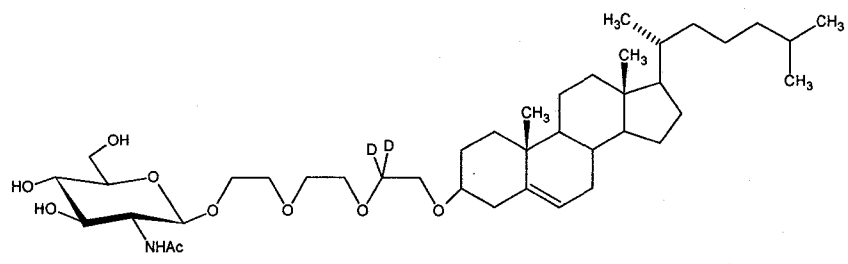


Figure V-6: ESI-QqToF spectrum of the neoglycolipid bearing GlcNAc with CH₂CH₂O CH₂CH₂O CD₂CH₂O spacer.

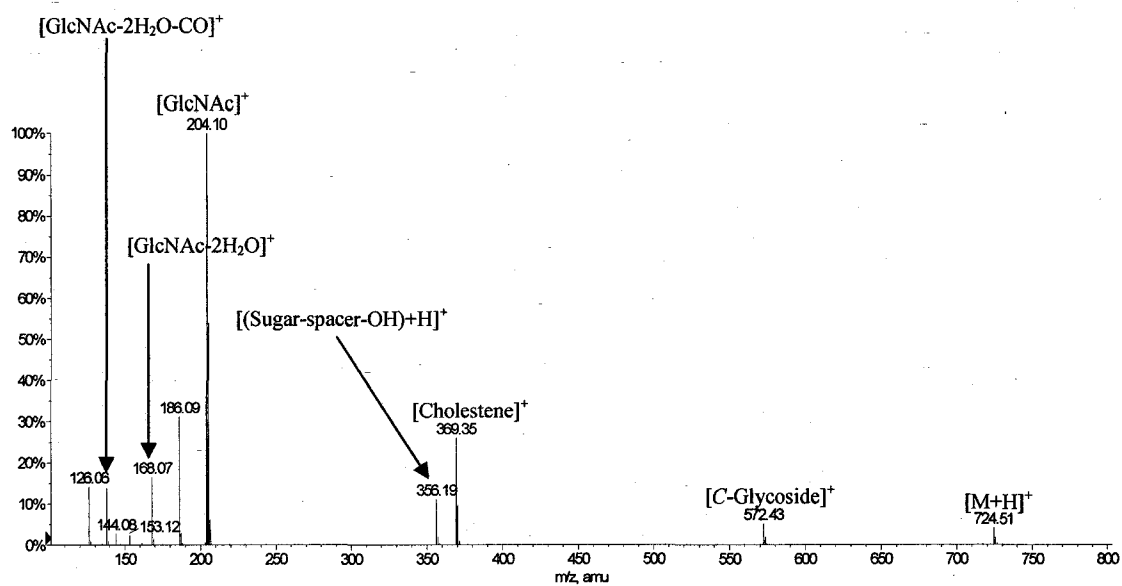
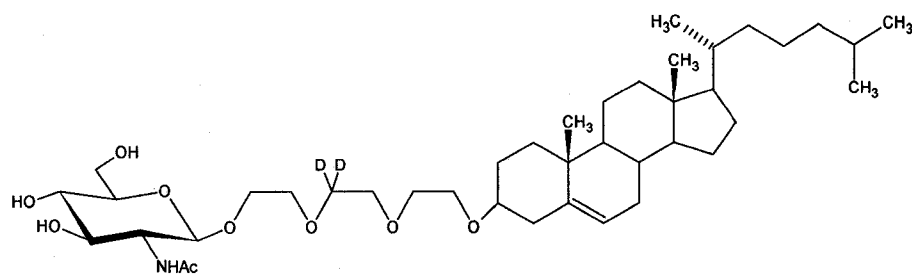


Figure V-7: ESI-QqToF spectrum of the neoglycolipid bearing GlcNAc with CH₂CH₂OCD₂CH₂OCH₂CH₂O spacer.

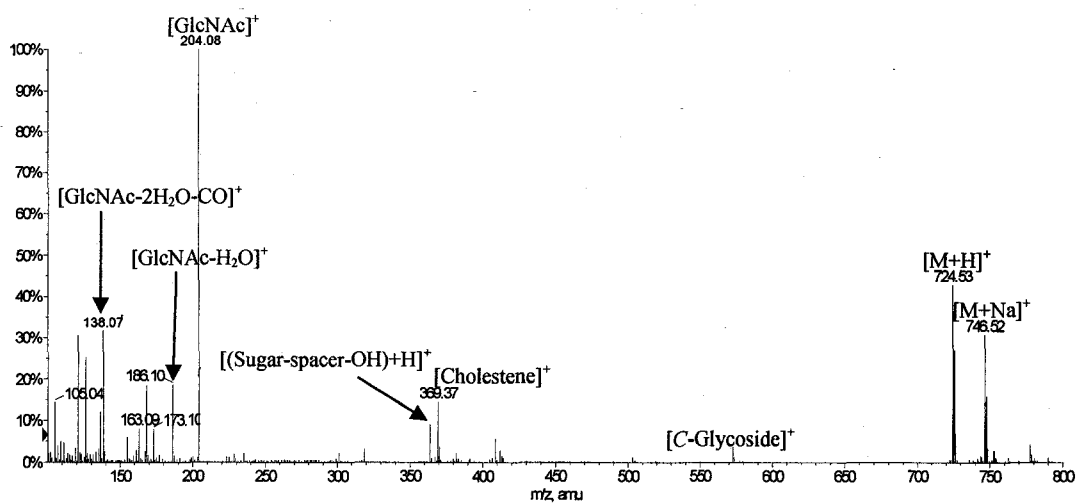
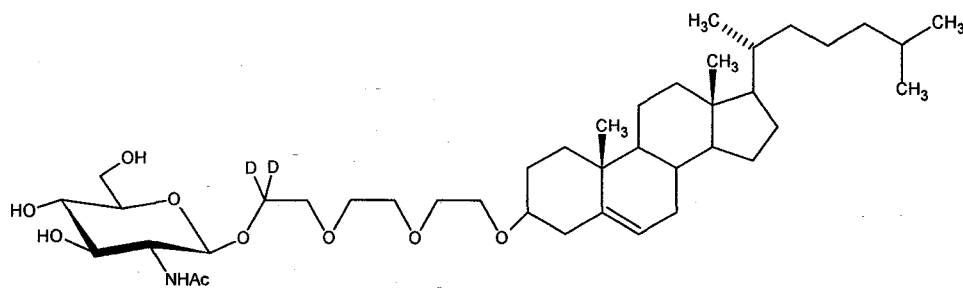


Figure V-8: ESI-QqToF spectrum of the neoglycolipid bearing GlcNAc with CD₂CH₂OCH₂CH₂OCH₂CH₂O spacer.

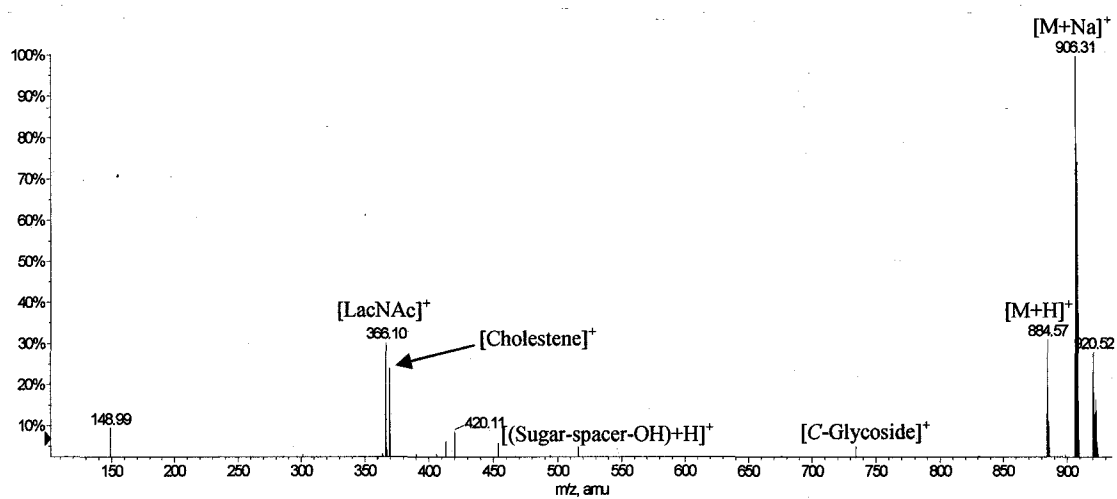
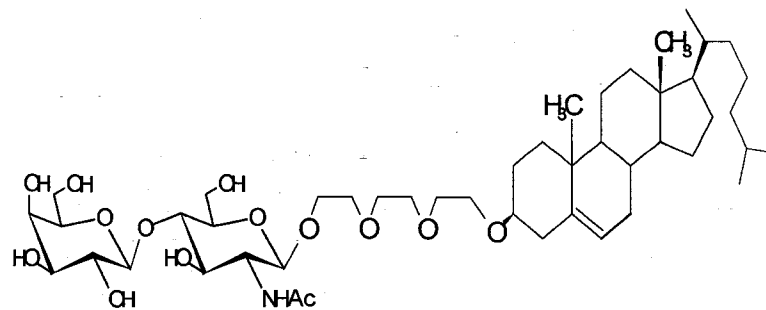


Figure V-9: ESI-QqToF spectrum of the neoglycolipid bearing LacNAc with $(\text{CH}_2\text{CH}_2\text{O})_3$ spacer $(4(\text{CH}_2\text{CH}_2\text{O})_3)$.

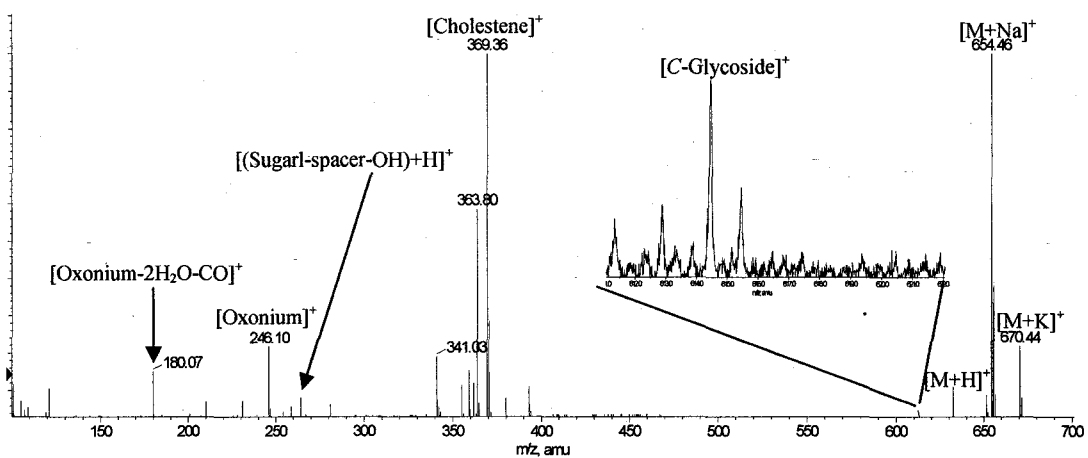
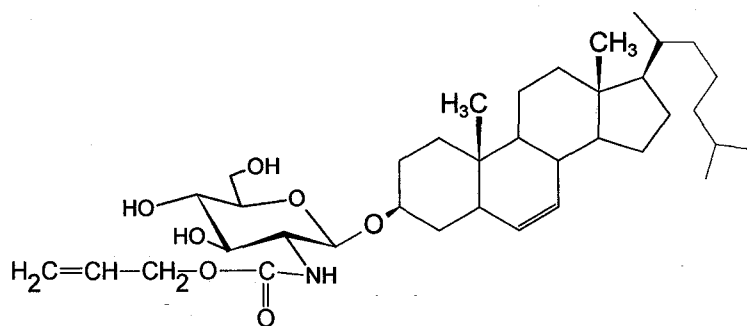


Figure V-10: ESI-QqToF spectrum of the neoglycolipid bearing GlcNAloc with *O*-glycoside as spacer (*6O*-glycoside).

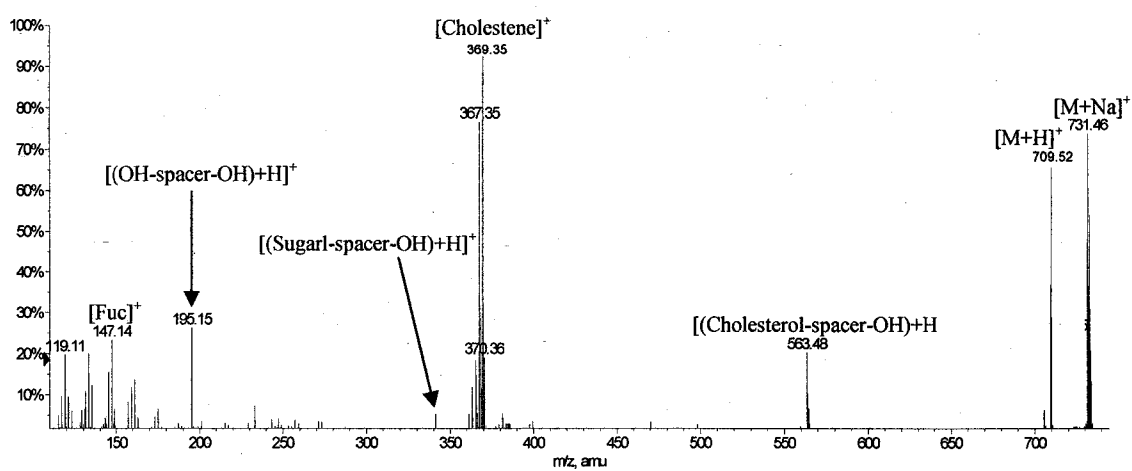
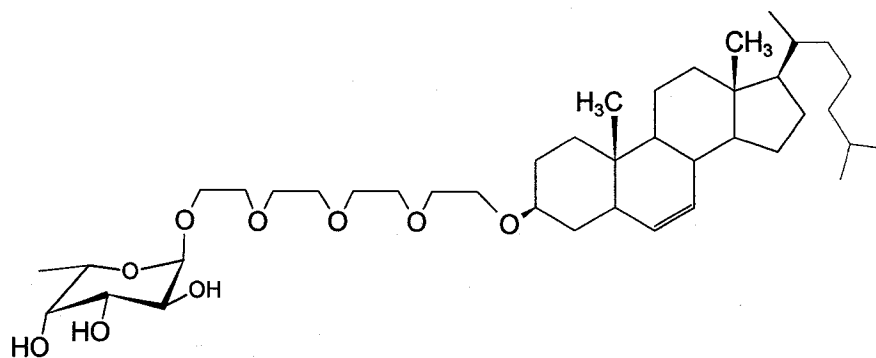


Figure V-11: ESI-QqToF spectrum of the neoglycolipid bearing Fuc with $(\text{CH}_2\text{CH}_2\text{O})_4$ spacer ($5(\text{CH}_2\text{CH}_2\text{O})_4$).

Appendix VI: Positive ESI-QqToF-MS spectra of the protected neoglycolipids

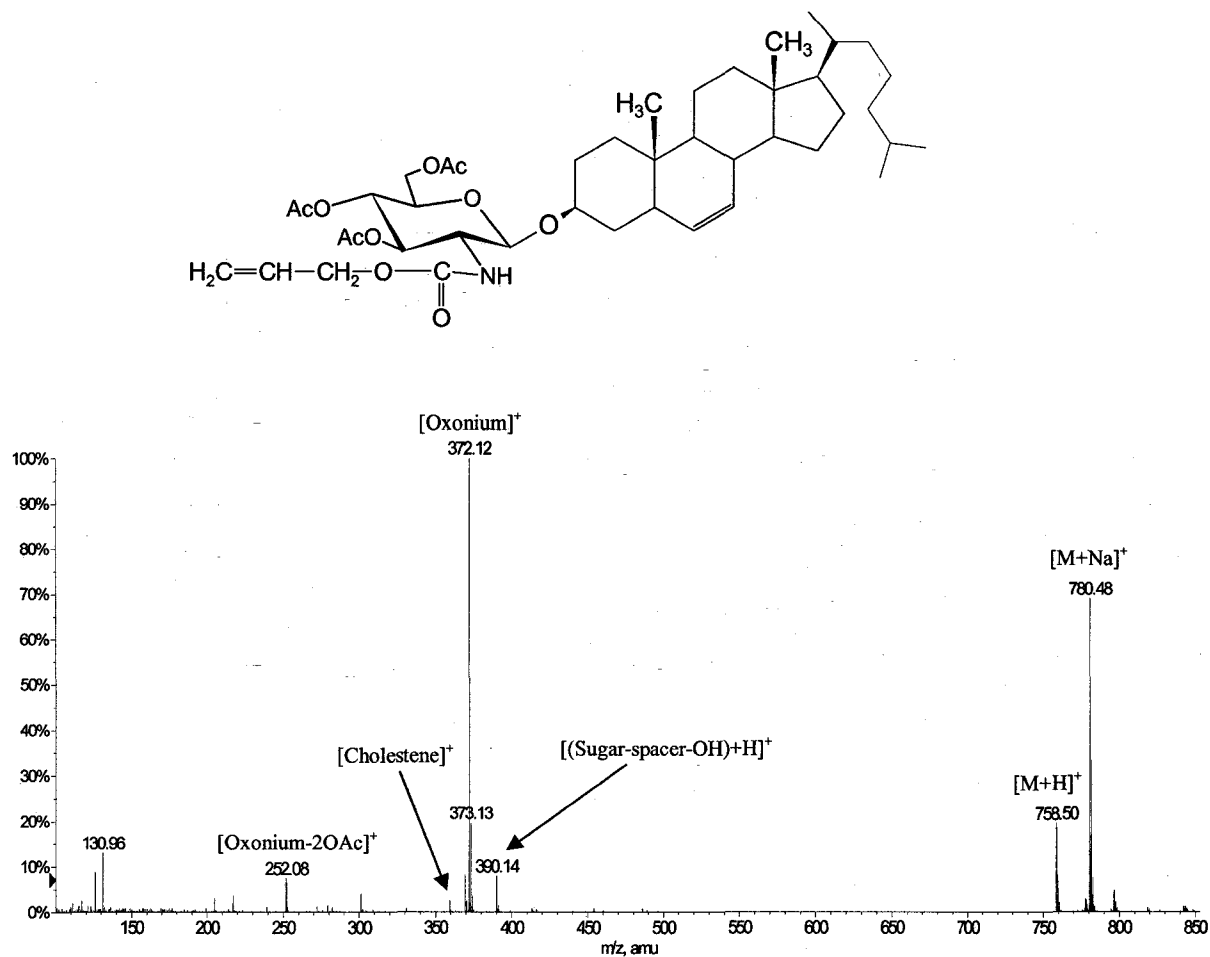


Figure VI-1: ESI-QqToF-MS spectrum of the neoglycolipids bearing GlcNAloc with *O*-glycoside as spacer (6*O*-glycoside).

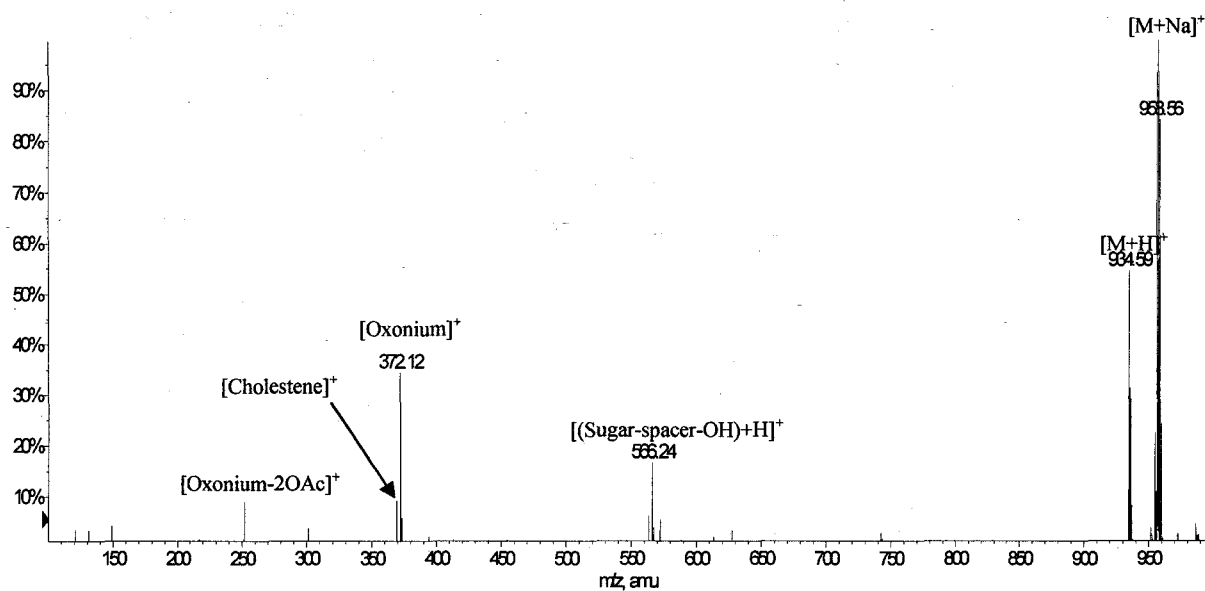
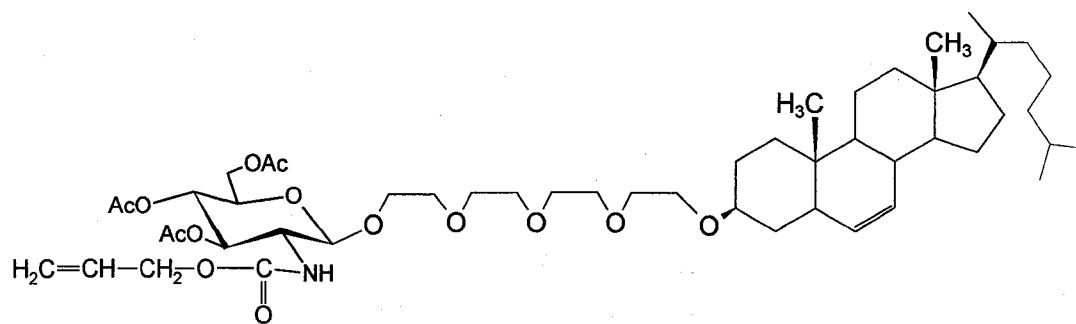


Figure VI-2: ESI-QqToF-MS spectrum of the neoglycolipids bearing GlcNAloc with $(\text{CH}_2\text{CH}_2\text{O})_4$ as spacer ($6(\text{CH}_2\text{CH}_2\text{O})_4$).

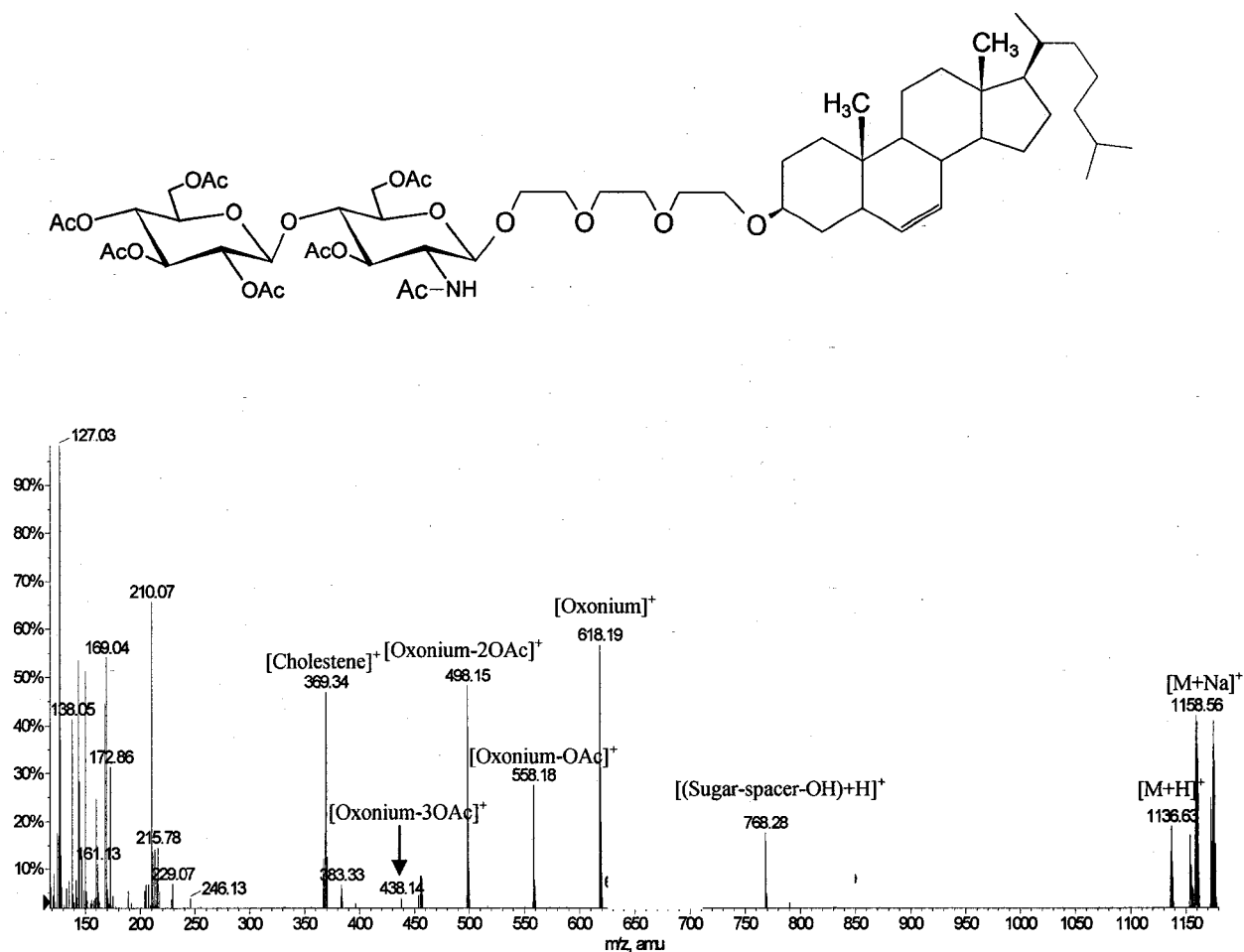


Figure VI-3: ESI-QqToF-MS spectrum of the neoglycolipids bearing LacNAc with (CH₂CH₂O)₃ as spacer (4(CH₂CH₂O)₃).

Appendix VII: ESI-QqToF-MS/MS spectra of the protonated molecules of the neoglycolipids, except for the ones presented within Chapter 7 (i.e. Figures 6-4 and 6-7)

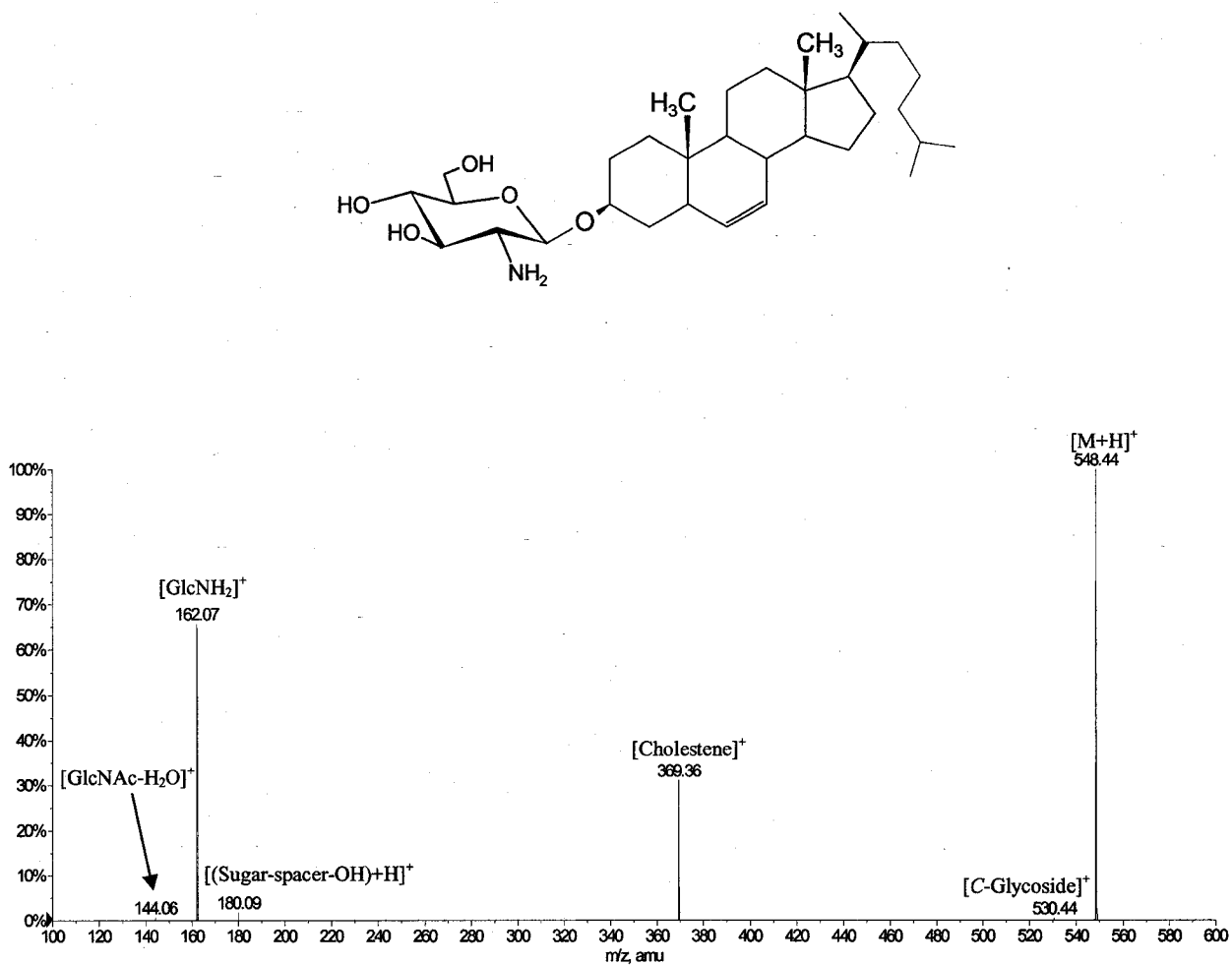


Figure VII-1: ESI-MS/MS spectrum of the neoglycolipid bearing GlcNH₂ with *O*-glycoside linkage (1*O*-glycoside).

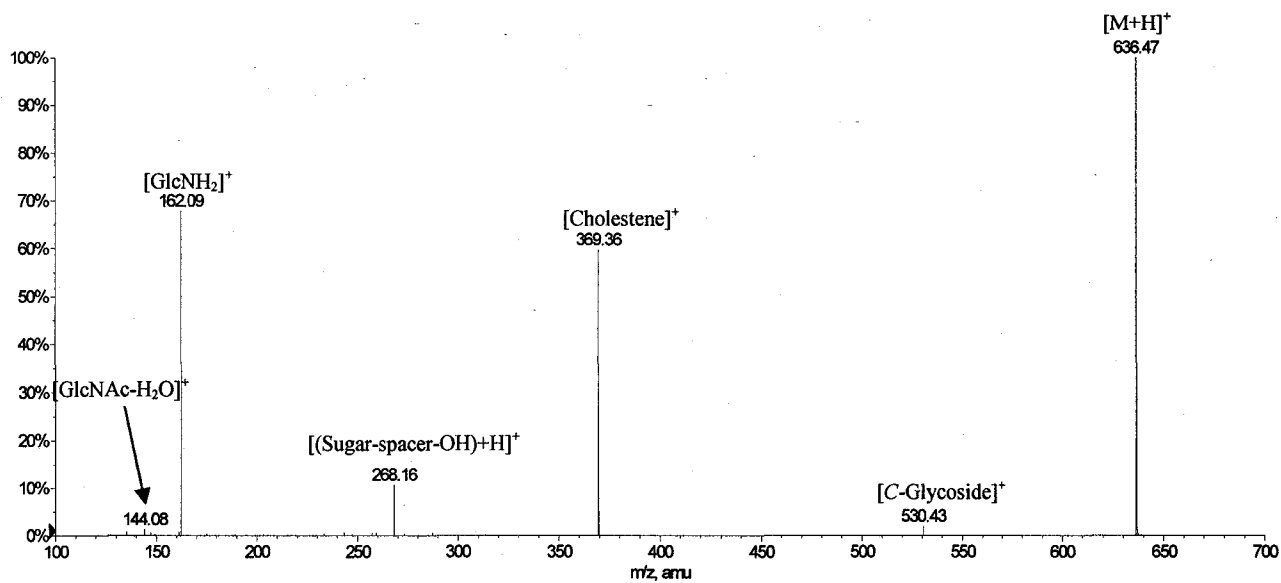
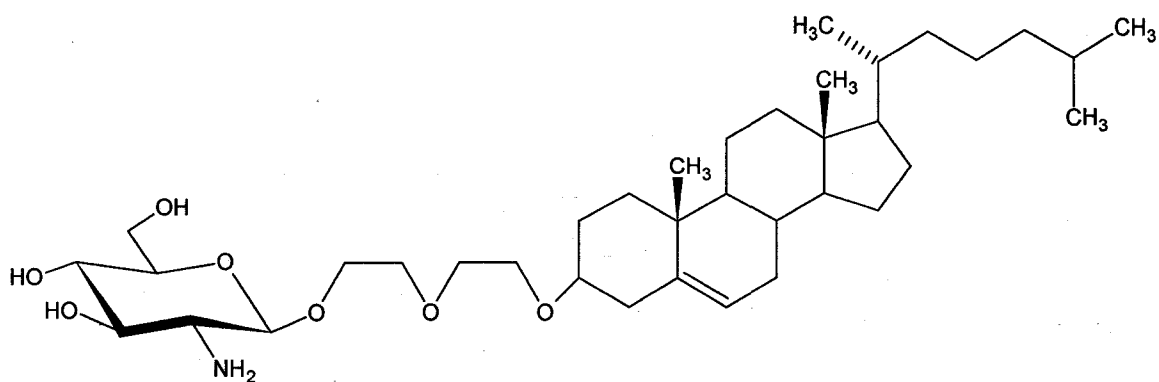


Figure VII-2: ESI-MS/MS spectrum of the neoglycolipid bearing GlcNH₂ with (CH₂CH₂O)₂ linkage (1(CH₂CH₂O)₂).

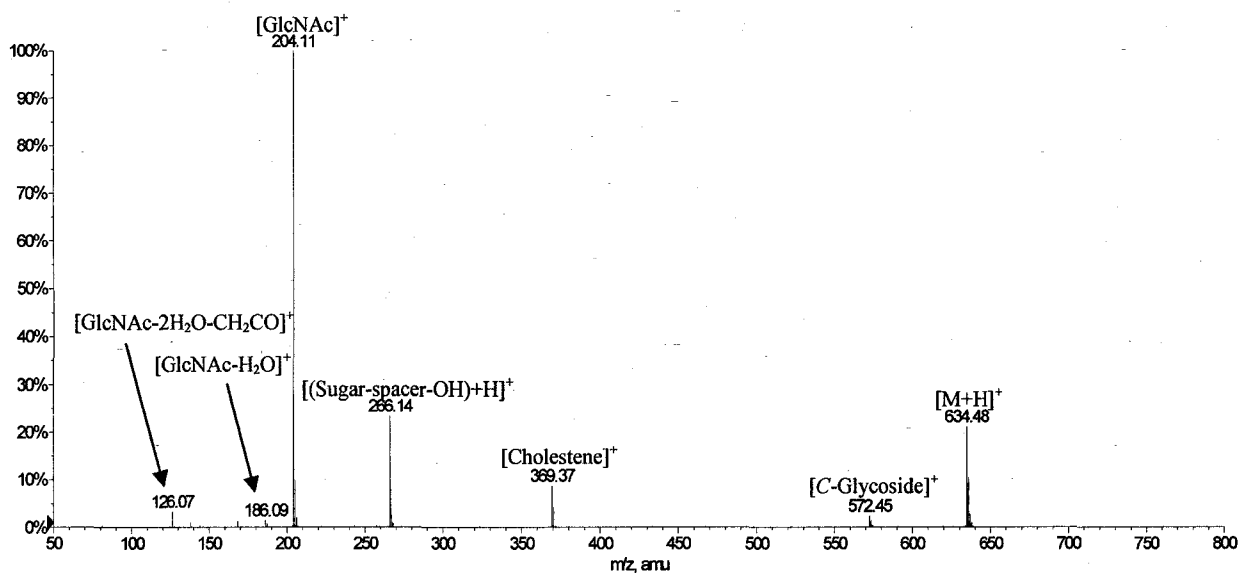
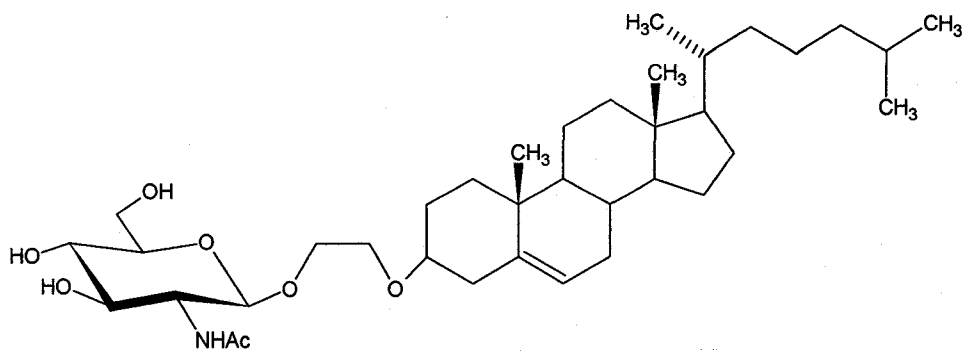


Figure VII-3: ESI-MS/MS spectrum of the neoglycolipid bearing GlcNAc with CH₂CH₂O linkage (2CH₂CH₂O).

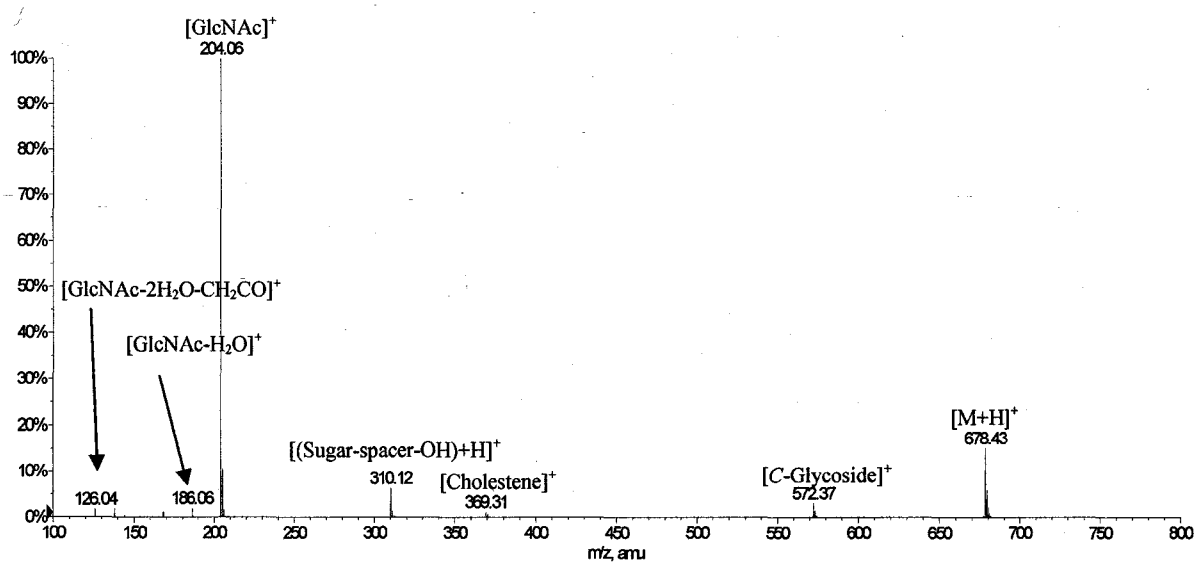
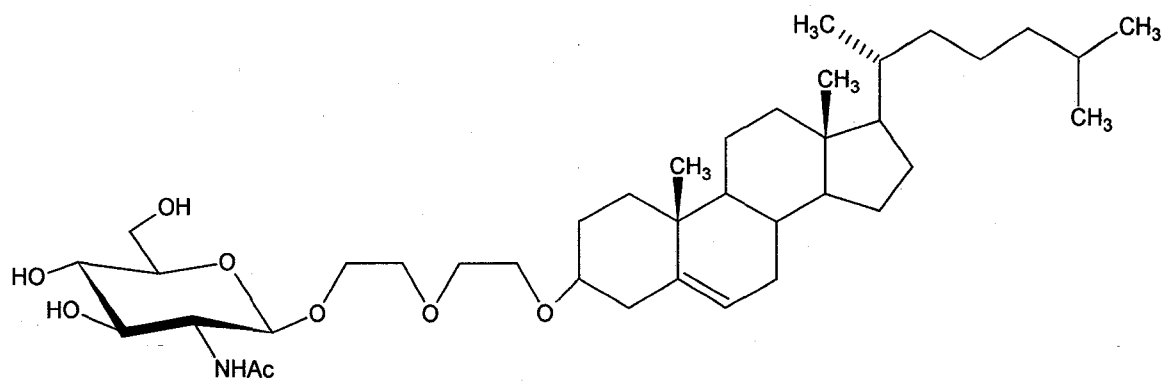


Figure VII-4: ESI-MS/MS spectrum of the neoglycolipid bearing GlcNAc with $(\text{CH}_2\text{CH}_2\text{O})_2$ linkage ($2(\text{CH}_2\text{CH}_2\text{O})_2$).

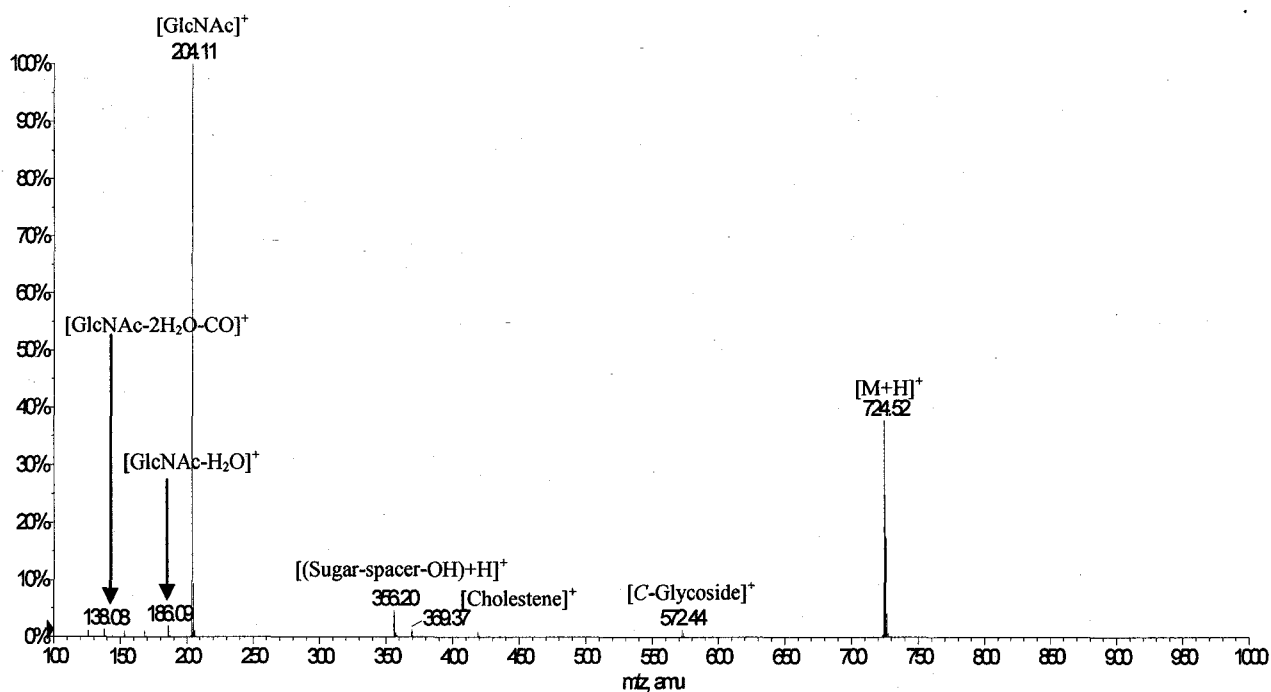
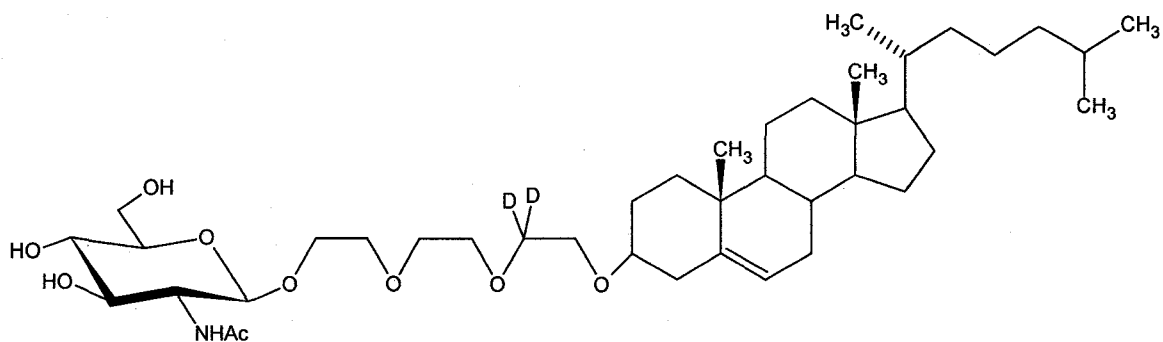


Figure VII-5: ESI-MS/MS spectrum of the neoglycolipid bearing GlcNAc with $\text{CH}_2\text{CH}_2\text{OCH}_2\text{CH}_2\text{OCD}_2\text{CH}_2\text{O}$ linkage.

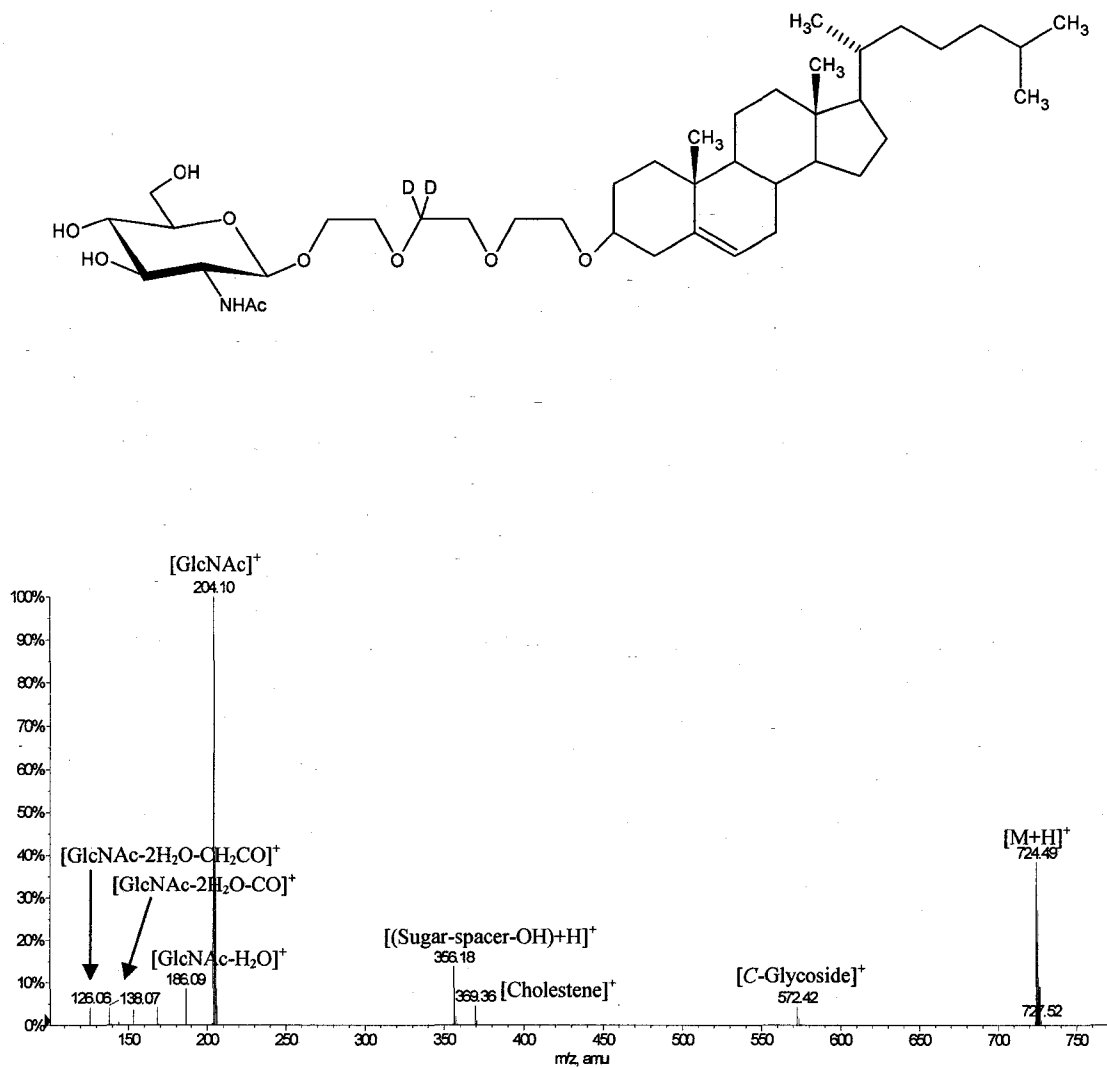


Figure VII-6: ESI-MS/MS spectrum of the neoglycolipid bearing GlcNAc with CH₂CH₂OCD₂CH₂OCH₂CH₂O linkage.

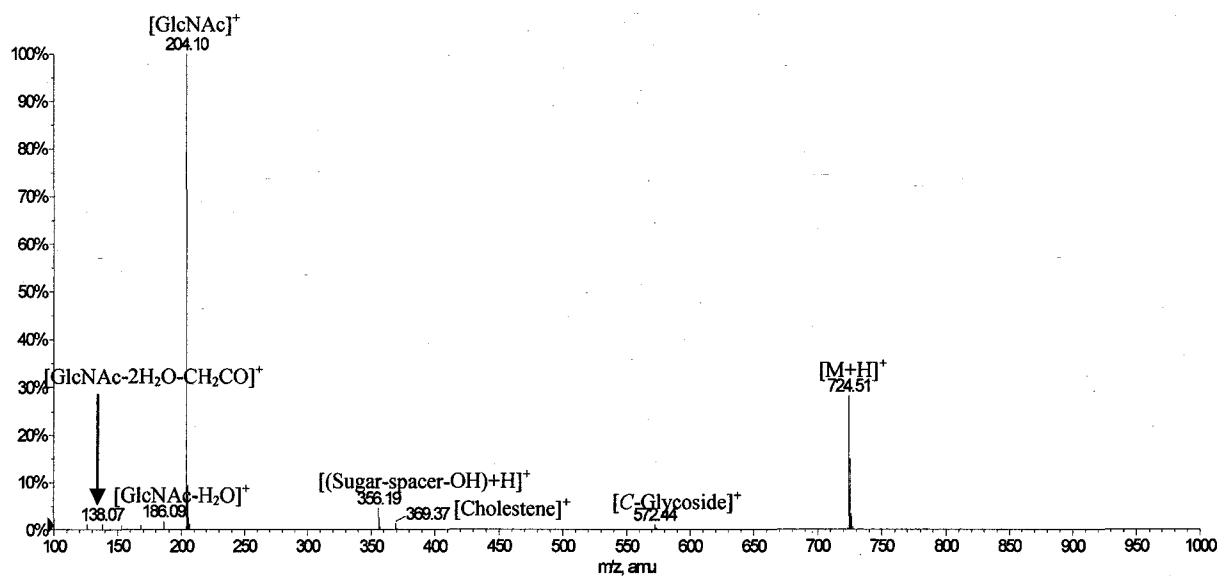
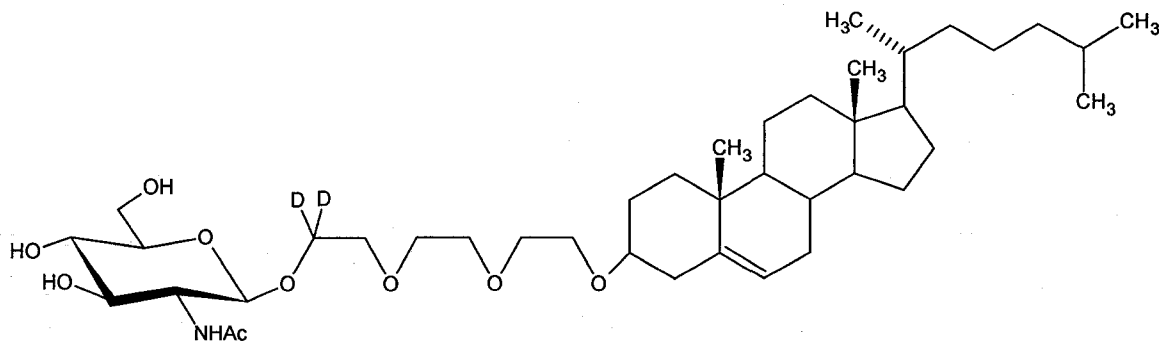


Figure VII-7: ESI-MS/MS spectrum of the neoglycolipid bearing GlcNAc with CD₂CH₂OCH₂CH₂OCH₂CH₂O linkage.

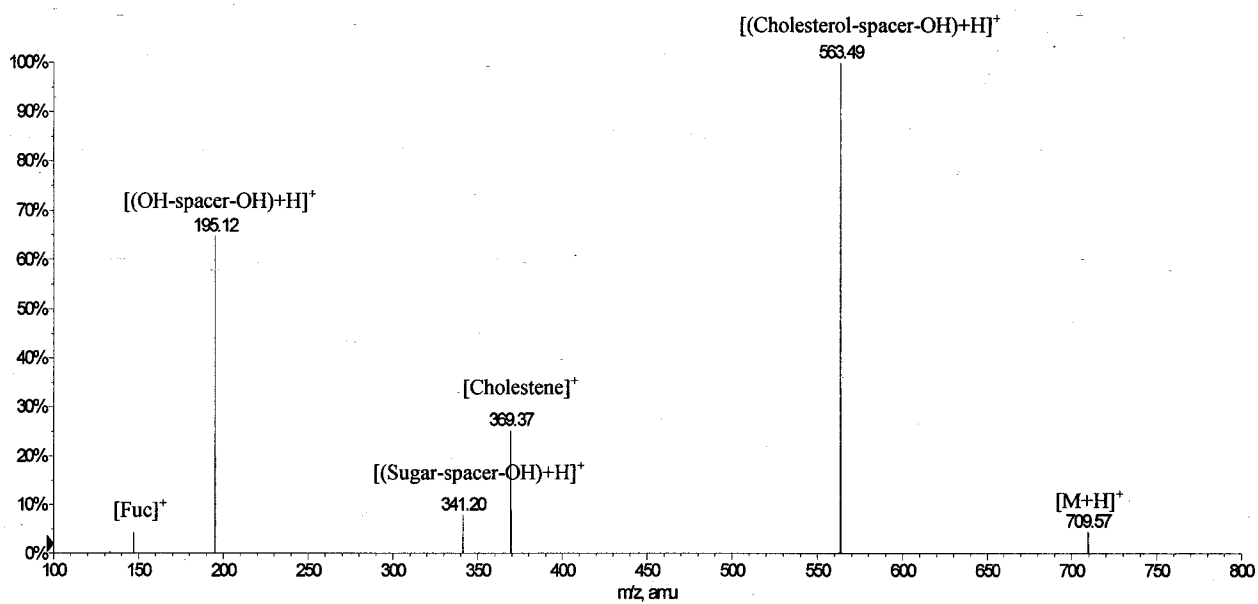
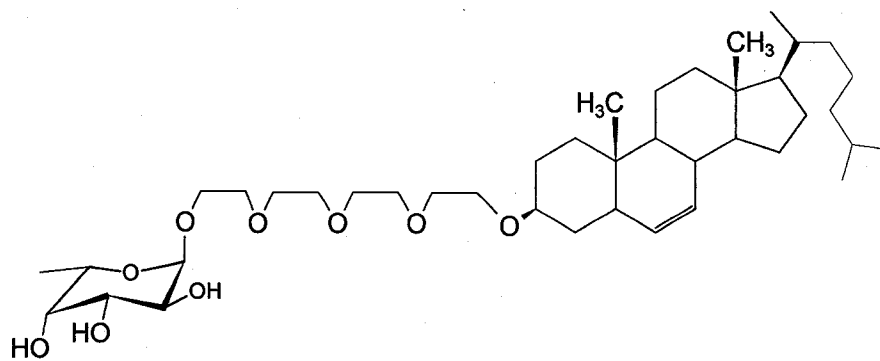


Figure VII-8: ESI-MS/MS spectrum of the neoglycolipid bearing Fuc with (CH₂CH₂O)₄ linkage (5(CH₂CH₂O)₄).

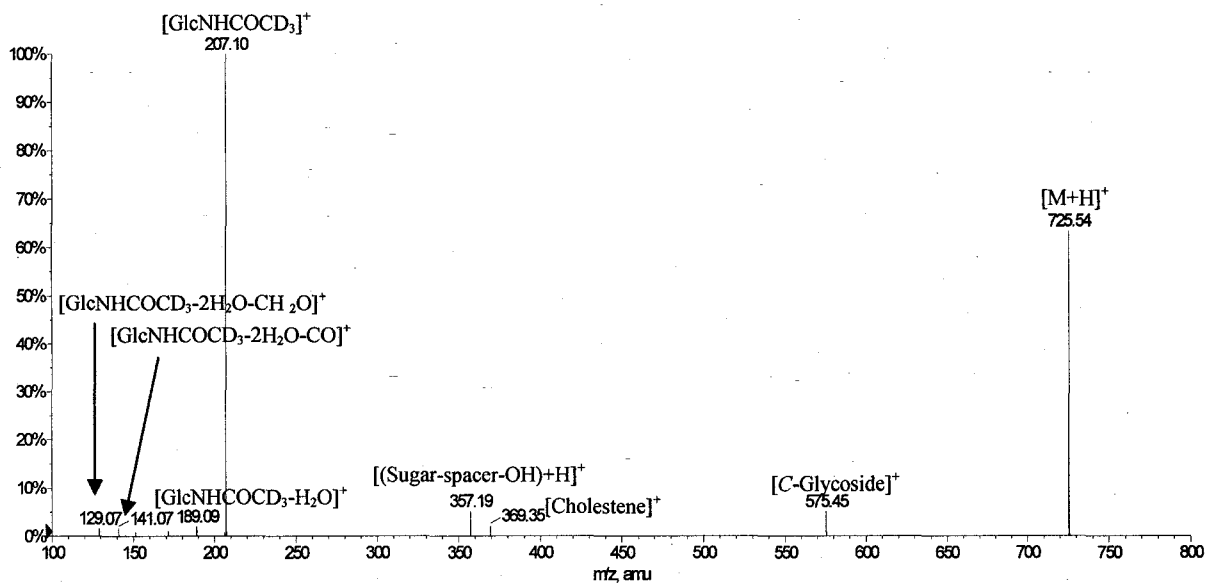
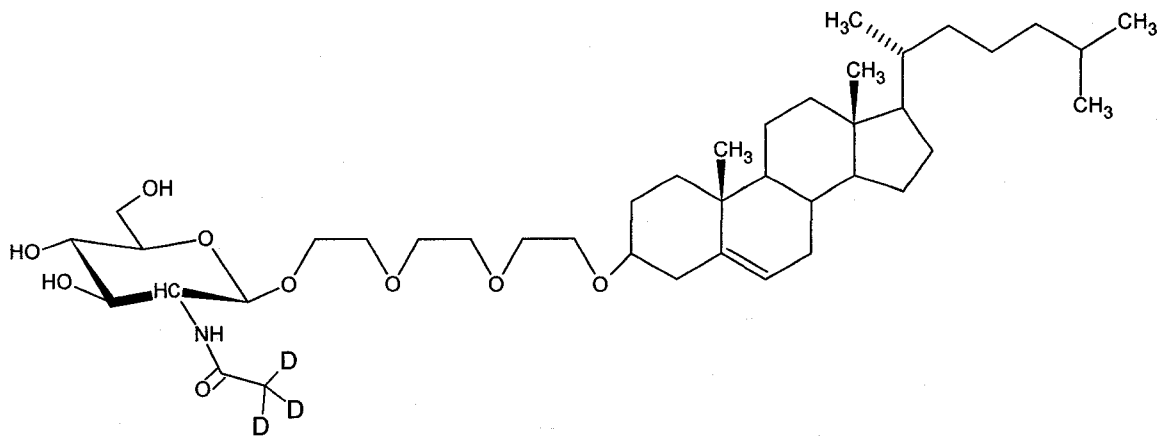


Figure VII-9: ESI-MS/MS spectrum of the neoglycolipid bearing GlcNHCOD₃ with (CH₂CH₂O)₃ linkage (3(CH₂CH₂O)₃).

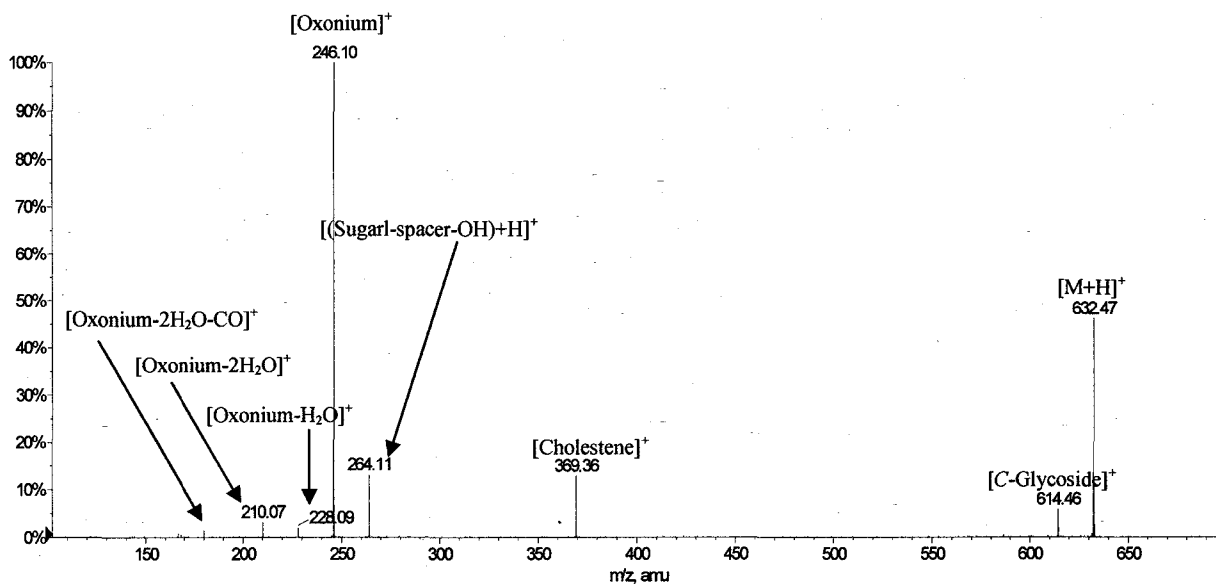
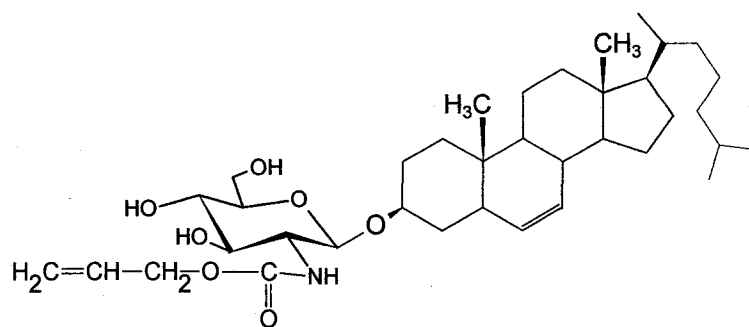


Figure VII-10: ESI-MS/MS spectrum of the neoglycolipid bearing GlcNAloc with *O*-glycoside as spacer (*6O*-glycoside).

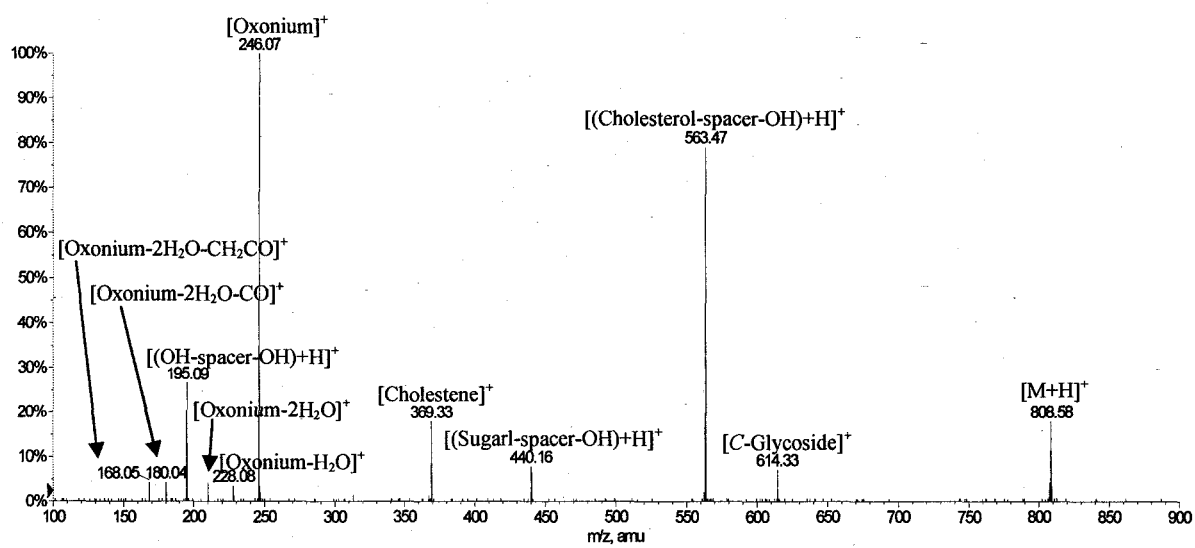
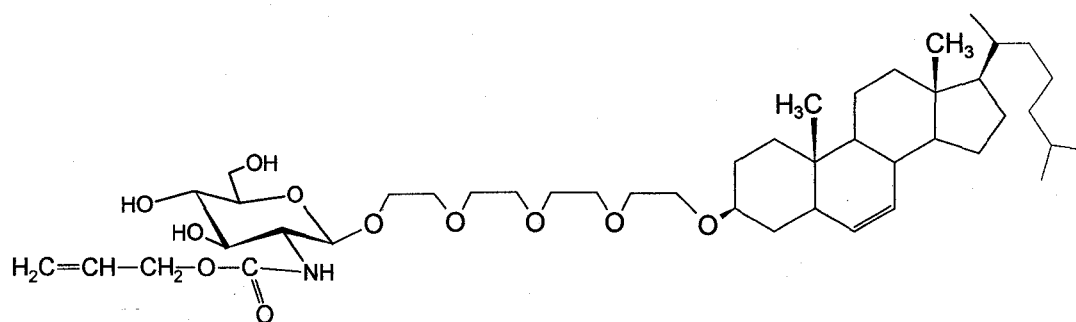


Figure V-11: ESI-MS/MS spectrum of the neoglycolipid bearing GlcNAc with $(\text{CH}_2\text{CH}_2\text{O})_4$ as spacer ($6(\text{CH}_2\text{CH}_2\text{O})_4$).

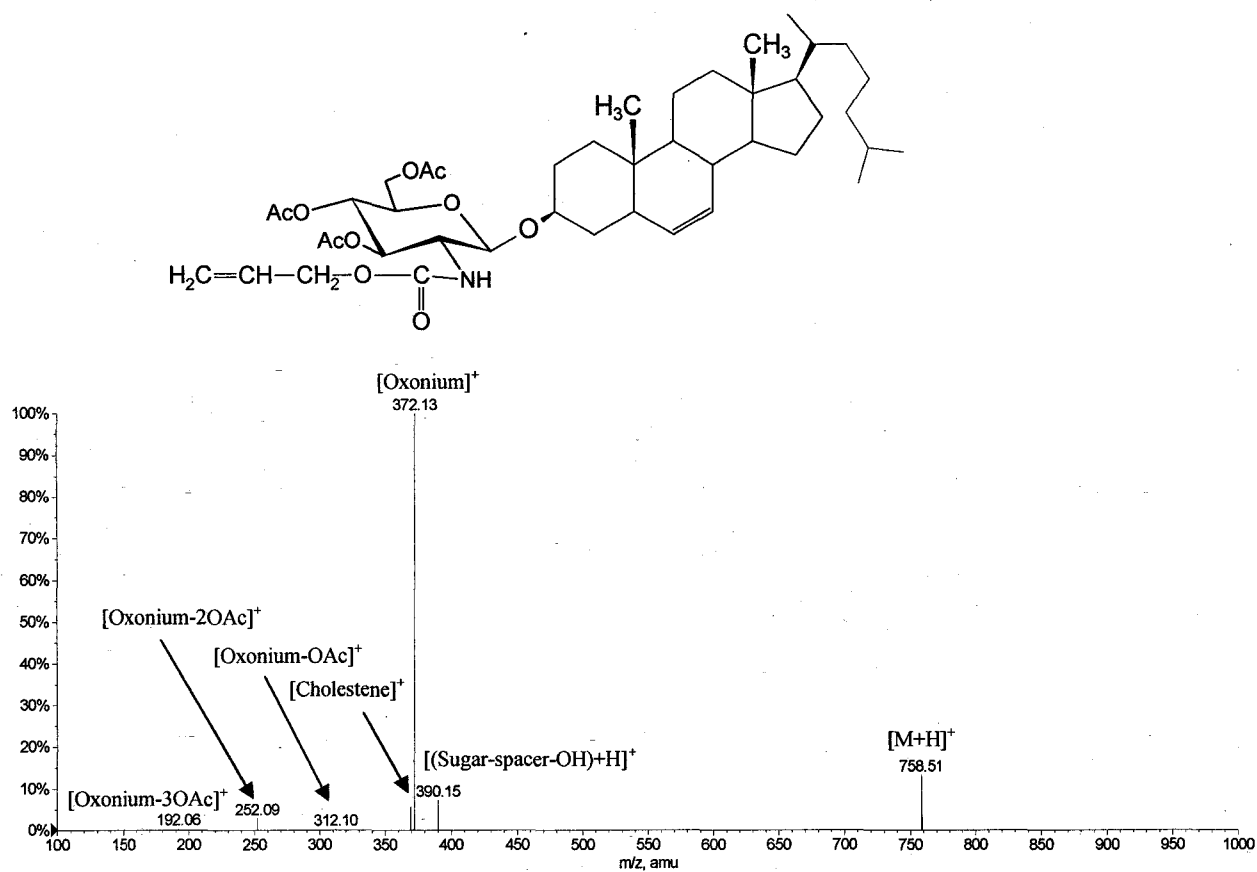


Figure VII-12: ESI-MS/MS spectrum of the neoglycolipids bearing GlcNAloc with *O*-glycoside as spacer-acetylated form (6*O*-glycoside).

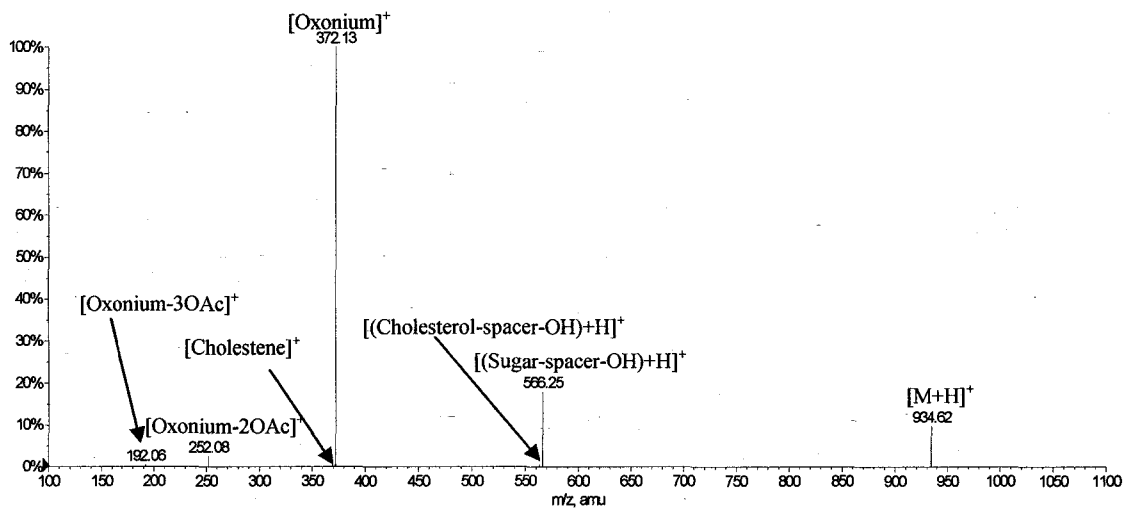
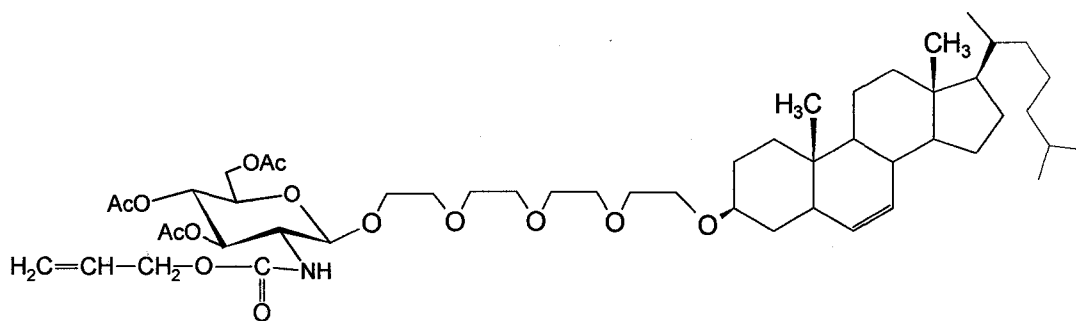


Figure VII-13: ESI-MS/MS spectrum of the neoglycolipids bearing GlcNAloc with $(\text{CH}_2\text{CH}_2\text{O})_4$ as spacer-acetylated form $(6(\text{CH}_2\text{CH}_2\text{O})_4)$.

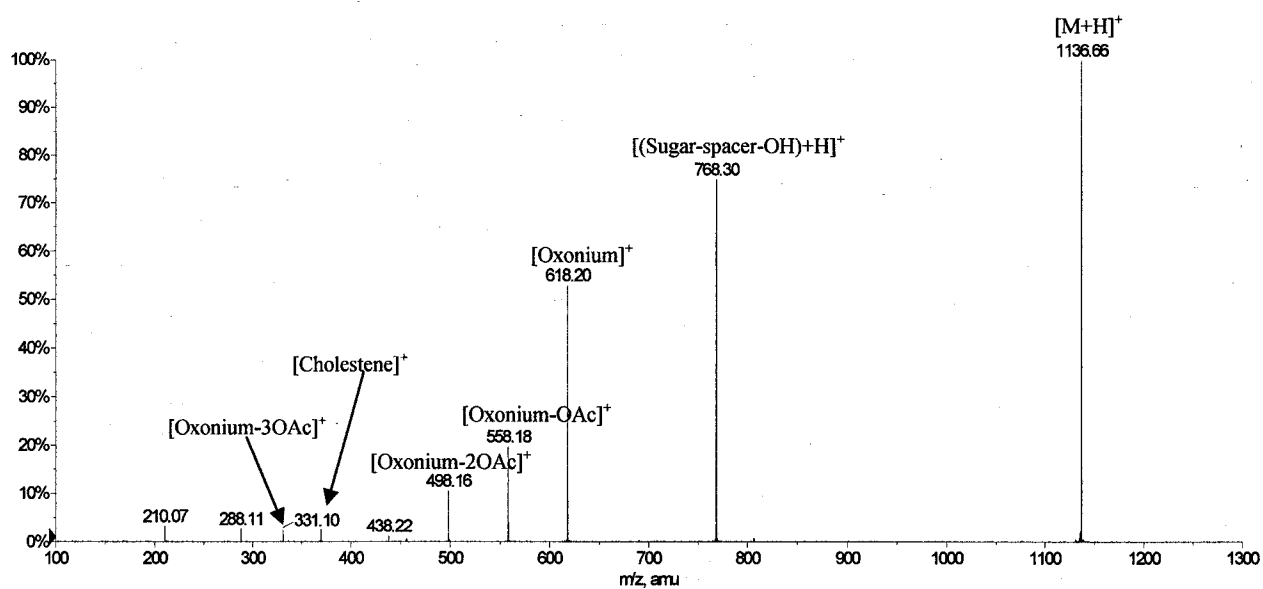
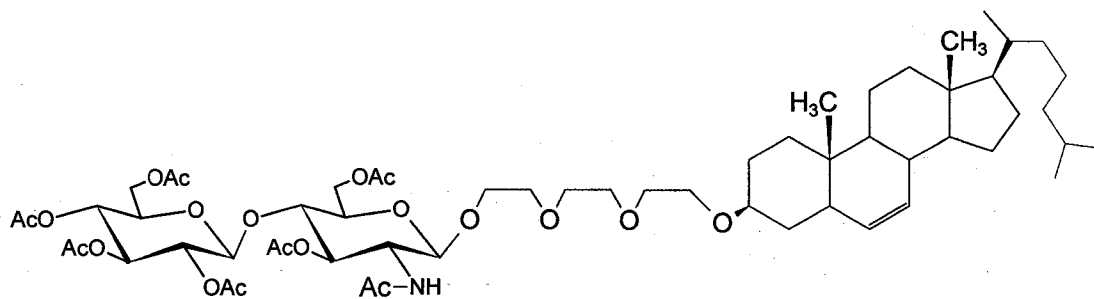


Figure VII-14: ESI-MS/MS spectrum of the neoglycolipids bearing LacNAc with $(\text{CH}_2\text{CH}_2\text{O})_3$ as spacer- acetylated form $(4(\text{CH}_2\text{CH}_2\text{O})_3)$.

